

**SITING A LOW-LEVEL RADIOACTIVE WASTE DISPOSAL FACILITY IN TEXAS
VOLUME FOUR - GEOLOGIC AND HYDROLOGIC INVESTIGATIONS
OF STATE OF TEXAS AND UNIVERSITY OF TEXAS LANDS**

August 1987

Report prepared by
Bureau of Economic Geology
The University of Texas at Austin

By

C. W. Kreidler, J. A. Raney, R. Nativ, E. W. Collins,
W. F. Mullican, III, T. C. Gustavson, and C. D. Henry

DISCLAIMER

The views expressed and conclusions reached in this report are those of the Bureau of Economic Geology, The University of Texas at Austin, and do not necessarily represent the views of the Texas Low-Level Radioactive Waste Disposal Authority or the Board of Directors of the Authority.

TEXAS LOW-LEVEL RADIOACTIVE WASTE DISPOSAL AUTHORITY

BOARD OF DIRECTORS

John E. Simek, Chairman

Elbert B. Whorton, Jr., Ph.D., Vice-Chairman

Jim R. Phillips, Secretary

James P. Allison

Milton J. Guiberteau, M.D.

William L. Fisher, Ph.D.

GENERAL MANAGER:

Lawrence R. Jacobi, Jr., P.E.

All programs and information of the Texas Low-Level Radioactive Waste Disposal Authority are available without regard to race, ethnic origin, religion, sex, or age.

CONTENTS

Section I	
EXECUTIVE SUMMARY.....	1
INTRODUCTION	5
REGIONAL SETTING, CULBERSON AND HUDSPETH COUNTIES, TEXAS.....	7
Regional geologic setting.....	7
Chemical and isotopic analysis.....	7
Regional seismicity.....	8
Climate	10
Section II	
RUSTLER HILLS, CULBERSON COUNTY INVESTIGATIONS.....	12
Location	12
Methods	12
Geologic setting.....	17
Karst topography of the Gypsum Plain.....	18
Geology of Site S-15.....	20
Geology of Block 46.....	21
Structures in Block 46.....	23
Faults in the Bell Canyon Formation.....	24
Fault/flexure grabens at the Bell Canyon-Castille contact.....	25
Northeast-striking faults in the Castille Formation.....	27
Northeast-striking faults in the Rustler Hills.....	27
Timing of northeast-striking faults.....	28
Joints.....	28
Sulfur mining in the Rustler Hills region.....	30
Surface flow.....	31
Hydrologic setting.....	32
Water-bearing characteristics.....	32
Recharge.....	32
Discharge.....	33
Potentiometric surface.....	33
Ground-water geochemistry.....	36
RUSTLER HILLS, CULBERSON COUNTY - CONCLUSIONS.....	47
Section III	
HUECO BOLSON, HUDSPETH COUNTY INVESTIGATIONS.....	54
Location	54
Methods	54
Geologic setting.....	57
Stratigraphy of Hueco Bolson deposits.....	58
Age of bolson sediments.....	59
Stratigraphy.....	60
Stratigraphic sections.....	61
Discussion.....	64
Structure	65
Quaternary faults.....	65
East-west fault along the Diablo Rim.....	67
Seismic survey.....	68
Drilling program.....	70
BEG drilling.....	70
URM drilling.....	75
Geophysical log interpretation.....	75

Discussion.....	77
Surface flow.....	83
Hydrologic setting.....	85
Water-bearing characteristics.....	85
Cretaceous formations.....	85
Bolson fill.....	86
Rio Grande alluvium.....	87
Recharge.....	87
Cretaceous formations.....	87
Bolson fill.....	89
Rio Grande alluvium.....	92
Discharge.....	93
Cretaceous formations.....	93
Bolson fill.....	93
Rio Grande alluvium.....	95
Potentiometric surface.....	95
Cretaceous formations.....	95
Bolson fill.....	95
Rio Grande alluvium.....	96
Ground-water geochemistry.....	97
Cretaceous formations.....	97
Bolson aquifer.....	105
Rio Grande alluvium.....	107
Summary.....	109
Site-specific hydrologic features.....	109
HUECO BOLSON, HUDSPETH COUNTY - CONCLUSIONS.....	110
Section IV	
DIABLO PLATEAU, HUDSPETH COUNTY INVESTIGATIONS.....	113
Location	113
Methods	113
Drilling programs.....	115
REGIONAL SETTING AND SEISMICITY.....	118
Geology	118
Structure	120
Babb Flexure.....	120
Faults, Folds, and Joints.....	121
HYDROLOGIC SETTING.....	122
Surface Flow.....	122
HU1A	122
HU1B	123
Unsaturated Zone.....	127
Saturated Zone.....	129
Water-bearing Characteristics.....	132
Potentiometric Surface.....	134
Recharge	137
Studies of recharge methods at HU1B.....	138
Flood management and recharge in the Dell City area.....	141
Discharge	142
Ground-water geochemistry.....	143
DIABLO PLATEAU, HUDSPETH COUNTY CONCLUSIONS.....	158
ACKNOWLEDGMENTS.....	161
REFERENCES	163

APPENDICES

1. Records of wells and springs in Culberson and Hudspeth Counties.....	173
2. Water chemistry and isotope data for wells and springs in Culberson and Hudspeth Counties.....	177
3. Pumping test data and interpretation - Diablo Plateau.....	183
3A. Hydrological parameters of the Cretaceous aquifer, Fort Hancock site, derived from a short-term pumping test.....	242
4. Application of isotope techniques to hydrology.....	245
5. Karst features of the Gypsum Plains.....	251
6. Stratigraphic sections of bolson deposits cropping out in Fort Hancock area, Hudspeth County.....	258
7. Hydraulic conductivity measurements in the unsaturated zone	266
8. Permeability of bolson fill based on core and grain size analyses.....	271
9. Lithologic logs for Hudspeth County test holes.....	275
10. Geophysical log data.....	286
11. Estimation of annual recharge based on soil coring and chloride analysis.....	296
12. Geologic and hydrologic data from El Paso Natural Gas Company Pump Station #2 water wells, Hudspeth County, Texas.....	299
13. Lithologic and structural descriptions of test holes cored in the Diablo Plateau.....	314
14. Climate and vegetation controls on surface recharge.....	318
15. B-14 water well summary.....	325

Figures

1. Location and stratigraphy of Block 46 and S-15 study areas, Culberson County.....	13
2. Base map and location of springs in the vicinity of S-15 study area in Culberson County.....	15
3. Base map and location of springs and wells in the vicinity of Block 46 study area in Culberson County.....	16
4. Geomorphic map of Culberson County study region.....	19
5. Geologic map of S-15 study area.....	22
6. Rose diagram plots of joints in Block 46 strata.....	29
7. Tritium and ^{14}C activity distribution in ground water of Site S-15, Culberson County.....	34
8. Tritium and ^{14}C activity distribution in ground water of Block 46 site, Culberson County.....	35
9. Water-level distribution of Site S-15, Culberson County.....	37
10. Water-level distribution of Block 46 site, Culberson County.....	38
11. Total dissolved solids distribution in ground water of Site S-15, Culberson County.....	39
12. Total dissolved solids, SO_4^{2-} , and Cl^- distribution in ground water of Block 46 Site, Culberson County.....	40
13. SO_4^{2-} concentration versus altitudes of ground-water samples in Site S-15, Culberson County	41
14. SO_4^{2-} concentration versus TDS concentration in ground water of Culberson County sites.....	42
15. SO_4^{2-} concentration versus Ca^{2+} , Na^+ , and Mg^{2+} concentrations in ground water of Culberson County sites.....	43
16. $\delta^{34}\text{S}$ distribution in ground-water samples of Site S-15, Culberson County (in ‰ deviation from the Canyon Diablo Troilite).....	45
17. $\delta^{34}\text{S}$ distribution in ground-water samples of Block 46, Culberson County (in ‰ deviation from the Canyon Diablo Troilite).....	46
18. Tritium activity versus altitude of ground-water samples from Site S-15, Culberson County.....	48

19.	$\delta^{18}\text{O}$ and $\delta^2\text{H}$ distribution in ground water of Site S-15, Culberson County (in ‰ deviation from SMOW).....	49
20.	$\delta^{18}\text{O}$ and $\delta^2\text{H}$ distribution in ground water of Block 46, Culberson County (in ‰ deviation from SMOW).....	50
21.	$\delta^{18}\text{O}$ versus $\delta^2\text{H}$ (‰) in Culberson County sites.....	51
22.	Map of geologic setting and location of S-34a and Hudspeth County study areas.....	55
23.	a) Map of topography, drainage, and test holes at primary study area in Hudspeth County.....	71
	b) Geologic map of primary study area in Hudspeth County.....	72
24.	a) Map of topography and test holes at S-34b in Hudspeth County.....	73
	b) Geologic map of S-34b in Hudspeth County.....	74
25.	Cross section A-A' across primary study site in Hudspeth County.....	78
26.	Cross section B-B' across primary study site in Hudspeth County.....	79
27.	Lithologic log for LLWA 1.....	80
28.	Base map of the Hudspeth County study area.....	84
29.	Tritium and ^{14}C activities in the Hudspeth County site.....	88
30.	Variations of grain size, water content, and chlorides in soil cores of five boreholes in the bolson gravel cover.....	91
31.	Potentiometric surfaces of water in the aquifers in Hudspeth County site.....	94
32.	Total dissolved solids, SO_4^{2-} , and Cl^- distribution in Hudspeth County site.....	98
33.	Salinity diagram of ground water from the Cretaceous aquifer in the Hudspeth County site.....	99
34.	^{14}C activity in ground water samples of the Cretaceous aquifer versus the distance from the recharge area at the Diablo Plateau.....	100
35.	Tritium activity versus temperature in water samples in Hudspeth County site.....	101
36.	$\delta^{18}\text{O}$ and $\delta^2\text{H}$ distribution in ground water in Hudspeth County site (in ‰ deviation from SMOW).....	102

37. $\delta^{18}\text{O}$ versus $\delta^2\text{D}$ (‰) in ground water of S-34 study area (in ‰ deviation from SMOW).....	103
38. $\delta^{18}\text{O}$ (‰) versus $\delta^{14}\text{C}$ corrected ages in ground water of S-34 study area.....	104
39. Salinity diagram of ground-water samples of the bolson-fill aquifer in the S-34 study area.....	106
40. Salinity diagram of ground-water samples of the Rio Grande alluvium in the vicinity of the Hudspeth County site.....	108
41. Location and regional geologic setting of Pump Station Hills study area	114
42. Surface drainage and location of wells within the study area.....	116
43. Photograph of flooding at Antelope Draw where it crosses Ranch-to-Market Road 1111.....	124
44. Flood Insurance Rate Map (FIRM) for area around site HU1A.....	125
45. Flood Insurance Rate Map (FIRM) for area around site HU1B.....	126
46. Map showing potentiometric surface elevations in the study area.....	128
47. Potentiometric surface map, Aquifers A and B.....	131
48. Map showing borehole locations and chloride profiles at HU1B.....	140
49. Map of TDS, Cl, and SO_4 distribution.....	145
50. Map of Na, Ca, and Mg distribution.....	146
51. Chemical facies map, Aquifers A and B.....	147
52. Piper diagram, Aquifers A and B.....	148
53. Salinity diagrams, Aquifers A and B.....	149
54. Map of NO_3 distribution.....	150
55. Map of ^{14}C and tritium distribution.....	152
56. Map of $\delta^{18}\text{O}$ and δD distribution.....	154
57. Plot of $\delta^{18}\text{O}$ versus δD	155
58. Map of $\delta^{34}\text{S}$ and $\delta^{13}\text{C}$ distribution.....	157

Appendix Figures

A3-1. Location map of the seven wells used for pumping tests.....	184
A3-2. Location map of wells used in pumping test no. 1.....	185

A3-3.	Time-drawdown curve matched to Walton type curves for pumping test no. 1 in well LL162.....	187
A3-4.	Time-drawdown plot interpreted using Jacob's method for pumping test no. 1 in well LL162.....	188
A3-5.	Time-recovery curve matched to Walton type curves for pumping test no. 1 in well LL162	191
A3-6.	Time-recovery plot interpreted using Theis' method for pumping test no. 1 in well LL162.....	197
A3-7.	Time-drawdown plot interpreted using Jacob's method for pumping test no. 2 in well LL156.....	200
A3-8.	Time-drawdown curve matched to Walton type curves for pumping test no. 3 in well LL155.....	204
A3-9.	Time-drawdown plot interpreted using Jacob's method for pumping test no. 3 in well LL155.....	205
A3-10.	Time-recovery curve matched to Walton type curves for pumping test no. 3A in well LL155.....	206
A3-11.	Time-recovery plot interpreted using Theis' method for pumping test no. 3A in well LL155.....	207
A3-12.	Time-drawdown curve matched to Walton type curves for pumping test no. 4A in well LL148.....	218
A3-13.	Time-drawdown curve matched to Walton type curves for pumping test no. 5 in well LL141.....	224
A3-14.	Time-recovery curve matched to Walton type curves for pumping test no. 5 in well LL141.....	225
A3-15.	Time-drawdown plot interpreted using Jacob's method for pumping test no. 5 in well LL141.....	226
A3-16.	Time-recovery plot interpreted using Theis' method for pumping test no. 5 in well LL141.....	227
A3-17.	Time-drawdown curve matched to Walton type curves for pumping test no. 6 in well LL132.....	233
A3-18.	Time-recovery curve matched to Walton type curves for pumping test no. 6 in well LL132.....	234
A3-19.	Time-drawdown plot interpreted using Jacob's method for pumping test no. 6 in well LL132.....	236
A3-20.	Time-recovery plot interpreted using Theis' method for pumping test no. 6 in well LL132.....	237

A3-21.	Time-drawdown curve matched to Walton type curves for pumping test no. 7 in well LL138.....	238
A8-1.	Variations in grain size and vertical permeability with depth in borehole 7.....	273
A8-2.	Correlation of porosity and vertical permeability in borehole 7.....	274
A9-1.	Lithologic log, LLWA1, Hudspeth County.....	276
A9-2.	Lithologic log, LLWA2, Hudspeth County.....	277
A9-3.	Lithologic log, LLWA3, Hudspeth County.....	278
A9-4.	Lithologic log, LLWA4, Hudspeth County.....	279
A9-5.	Lithologic log, LLWA5, Hudspeth County.....	280
A9-6.	Lithologic log, LLWA6, Hudspeth County.....	281
A9-7.	Lithologic log, LLWA7, Hudspeth County.....	282
A9-8.	Lithologic log, LLWA8, Hudspeth County.....	283
A9-9.	Lithologic log, LLWA9, Hudspeth County.....	284
A9-10.	Lithologic log, LLWA10, Hudspeth County.....	285
A10-1.	Composite geophysical log for borehole 7.....	287
A10-2.	Composite geophysical log for borehole 11.....	288
A10-3.	Composite geophysical log for borehole 12.....	289
A10-4.	Composite geophysical log for borehole 13.....	290
A10-5.	Composite geophysical log for borehole 10.....	291
A13-1.	Lithologic log for rhyolite core from HU1A site.....	315
A13-2.	Lithologic log for limestone core from HU1B site.....	316
A14-1.	Weather station location map.....	320

TABLE

1.	Summary of climatic data, El Paso County.....	11
----	---	----

APPENDIX TABLES

A3-1.	Drawdown data from pumping test no. 1 in well LL162.....	189
A3-2.	Recovery data from recovery test no. 1 in well LL162.....	192

A3-3.	Drawdown data from pumping test no. 2 in well LL156.....	199
A3-4.	Recovery data from pumping test no. 2 in well LL156.....	202
A3-5.	Drawdown data from pumping test no. 3 in well LL155.....	208
A3-6.	Drawdown data from pumping test no. 3A in well LL155.....	209
A3-7.	Recovery data from pumping test no. 3A in well LL155.....	210
A3-8.	Drawdown data from pumping test no. 4 in well LL148.....	215
A3-9.	Recovery data from pumping test no. 4 in well LL148.....	216
A3-10.	Drawdown data from pumping test no. 4A in well LL148.....	217
A3-11.	Drawdown data from pumping test no. 5 in well LL141.....	221
A3-12.	Recovery data from pumping test no. 5 in well LL141.....	222
A3-13.	Drawdown data from pumping test no. 6 in well LL132.....	229
A3-14.	Recovery data from pumping test no. 6 in well LL132.....	231
A3-15.	Drawdown data from pumping test no. 7 in well LL138.....	240
A11-1.	Chloride and annual recharge data at HUIB.....	298
A14-1.	Climatic data for Hueco Bolson and Diablo Plateau.....	321

PLATES (in pocket)

- Plate 1. Geologic map of State Land S-15, Culberson County, Texas
- Plate 2. Geologic map of University Lands Block 46, Culberson County, Texas
- Plate 3. Geologic map of study area in Hudspeth County, Texas
- Plate 4. Geologic map of the Pump Station Hills area, Hudspeth County, Texas
- Plate 5. Floodprone areas in Hudspeth County

EXECUTIVE SUMMARY

The Bureau of Economic Geology, The University of Texas at Austin, conducted preliminary investigations of the geology and hydrology of 5 areas in Culberson and Hudspeth Counties, Texas, selected by the Texas Low-Level Radioactive Waste Disposal Authority as potential sites for a low-level radioactive waste repository. This report discusses the results of those studies.

Two areas in Culberson County, Texas, Site S-15 and Block 46 and adjacent regions, were investigated. The Permian Castile Formation underlies all of Site S-15 and the eastern half of Block 46. The Castile Formation displays evidence of extensive solution and local collapse and appears to contain a complex system of karst features and underground solution channels. The western half of Block 46 is underlain by the Permian Bell Canyon Formation, consisting of interbeds of sandstone and limestone. Both the Castile and subjacent Bell Canyon Formations contain prominent joint systems and local areas of normal faults. Surficial deposits are commonly composed of detritus derived from local formations and appear to be both porous and permeable.

The ground-water flow in both areas is governed by karst dissolution and collapse features. The chemical and isotopic composition of ground water indicates active recharge through the thin unsaturated zone combined with older water flowing from the west. Residence time of ground water in the aquifers is relatively short, and numerous springs discharge from the shallow ground-water table.

Hudspeth County, Texas, includes a large area of State-owned lands to the north and east of the town of Fort Hancock (S-34) within the Hueco Bolson and 2

large University of Texas-owned areas, HU1A and HU1B, south and west of the town of Dell City on the Diablo Plateau. The Authority selected these areas for more detailed investigations based on the areas' low topographic relief, surface drainage, and depth to ground water.

The Fort Hancock area drains into Alamo Arroyo, which does not pass through any populated areas. This area has an arid climate and usually receives less than 10 inches (25 cm) of rainfall a year. Drill testing in the Fort Hancock study area indicates that about 40 ft (13 m) of alluvial silts, sands, and gravels with near-surface calcrete horizons overlie a thick sequence of silty and clayey older bolson-fill deposits. The older bolson-fills, as shown by both drilling and surface exposure, are an interbedded sequence of clay, silt, and fine sand. The clays are expansive, and local selenite crystals are present at the surface. The depth to Mesozoic bedrock is variable, but drilling in the study area encountered probable bedrock at approximately 400 to 500 ft (122 to 152 m). Seismic investigations in the same area, however, indicate that the depth to bedrock may actually be 800 to 900 ft (244 to 274 m). The Fort Hancock study area lies about 4 mi (6 km) northeast of a northwest-striking fault that cuts the bolson-fill deposits and at least the base of the overlying alluvial deposits. The age of most recent faulting has not been determined.

Three aquifers, located in the Cretaceous rocks, the bolson fill, and the Rio Grande alluvium, are present regionally near the Fort Hancock site. In the site area proper, no ground water was encountered in the bolson fill, and in what is considered to be a Cretaceous aquifer, the static water level was measured at 478 ft (145.7 m) below land surface. Water in the Cretaceous aquifer was old, suggesting either slow movement of ground water in the aquifer or hydraulic disconnection of the aquifer in the site area from the recharge zone at the Cretaceous plateau due to

faulting. There are, however, indications of limited current recharge into the Cretaceous. Water in the bolson fill occurs 2 to 6 mi (3 to 9 km) southwest of the site, where the thickness of the unsaturated zone varies from 90 to 360 ft (27 to 110 m). Water in the bolson fill is old and may be recharged from water moving upward from the Cretaceous aquifer. In the Rio Grande valley, water in the bolson is modern and is mainly recharged by the Rio Grande alluvium aquifer. Average annual recharge rate into the ground cover that overlies the bolson fill is estimated to be 0.003 to 0.02 inch/year (0.07 to 0.5 mm/year). Ground-water flow within the Hueco Bolson in both the Cretaceous and bolson-fill aquifers is to the southwest toward the Rio Grande valley. The Rio Grande alluvium in the valley contains an aquifer that is fed by the Rio Grande and discharges to numerous irrigation wells in the valley and also probably discharges into the bolson fill in the valley.

Sites HU1A and HU1B on the Diablo Plateau are underlain by different bedrock lithologies covered by alluvium, which necessitated drilling for site-specific investigations. Because of the lack of exposed bedrock, studies of the regional geologic setting were used to infer the probable nature of the subsurface geologic environment at each site. Hydrologic investigations for HU1A and HU1B were also regional in nature because of the limited data available at either site and the availability of water-level data and water samples from previously drilled wells in the region.

Subsurface lithologies at HU1A and HU1B are Precambrian rhyolite porphyry and Cretaceous limestone interbedded with some silty and muddy interbeds, respectively. The rhyolite porphyry is fractured, and the fractures strike in many directions and dip from vertical to horizontal. Most fractures contain no mineral fillings, indicating they are not sealed. Cretaceous limestone at HU1B is not as fractured as the

rhyolite porphyry at HU1A. There is evidence of carbonate dissolution and formation of some solution permeability.

The Babb flexure is north of both HU1A and HU1B. Fractures that are evident away from the inferred margin of the flexure may be related to flexure deformation. The flexure may be the Permian or post-Permian expression of a major pre-Permian strike-slip fault (Hodges, 1975). It is unknown if Cretaceous rocks have been warped by recurrent movement along the structure.

Regional ground-water flow on the Diablo Plateau is predominantly from southwest to northeast. The ground-water divide is not located along the Babb flexure but is close to the southern edge of the Diablo Plateau. Two aquifers are present, a shallow aquifer in the southwestern Diablo Plateau with depths to water generally less than 200 ft (61 m) and a deeper aquifer through most of the region with depths to water of as much as 800 ft (244 m).

Recharge occurs over the entire study area and is not restricted to the updip part of the potentiometric surface in the areas of higher elevation. Tritium occurs in nearly all wells regardless of their location within the regional water table. Most recharge probably occurs during flooding of the arroyos that traverse the plateau. Recharge along fractures, typically concentrated in arroyos, permits recently recharged water to move rapidly through a thick unsaturated section. Three separate fracture sets were identified during pumping tests no. 1 and no. 6 of this study. Because of the fracture control on ground-water flow, flow velocities cannot be estimated but are expected to be high. Discharge is either by evaporation on the salt flats or through pumping wells.

The shallower aquifer may or may not be present at either site, though it is not

used at either site. Depth to ground water in the deeper aquifer beneath the sites is probably greater than 600 ft (183 m). Fractures in bedrock beneath the arroyos are important pathways for recharge in the vicinities of the sites, as has been documented through chloride analysis and vadose permeability tests.

Flooding down Antelope Draw, which bounds site HU1A, may be very intense for short durations, and consideration should be given to any siting with respect to potential flooding.

INTRODUCTION

In December 1985 and June 1986 the Bureau of Economic Geology (BEG) was asked by the Texas Low-Level Radioactive Waste Disposal Authority to conduct a preliminary study of the geology and hydrology of five sites being considered for construction of a low-level radioactive waste repository. The sites are located in Culberson and Hudspeth Counties, Texas, and the repository is to be constructed within the unsaturated zone.

The rocks below potential sites are Permian evaporites in Culberson County and Cenozoic gravels and silty clays of the Hueco Bolson and Precambrian rhyolite porphyry and Cretaceous limestones and sandstones on the Diablo Plateau in Hudspeth County. These geologic investigations provide (1) general data for evaluation of the geologic framework of the proposed sites and (2) site-specific data for evaluation of active geomorphic processes and physical and structural character of the units.

Our hydrologic investigations emphasize six major issues:

- (1) Are there any regional aquifers (water-bearing formations capable of

producing water from a well) below these sites that can be affected by radioactive waste disposal?

(2) What is the depth to the uppermost regional ground-water table at each site? Is the unsaturated zone sufficiently thick to prevent vertical migration of contaminants from the repository to the water table?

(3) What are the flow directions of ground water?

(4) What is the residence time of water in the regional aquifers? Are flow rates sufficiently low that radionuclides would not spread contaminants away from the site in case of an accidental spill?

(5) What are the methods and rates of recharge to these aquifers? How much of the recharge comes from direct precipitation and surface flooding on the sites' land surface? How much recharge water could percolate through the layers being considered as host rocks for the repository?

(6) Where are the discharge points (natural and wells) of these aquifers and what is their distance from the site? In case of an accidental spill, is the distance large enough to allow complete radioactive decay before water reaches the biosphere?

Hydrogeologic study of both the unsaturated and the saturated zones at each site was conducted to provide an initial assessment of these concerns. Topics of regional scope that apply to both counties are discussed, then the results of the geologic and hydrologic investigations that are more specific to each area are presented. C. W. Kreitler and J. A. Raney are co-principal investigators for the geologic and hydrologic studies. E. W. Collins, T. C. Gustavson, and C. D. Henry conducted much of the geologic work, and W. F. Mullican, R. Nativ, and D. A. Smith investigated the hydrology of the sites. S. C. Caran provided information on present climate of the areas. We appreciate the cooperation, help, and hospitality of the local landowners during these investigations.

REGIONAL SETTING: CULBERSON AND HUDSPETH COUNTIES, TEXAS

Regional Geologic Setting

Culberson and Hudspeth Counties lie in Trans-Pecos Texas in the southeastern part of the Basin and Range structural province. This province consists of topographically high ranges separated by major normal faults from adjacent topographically low basins. Structural development of the province began about 24 million years ago (mya) during east-northeast-oriented extension. Faulting and associated relative subsidence of the basins began at that time and continue to the present. The basins were progressively filled by detritus eroded from the adjacent ranges.

Only the northern and western parts of Trans-Pecos Texas have well-developed northwest-trending basins and ranges, having as much as 5,000 ft (1,500 m) of relief. The two Culberson County study areas are in the easternmost part of the province at its transition to the Great Plains. Basin and Range faults are present but they are of small displacement, and the study region lies outside the area of distinct Basin and Range topography. The Fort Hancock site in Hudspeth County is along the margin of Hueco Bolson, a major Basin and Range graben. Hueco Bolson is bordered on the west and south by the Chihuahua Tectonic Belt, a part of the Laramide fold belt. HU1A and HU1B are located centrally on the Diablo Plateau, a horst block north of the Hueco Bolson.

Chemical and Isotopic Analysis

Chemical analyses of ground water from wells in the Dell City area, Rio Grande Valley, and in the Salt Basin were obtained from Texas Water Commission files.

Data for wells near the selected sites were unavailable, but 58 active water wells and springs within the study region were sampled. All samples were analyzed for general chemistry, $\delta^{18}\text{O}$, δD , tritium, $\delta^{34}\text{S}$, $\delta^{13}\text{C}$, and ^{14}C . Chemical analyses were performed by Mineral Studies Laboratory (BEG); ^{14}C analyses, by Radioisotopes Laboratory, Balcones Research Center (UT-Austin); other isotopic analyses ($\delta^{18}\text{O}$, δD , tritium, $\delta^{34}\text{S}$, and $\delta^{13}\text{C}$), by Environmental Isotope Laboratory, University of Waterloo, Ontario, Canada; Geochron Laboratories, Krueger Enterprises; and University of Miami, Tritium Laboratory. Water temperatures were measured at the sampling sites. Water well and spring locations, elevations, and water levels are reported in appendix 1. All chemical and isotopic data collected during this study are reported in appendix 2.

Drilling programs at S-34 were contracted to Underground Resource Management and at HU1A and HU1B to Byrl Binkley Drilling Contractor. Additional shallow drilling and soil sampling were performed with the BEG drilling rig under the supervision of James Doss. Stratigraphic test holes at the S-34 were electrically logged by Schlumberger. Monitoring equipment was installed by Byrl Binkley in seven water wells for pumping tests on the Diablo Plateau. Results of these tests are reported in appendix 3.

Regional Seismicity

Because no detailed studies of seismicity are available, information on possible seismic activity is based on a consideration of the tectonic setting of Trans-Pecos Texas and of recent seismicity in and near the Basin and Range structural province. Quaternary fault scarps occur throughout much of Trans-Pecos Texas (Muehlberger and others, 1978; Henry and Price, 1985) and are abundant in the Salt Basin, a large Basin and Range graben oriented north-south along the Culberson-Hudspeth

County line. Quaternary scarps have not been found near either Block 46 or Site S-15, but recognition of scarps is hindered by the paucity of Quaternary outcrops. Quaternary scarps are abundant in the northern part of Hueco Bolson 30 mi (50 km) northwest of S-34, and a distinct Quaternary scarp lies 3 mi (5 km) southwest of the initial drillhole in S-34. This scarp and related structures are discussed more thoroughly below.

Recent compilations of regional seismicity data include studies of (1) the entire Basin and Range province (Askew and Algermissen, 1983), (2) southeastern New Mexico (Sanford and Topozada, 1974), and (3) southern Culberson County and adjacent areas (Dumas, 1980). Askew and Algermissen (1983) list six earthquake epicenters in the Trans-Pecos region between 1803 and 1977, two with Richter magnitudes (surface waves) of 5 and 6. Both of these latter earthquakes occurred near Valentine, 50 mi (80 km) south of the Culberson County sites; one, the 1931 Valentine earthquake, had a Modified Mercalli intensity of VIII and was the strongest reported earthquake in Texas. The 1955 earthquake near Valentine had a Modified Mercalli intensity of IV (Reagor and others, 1982). Dumas (1980) detected about 300 earthquakes, all with magnitudes less than 3.7, between 1976 and 1980 near the site of the Valentine earthquake. Dumas (1980) also identified a seismically active area along the eastern margin of the Salt Basin in the area of abundant Quaternary fault scarps. However, this area could not be located precisely because it was outside the seismic network. Sanford and Topozada (1974) listed 11 felt earthquakes prior to 1961 and 6 instrumentally detected quakes between 1961 and 1972 in southeastern New Mexico and West Texas. Askew and Algermissen (1983) identified a swarm of earthquakes, all having magnitudes less than 4, near Juarez, Chihuahua, Mexico, about 45 mi (70 km) northwest of the Hudspeth County site.

Climate

The Hudspeth and Culberson study areas lie within the northern Chihuahuan Desert, south and southwest of the southern Guadalupe Mountains (King, 1948, his fig. 2; Miller, 1977, his fig. 1). The region has a subtropical arid climate (classification of Thornthwaite, 1931, as modified by Larkin and Bomar, 1983). Such climates are characterized by (1) high mean temperatures with marked fluctuations over broad diurnal and annual ranges and (2) low mean precipitation with widely separated annual extremes (Orton, 1964). For example, total annual precipitation at Carlsbad, New Mexico, north of the study areas, ranges from 2.95 to 33.94 inches (7.5 to 86.2 cm) (Orton, 1964). Winds generally are from the north and west in fall and winter and from the south and west in spring (Bomar, 1983b). None of these winds carry significant moisture (Carr, 1967), except under unusual circumstances such as the intrusion of Pacific Hurricane Paul in September 1982, which introduced enormous quantities of moisture over the highlands of Mexico and into West Texas (Bomar, 1983a). Precipitation is primarily late summer and early autumn rainfall from thundershowers. These storms occur when moist air from the Gulf of Mexico penetrates northwestward and rises to higher elevations as it approaches the mountains (Carr, 1967).

Rainfall events are locally intense but short-lived, and surface water is ephemeral because of consistently high evaporative rates. Mean annual lake-surface evaporation potential in the study areas is approximately 83 inches (211 cm) (Larkin and Bomar, 1983). Evaporation is aided by strong winds that also produce conditions of blowing dust several days each year, primarily during early spring (Bomar, 1983b). High evaporation and low, highly localized rainfall combine to form droughts during all or part of most years. During 19 of the 31 years from 1951 to 1981, Hudspeth, Culberson, and adjacent counties recorded the lowest annual precipitation of any reporting stations in Texas (Bomar, 1983a). Climatic data from stations of long record near the study areas are summarized in table 1.

Table 1. Summary of climatic data, El Paso County.

Temperature

Maximum (1960)	109°F	(43°C)
Minimum (1962)	-8°F	(-22°C)
Mean (1951-80)	63.4°F	(17°C)

Precipitation

Mean (1951-80)	7.82 inches	(20 cm)
----------------	-------------	---------

Wind

Mean velocity (1931-60)	10.0	(mph)
Mean direction	N	

*Orton, (1969, p. 33, 39); National Climatic Data Center (1985, p. 15)

RUSTLER HILLS, CULBERSON COUNTY INVESTIGATIONS

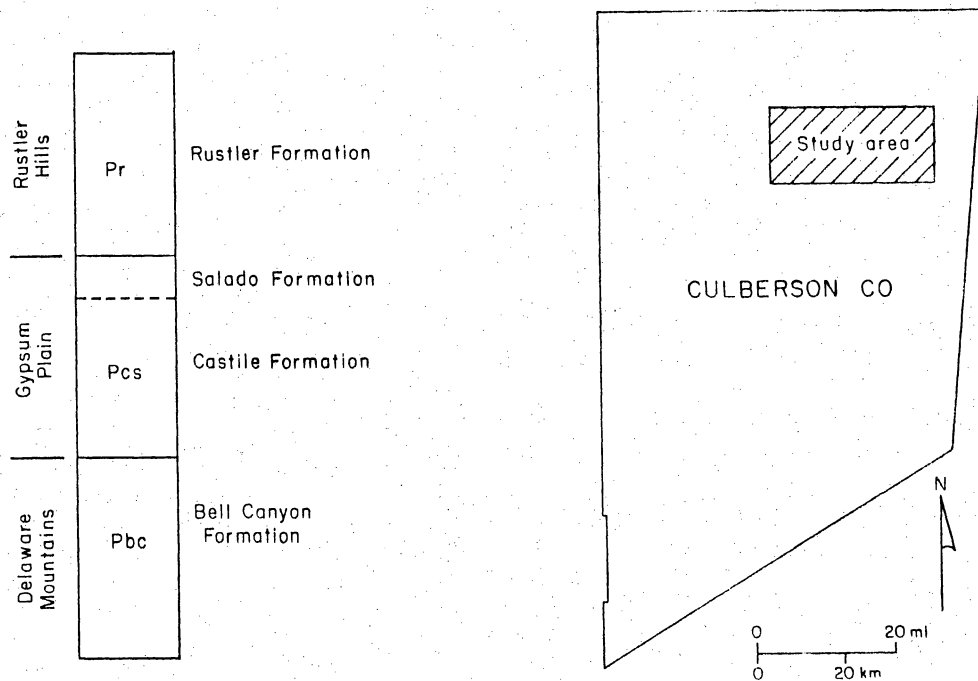
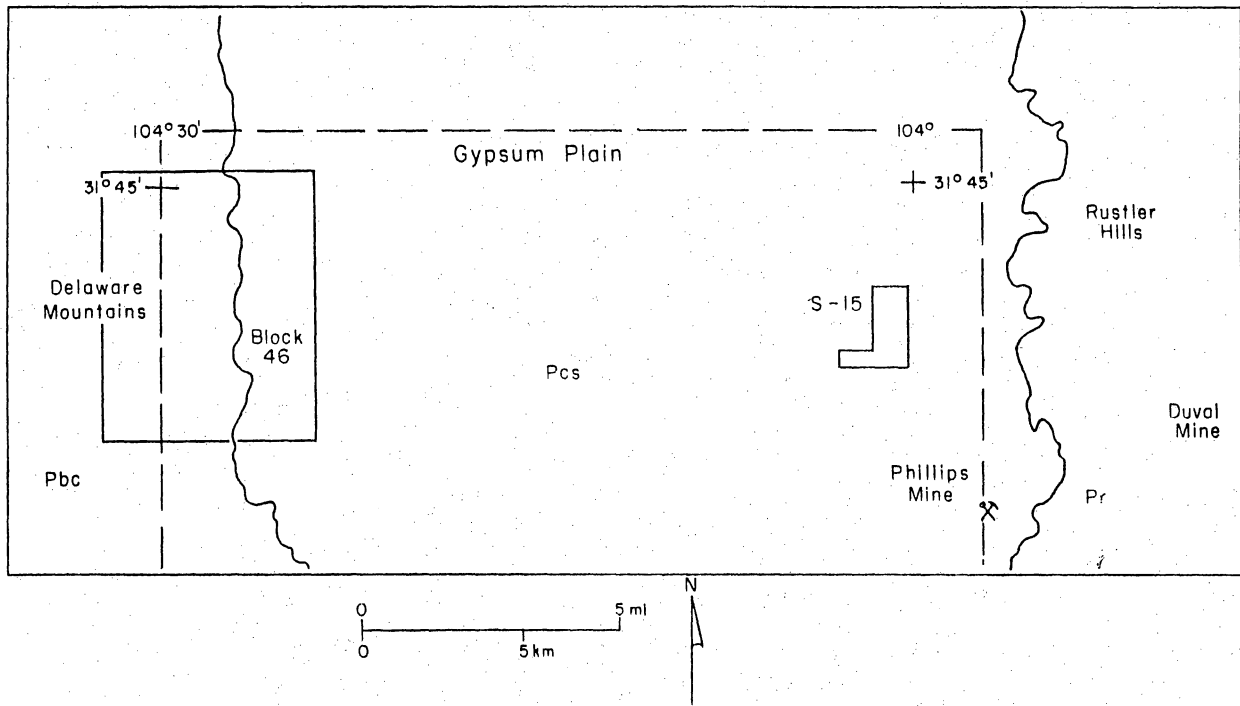
Location

The Texas Low-Level Radioactive Waste Disposal Authority selected two areas in Culberson County, Texas, for evaluation as possible sites for a low-level radioactive waste repository. The two areas are shown in figure 1 and are referred to as Site S-15 and Block 46.

Site S-15 consists of Sections 16 and 21 in PSL Block 114, which is administered by the General Land Office of Texas. Block 46 is owned and administered by The University of Texas System. Site S-15 is located on the Gypsum Plain west of the Rustler Hills. It lies on the Seven L Peak NE 7.5-minute quadrangle approximately 8 mi (13 km) west-northwest of the Pennzoil Sulphur Mine. Access to Site S-15 and adjacent areas was obtained from property owners J. Covington, R. L. Harrison, and H. M. Phillips, Jr., and from lessee F. Armstrong. Block 46 is about 8 mi (13 km) west of Site S-15 and lies mostly on the Seven L Peak and Chico Draw East 7.5-minute quadrangles. Block 46 straddles the boundary between the western edge of the Gypsum Plain and the eastern margin of the Delaware Mountains. Access to Block 46 was obtained from the Rounsavill family, owners of the KC Ranch and lessees of surface grazing rights in Block 46.

Methods

The general proximity and geologic similarity of Site S-15 and Block 46 required that a somewhat larger region encompassing both areas be considered.



QA 5955

Figure 1. Location and stratigraphy of Block 46 and S-15 study areas, Culberson County. Stratigraphy from Barnes (1983). Dashed lines locate figure 4.

Low-sun-angle aerial photographs of the region, printed at a scale of 1:12,000 (1 inch = 1,000 ft), were acquired. The area flown includes part of the Rustler Hills east of S-15 and a portion of the Delaware Mountains west of Block 46. Particular attention was focused on features such as faults, fractures, and evidence of solution or collapse that are pertinent in evaluating the viability of the areas to host a low-level radioactive waste repository.

Surface geologic investigations attempted to document geologic features identified on the aerial photographs and to refine understanding of the structural geology, geomorphology, and near-surface lithologic units of the two areas. Six staff-days were spent at S-15, and 12 staff-days were spent at Block 46. Access to the areas is restricted by the local landowners, and no drilling or excavations were done in S-15 or Block 46. Engineers from the Civil Engineering Department of The University of Texas at Austin collected surface samples from S-15.

Water levels were available only from wells east of the S-15 site near the Pennzoil Sulphur Mine. No water levels from wells were available within S-15 or in neighboring areas to the north, west, or south. However, many springs are present in this area, and their altitudes were used as water-level altitude markers (fig. 2). Information on water levels in Block 46 was too scarce (two wells and two springs, fig. 3) to permit potentiometric surface mapping of the site. All water-level information is presented in appendix 1.

No data were available for porosities, hydraulic conductivities, or transmissivities of the unsaturated or saturated zones of either site in Culberson County.

The only chemical analyses available from the Texas Water Commission files for the Culberson County sites are of water from remote wells near Van

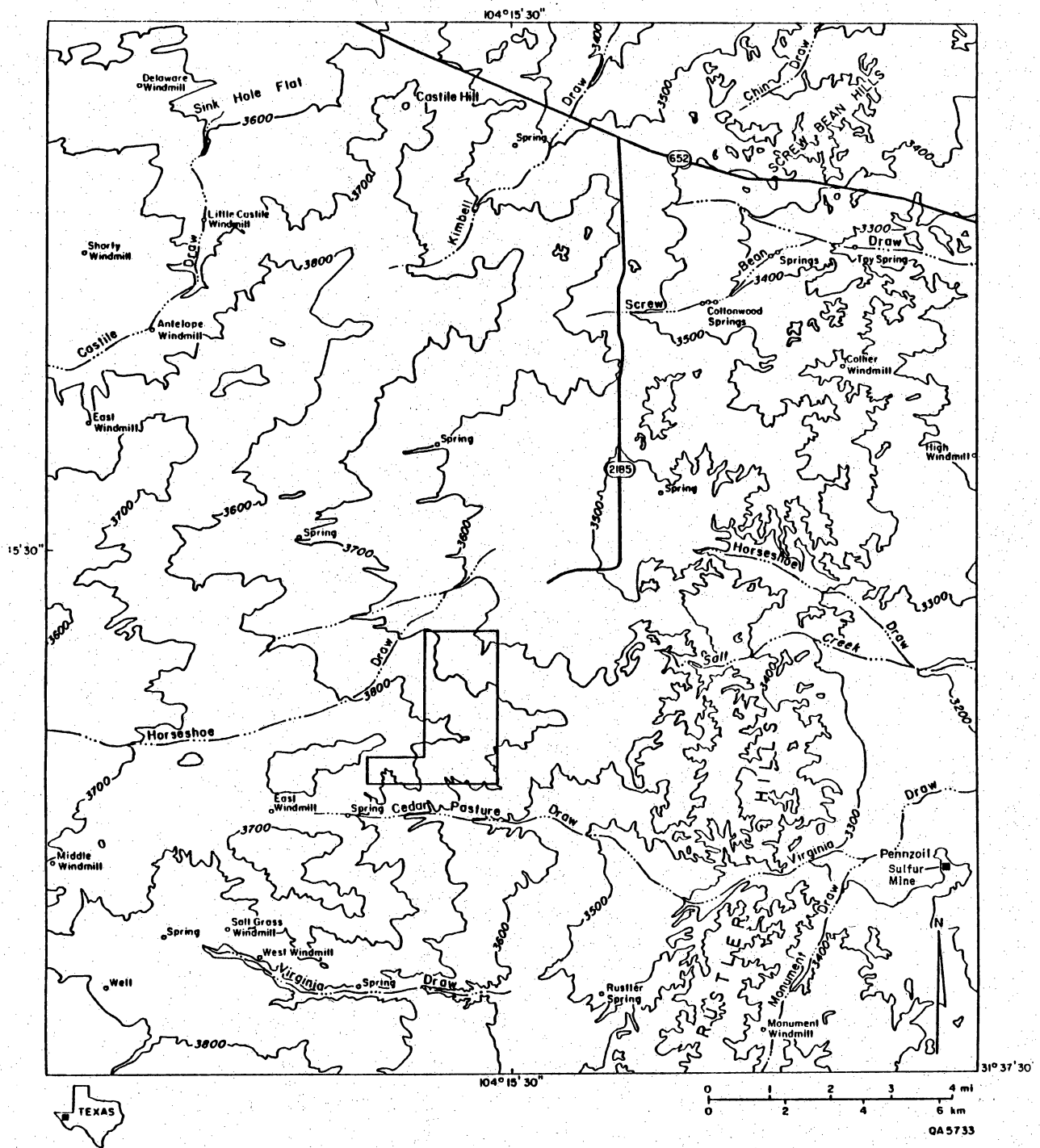


Figure 2. Base map and location of springs in the vicinity of S-15 study area in Culberson County. Bold line approximately locates the site area.

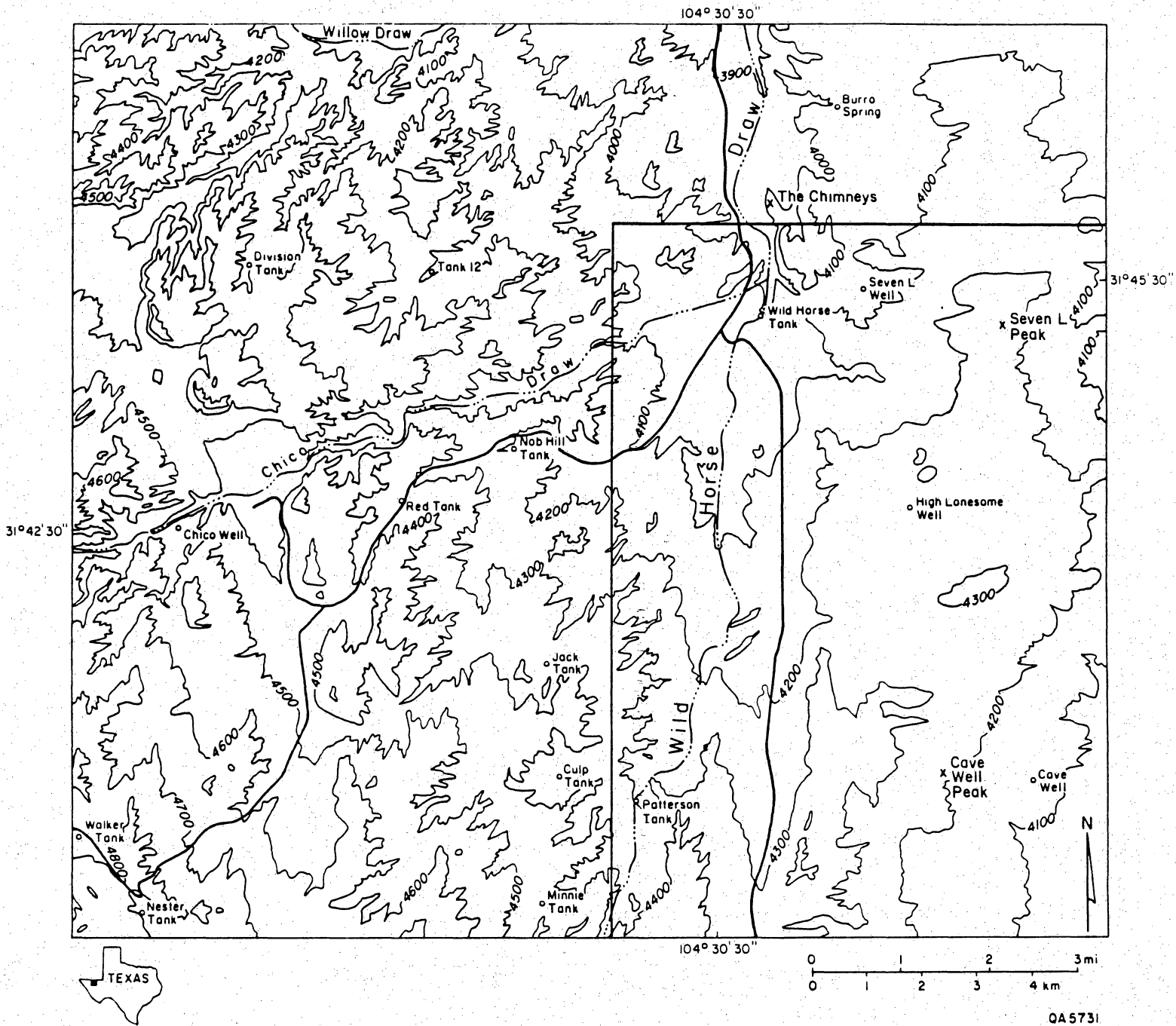


Figure 3. Base map and location of springs and wells in the vicinity of Block 46 study area in Culberson County. Bold line approximately locates the site area.

Horn, Dell City, Orla, and Kent. Some chemical analyses of wells located near the Pennzoil Sulphur Mine, east of S-15, were also available. As a result, all the wells and springs at each site, and nearby wherever possible, were sampled. All samples were analyzed for general chemistry, $\delta^{18}\text{O}$, $\delta^2\text{H}$, tritium, and $\delta^{34}\text{S}$. Well-water samples were also analyzed for ^{14}C and $\delta^{13}\text{C}$. (Springs that discharge into ponds are not suitable for ^{14}C sampling because of probable equilibration with atmospheric CO_2 .) Temperatures were measured at each sampling site. However, temperatures of springs were measured using water samples from ponds that had probably equilibrated with the ambient air temperature. These measurements are therefore unreliable. All chemical, isotopic, and temperature data are reported in appendix 2. The application of isotope techniques to ground-water studies is explained in appendix 4.

Geologic Setting

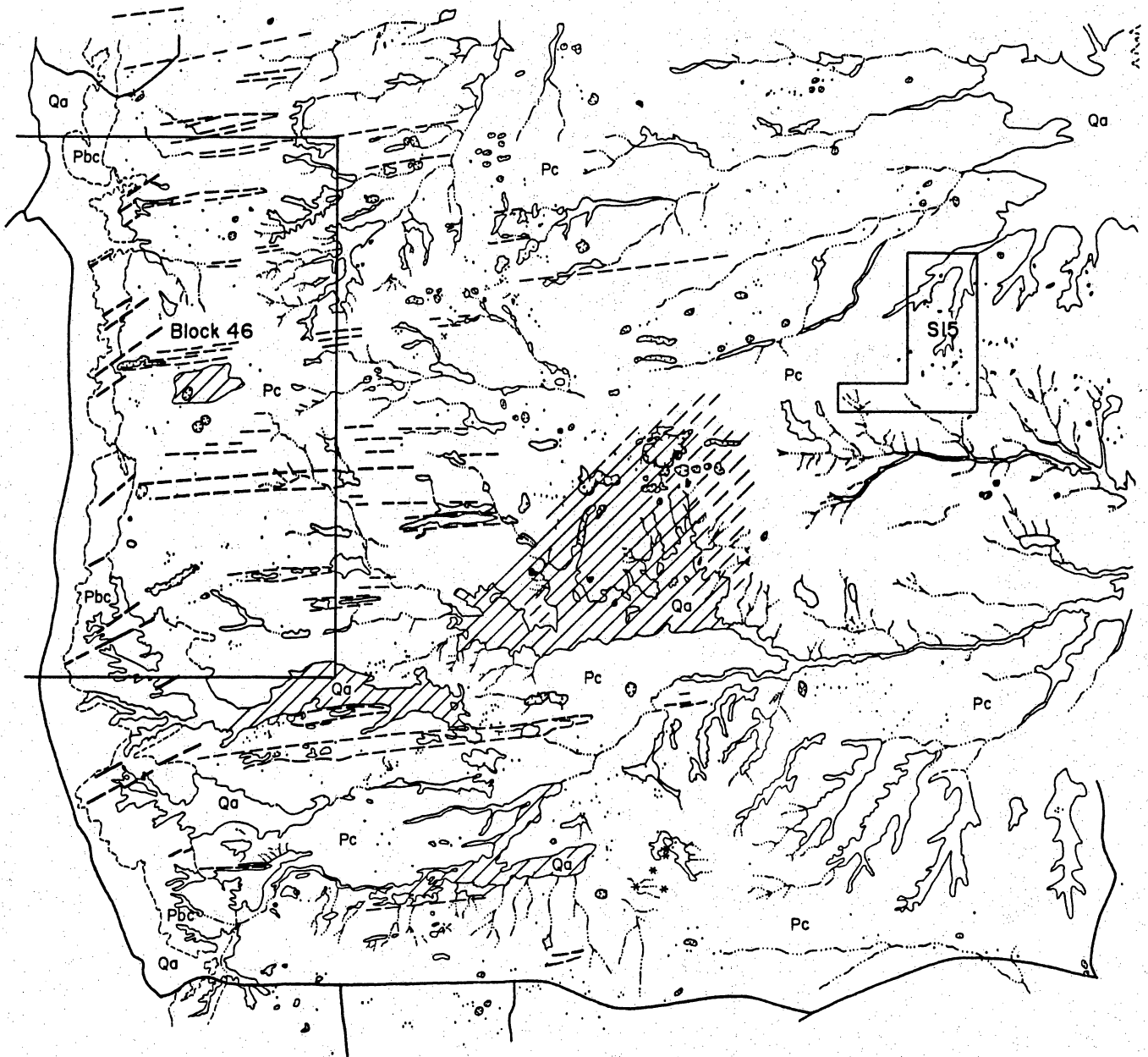
Three Permian-age formations have been mapped by Barnes (1983) throughout the area of Culberson County investigated for this study (fig. 1). These units are, from youngest to oldest, the Rustler, Castile, and Bell Canyon Formations (fig. 1). The Rustler Formation consists of limestone, siltstone, sandstone, gypsum, and clay as much as 140 ft (45 m) thick (Barnes, 1983). The Castile Formation (Anderson and others, 1972) consists of gypsum, anhydrite, and limestone as much as 2,000 ft (610 m) thick; halite (salt) occurs in the subsurface (eastward) but does not crop out. Limestone lenses occur within the bedded gypsum of the Castile Formation. At the surface these resistant limestone bodies resemble castlelike hills and are termed castiles (Adams, 1944; Motsch, 1951). Salado Formation strata may crop out between

the Castile and Rustler Formations. Barnes (1983) did not differentiate the upper Castile and Salado Formations, probably because of their similar lithologies and poor exposures. The Bell Canyon Formation is 700 to 1,000 ft (215 to 305 m) thick and consists of fine-grained sandstone and interbedded thin limestone lenses. The formations dip 1° to 2° toward the east. The three formations have distinctive physical and weathering properties such that the outcrop areas are physiographically distinct. The Rustler Formation forms irregular low hills (the Rustler Hills) having as much as 330 ft (100 m) of relief. The nonresistant evaporite beds of the Castile Formation form a gently rolling topography called the Gypsum Plain. More resistant beds in the Bell Canyon Formation form hills of greater relief in the eastern part of the Delaware Mountains.

Karst Topography of the Gypsum Plain

Karst landforms and landforms possibly indicative of ancient karst processes are common throughout both of the potential low-level radioactive waste sites in Culberson County. These features include, from smallest to largest, karren, swallow holes, collapse sinks, dolines, blind valleys, and subsidence basins (fig. 4). Castiles are landforms that are not true karst features but that perhaps result in part from karst processes. Troughlike features in the western part of the study area also have been attributed to solution and subsidence (Olive, 1957). Karst landforms are discussed in detail in appendix 5.

Widespread distribution of karst landforms and related features in Culberson County is strong evidence that the study area, including both potential repository



EXPLANATION

<p>Quaternary</p> <p>Qa Alluvium</p> <p>Permian</p> <p>Pa Castile Formation</p> <p>Pbc Bell Canyon Formation</p>	<p>--- Fault</p> <p>- - - Ridge</p> <p>(small) (large) Sinkhole</p> <p>* (small) (large) Castles and hills</p> <p>////// Subsidence basin</p>	<p>Study site</p> <p>0 1 2 mi</p>	<p>N</p>
---	---	-----------------------------------	----------

Figure 4. Geomorphologic map of Culberson County study region. See figure 1 for location of figure 4.

sites, is underlain by a cavern system or systems. The karst drainage system underlying the proposed Culberson County sites is difficult to characterize; for example, the cavern system extends to the surface, but the depth of cavern development is unknown. Although the general direction of ground-water movement can be determined from potentiometric head maps, the actual paths and velocities of ground-water movement through cavern systems have not been determined. Furthermore, because the distribution of caverns is unknown, the potential for new sinkholes or other subsidence features developing anywhere in the study area cannot be determined, nor can the potential location of these features be predicted.

Parallelism between cavern segments and joints is common in areas of karst drainage. Field and aerial photographic evidence suggests that surface drainage in the study area is influenced by joint systems. The presence of joints and several groups of sinkholes, castles, and subsidence basins that parallel northeasterly striking joints and faults suggests that subsurface drainage also has been influenced by joint systems.

Geology of Site S-15

Site S-15 is an area of about 3 mi² (5 km²) (fig. 5, pl. 1). The topography is rolling and includes several small hills with 35 to 65 ft (10 to 20 m) of relief that project above the surface of the Gypsum Plain. The hills contain outcrops and surface rubble of a massive to platy dolomite and a siliceous sandstone and conglomerate. Cobbles in the conglomerate consist of chert, quartzite, and siliceous volcanic clasts. A lithologically similar conglomerate, which contains fossils probably reworked from Cretaceous marine

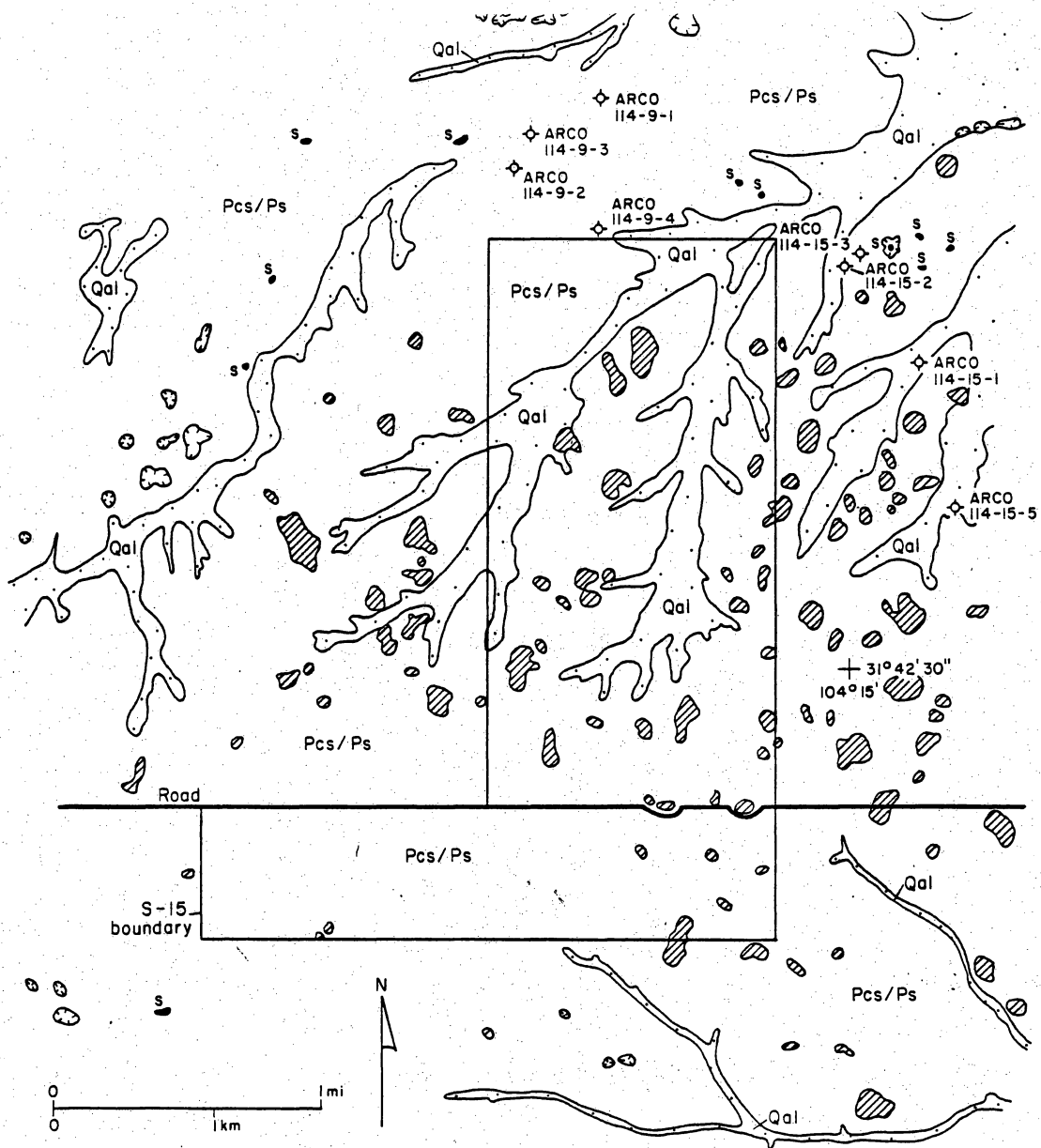
sedimentary rocks, occurs on hills about 6 mi (10 km) southwest of S-15 near Virginia Draw.

Outcrops are rare on the hills at S-15, but the sandstone tends to occur as steeply inclined blocks that appear to dip toward the core of the hills. The dolomite, sandstone, and conglomerates are interpreted to be collapsed remnants of overlying units that fill relict sinkholes in the Castile Formation. The dolomite is interpreted to be from either the Salado or the Rustler Formation, and the sandstones and conglomerates are probably post-Cretaceous in age. A clay-rich soil that may be a residue from solution of more soluble units is locally present on the hills.

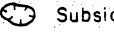
Strata at the S-15 site are generally poorly exposed. Sediments from either the upper section of the Castile Formation or the Salado Formation crop out around the hills (fig. 5, pl. 1). Near-surface gypsum exposures have decomposed to gypsite, although some bedded gypsum is also exposed. Driller's logs of several sulfur exploration wells near the site suggest that 20 to 60 ft (6 to 18 m) of interlayered clay, sand, and gypsum may overlie thicker sequences of gypsum. Although no recently formed karst landforms are present in S-15, they do occur in the immediate vicinity of the site. Relict sinkhole fillings in the hills of S-15, coupled with nearby karst landforms of more recent origin, imply that a system of subsurface solution channels may be present near or within the study area. Some of the intense deformation in the Rustler Formation, 2.5 mi (4 km) east of S-15, was probably caused by evaporite dissolution and subsidence.

Geology of Block 46

The Permian Bell Canyon and Castile Formations crop out in Block 46 (fig. 1, pl. 2). The contact between the formations runs roughly north-south



EXPLANATION

- | | |
|--|--|
|  Quaternary alluvium |  Sinkhole |
|  Hills composed of Permian Salado or Rustler Formation dolomites and/or post-Permian conglomerates and sandstones |  Subsidence depression |
|  Pcs/Ps Permian Castile and/or Salado Formations; predominantly covered, some gypsite and bedded gypsum |  Sulfur exploration test hole |

QA 5956

Figure 5. Geologic map of S-15 study area. Location in Culberson County is shown in figure 1.

through the middle of the block; the Bell Canyon Formation crops out in the western part and the Castile Formation in the eastern part. The Bell Canyon Formation consists of fine-grained sandstones and numerous thin limestone lenses. The Castile Formation consists of a distinctively banded rock composed of alternating layers of calcite and anhydrite. This rock does not commonly crop out; a weathered residuum of gypsum and clay mantles the bedrock to variable depths.

The stratigraphic section at the contact between the two formations was examined in detail to define the contact and to interpret structure. The section is:

Castile Formation	
Massive banded limestone; typical rhythmic Castile bedding but contains little if any anhydrite	
Bell Canyon Formation	
Platy, dark-brown limestone, laminated at a scale of a few mm, petroliferous; forms bench	1.64 ft (0.5 m)
Finely laminated, thin-bedded sandstone, a few 5- to 10-cm-thick beds of sandstone; forms slope	9.84 ft (3 m)
Platy, gray limestone, petroliferous, nonlaminated; forms bench	1.64 to 3.28 ft (0.5 to 1 m)
Finely laminated, thin-bedded sandstone	6.56 ft (2 m)
Massive, crossbedded sandstone	2.62 ft (0.8 m)
Finely laminated, thin-bedded sandstone	6.56 ft (2 m)
Massive, crossbedded sandstone with laminated, thin-bedded sandstone	9.84 ft (3 m)

Structures in Block 46

Significant structures in Block 46 (King, 1949) include a major set of northeast-striking normal faults, a lesser set of north-striking faults, and several prominent joint sets that are in part parallel to the fault trends (pl. 2).

Northeast-striking faults, oriented between N 45 E and N 65 E, are the most prominent structures in Block 46, although they generally have less than 35 ft (10 m) of displacement. On aerial photographs, these faults are easily observable both within the Bell Canyon Formation and where the contact between the Bell Canyon and Castile Formations is displaced. Northeast alignment of sinkholes, castiles, and sulfur deposits in the Castile Formation indicates continuation of these faults at least as far east as the Rustler Hills.

Faults in the Bell Canyon Formation

Northeast-striking faults (N 45-65 E) cutting the Bell Canyon Formation are common throughout Block 46. Several north-striking faults (N 0-10 E) also occur in the western part of the site. Fault traces up to 1.2 mi (2 km) long were observed on aerial photographs and throws up to 25 ft (7 m) were estimated from outcrop exposures. Some of the northeast-striking fault traces exhibit an en echelon pattern, indicating that these faults are part of a 1,300-ft- (400-m-) wide zone that crosses Block 46 and cuts Bell Canyon and older strata at least 5 mi (8 km) to the southwest. Many of the northeast-striking faults that occur at the Bell Canyon-Castile contact appear to die out southwestward; however, they project into zones of closely spaced joints. The fault traces are usually poorly exposed in outcrop. Where strata are exposed, closely spaced joints striking parallel to the fault traces are abundant. A few small-scale normal faults dipping between 65° and 90° also were identified along the major fault traces, suggesting that the major faults are high-angle normal faults.

Fault planes were observed at two locations: near hill 4144 at the eastern edge of the Chico Draw East Quadrangle and west of hill 4295 just east of the main road on the Seven L Peak Quadrangle. Near hill 4144, two small faults (N 61 E, 68 SE, ~3 ft [\sim 1 m] of displacement; N 52 E, 76 SE, ~1 ft [\sim 30 cm] of displacement) occur in massive sandstones. Observed displacement of beds and slickensides on the fault planes indicates normal displacement down to the southeast. These small faults parallel a prominent topographic escarpment immediately to the north, which probably marks a fault of greater displacement.

West of hill 4295, a fault striking N 57 E and dipping 68 NW displaces massive and laminated sandstones in the upper part of the Bell Canyon Formation just below its contact with the Castile Formation. Displacement of beds and slickensides in the fault plane shows that displacement is normal down to the northwest. Total displacement is approximately 10 ft (3 m). The northeastward continuation of the fault toward the contact with the Castile Formation is poorly exposed. However, the fault is adjacent to one of the northeast-striking fault/flexure grabens that occur along the contact, as described below.

Fault/Flexure Grabens at the Bell Canyon - Castile Contact

At least seven fault/flexure grabens occur along the Bell Canyon - Castile contact within or immediately adjacent to Block 46. These structures are the continuation of northeast-striking faults from the Bell Canyon Formation; however, their style of displacement is considerably more complex than the simple normal motion observed in the Bell Canyon. All are marked by linear topographic depressions resulting from erosion of the Castile Formation within the graben. The margins consist of the resistant banded carbonate rock that is

considered to be the lowest part of the Castile Formation.

Structures at the margins of the grabens are faults, flexures, or both. Actual fault displacement at the margins is indicated by apparent abrupt termination of some rock units but is difficult to demonstrate due to poor exposure. Exposed flexures consist of the banded carbonate rock that forms resistant northeast-trending ridges. The beds generally dip into the graben as much as 65° . Several flexures appear to be monoclines having no fault displacement. Some flexures are asymmetric anticlines; beds dip gently away from the grabens on the outer limb and more steeply into the graben on the interior limb. The floors of the grabens are commonly slightly asymmetric, the structurally lowest part being near one margin. Beds on the higher side dip gently toward the structurally lower side.

Total displacement across these grabens includes both the displacement from the structural margin into the graben and the displacement across the faulted margin. Displacement in the grabens ranges from as much as 100 ft (30 m) on one of the structures at the south end of the Seven L Peak Quadrangle south of Block 46, to about 10 to 15 ft (3 to 5 m) on structures within Block 46. Net displacement across the grabens is small and cannot be determined precisely; displacement is apparently almost canceled by nearly equal but opposite senses of motion on the paired graben faults. This net displacement may be comparable to that shown by the faults in the Bell Canyon Formation. Although dominant motion appears to be normal, microfaults, shear zones, and tension gashes in the banded carbonate at the base of the Castile Formation indicate at least some component of right-lateral strike-slip motion.

A similar grabenlike structure, discussed below, has been mapped in the subsurface about 9 mi (15 km) to the east, where it localizes sulfur mineralization at the Phillips Ranch deposit. Several small sulfur prospects occur along the structures in Block 46; all were in the laminated sandstone between the two petroliferous limestones at the top of the Bell Canyon Formation.

Graben origin is unclear, although the grabens are clearly continuations of the northeast-striking faults. Restriction of the grabens to the basal Castile Formation indicates that their complex geometry is a result of the contrast in mechanical properties of the Bell Canyon and Castile Formations.

Northeast-striking Faults in the Castile Formation

Continuations of northeast-striking faults and the fault/flexure structures into the Castile are indicated by photolineations and alignment of castiles and sinkholes. Most notably, several castiles, including Cave Well Peak, and several large sinkholes occur along a photolineation that extends from the northern limb of a prominent graben near the southern boundary of Block 46 (fig. 3). Two castiles north of High Lonesome Well lie on the continuations of each limb of a graben.

Northeast-striking Faults in the Rustler Hills

Test drilling for sulfur has delineated several northeast-striking faults in the vicinity of the Rustler Hills (Smith, 1980). These faults trend about N 65 E and have 25 to 80 ft (8 to 25 m) of displacement. They commonly localize sulfur deposits, including the major Culberson Mine and Phillips Ranch deposits. Smith's (1980) isopach and structure-contour maps depict these faults.

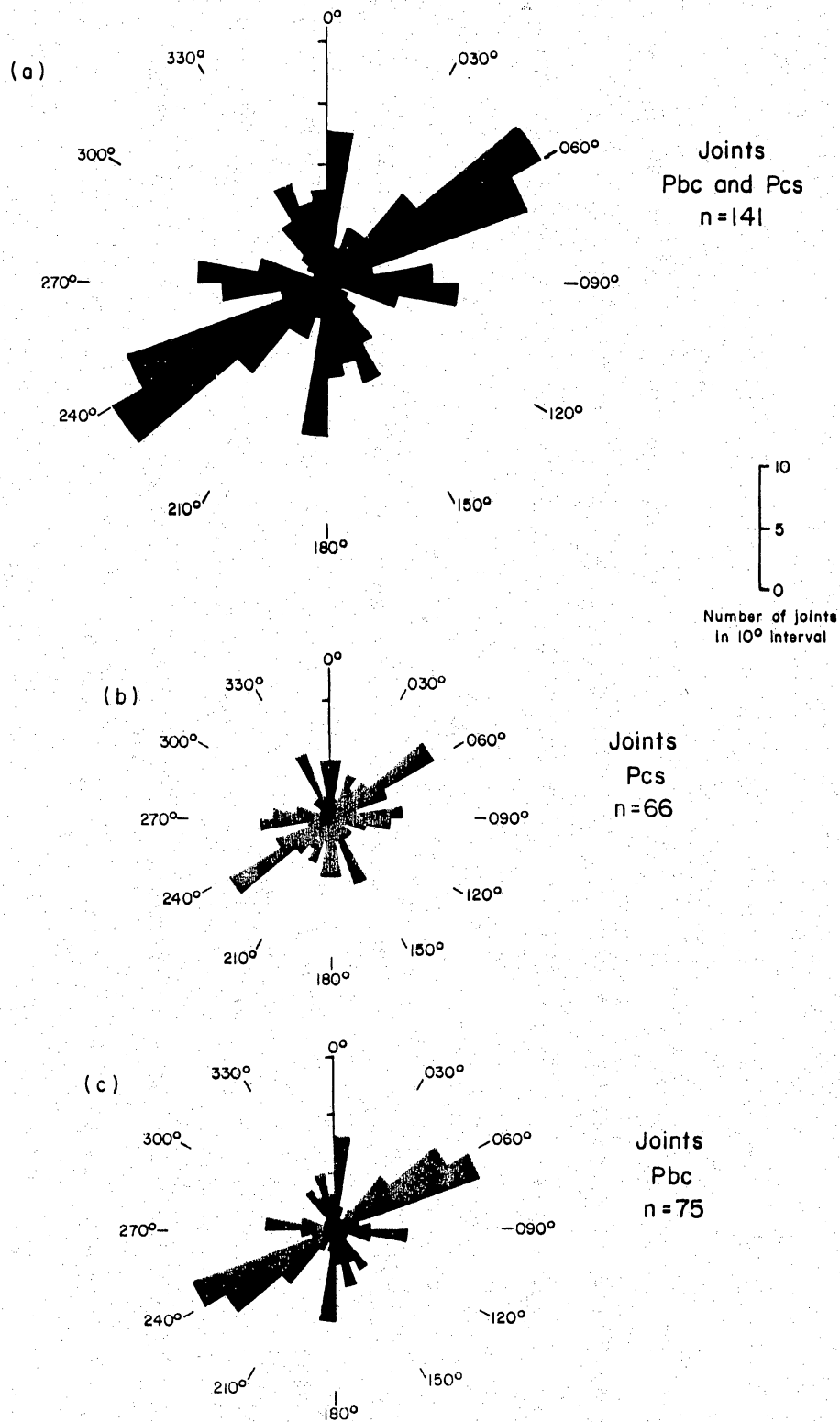
The Phillips Ranch deposit occurs at the base of the Castile Formation in a narrow graben about 985 ft (300 m) wide and 1.2 mi (2 km) long. The structure-contour map of the deposit (Smith, 1980, his fig. 5) shows a feature remarkably similar to the fault/flexure grabens we mapped at the same contact.

Timing of Northeast-striking Faults

The time of displacement along the northeast-striking faults is poorly constrained by available data. The northeast-striking faults are most likely related to Basin and Range extension, which began about 24 mya but occurred in two different episodes of different stress orientations. East-northeast-oriented extension during the earlier episode produced the characteristic northwest-striking faults that dominate the Basin and Range province of Trans-Pecos Texas. During the younger episode, possibly from 15 or 10 mya to the present, extension was oriented northwest, which would have produced northeast-striking faults. The northeast strikes of the faults and of the slickensides within them indicate northwest extension and suggest that the faults formed during the younger episode of late Basin and Range extension.

Joints

Four joint sets occur in Bell Canyon and Castile strata. Orthogonal sets are comprised of joints striking N 40-70 E and N 20-30 W, and joints striking N 80-100 E and N 10 W to N 10 E. Northeast-striking joints (N 40-70 E) are the most common (fig. 6, pl. 2). Zones of closely spaced joints exist throughout the area for all four joint sets; however, most of the zones strike northeast (N 40-70 E). Some of the closely spaced joint zones are related to the fault traces that cross the area. Joint zones may be as wide as 130 ft (40 m), and the joint spacing within the joint zones is as great as 12 joints/6 ft (2 m) in beds that are



QA 6068

Figure 6. Rose diagram plots of joints in Block 46 strata of (a) Bell Canyon (Pbc) and Castile (Pcs) Formations, (b) Castile Formation (Pcs), and (c) Bell Canyon Formation (Pbc). n= number of joint measurements.

5 to 6 ft (1.5 to 2 m) thick. Dissolution and erosion along joints have developed caverns in the gypsum strata of the Castile Formation. Joints also locally control the direction of surface drainage in Bell Canyon and Castile strata.

Sulfur Mining in the Rustler Hills Region

The Rustler Hills region of Culberson County contains substantial sulfur deposits that have been mined at two locations by means of the Frasch process. Future sulfur mining near Site S-15 could alter the geology of the site because the Frasch process involves injecting hot water, melting the sulfur, and pumping the liquid sulfur to land surface. Land subsidence results from the sulfur extraction.

The Pennzoil Sulphur Company Culberson Mine (formerly Duval Sulphur Mine), located 6.5 mi (10.5 km) east of Site S-15 and 39 mi (63 km) west of Pecos, Texas, on FM 2119, is the only operating Frasch sulfur mine in West Texas. Production of sulfur began September 30, 1969, and cumulative production is 28,703,157 long tons (LT). Containing estimated recoverable resources of 31,524,000 LT, the Culberson Mine is the largest producing sulfur mine in the Western Hemisphere. Currently, sulfur is being produced from the Permian Salado Formation at depths of approximately 300 to 600 ft (90 to 180 m) below land surface. The total interval of sulfur occurrence in the area ranges from the top of the Permian Bell Canyon Formation to ground surface (fig. 1) (Joseph W. Mussey, Chief Geologist, Pennzoil Sulphur Company Culberson Mine, personal communication, 1986). Production formerly occurred at the Phillips Mine, 1.5 mi (2.4 km) southeast of Site S-15, but the mine is now inactive.

Land-surface subsidence and collapse are common natural features around the Culberson Mine, resulting from the dissolution and removal of Permian-age

evaporites by ground water in the subsurface (Snyder and Gard, 1982). Subsidence at the Culberson Mine, however, is man-induced, resulting from the removal of sulfur by Frasch mining. This type of subsidence is generally a slow, controlled occurrence and is classified as trough subsidence (Obert and Duvall, 1967). As of December 31, 1985, maximum vertical subsidence was 60 ft (18 m). Subsidence is contained within the mine area ($\sim 4 \text{ mi}^2$ [$\sim 10.4 \text{ km}^2$]) and is not expected to affect Site S-15, which is 6.5 mi (10.5 km) away.

Future mining in areas that are closer, if not directly adjacent, to S-15 could result in subsidence at the site. Porsch (1917) identified sulfur deposits throughout the Rustler Hills area as potential or active areas of sulfur mining. Field investigations conducted in the vicinity of Site S-15 found several localities of sulfur at the surface and springs that contain sulfur-bearing water, indicating sulfur mineralization in the subsurface.

Surface Flow

Both sites are dissected by narrow valleys that contain ephemeral streams (figs. 2 and 3). The direction of the surface flow is locally affected by dissolution features. Dissolution arches made of gypsum that represent formerly breached land surface hang above current, lower surface drainage systems.

Close relationships exist between the surface drainage system and ground water at both sites. The presence of many springs in the draws indicates that the draws serve as a discharge zone for the shallow aquifer. Some ground water discharges into the draws by direct evaporation, which is indicated by large moist areas covered with salt crust (such as Virginia Draw west of Rustler Spring, fig. 2).

Prolonged periods of drought, during which no surface-flow runoff is observed, are common in this area (Olive, 1957).

Hydrologic Setting

Water-bearing Characteristics

The Castile Formation at Site S-15 and Block 46 contains aquifers. Porosity and permeability distributions in these aquifers are dominated by dissolution processes. The limestone and evaporite beds have vugular porosity and in some cases form caverns (Cave Well, Block 46 site). Hollow spaces that underlie a thin crust of soil are common at both sites, possibly suggesting soil piping. No data on transmissivity and storativity coefficients were available for the study area. Water-level declines so severe that wells run dry after several years' use (Seven L Well, Block 46 site) or even after 1 year of drought (Cave Well, Block 46 site) (K. Moore, University Land Office, personal communication, 1986) indicate that the values of transmissivity and storativity are probably small (also Brown and others, 1973). Aquifer thicknesses at the sites are unknown.

Recharge

Recharge into the Castile aquifers results from direct precipitation on outcrops and from flash floods in permeable riverbed clastics at the washes. Olive (1957) suggests that most of the water that flows through underground channels in the Castile Formation is derived from the underlying Delaware Mountains Group (whose upper formation is the Bell Canyon) and that only a minor amount comes from surface runoff.

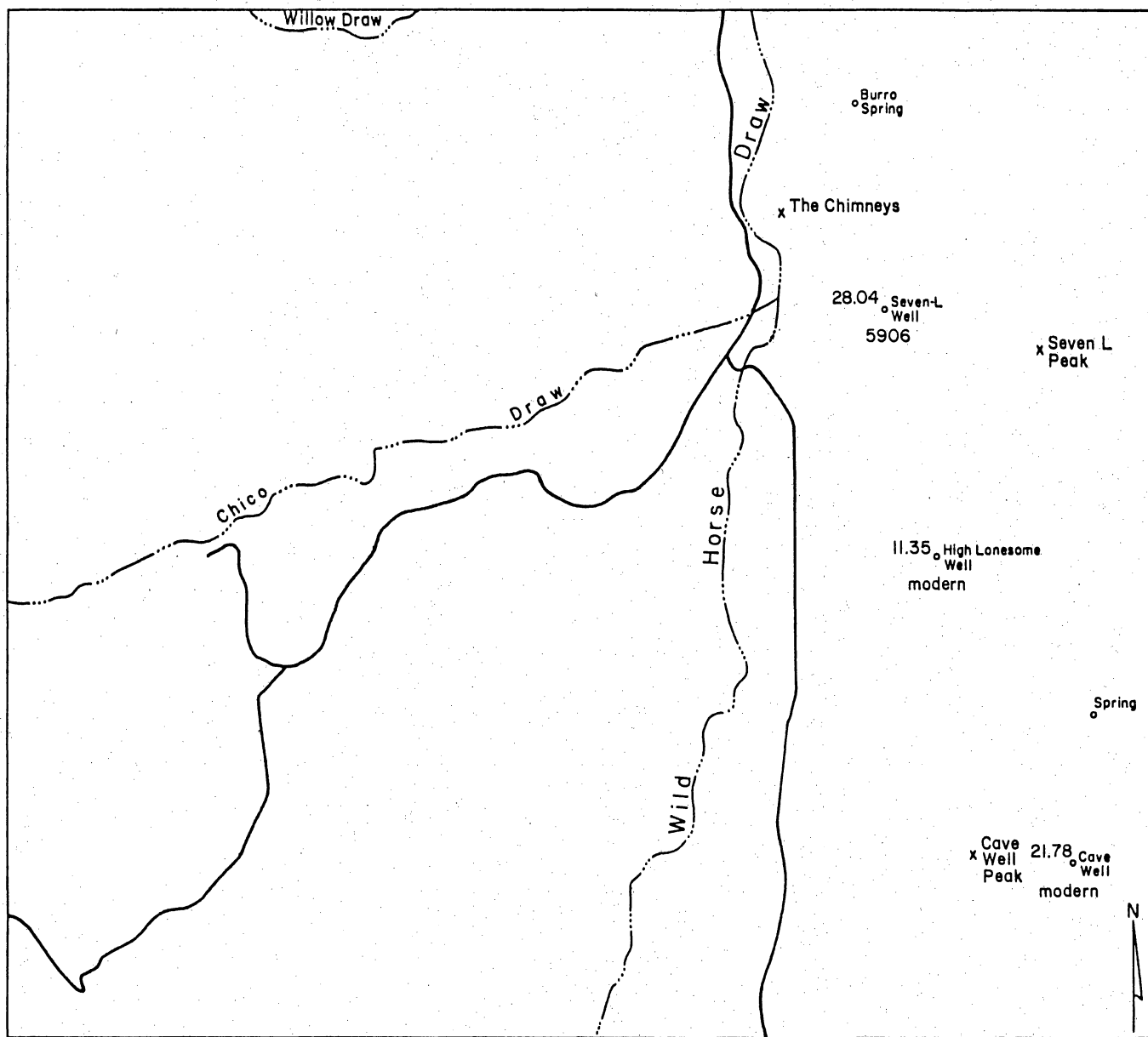
Ground-water samples were collected and analyzed for tritium and ^{14}C . Tritium and ^{14}C are radioactive isotopes used to estimate the age of water. Tritium may be used to qualitatively identify waters less than 40 yr old, and ^{14}C can be used for water less than 30,000 yr old (see app. 4 for method of calculation of ^{14}C ages). Ground-water analyses from both sites show high tritium activities (6.7 to 28 TU) in combination with high to moderate values of ^{14}C (modern to 5,900 yr old) (figs. 7 and 8, app. 2). This observation supports Olive's suggestion of ground water "base flow" coming from the west (fig. 9), parallel to the regional dip (characterized by lower ^{14}C values), that is supplemented by recent recharge sources (with high tritium activities) from local rains and surface water.

Discharge

Many springs occur in the S-15 site and vicinity. Some of them issue directly from the Castile Formation, whereas others discharge from the contact between the Castile Formation and overlying permeable alluvial deposits. Annual discharge of these springs is relatively small and varies from seeps to 111 gpm (7.0 lps) (Brune, 1981). In topographically low areas, discharge may also take place through direct evaporation from an extremely shallow water table, resulting in the formation of gypsum crusts and increased salinity of the ground water (as in Virginia Draw, south of Site S-15, fig. 2). Changes in vegetation types were observed in many of the low areas, which may indicate a shallow water table and discharge via evapotranspiration.

Potentiometric Surface

On the basis of shallow depth to water (from 0 to 150 ft, 0 to 46 m, app. 1) we assume that water in the Castile Formation flows under water-table



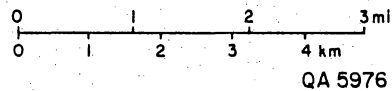
EXPLANATION

28.04
 ○
 5906

 Water sample with 28.04 TU and corrected ¹⁴C age of 5906 years.

x

 modern 100 years old or less (corrected age of ¹⁴C)



QA 5976

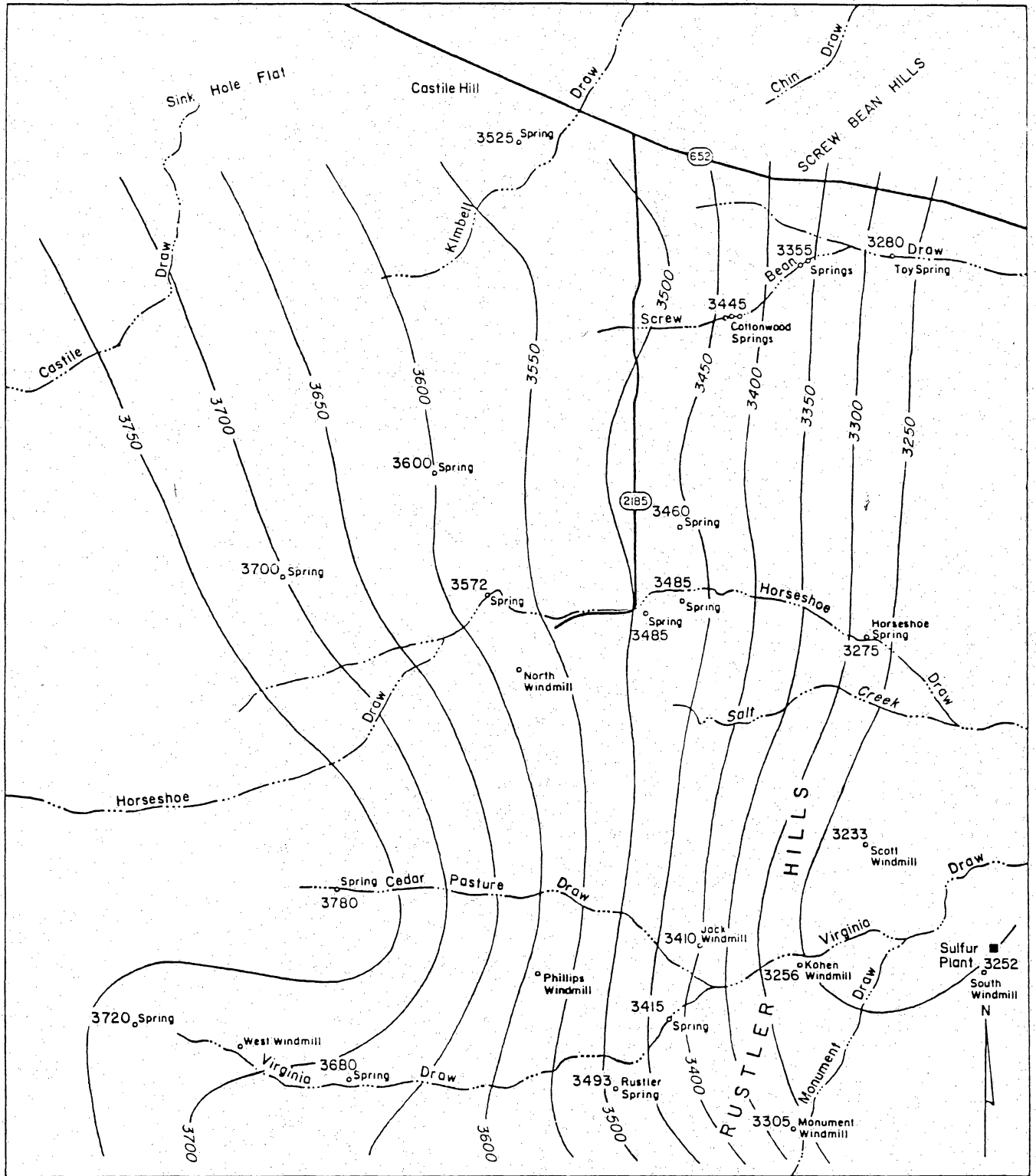
Figure 8. Tritium and ¹⁴C activity distribution in ground water of Block 46 site, Culberson County.

conditions. Water levels (fig. 9) at Site S-15 range from 3,700 to 3,250 ft (1,130 to 990 m). The gradient of water-level surface ranges from 13 to 120 ft/mi (2.5 to 23 m/km). Ground water follows the regional topographic and geologic dip from west to east. Water-level contours were interpolated between all wells and springs, regardless of which aquifers they penetrate, because that information was unavailable. However, the presence of a regional potentiometric surface suggests some interconnectedness between the regional aquifers.

No potentiometric map could be produced for the Block 46 site, owing to scarcity of data. Despite the shallow water table, indicated by the minimal depth to water (20 to 30 ft, 6 to 9 m) in Block 46 wells (app. 1), only two springs could serve as additional control points for a water-table map (fig. 10). Flow is assumed to be under water-table conditions, and water heads range from 4,130 to 4,006 ft (1,260 to 1,221 m). Wells reported to run dry after several years of pumpage (the old abandoned well next to the new Seven-L well) or after a year with little rain (Cave Well) may indicate a poorly developed karstic system with a low degree of interconnectedness. Water having large ranges of tritium (11.35 to 28.04 TU) and ^{14}C (modern to 5,900 yr old) (fig. 8) support this assumption.

Ground-water Geochemistry

All ground-water samples that were collected in Block 46 and in the vicinity of the S-15 site are brackish, total dissolved solids (TDS) ranging between 1,200 and 4,000 ppm (figs. 11 and 12, app. 2). Salinity increases toward the east of the S-15 site with the direction of flow (figs. 9, 11, and 13) and indicates a longer time of interaction with the host rocks. Ground water in the area is of the Ca-SO_4 facies, as expected based on the gypsiferous nature of the host formations. In addition, sulfate correlates well with Na^+ , Mg^{2+} , and TDS (figs. 14 and 15).



QA 5975

Figure 9. Water-level distribution (ft) of Site S-15, Culberson County.

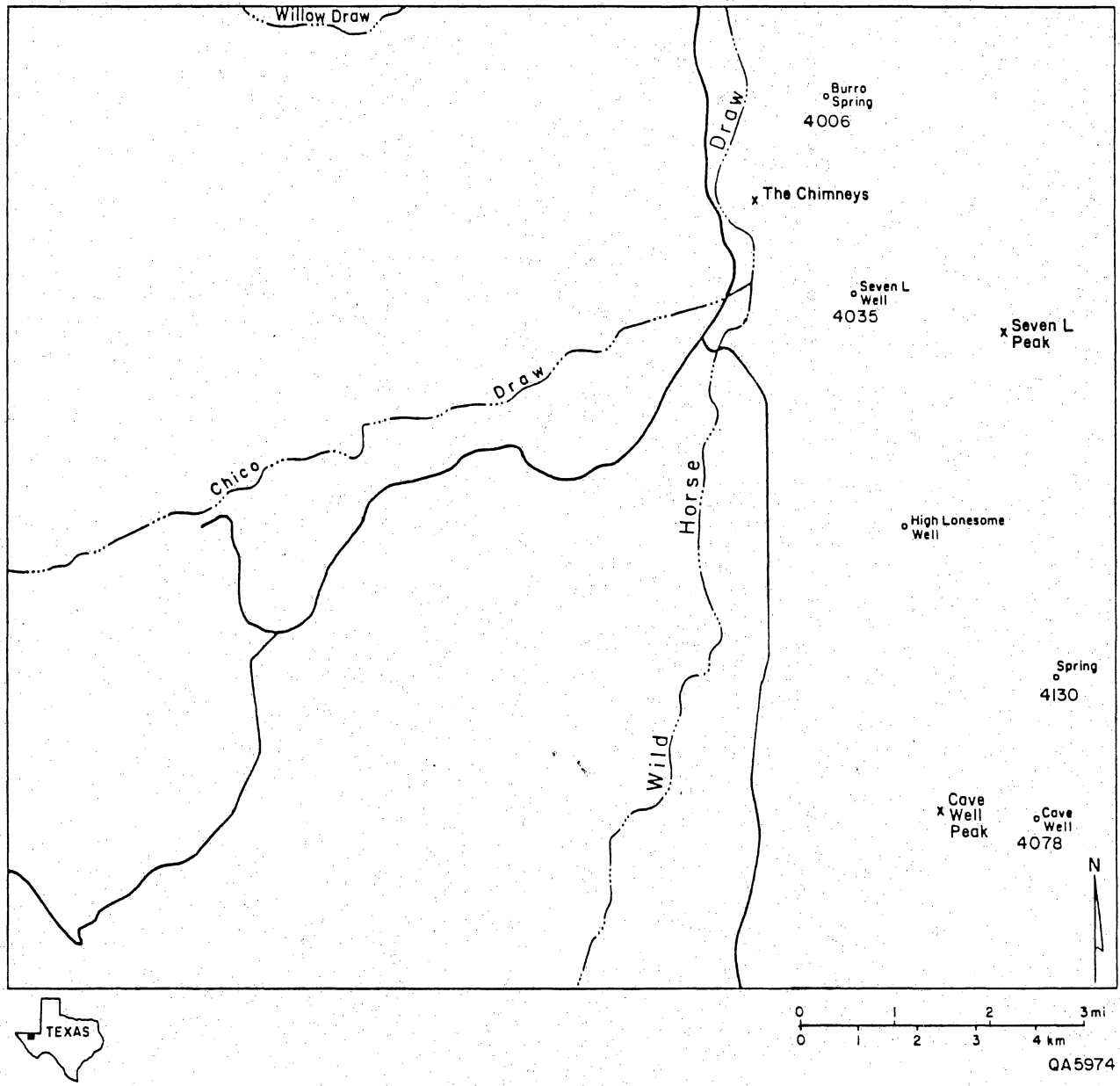
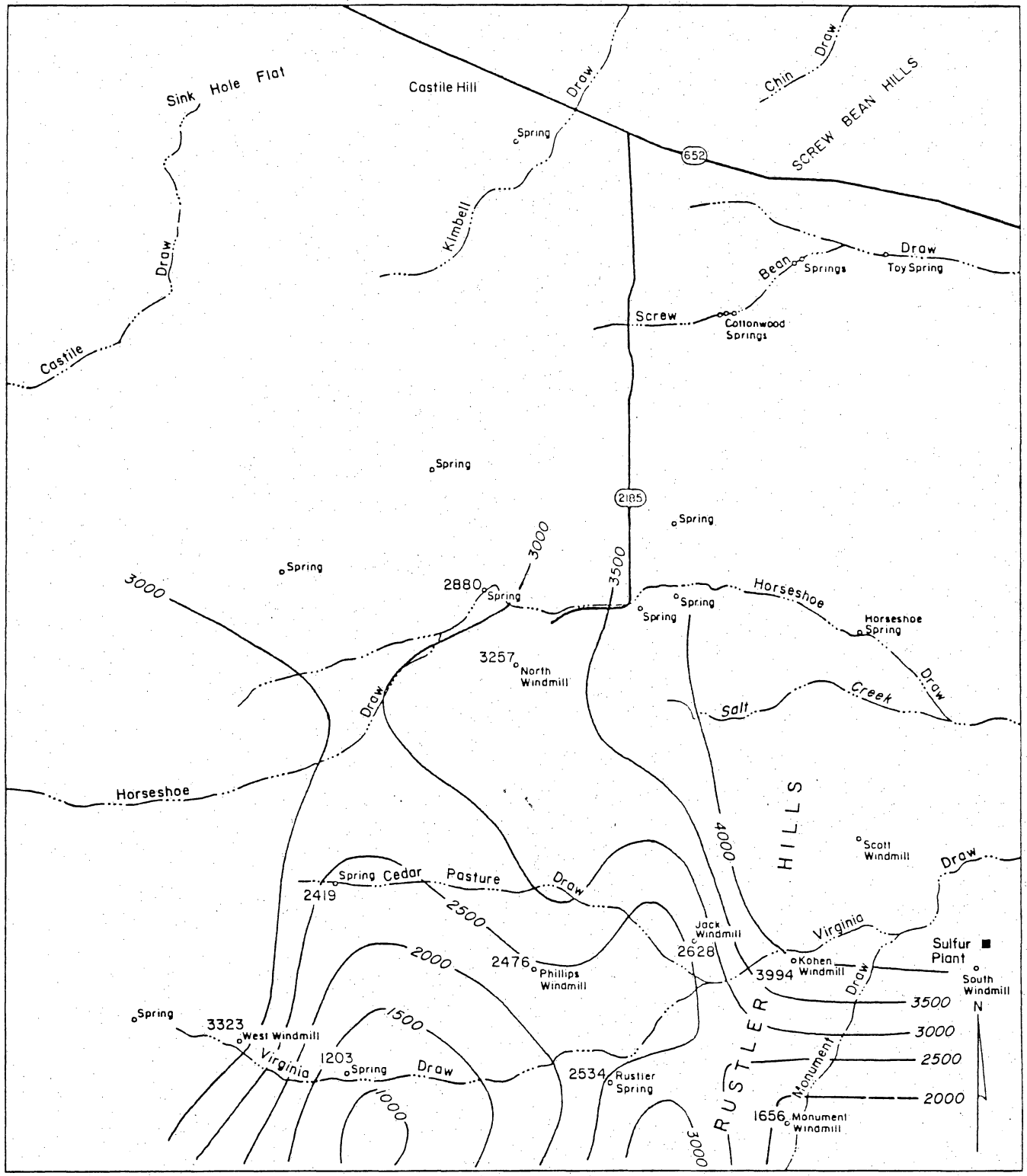


Figure 10. Water-level distribution (ft) of Block 46 site, Culberson County.



QA 5973

Figure 11. Total dissolved solids (TDS) (mg/L) distribution in ground water of Site S-15, Culberson County.

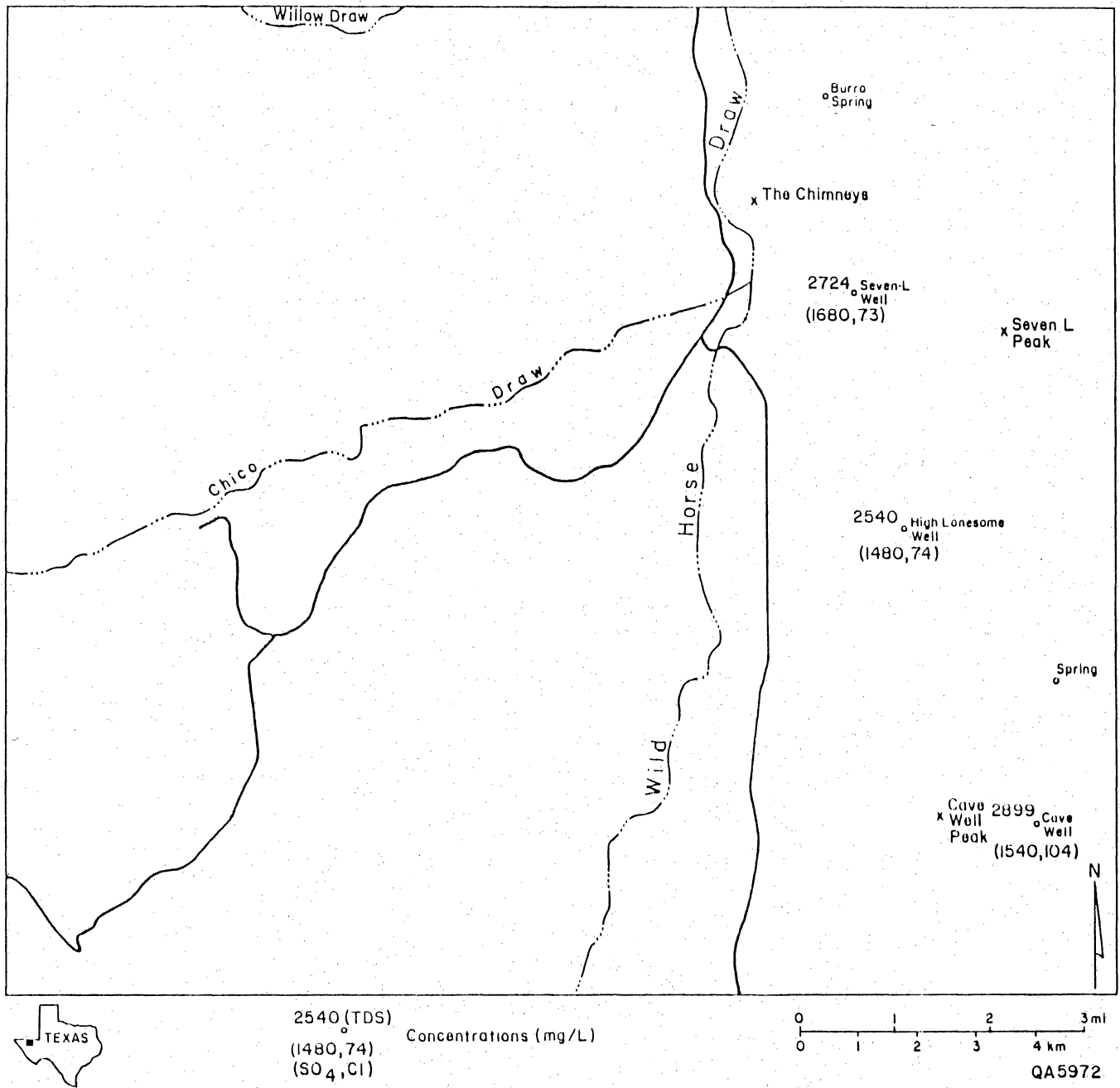
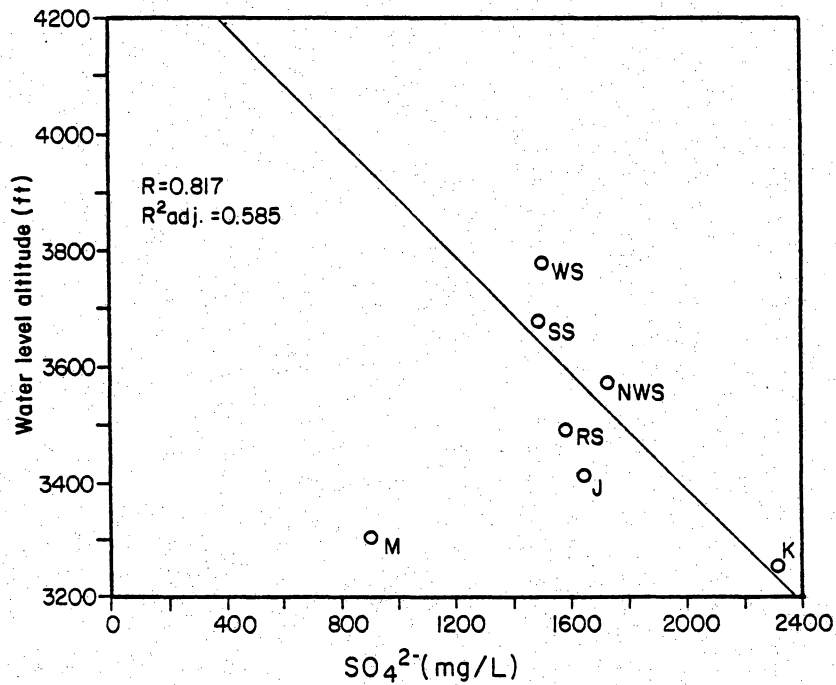


Figure 12. Total dissolved solids (TDS) SO_4^{2-} , and Cl^- (all in mg/L) distribution in ground water of Block 46 site, Culberson County.

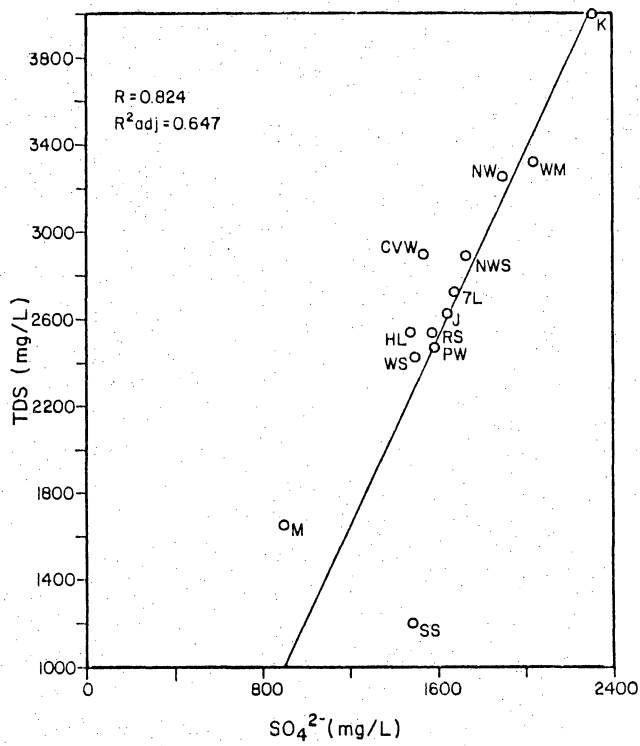


EXPLANATION

J - Smilin Jack Windmill	SS - South Spring
K - Kohen Windmill	WS - West Spring
M - Monument Windmill	NWS - North Windmill Spring
RS - Rustler Spring	

QA 6000

Figure 13. SO_4^{2-} concentration (mg/L) versus altitudes (ft) of ground-water samples in Site S-15, Culberson County. Well locations are shown in figure 11.



EXPLANATION

- | | |
|-----------------------------|-----------------------------|
| J - Smilin Jack Windmill | RS - Rustler Spring |
| K - Kohen Windmill | SS - South Spring |
| M - Monument Windmill | WM - West Windmill |
| 7L - Seven-L Windmill | WS - West Spring |
| HL - High Lonesome Windmill | NWS - North Windmill Spring |
| NW - North Windmill | CVW - Cave Well |
| PW - Phillips Windmill | |

QA 6002

Figure 14. SO_4^{2-} concentration versus TDS concentration in ground water of Culberson County sites. ⁴Well locations are shown in figures 11 and 12.

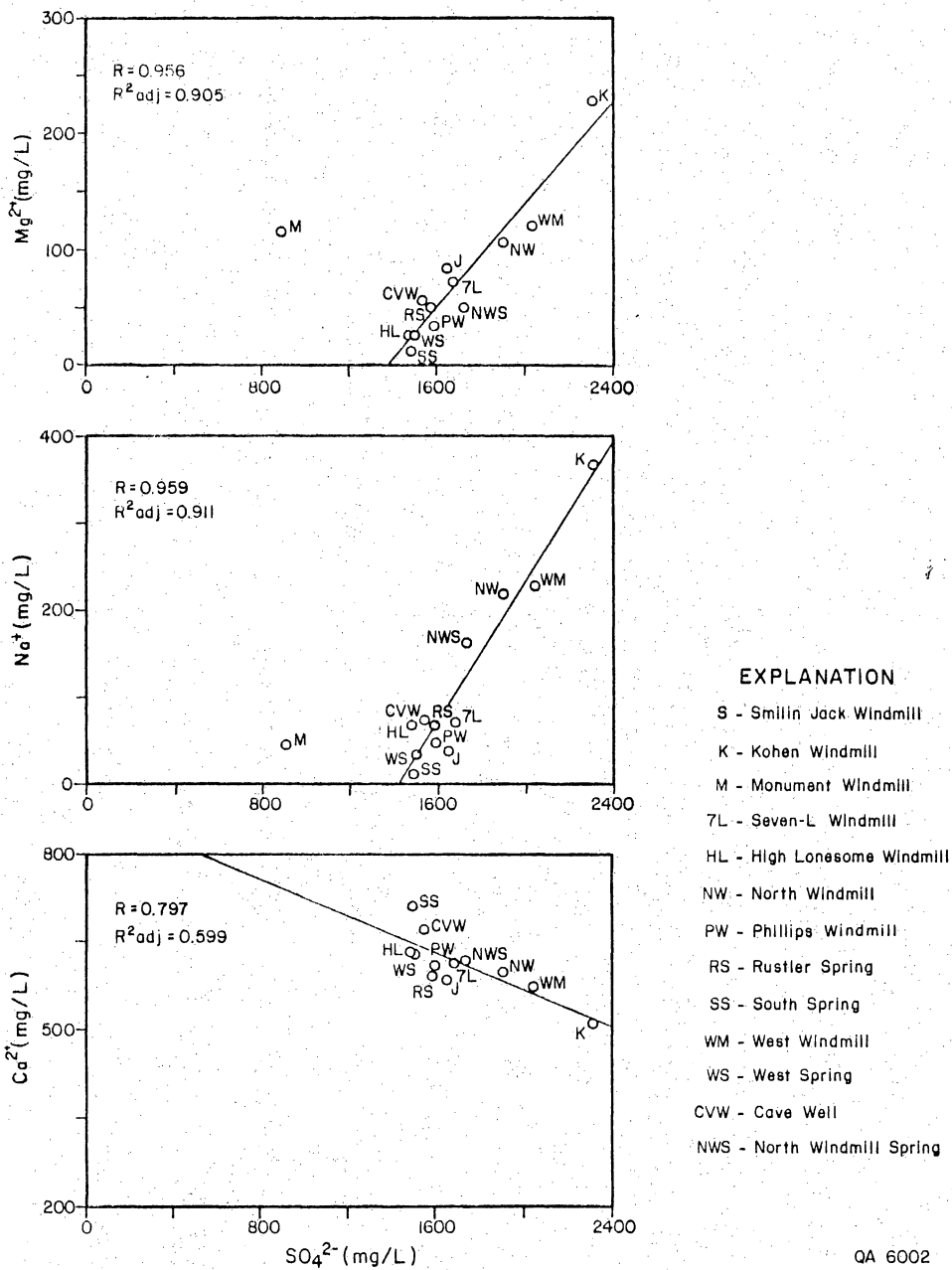


Figure 15. SO_4^{2-} concentration versus Ca^{2+} , and Na^+ and Mg^{2+} concentrations (all in mg/L) in ground water of Culberson County sites. Well locations are shown in figures 11 and 12.

suggesting that other salts are dissolving.

Site S-15 $\delta^{34}\text{S}$ values (figs. 16 and 17) indicate that the dissolved SO_4^{2-} in ground water is from dissolution of the gypsum in the host rock. These $\delta^{34}\text{S}$ values of dissolved sulfate are typical of Permian sulfate minerals (12 ‰) (Hoefs, 1973), as shown by a range of +9.3 to +11.3 ‰. Samples from Monument Windmill and the South Spring near the S-15 site had $\delta^{34}\text{S}$ values of +5.8 and +17 ‰, respectively, which differ from the normal range. In the case of Monument Windmill, the value can be attributed to the dissolution of the native sulfur (which has lighter $\delta^{34}\text{S}$ values than those of SO_4^{2-} in the gypsum because of isotopic fractionation [Hoefs, 1973]) that is mined in the immediate vicinity. The high values of $\delta^{34}\text{S}$ in South Spring may be attributed to local bacterial reduction of the Permian sulfate, which results in higher $\delta^{34}\text{S}$ values in the gypsum host rocks.

Some of the ground water at both sites has been recharged recently (indicated by tritium values ranging from 6.3 to 28 TU) and mixed with an older component of ground-water flow (indicated by ^{14}C ages of up to 5,900 yr). Alternatively, the apparent old ^{14}C ages of some of the water samples may result from calcite precipitation, as suggested by the negative correlation between Ca^{2+} and SO_4^{2-} (fig. 15) in ground water at these sites. Solution of gypsum causes increased concentrations of Ca^{2+} and SO_4^{2-} and the subsequent precipitation of less soluble calcite that contains ^{14}C . The residual ground water becomes depleted in ^{14}C and therefore appears older than it really is. Thus, no older component of ground water may exist, and all the ground water may be young, as suggested by the tritium activities. Variations occur in tritium and ^{14}C activities over short distances (as at High Lonesome Well and Cave Well, Block 46 site) that are typical of karstic systems and that probably reflect hydraulic discontinuity and independent

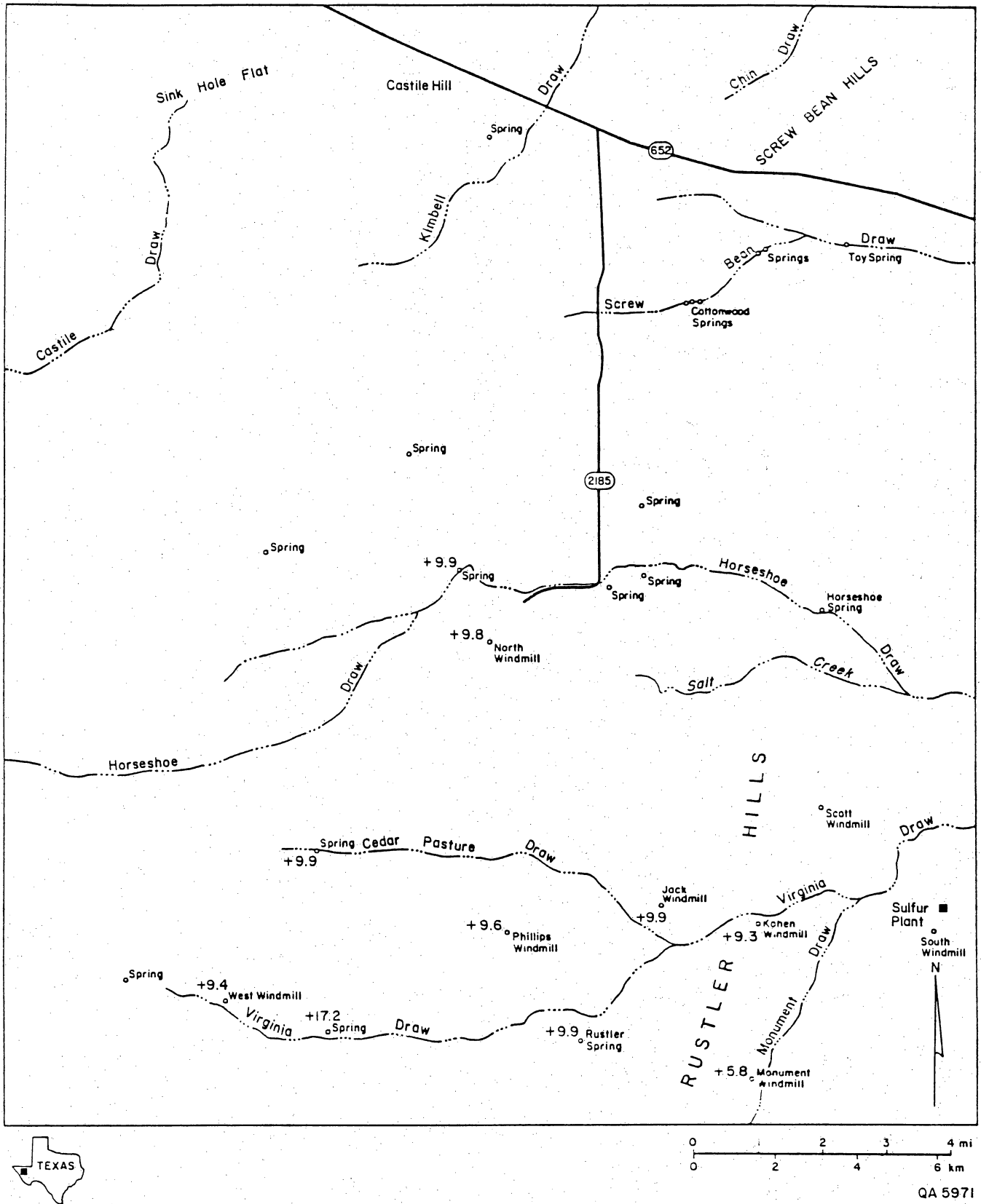


Figure 16. $\delta^{34}\text{S}$ distribution in ground-water samples of Site S-15, Culberson County (in ‰ deviation from the Canyon Diablo Troilite).

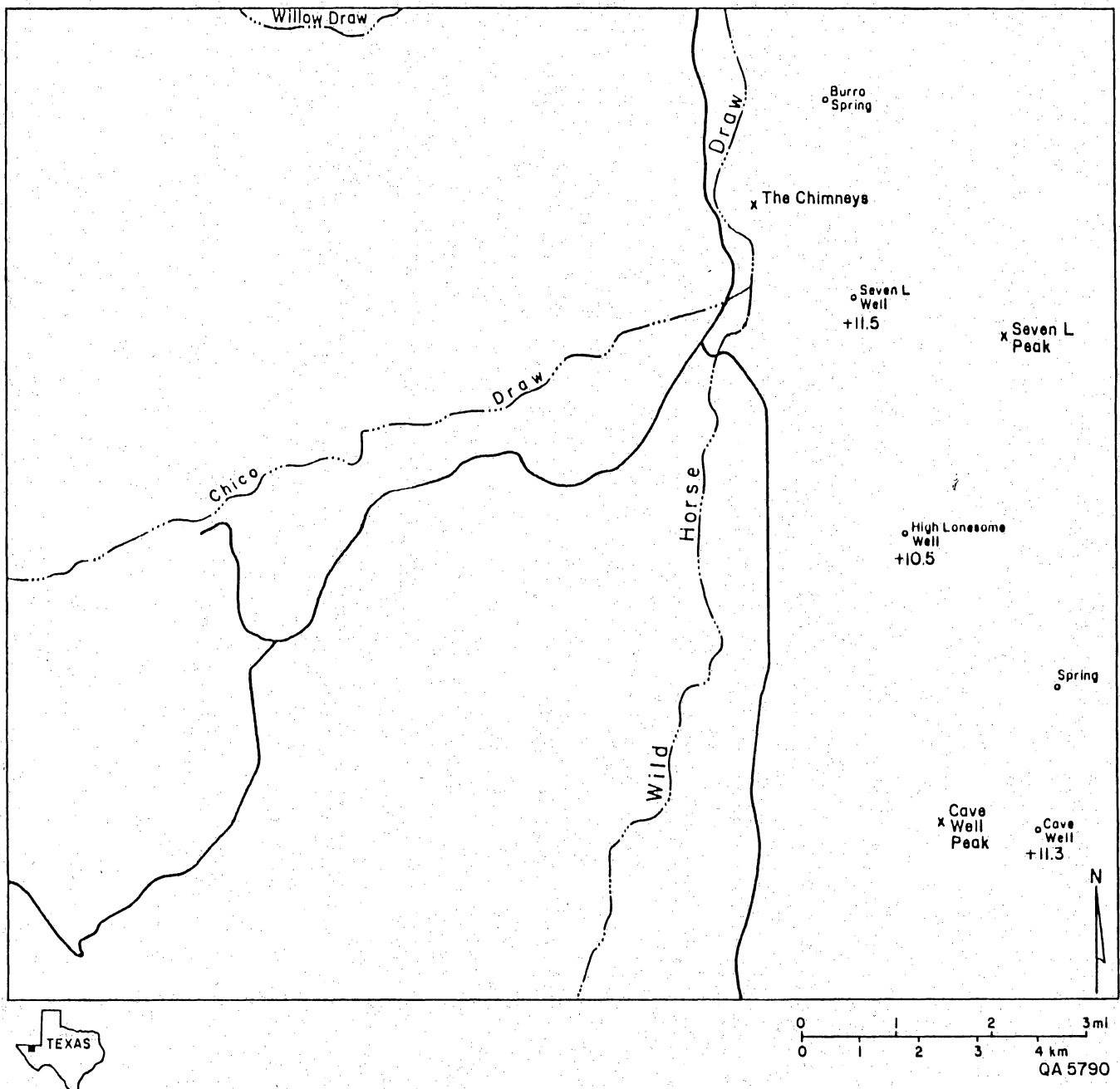


Figure 17. $\delta^{34}\text{S}$ distribution in ground-water samples of Block 46, Culberson County (in ‰ deviation from the Canyon Diablo Troilite).

recharge pathways. However, some degree of connectedness in the S-15 site is indicated by the good correlation between decreasing tritium activities and lower water-level altitudes (fig. 18). As shown in figure 18, water that flows into the site from the west at higher water-level elevations has higher tritium activities and perhaps a shorter residence time in the aquifer. Local $\delta^{18}\text{O}$ and $\delta^2\text{H}$ values indicate recharge from current precipitation (figs. 19 through 21). Their narrow range (-7.4 to -6.1 ‰ for $\delta^{18}\text{O}$ and -56 to -40 ‰ for $\delta^2\text{H}$) does not support the concept of ground-water base flow coming from higher elevations in the west; perhaps it indicates a well-mixed ground water system.

Chemical and isotopic characteristics of the water at both Culberson County sites reflect fast-moving flow systems (high tritium and ^{14}C activities) in karstic channels and other dissolution features, and with a high degree of interaction with the evaporitic host rocks (high values of TDS, SO_4^{2-} , and $\delta^{34}\text{S}$).

RUSTLER HILLS, CULBERSON COUNTY--CONCLUSIONS

Geologic investigations in the Culberson County area produced the following preliminary conclusions applicable to evaluation of Site S-15 and Block 46 as potential sites for a low-level radioactive waste repository. The part of Culberson County that is underlain by the Castile Formation includes all of S-15 and the eastern portion of Block 46, areas repeatedly subjected to dissolution and collapse. These processes have resulted both in modern, sharply defined geomorphic features and in paleofeatures having relatively subtle expression. The density of these features suggests that the area is underlain by a complex system of dissolution channels whose geometry and precise distribution cannot be precisely described.

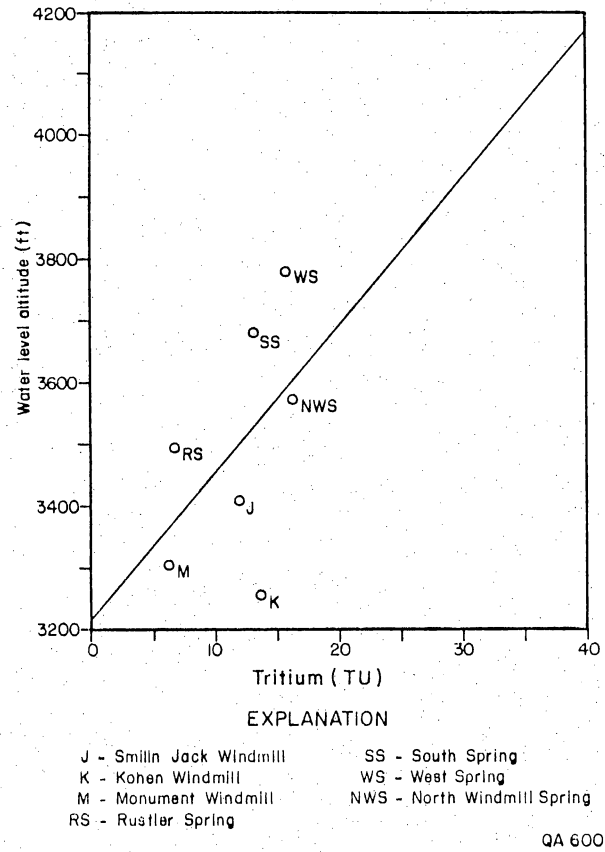
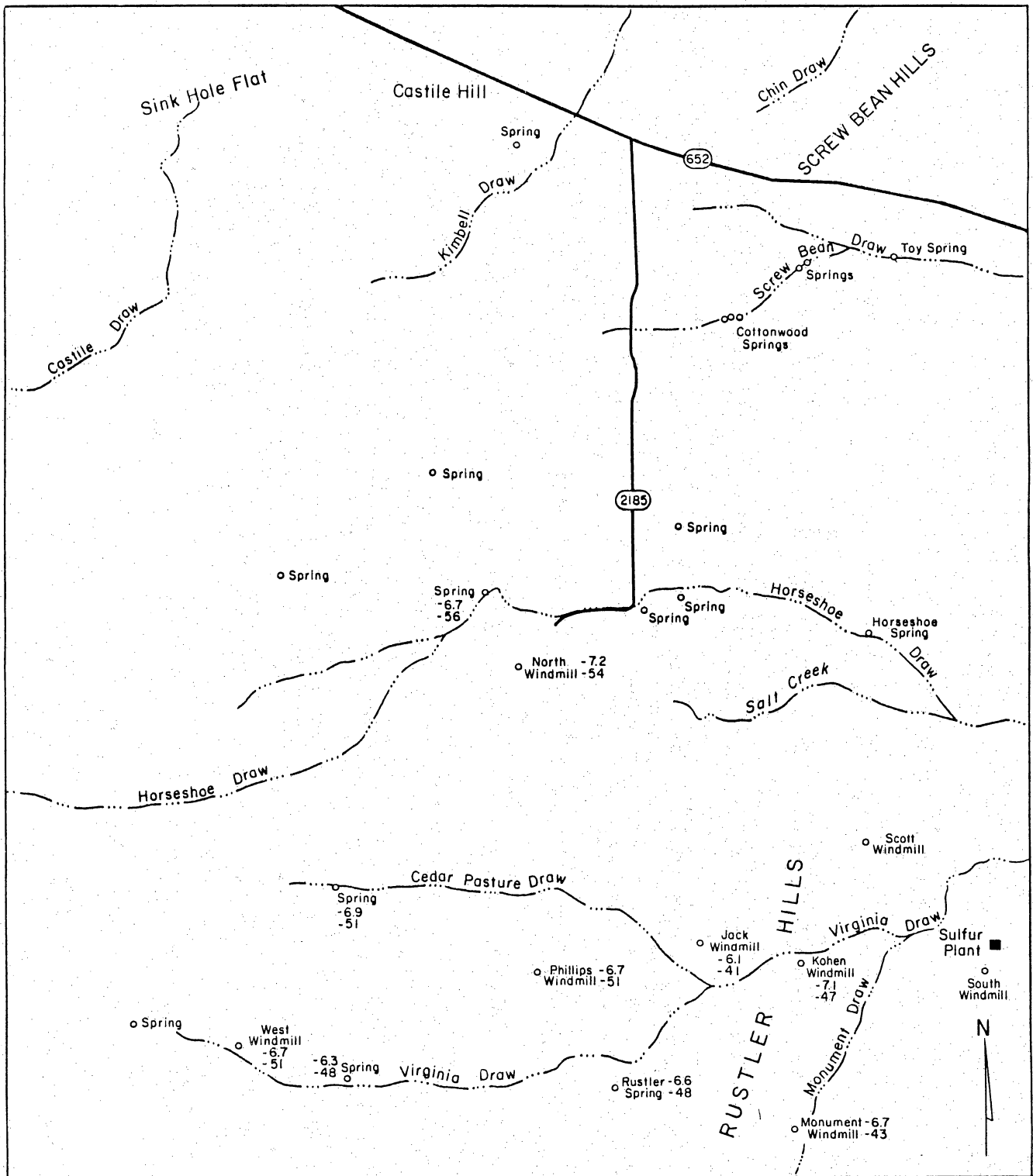
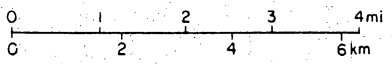


Figure 18. Tritium activity (TU) versus altitude (ft) of ground-water samples from Site S-15, Culberson County. Well location is shown in figure 7.

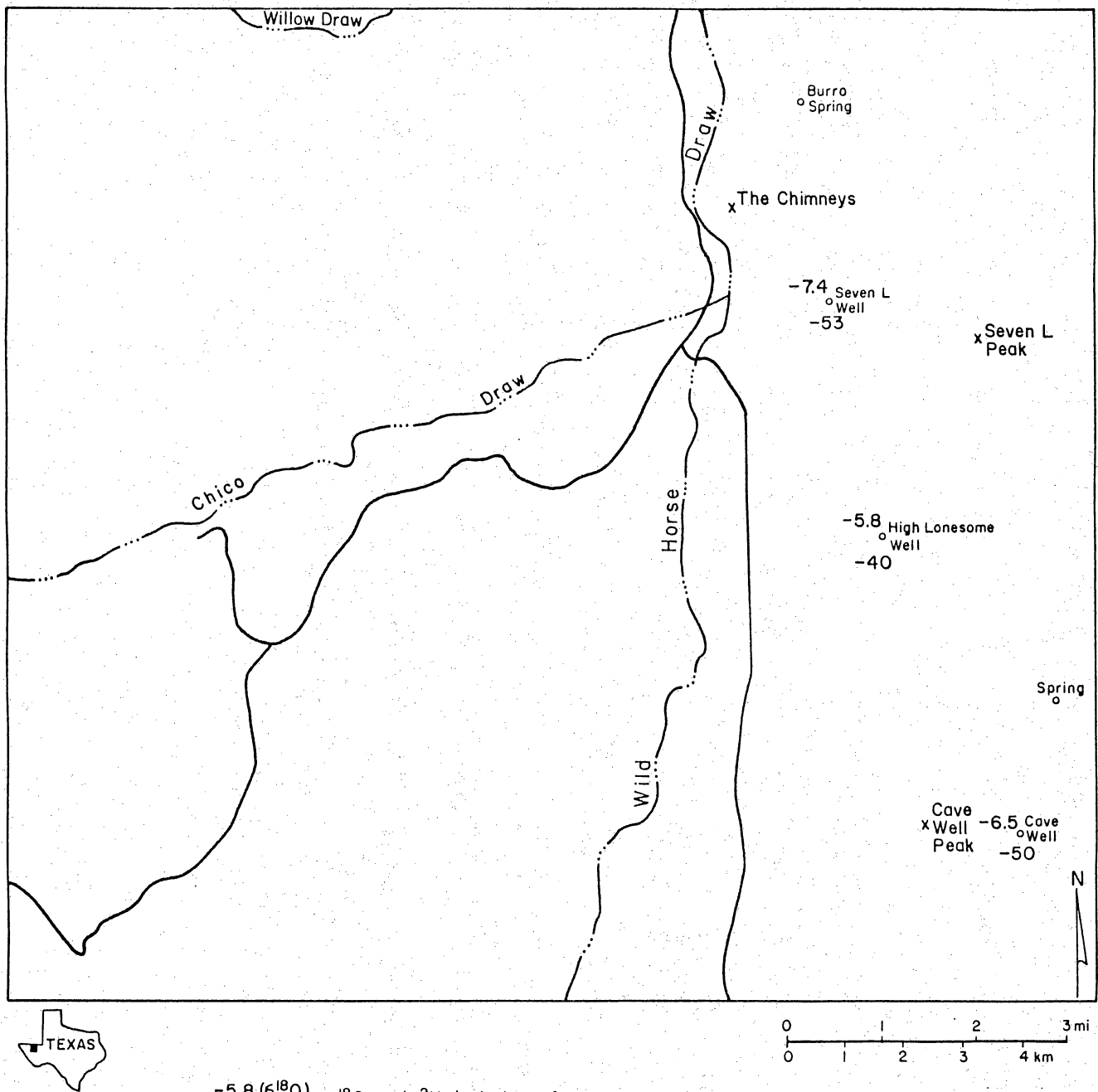


○ -5.1 ($\delta^{18}\text{O}$) ^{18}O and ^2H deviations from
 ○ -56 (SD) SMOW in water sample (‰)



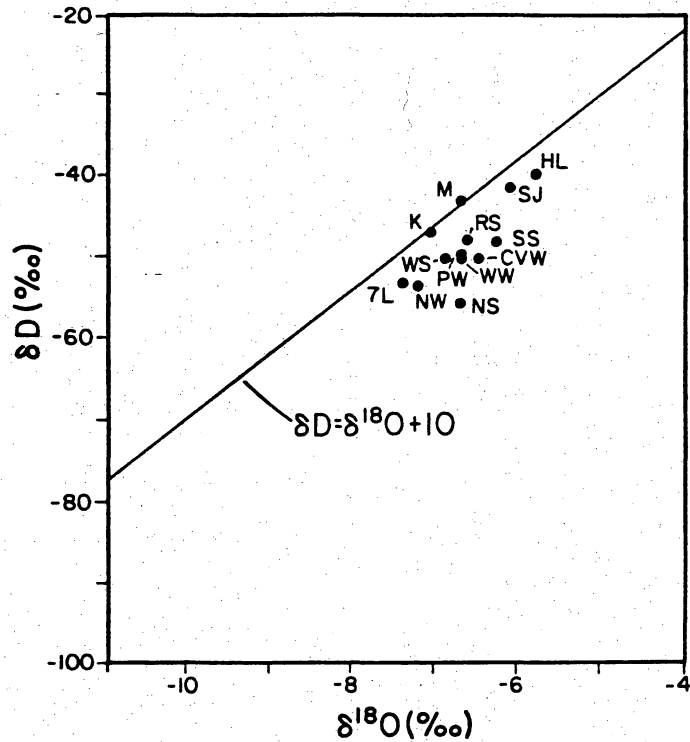
QA-6123

Figure 19. $\delta^{18}\text{O}$ and $\delta^2\text{H}$ distribution in ground water of Site S-15, Culberson County (in ‰ deviation from SMOW).



-5.8 ($\delta^{18}O$) ^{18}O and ^{2}H deviations from
 -40 (δD) SMOW in water sample (‰).

Figure 20. $\delta^{18}O$ and $\delta^{2}H$ distribution in ground water of Block 46, Culberson County (in ‰ deviation from SMOW).



EXPLANATION

M	Monument Windmill	CVW	Cave Well Windmill
SJ	Smilin Jack Windmill	WW	West Windmill
KW	Kohen Windmill	7L	Seven-L Windmill
P	Phillips Windmill	SS	South Spring
NW	North Windmill	WW	West Spring
HL	High Lonesome Windmill	NS	North Spring
RS	Rustler Spring		

QA-6120

Figure 21. $\delta^{18}\text{O}$ versus $\delta^2\text{H}$ (‰) in Culberson County sites. Well location is shown in figures 19 and 20.

Lack of exposure of the Castile Formation over much of the Gypsum Plain, except for deeply incised drainages and in castiles, makes structural interpretations difficult. However, many of the surface drainages are controlled by a system of joints, and local areas of faulting are present. These faults are commonly inferred by projection from exposures in the Delaware Mountains. In the Gypsum Plain, the faults are expressed as linear northeast-trending drainages and aligned zones of sinkholes and castiles, but the displacement on these faults, although believed to be small, cannot be demonstrated.

Surficial materials in the Gypsum Plain consist mostly of gypsite, a granular product formed by the breakdown of bedded gypsum, and other locally derived alluvium. These materials could be easily excavated, but they appear to be highly porous. The gypsite and other alluvial sediments mantle much of the surface and fill valleys and depressions. Some of these features appear to have been formed by dissolution and collapse of the underlying Castile Formation.

The western portion of Block 46 is underlain by the Bell Canyon Formation. Most of the Bell Canyon Formation is a weakly cemented sandstone that appears to be highly porous and permeable. It is well jointed and is locally faulted by small displacement normal faults. Northeast-striking faults are the most prominent, especially at the contact between the Bell Canyon and Castile Formations. Locally drainages are joint controlled.

Surficial materials in Block 46 consist of recent and older alluvium derived from erosion of the Bell Canyon Formation. The alluvium, which could be easily excavated but which appears to be very porous, occurs in small alluvial fans and as valley-fill deposits.

Six hydrologic issues relevant to evaluation of the two Culberson County sites were addressed in this report. The following preliminary conclusions were based on our findings.

(1) Karstic aquifers underlie both study areas in Culberson County. The aquifer underlying the S-15 area seems to have a regional distribution and to have more connectedness than the aquifer underlying the Block 46 area.

(2) The water table is shallow in both areas, ranging from 0 to 150 ft (0 to 46 m).

(3) Ground-water flow at the S-15 study area is from west to east, following the topographic and geologic dip. At the Block 46 study area, flow direction in the aquifer could not be determined because of a scarcity of data.

(4) The residence time of water in the aquifer varies from a few tens of years to several thousand years. The oldest water sampled (5.906 yr old) is a mixture of younger and older water. Calculated ^{14}C ages may be too old because of possible calcite precipitation in the site area. Therefore, the high tritium activities in ground water sampled in the sites may be a better indicator of short residence time of recently recharged ground water. Because of the karstic nature of the system, residence time of the ground water may be highly variable.

(5) Recharge to the aquifers of both areas seems to combine water coming from a remote distance (perhaps the Delaware Mountains) with water from local precipitation that percolates through the relatively thin unsaturated zone.

(6) Natural discharge points are scattered all over the S-15 study area as springs that issue water from the shallow aquifer. In some locations, the water table is close enough to land surface to permit large areas of seepage and direct evaporation. Both sites have nearby pumping wells that provide water mainly for grazing cattle. Future mining activities closer to the S-15 site may result in man-induced dissolution features and unpredicted flow directions and discharge points.

HUECO BOLSON, HUDSPETH COUNTY INVESTIGATIONS

Location

One area in Hudspeth County includes 2 sites (S-34a and S-34b) selected by the Texas Low-Level Radioactive Waste Disposal Authority for consideration as the location of a low-level radioactive waste repository. The study area is located in the Hueco Bolson on State-owned lands lying between the Rio Grande to the south and the Diablo Plateau to the north (fig. 22). The Finlay Mountains lie about 4 mi (6.5 km) east of the primary study site.

The primary study area, S-34a (fig. 22), is located in the Diablo Canyon West 7.5-minute Quadrangle and is close to the northern border of the lands owned by the State of Texas. It is accessed by a well-maintained gravel road that leads from Fort Hancock, about 9 mi (15 km) to the southwest, to the Lee Moore Ranch. The site is an area of low relief, having surface drainage to the west and south into Alamo Arroyo. Alluvial sands with some pebbles and cobbles occur at the surface, locally overlain by windblown sands. Camp Rice Arroyo lies south of the primary study area.

This second study site, S-34b, was selected for preliminary drill testing by BEG. It lies in an area of low relief on the west side of Diablo Arroyo about 2 mi (3 km) southwest of Campagrande Mountain (fig. 22). The area is overlain by a surface veneer of windblown sand.

Methods

Aerial photographs at a scale of 1:12,000 (1 inch = 1,000 ft) were acquired for a large area around the proposed site, including the drainages of most of the major arroyos from near their headwaters at the rim of the Diablo Plateau to their mouths on the Rio Grande. Particular attention was placed on identification of

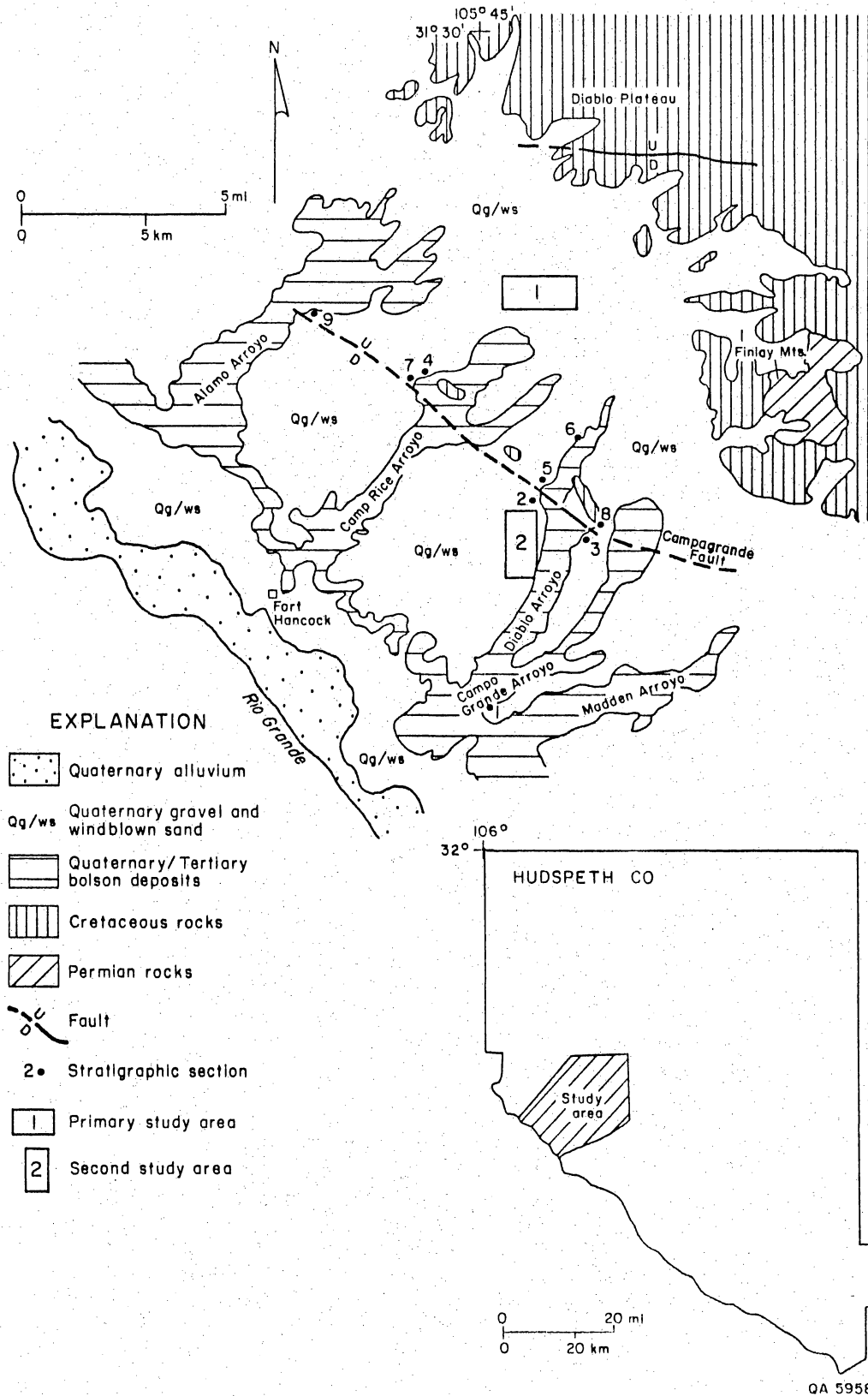


Figure 22. Map of geologic setting and location of (1) S-34a and (2) S-34b in Hudspeth County. Geology after Barnes (1983). Described stratigraphic sections are in appendix 6.

fault traces and the location of well-exposed stratigraphic sections. Local areas were interpreted in detail, and the results were compared with published maps of the region. Aerial photographs were also used to extend the published mapping into previously unmapped areas farther west. Interpretations made from aerial photographs were verified, sections were measured, landforms were studied, and areas of faulting were investigated.

Five shallow holes were drilled by BEG personnel to assist in the location of deeper holes subsequently drilled by Underground Resource Management, Inc. (URM). URM drilled four holes for defining the local stratigraphy and five holes for hydrologic testing. Geophysical logs were run in five holes by Schlumberger. BEG personnel were on site during all drilling operations and supervised sample collection.

Water-level data for the Rio Grande alluvium aquifer in Hudspeth County near the proposed site were obtained from the Texas Natural Resources Information System (TNRIS) computerized data base and from open-file reports of the Texas Water Commission. Water levels in the Hueco Bolson and the Cretaceous aquifers in the vicinity of the site were reported by the well owners and may be considered as approximations only. All information about water levels is presented in appendix 1.

No data were available for porosities, hydraulic conductivities, or transmissivities of the unsaturated or saturated zones of this site. Two permeability tests were performed during this study in the unsaturated zone of the bolson fill at the site. The tests were performed in gravels and in the entire lithologic sequence beneath the gravels to a depth of 150 ft (48 m). These data are reported in appendix 7. Six additional permeability tests and 12 grain-size analyses on core samples from the unsaturated zone of this formation at this site were carried out by URM labs. These data are reported in appendix 8. A pumping

test in the saturated zone of the Cretaceous aquifer was part of the completion program of the water well drilled at this site. These data are reported in appendix 3A.

Chemical analyses of water from wells that penetrate the Rio Grande alluvium near the site in Hudspeth County were obtained from the Texas Water Commission files. No data were available for wells that penetrate the bolson sediments or the Cretaceous rocks in the vicinity of this site. Therefore, all bolson and Cretaceous wells adjacent to the site were sampled. All samples were analyzed for general chemistry, $\delta^{18}\text{O}$, $\delta^2\text{H}$, tritium, and $\delta^{34}\text{S}$. Well-water samples were also analyzed for ^{14}C and $\delta^{13}\text{C}$. Temperatures were measured at the sampling sites. All chemical and isotopic data are reported in appendix 2.

Chloride and water content analyses were done on cores that were collected from shallow boreholes by BEG personnel. These boreholes were augered into gravels to a total depth of 40 to 50 ft (12 to 15 m) at the two sites.

The well numbering method used for some of the wells in Hudspeth County follows the system adopted by the Texas Water Commission (Alvarez and Buckner, 1980).

Geologic Setting

The Fort Hancock sites lie at the eastern edge of the Hueco Bolson, a major Basin and Range graben. Rocks in the area range in age from Permian to Recent; the strata most important to this investigation are late Tertiary to Recent sediments that fill the Hueco Bolson. They were deposited on a high-relief surface composed of massive, indurated Lower Cretaceous sandstones and limestones and

Upper Cretaceous marly limestones and shales. These Cretaceous rocks were folded and faulted during early Tertiary Laramide deformation. During this deformation, the rocks were folded and thrust northeastward toward the relatively undeformed Diablo Plateau. The boundary between highly deformed rocks to the west and relatively undeformed rocks to the east approximately underlies the primary study area. Deformed rocks are exposed at Campgrande Mountain about 5 mi (8 km) south of the site; relatively undeformed rocks occur along the Diablo Rim less than 3 mi (5 km) to the northeast. Plate 3 displays the geology of the Hudspeth County area.

Stratigraphy of Hueco Bolson Deposits

Tertiary deposits that fill the Hueco Bolson are being considered as potential host sediments for a low-level radioactive waste repository. These strata include the informally named older basin deposits described by Albritton and Smith (1965); the same strata, but named the Fort Hancock Formation, are described by Strain (1966). Relatively coarse bolson deposits unconformably overlie the Fort Hancock Formation and were called the Camp Rice Formation (Strain, 1966). This unit is apparently equivalent to the younger basin deposits as well as to the Miser, Madden, Gills, Ramey, and Balluco Gravels of Albritton and Smith (1965). Very similar sequences of sediments also have been described in the Presidio Bolson, the next basin to the southeast along the Rio Grande (Groat, 1972).

In this study the term "bolson deposits" means all bolson deposits; the term "older bolson deposits" is equivalent to both the older bolson deposits described by Albritton and Smith (1965) and the Fort Hancock Formation of Strain (1966). The term "younger bolson deposits" is equivalent to younger bolson deposits as defined by Albritton and Smith (1965), but it also includes some near-surface gravels that

may be equivalent to the Miser, Madden, Gills, Ramey, or Balluco Gravels of Albritton and Smith (1965). In this usage, younger bolson deposits are probably equivalent to the Camp Rice Formation of Strain (1966).

The base of the bolson deposits is not exposed in the study area. Locally, small erosional outliers of Cretaceous sediments crop out within exposures of bolson deposits. The upper part of the bolson deposit sequence has been eroded to form a pediment surface in which progressively older bolson deposit sediments are exposed toward the Rio Grande. Bolson sediments are overlain by thin fluvial gravels, and both the modern surface and the erosional surface that are cut into bolson deposits slope toward the Rio Grande at about 30 to 50 ft/mi (6 to 9 m/km).

Age of Bolson Sediments

On the basis of a vertebrate fauna identified from Madden Arroyo, the arroyo southeast of the area investigated, Strain (1966) interpreted the age of the Hudspeth local fauna, which is preserved in the Fort Hancock Formation, to be Blancan. In its present usage the Blancan Age is late Pliocene.

On the basis of vertebrate remains and volcanic ash beds identified as the Pearlette Ash, Strain (1966) considers the Camp Rice Formation to be middle Pleistocene. Izett and Wilcox (1982) showed that volcanic sediments identified as Pearlette Ash by Strain (1966) are actually part of the Huckleberry Ridge ash bed of the Pearlette family of ash beds, which has a fission-track zircon age of 2.02 million yr. Therefore, the lower part of the Camp Rice Formation and presumably the lower part of the younger bolson deposits are late Pliocene. The age of the upper part of the younger bolson deposits or of the upper part of the Camp Rice Formation is unknown but presumed to be Pliocene (Gile and others, 1981).

Stratigraphy

Eleven stratigraphic sections through bolson deposits and younger fluvial sediments in Hudspeth County are described from outcrops along Alamo, Camp Rice, and Diablo Arroyos and unnamed tributaries of these arroyos (app. 6). Collectively, these sections include ~720 ft (~220 m) of strata, but no single section includes more than ~100 ft (~30 m) of strata. In many places parts of the valley walls leading into the arroyos are covered with colluvium or terrace deposits, and correlation from upstream to downstream sections is impossible. Thus, the described sections represent only increments of the entire stratigraphic thickness of the bolson deposits, and they characterize bolson deposits in specific geographic areas rather than define or fully describe the formation.

A single section is described to characterize coarse-grained facies of the younger bolson deposits exposed in the downstream part of Diablo Arroyo southeast of Fort Hancock. Most of the remaining sections described are on either side of the Campagrande fault, which strikes northwest-southeast across the study area. In these sections, relatively coarse, younger bolson deposits composed of fluvial sand and gravel are exposed in downthrown blocks southwest of the fault, and fine silty clay and clayey silt of the older bolson deposits are exposed in the upthrown block northeast of the fault. Additional observations indicate that surface exposures of bolson deposits become progressively coarser northeast of the fault. Albritton and Smith (1965) and Groat (1972) recognized similar lithologic variations south of this study area.

Stratigraphic Sections

Stratigraphic sections that form the basis for the following descriptions of facies of the bolson deposits are in appendix 6. Generalized descriptions of surface outcrops are given for four representative areas: (1) an outcrop near the Rio Grande, (2) outcrops in the downthrown block and within a few hundred meters of the fault, (3) outcrops in the upthrown block within a few hundred meters of the fault, and (4) an outcrop far northeast of the fault.

Section Near the Rio Grande River.--Nearly 23 ft (8 m) of younger bolson deposits are exposed on the southeast valley wall of Diablo Arroyo, approximately 0.5 mi (0.8 km) northeast of the Diablo Reservoir No. 2 (app. 6). These sediments consist of approximately 20 ft (6.3 m) of fluvial sands and gravels interbedded with bioturbated clayey silt. This section is apparently equivalent to part of the Camp Rice Formation of Strain (1966).

Composite Section, Downthrown Side of Campagrande Fault.--Coarse-grained sediments of the younger bolson deposits crop out in stream cuts southwest of the Campagrande fault (fig. 22). Sections described in these sediments occur in Diablo Arroyo and Alamo Arroyo, and both occur within 100 ft (30 m) of the Campagrande fault (app. 6). Older bolson deposits consisting of pale-red-brown silty clay and pale-brown laminated clayey silt occur at the base of the section. Preserved primary sedimentary structures, which are rare in the silty clay unit, consist of very fine graded laminae of silty clay and clay. The silty clay lithology makes up approximately 78 percent of the section. Desiccation cracks, slickensides on fracture surfaces, and a popcornlike surface texture indicate that the red-brown clays contain a high proportion of expansive clay minerals, most likely montmorillonite.

Younger bolson deposits composed of sand and gravel overlie an erosion surface cut into the older bolson deposits. Typically these sands and gravels are a series of upward-fining sequences and are as much as 90 ft (27.5 m) thick. Sequences commonly overlie an erosion surface and consist of basal, horizontally bedded, clast-supported limestone pebble to cobble gravel overlain by horizontally to crossbedded coarse to medium sand. Pedogenic calcrete nodules occur throughout the sandy sections, and CaCO_3 films cover the lower part of gravel clasts. As many as three pedogenic CaCO_3 calcretes, known as Stage III calcretes in the classification of Bachman and Machette (1977), may be preserved in the lower part of this unit. The younger bolson deposits are capped by a massive pedogenic calcrete that is locally as much as 6 ft (2 m) thick. At least one cycle of brecciation has resulted in a polygonal fracture system in which carbonate laminae are deposited. The upper part of the calcic horizon is well indurated and weathers to a platy structure. This calcrete is probably a Stage IV or Stage V calcrete in the Bachman and Machette (1977) classification.

Composite Section, Uplifted Side of Campagrande Fault.--Sections on the uplifted side of the Campagrande fault were described from Alamo, Camp Rice, and Diablo Arroyos. Fine-grained older bolson deposits are exposed in the uplifted block northeast of the Campagrande fault in each of these areas. Because there are no distinctive lithologic units nor any datable material in these sections, it is impossible to correlate them with sections of older bolson deposits exposed south of the Campagrande fault.

Older bolson deposits in sections within the uplifted block and within a few hundred meters of the Campagrande fault are as much as 90 ft (27.5 m) thick and consist of interbedded pale-red-brown silty clay and pale-brown clayey silt. The

silty clay is devoid of preserved sedimentary structures and the clayey silt is commonly laminated. In these sections silty clay makes up from 48 to 78 percent of the older bolson deposits. In the section northwest of Diablo Reservoir, a 6-ft (2-m) thick sequence of deltaic topset, foreset, and bottomset beds is preserved. These strata are primarily clayey silt and very fine sand.

As much as 43 ft (13 m) of younger bolson deposits overlie an erosion surface developed on the older bolson deposits. The younger bolson deposits in these sections consist of thin units of silty clay and clayey silt and thick units of flat-bedded to trough and planar crossbedded and ripple cross-laminated sand. Mud drapes with desiccation cracks are preserved within the sequence. Pedogenic calcrete nodules are dispersed throughout the younger bolson deposits. Thin ground-water calcretes cement some very thin sandstones. Layers of ground-water calcrete nodules are locally preserved above mud drapes.

Locally, the younger bolson deposits are overlain by Recent eolian sand or by a thin layer of gravel that underlies the regional pediment surface. The gravel contains a pedogenic calcrete that appears to have been partly stripped away in the areas where these sections were described. The calcrete is massive to platy in outcrop and up to 5 ft (1.5 m) thick. At least one cycle of fracturing has occurred, and fractures 0.4 inch (1 cm) wide are filled with laminated CaCO_3 . These are Stage IV calcretes in the classification of Bachman and Machette (1977) and may actually be Stage V calcretes.

Section Near Bolson Margin.--A section of sediment was examined at Alamo Tank in the headwaters of Alamo Arroyo. This outcrop occurs only about 0.6 mi (1 km) downslope from the projected margin of the Hueco Bolson (the contact between

bolson deposit sediments and Cretaceous rocks) and thus may expose coarse proximal bolson deposit facies. This section consists of approximately 15 ft (5 m) of sand and gravel. The sediments are flat bedded and contain pedogenic calcrete nodules. Three pedogenic calcrete horizons are preserved. The Alamo Tank section appears to be representative of proximal coarse-grained younger bolson deposits, but correlation of this section to bolson deposits farther south is unclear because no datable material has been found and outcrops are discontinuous.

Discussion

Bolson deposits consist of a lower sequence of silty clays and clayey silts that are apparently equivalent to the older bolson deposits of Albritton and Smith (1965) and to the Fort Hancock Formation of Strain (1966). Unconformably above these fine-grained sediments lie sands and gravels that are equivalent to the younger bolson deposits of Albritton and Smith (1965) and the Camp Rice Formation of Strain (1966). These strata become progressively coarser to the northeast toward the margin of the Hueco Bolson. The silty clay content decreases from nearly 80 percent to the southwest to only 32 percent near the Campagrande fault. Thick sands and gravels overlie older bolson deposits in the hanging wall south of the fault. Fine-grained older bolson deposits are exposed in the foot wall north of the Campagrande fault and contain from 48 to 78 percent silty clay. The percentage of silty clay in this sequence decreases to the northeast toward the basin margin. As much as 43 ft (13 m) of younger bolson deposits, sands, and gravels occur above the silt and clay beds of the older bolson deposits north of the Campagrande fault. Younger bolson deposits and surface gravels also appear to coarsen toward the basin margin.

Within the study area, fine-grained and presumably low-permeability rocks crop out in arroyos near the Rio Grande valley and short distances northeast of the Campagrande fault. At equivalent stratigraphic horizons these fine-grained sediments become progressively coarser toward the northeast.

Relatively thin sections of younger bolson deposits, consisting of sand and gravel, overlie silt and clay units of the older bolson deposits in the southern part of the study area. North of the Campagrande fault as much as 43 ft (13 m) of sand and gravel overlie fine-grained sediments of the older bolson deposits.

Site-specific geologic investigations will be discussed later in the text.

Structure

Quaternary Faults

A fault system cutting the Quaternary and late Tertiary alluvial and basin-fill deposits in the vicinity of the study area was mapped by Albritton and Smith (1965). The main fault is well exposed in several branches of Diablo Arroyo near Campagrande Mountain and is informally referred to as the Campagrande fault. The fault is also exposed in Alamo Arroyo. The trace of the Campagrande fault, shown in figure 22 and plate 3, lies about 4 mi (6 km) southwest of the primary study area and about 2 mi (3 km) northeast of the alternate study area. No evidence of faulting was observed in other outcrops closer to the main areas of detailed investigation.

The Campagrande fault can be traced as a nearly continuous scarp of slightly higher slope than the pediment surface and is cut only by incised arroyos from the eastern edge of the Campagrande Mountain Quadrangle northwest onto the southern

edge of the Cavett Lake Quadrangle, a distance of about 7.5 mi (12 km). A topographic scarp, locally covered by windblown sand, probably marks the continuation of the fault another 9 mi (15 km) to the northwest, giving an inferred total length of about 17 mi (27 km). The apparent Quaternary displacement becomes imperceptible to the southeast and increases to a maximum of about 15 ft (5 m) just west of Campagrande Mountain. The amount of displacement may be greater to the northwest because the size of the sand-veneered scarp increases; however, the displacement cannot be determined precisely.

The Quaternary scarp probably marks a major fault, having much greater displacement in the subsurface, that makes up part of the eastern boundary of the Hueco Bolson. Well and geophysical data collected by the U.S. Geological Survey for ground-water exploration (Gates and Stanley, 1976; Alvarez and Buckner, 1980) indicate that basin fill thickens significantly toward the southwest near the Quaternary scarp. The geophysical data are not sufficiently detailed to locate the area of thickening more precisely. Nevertheless, the Quaternary scarp probably marks the location of most recent movement on a fault or fault zone that forms the eastern boundary of the Hueco Bolson. Net displacement on this fault may be as much as 3,300 ft (1 km).

Where seen in outcrop, the main strand of the Campagrande fault strikes about N 50 to 55 W and dips approximately 65° to 85° southwest. It commonly consists of several fault strands, each of which has up to 10 ft (3 m) of normal displacement. Stratigraphic studies of the older bolson fill suggest that as much as 100 ft (30 m) of displacement may be the aggregate displacement across the zone in some localities. The total width of the zone of demonstrable faulting seldom exceeds 165 ft (50 m). The one exception to this occurs in outcrops exposed in a major tributary of Diablo Arroyo south-southeast of Campagrande Mountain. At

this locality there is a second zone of faulting about 3,300 ft (1 km) south of the main fault trace. The faults are presumed to be related to the same period of activity that formed the main Campagrande fault, but fault strikes are both northwesterly and almost due north-south. The north-south faults are also normal faults, but some occur as an antithetic set dipping to the east in the hanging wall of a "typical" northwest-striking fault. Farther down the arroyo there is a large outcrop of highly disturbed sandstone that may result from soft-sediment deformation; further investigation into its origin is needed.

The timing of the latest episode of movement along the Campagrande fault has not been established with confidence. The fault cuts the Camp Rice Formation, which contains the 2.02 million-yr-old Huckleberry Ridge ash bed (Izett and Wilcox, 1982) and displaces the pediment surface developed on Camp Rice Formation sediments. Deposition of the Camp Rice Formation probably ceased between 300,000 and 400,000 yr ago (Gile and others, 1981), indicating that the most recent displacement on the fault is younger than about 300,000 to 400,000 yr. The relationship of the fault to the caliche horizons is unclear. Nowhere is there definitive evidence of the fault cutting the caliche. If it can be demonstrated that the caliche caps the fault trace and is not offset by the fault, it may be possible to determine a minimum upper limit to the age of last fault movement.

East-West Fault along the Diablo Rim

An east-striking fault and monocline system displace Cretaceous rocks at the edge of the Diablo Plateau approximately 4 mi (7 m) north of the study area (fig. 22). Maximum displacement on a single fault strand is about 20 to 30 ft (6 to 9 m) down to the south; the displacement generally increases from east to

west. At the far east end, the fault dies out into a monocline, which continues to decrease in displacement still farther east until there is no displacement. Along much of the fault trend, at least part of the displacement is taken up by monoclinical warping.

An east-striking topographic escarpment about 2.5 mi (4 km) east of the study area may mark another east-striking fault. A ridge of Cretaceous rock, dominantly Cox Sandstone, is abruptly terminated on the south by a scarp with as much as 330 ft (100 m) of relief. Cretaceous rocks are covered by Quaternary deposits in the valley to the south and do not reappear for about 0.6 mi (1 km). East along the trend of the scarp, the Cox Sandstone overlies the Campagrande Formation. Albritton and Smith (1965) show the contact as being depositional. The abruptness of the scarp suggests joint or fault control, but no offset can be demonstrated.

A similar but north-northwest-trending geomorphic escarpment connects the two east-trending zones. The northern end, north of the east-striking fault, consists of a zone of closely spaced joints having no discernible displacement. It forms the large indentation into the Diablo Rim where the county road crosses. This trend continues to the south, where it forms a narrow valley, covered with alluvium, between ridges of Cretaceous rock. Displacement across the valley is at most minor, but dips on the western side are greater than on the eastern side, suggesting at least some flexure. Also, north-northwest-striking joints are abundant in rocks on both sides of the valley. The trend must be either a major joint zone or a minor fault.

Seismic Survey

Four seismic lines were run in the study area. One was located on the main road, from north of the study area, across the Campagrande fault, to south of the study area. The Campagrande fault is visible, as are nearly flat-lying bolson

sediments above gently dipping Cretaceous rocks in the vicinity of the study area. Displacement on the Campagrande fault is not apparent on the available seismic section, but the Cretaceous rocks may be deeply buried by younger sediments in the hanging wall block. Additional velocity control data will be required to allow better resolution of depth values.

An interesting feature seen in seismic data is a buried "basement" high of presumed Cretaceous rocks in the foot-wall block of the Campagrande fault. The basement high appears to be a continuation of the deformed mass of Cretaceous rocks that occur on Campagrande Mountain and in small isolated outcrops to the northwest. The northeast margin of the block shows no evidence of a bounding fault, but regional relationships suggest that this area may contain a southwest-dipping reverse fault that separates strongly deformed Cretaceous rocks to the southwest from gently dipping but little deformed Cretaceous rocks to the northeast. On the seismic section the structural block appears to locally constitute the southwestern boundary of the bolson sediments that underlie the proposed site. Bolson sediments in the study area may have been deposited in a basinal area that was locally topographically distinct from the nearly coeval sediments deposited closer to the present Rio Grande across the topographic divide formed by the structural block. The structural block also may hydrologically isolate the deep bolson sediments along the Rio Grande from those in the foot-wall block of the Campagrande fault. Additional definition of the topographic shape and continuity of the structural block is needed because the single seismic line cannot define the extent to which the structural block isolates older updip bolson sediments from downdip bolson sediments.

Drilling Program

The drilling program at both Hudspeth County sites was designed to provide detailed stratigraphic data to drill wells for hydrologic tests, and to provide control for the seismic study. An initial drilling program was carried out by BEG personnel using BEG equipment, and subsequent deeper holes were drilled by personnel from Underground Resource Management, Inc. (URM) of Austin, Texas, using their own equipment.

BEG Drilling

Lack of exposure of the silty and clayey older bolson fill deposits (Albritton and Smith, 1965) in the S-34a study area prompted an initial investigation to verify the depth of gravel overburden overlying the silty and clayey sediments. A second study area, S-34b, was also tested. Locations of the three holes drilled at S-34a are shown in figures 23a and 23b; two holes drilled at S-34b are displayed in figures 24a and 24b.

At S-34a three auger holes (LLWA 1, 2, and 3) were drilled to depths of about 44 ft (13 m). Dense, compact clays and silts prevented further penetration. The clays and silts are overlain by a sequence that is 30 to 40 ft (9 to 12 m) thick and composed of limestone gravel, sand, and silt. Calcrete, sand, and silt overlie the gravel sequence. The two holes (LLWA 4 and 5) augered at the second study site encountered a similar stratigraphic sequence. Hole LLWA 5 was abandoned at a total depth of 20 ft (6 m) because the small BEG drill rig was unable to penetrate the cobble-sized gravel. Results of the drilling at the second study area demonstrate that the depth to the top of the silt and clay is similar at both S-34a and S-34b. The gravel sequence may also be coarser grained at the second study area, although the larger sized gravel penetrated in LLWA 4 and 5 might be a local variation that occurs at both study areas.

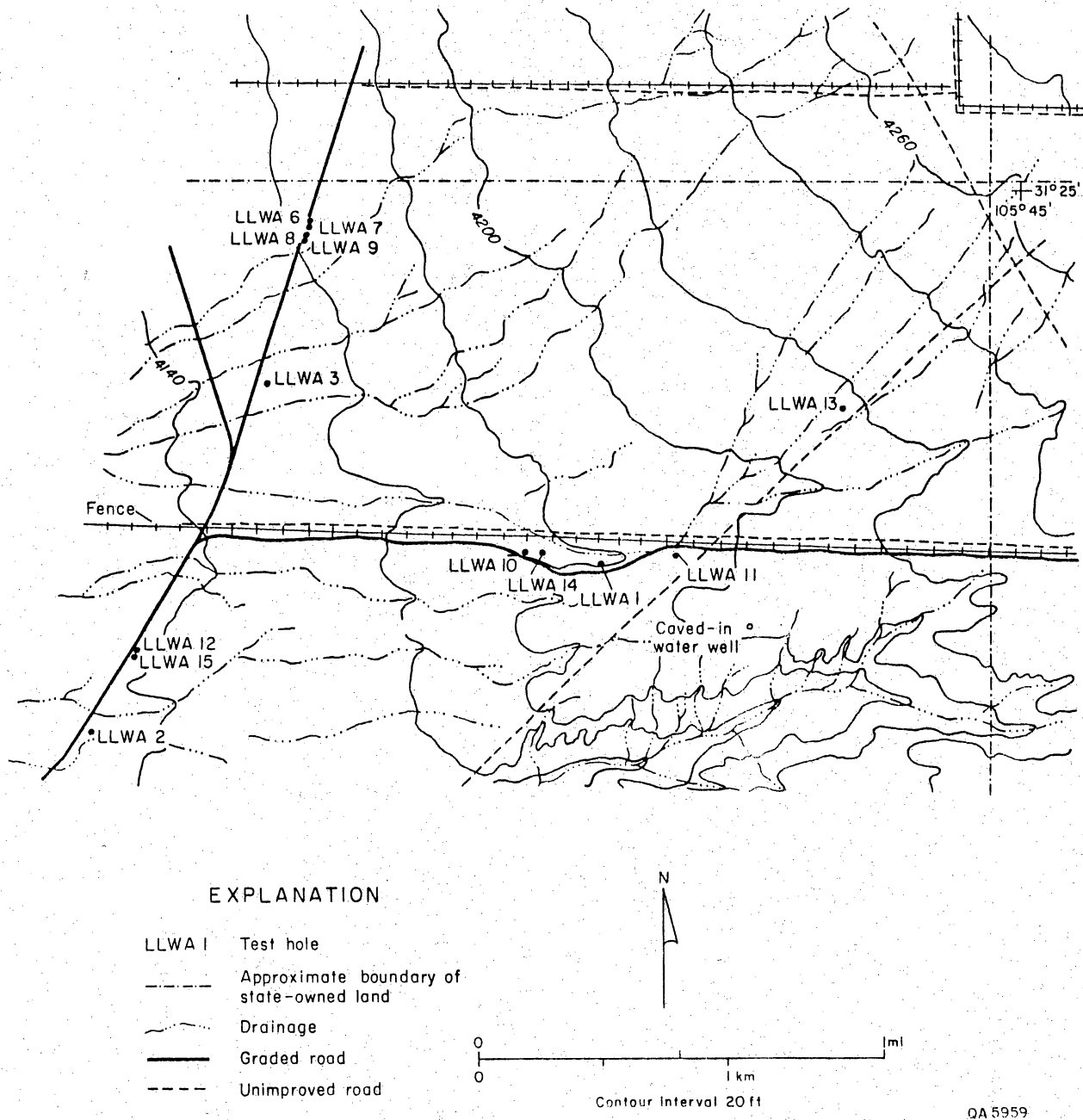
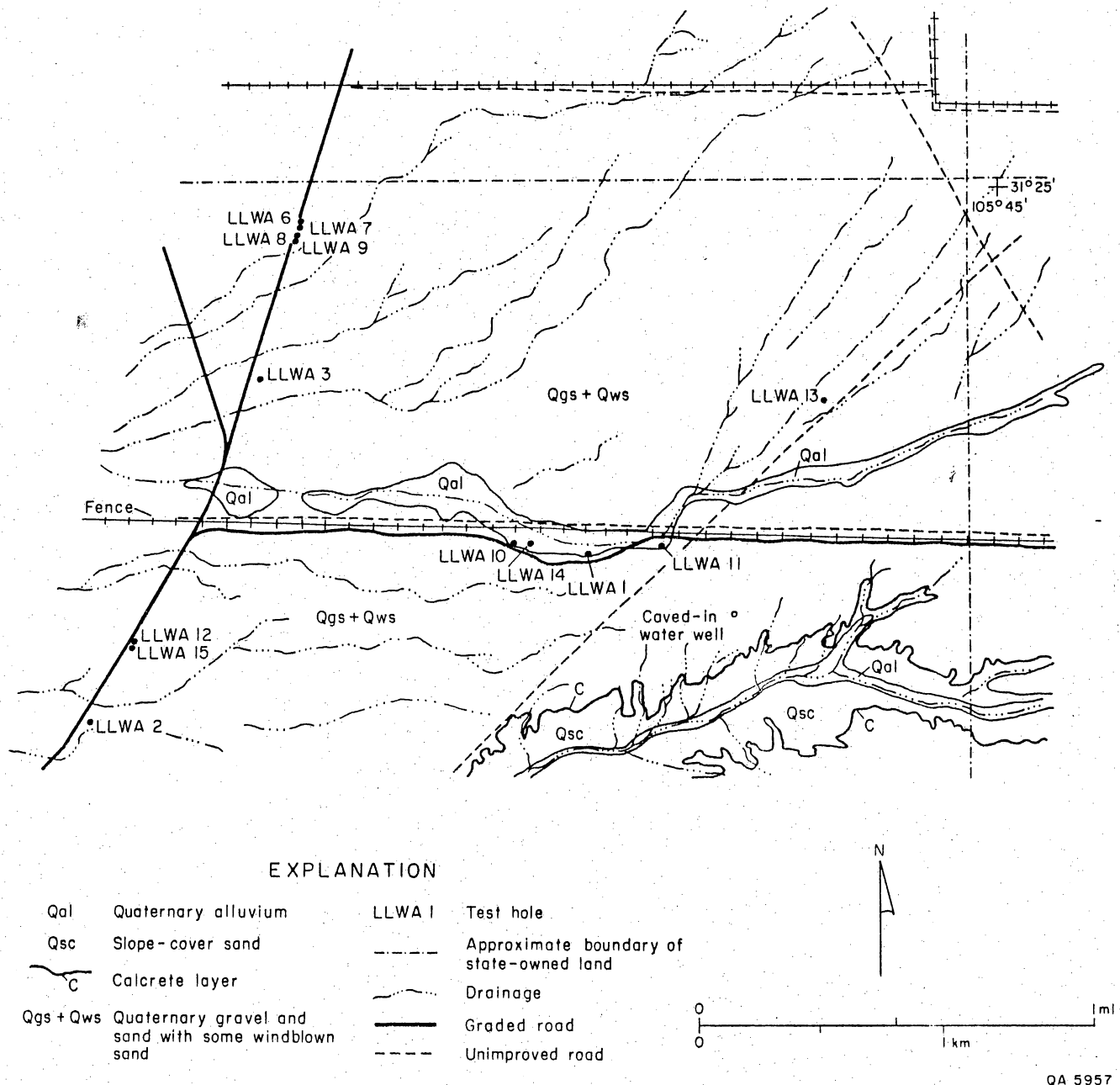


Figure 23(a). Map of topography, drainage, and test holes at S-34a in Hudspeth County. Location of area is shown in figure 22. Topography from U.S. Geological Survey Diablo Canyon West Quadrangle.



QA 5957

Figure 23(b). Geologic map of Site S-34a in Hudspeth County. Lithologic descriptions of core and cuttings from test holes are in appendix 9.

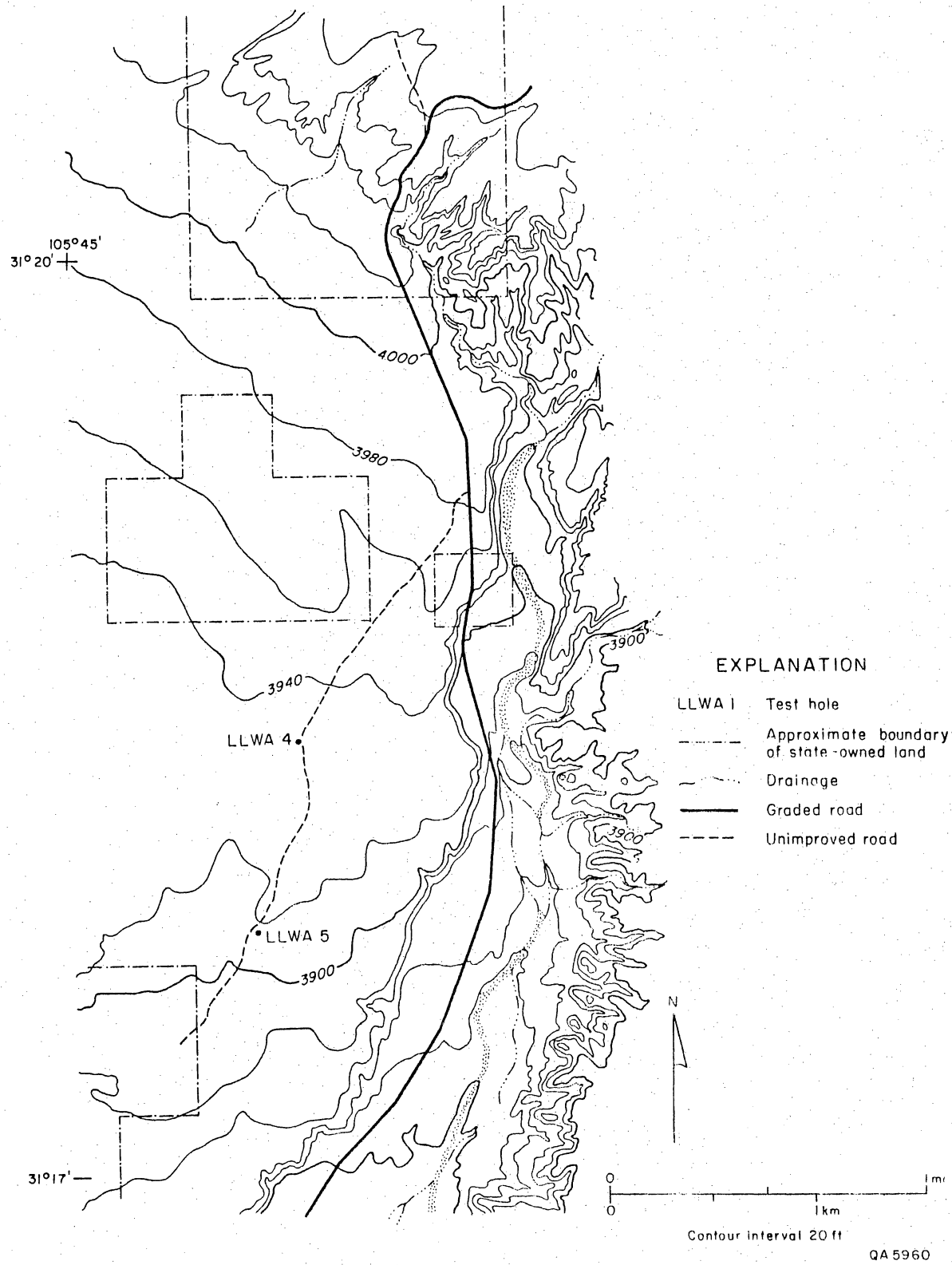


Figure 24(a). Map of topography and test holes at Site S-34b in Hudspeth County. Location of area is shown in figure 22. Topography from U.S. Geological Survey Campo Grande Mountain Quadrangle.

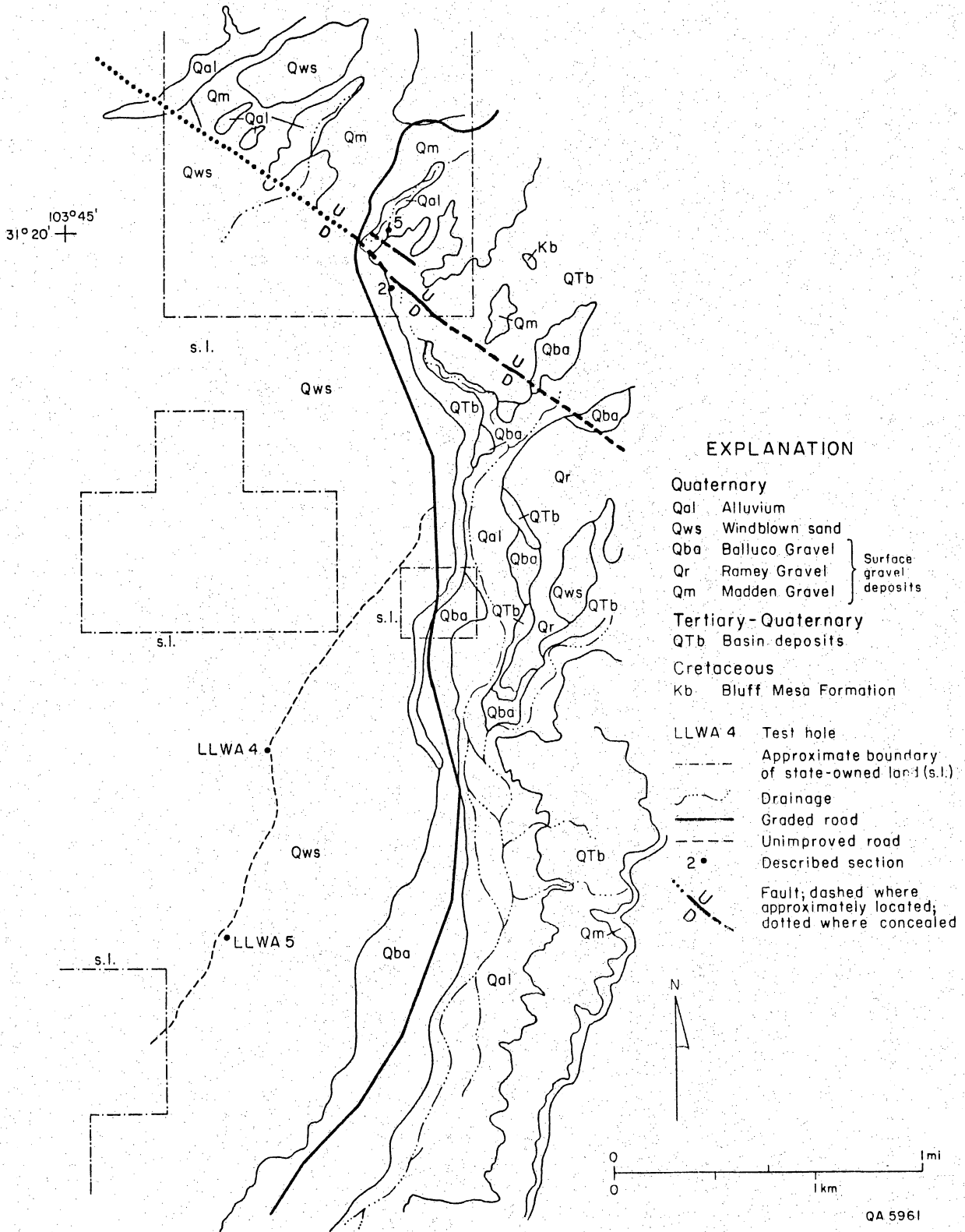


Figure 24(b). Geologic map of Site S-34b in Hudspeth County. Lithologic descriptions of cuttings from test holes are in appendix 9.

URM Drilling

URM drilled four holes (LLWA 7, 11, 12, and 13) 150 ft (45 m) deep to test the stratigraphy S-34a (figs. 23a and 23b). Additional holes were drilled for hydrologic purposes, although several of these holes also provide valuable stratigraphic control. Hole LLWA 6 was intended to be a 150-ft- (45-m-) deep stratigraphic test hole; however, sampling methods were inadequate, and the auger pipe broke at a depth of 65 ft (20 m), so the hole was abandoned. Holes LLWA 8, 9, and 15 were drilled for permeability tests. Hole LLWA 10, drilled to 465 ft (142 m), was intended to be a water well, but because the packer failed when the casing was being cemented, the test zone and screen were accidentally cemented also. Hole LLWA 14 was subsequently drilled to 500 ft (152 m) to replace the abandoned LLWA 10. Lithologic logs composed from on-site sample descriptions of test holes are displayed in appendix 9.

Geophysical Log Interpretation

Geophysical logging conducted in open boreholes 7, 11, 12, and 13 included the Spontaneous Potential curve (SP), Gamma-Ray log (GR), Dual Induction-Spherically Focused log (DIL-SFL), Compensated Neutron log (CNL), and the Litho-Density log (LDT). Depth of coverage for these four boreholes was 150 ft (46 m) to surface. This suite of logs was designed to support core analyses.

One cased hole, borehole 10 (a 470-ft cased water well), was also logged to provide information on the bolson intervals below 150 ft (46 m). Logging tools in cased holes were restricted to GR and CNL. Owing to casing conditions in this hole, the section logged was restricted to 303 ft (92 m) to surface.

Composite logs for the five boreholes are reproduced in appendix 10. Basic features of these logs and analysis of quantitative data are also provided in appendix 10.

Lithologic determination was accomplished using LDT and GR logs. One component of the LDT, the photoelectric curve (P_e), was useful in detecting the presence of limestone gravels because it indicates the presence of calcite and clean sands. This is best illustrated by the confirmation of the presence of a limestone gravel sequence from 94 to 97 ft (29 to 30 m) in borehole 13. Failure of the P_e to detect any calcite in the limestone gravels in borehole 12 may be a result of higher clay content masking the calcite response or greater depths of borehole invasion as recorded on SFL logs throughout this interval.

The GR is beneficial in stratigraphic and structural correlations and in quantification of clay content. GR logs indicate that 40 percent of the sequences contain 0 to 25 percent clay, 34 percent contain 26 to 50 percent clay, 17 percent contain 51 to 75 percent clay, and 8 percent contain 76 to 100 percent clay. Methods used to determine clay content are presented in appendix 10.

Porosity values were determined by crossplotting CNL values with LDT values. Porosity values from the four open boreholes range from a minimum of 19 percent in borehole 13 to a maximum of 54 percent in boreholes 7 and 12. Correction factors determined by crossplotting indicate that true porosity is 1 to 2 porosity units greater than the computer-derived average porosity curve (labeled PHIA) displayed in Track #3 of the geophysical logs (app. 10).

Quantification of formation water resistivity values from the DIL was impossible because of the unsaturated nature of the section logged. The DIL was a useful indicator of units containing higher irreducible water content, of intervals

where drilling fluid invasion of the borehole had exceeded 16 inches (41 cm) (thus a more permeable interval), and in stratigraphic correlation. True resistivity in unsaturated intervals is best represented by the deep-induction log (ILd).

Discussion

The test holes indicate three distinct units based on lithology: (1) limestone, (2) silt and clay, and (3) gravel. Limestone, which was penetrated in LLWA 10 and 14, is the deepest unit. It is approximately 480 ft (146 m) deep in the study area. The limestone cuttings are multicolored (tan, brown, gray, and black) and resemble a conglomerate unit within the Cretaceous Mesa Bluff Formation that is exposed in Camp Rice Arroyo about 3 mi (5 km) southwest of the boreholes. The cuttings could also be interpreted as a Tertiary limestone gravel overlying bedded Cretaceous limestone.

Above the limestone unit is a dominantly silt and clay unit that includes some sand layers. This unit has been described by Albritton and Smith (1965) as older basin fill. On the basis of the test holes and geophysical logs, the individual sand layers do not seem to correlate from hole to hole, suggesting they are not continuous; however, a silt-sand-clay sequence, or package, appears to extend across the area. The sandier package of older basin sediments is thickest in the northeastern part of the study site and thins west-southwestward (figs. 25, 26, and 27). The silt-sand-clay sequence comprises most of the older basin fill penetrated in test holes LLWA 11 and 13. LLWA 7 and 10 penetrated two sandier layers that are approximately 10 ft (3 m) and 30 ft (9 m) thick, respectively, whereas LLWA 12 penetrated only 10 ft (3 m) of the silt-sand-clay sequence.

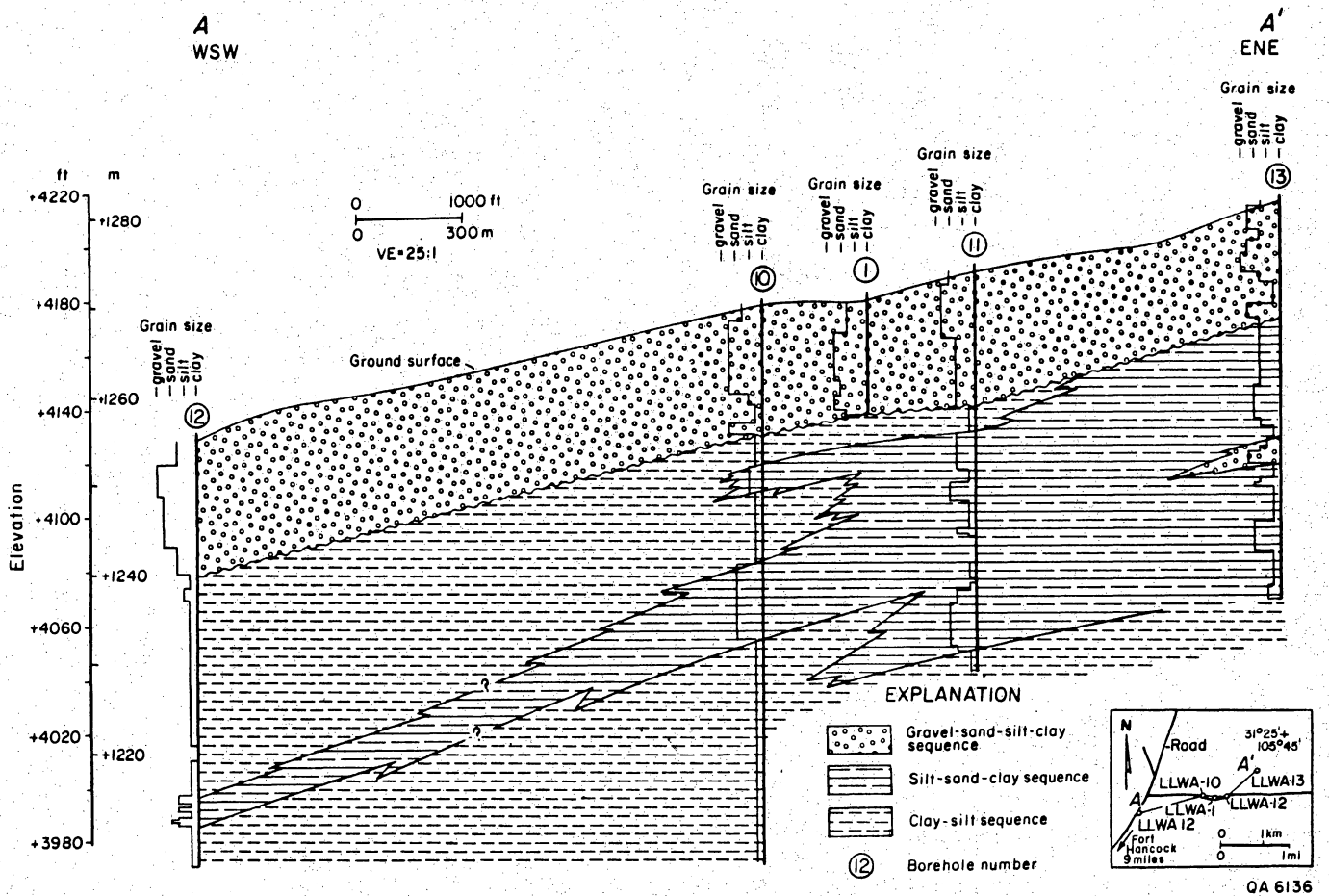
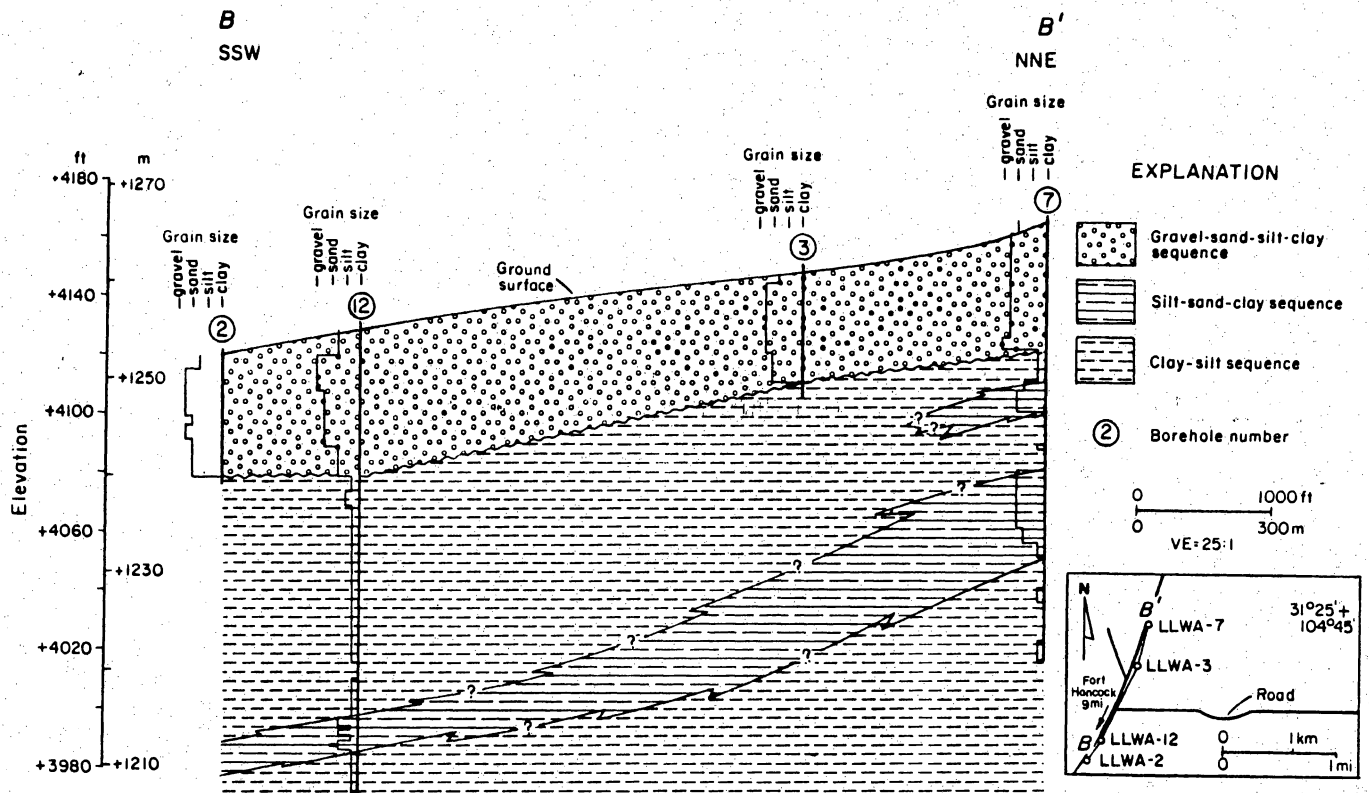


Figure 25. Cross section A-A' (west-southwest to east-northeast) across Site S-34a in Hudspeth County. Well locations are shown in figure 23.



QA 6138

Figure 26. Cross section B-B' (south-southwest to north-northeast) across S-34a in Hudspeth County. Well locations are shown in figure 23.

LLWA 10

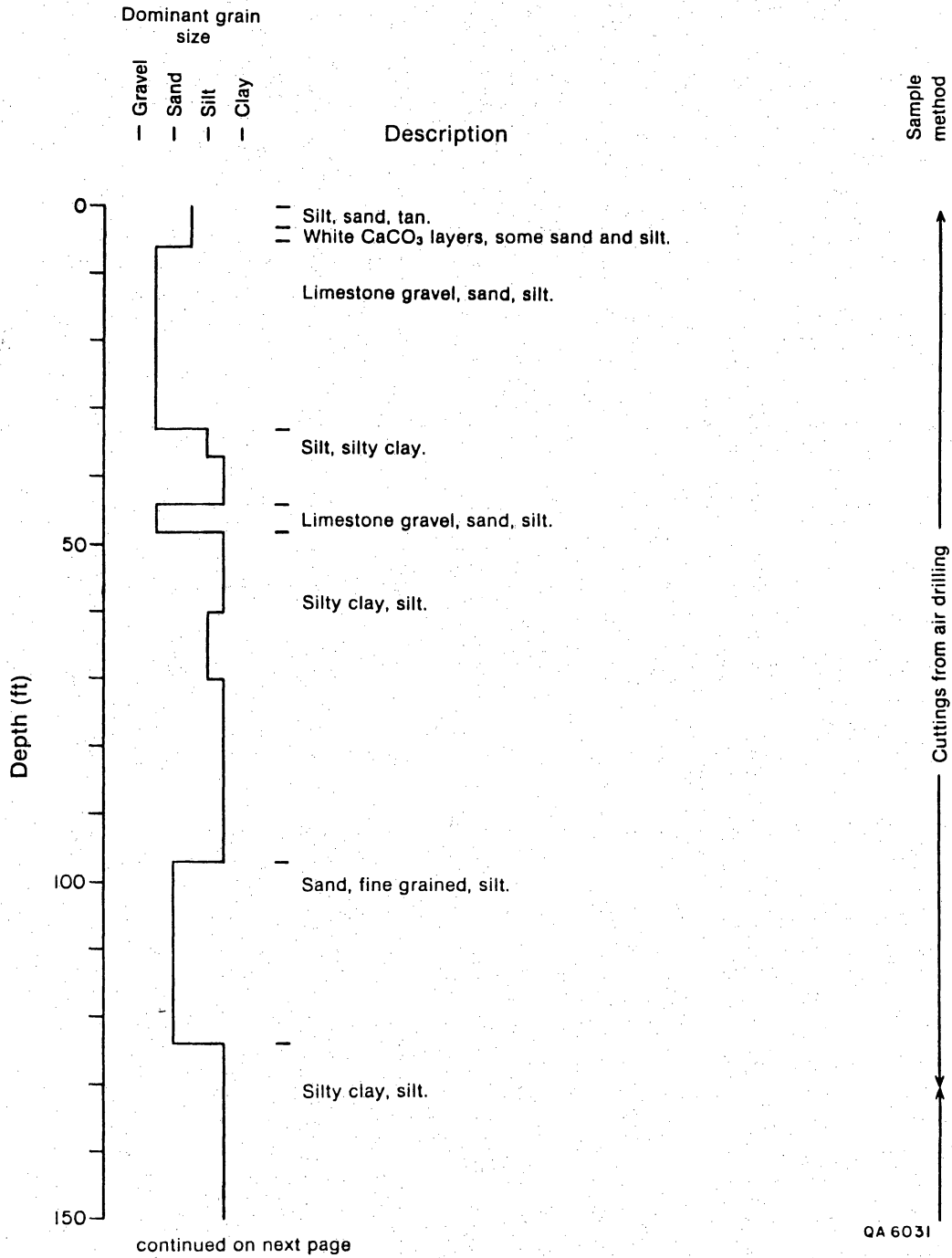


Figure 27. Lithologic log of cuttings from first water well, LLWA 10.

LLWA 10

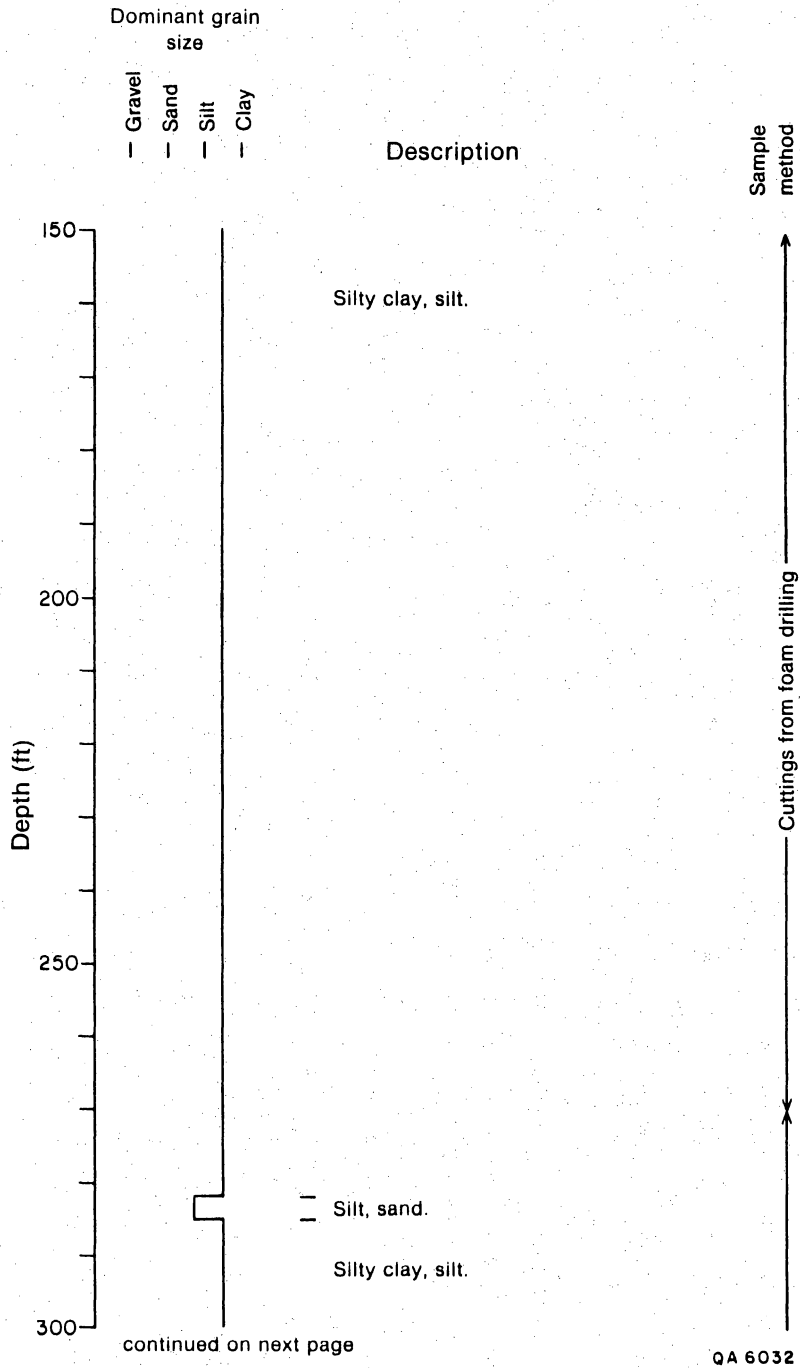


Figure 27 (cont.)

LLWA 10

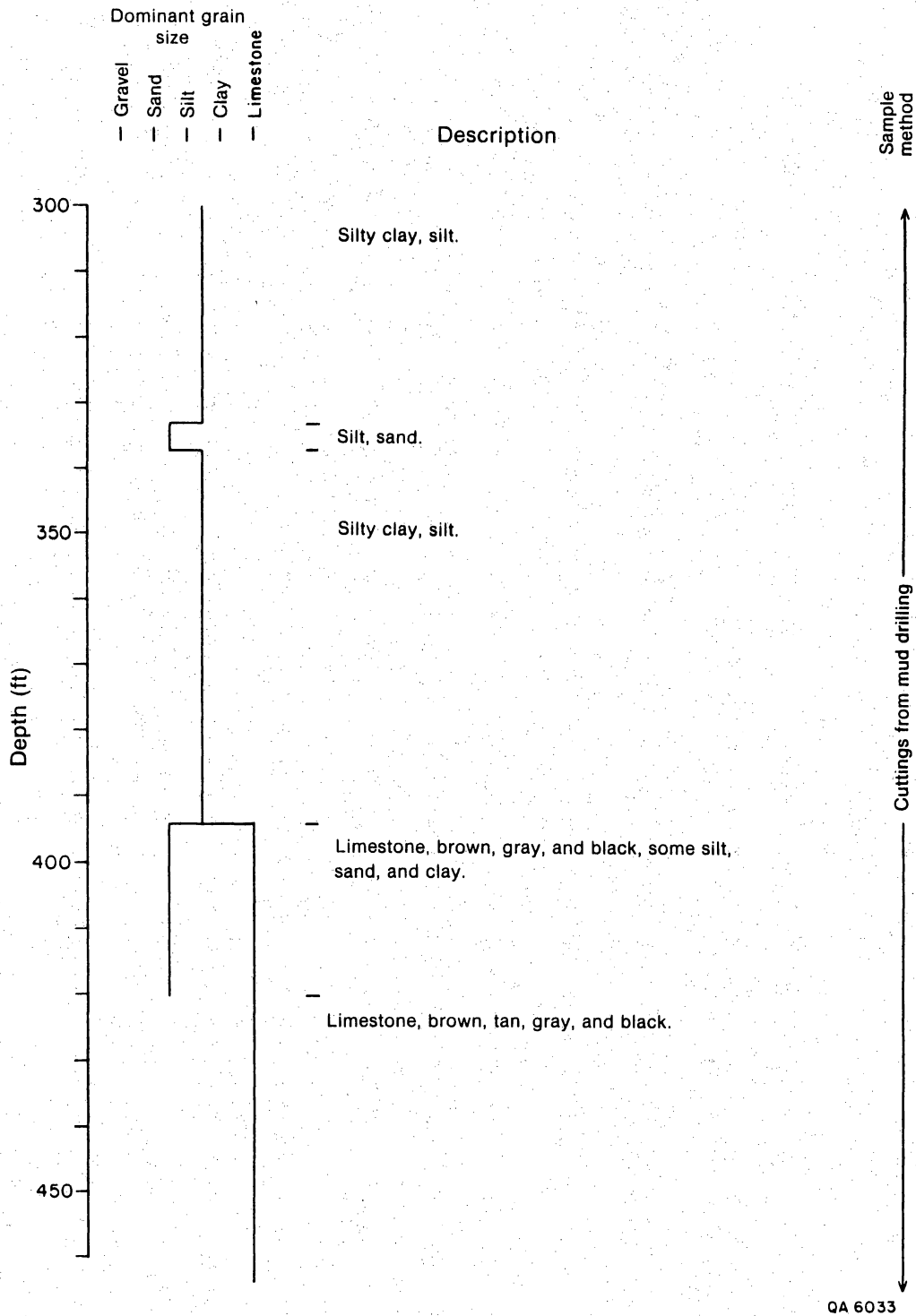


Figure 27 (cont.)

The upper unit, overlying the silt and clay unit, is composed of limestone pebble- and cobble-sized gravel, sand, silt, and some clay. This unit comprises younger basin fill and surface gravel deposits, which have been discussed by Albritton and Smith (1965). The upper gravel unit appears to be consistently 40 to 50 ft (12 to 15m) thick throughout the study area (figs. 25 and 26).

Surface Flow

Site S-34a is located on a sloping area that drains the Diablo Plateau and Finlay Mountains (Finlay Mountains and Smith Mesa in fig. 28) via narrow arroyos such as Diablo, Camp Rice, and Alamo Arroyos. These ephemeral washes extend from northeast to southwest toward the Rio Grande. They cut into the bolson fill, and near Campgrande Mountain and the plateau's escarpment they cut into Cretaceous formations such as Finlay limestone, Cox sandstone, and Bluff Mesa limestone. Water in the arroyos changes course from one flash flood to another. Although the depth of the alluvial fill in the arroyos is unknown, the absence of bolson fill in the riverbeds may suggest an alluvial thickness of several tens of feet. The presence of water storage tanks and of earth dams, which are constructed on these arroyos (two reservoirs on Diablo Arroyo, one on Camp Rice Arroyo, and three on Alamo Arroyo, fig. 28), suggests that surface water flow occurs regularly in this area. Residents (S. Wilkey and D. Walker, personal communication, 1986) say that these reservoirs receive water every year by August or September and hold water until January or February. No records of water depths in these reservoirs were available. Active floodplains are indicated in plate 4 (U.S. Department of Housing and Urban Development, Flood Insurance Administration, 1985a,b).

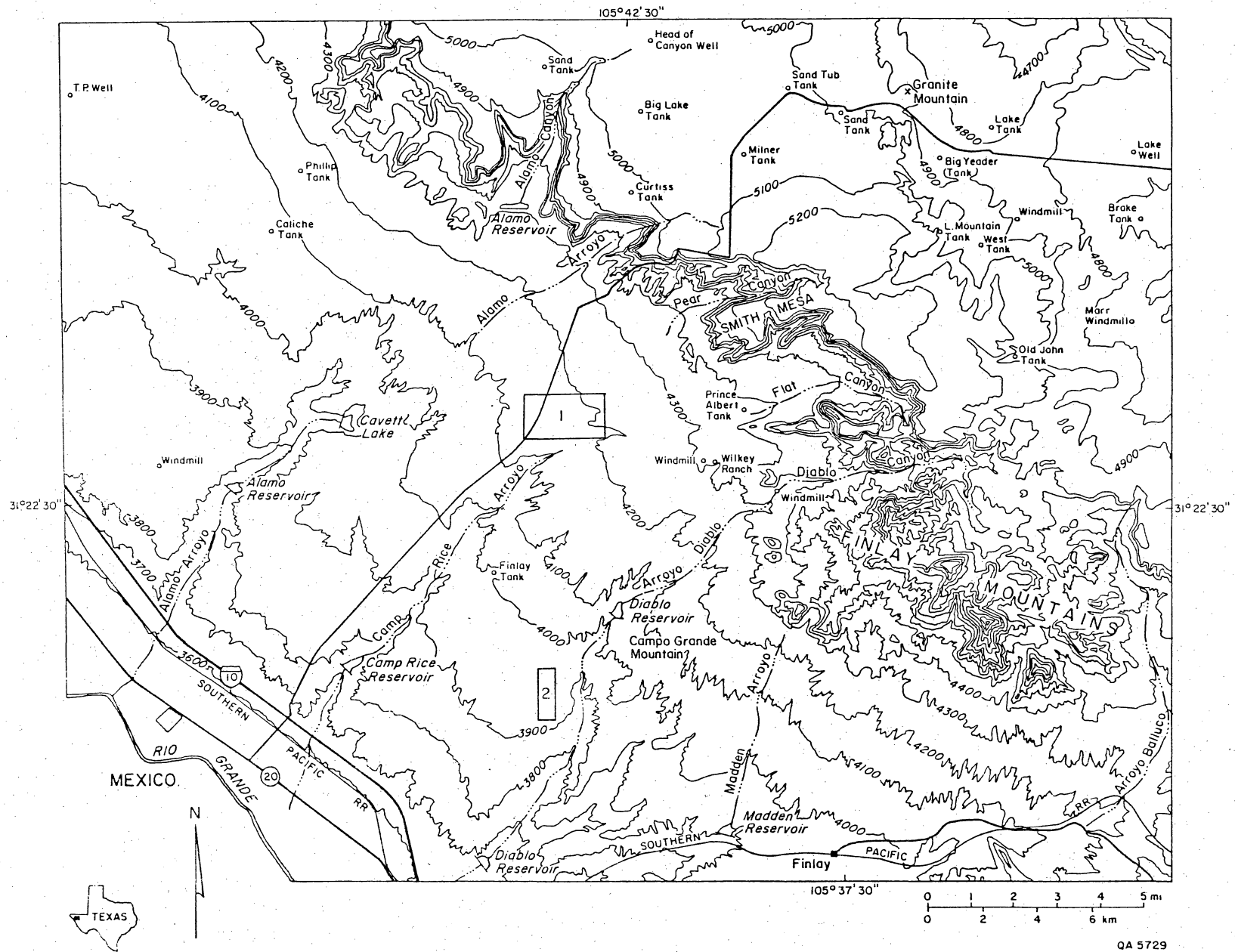


Figure 28. Base map of the Hudspeth County study area. Bold line approximately locates Sites S-34a and S-34b.

Hydrologic Setting

Three aquifers in Hudspeth County Cretaceous rocks form a plateau and underlie the lower area that is being considered for the potential site (fig. 28). Some of the wells in the plateau and the lower areas penetrate Cretaceous rocks of the Finlay, Cox, or Bluff Mesa Formations. It is not clear if there is one aquifer in the Cretaceous rocks or several aquifers in the various formations; for simplicity, the rest of this discussion will refer to only one aquifer in the Cretaceous rocks. Because of regional faulting and overthrusting, various parts of the aquifer west and south of the plateau may not be interconnected. A second aquifer occurs within the overlying Cenozoic bolson fill. Most of the wells in this aquifer pump from sand lenses that occur between the clays and silty clays in the older bolson fill. Basin and Range faults may cut the basin fill and cause hydrologic discontinuities in this aquifer. The bolson fill is characterized by a variety of clastic materials that pinch out or grade into materials of different grain size laterally and vertically, which could be another reason for hydrologic discontinuities (Guyton and Associates, 1971). Lateral continuity of the bolson fill at S-34 is discussed in the geologic investigations section. The third aquifer is in the young Quaternary Rio Grande alluvium that stretches along the Rio Grande from the El Paso area to Fort Quitman.

Water-bearing Characteristics

Cretaceous Formations

A minimum value of 27 gpd/ft ($0.33 \text{ m}^2/\text{d}$) was estimated for the transmissivity coefficient of the Cretaceous aquifer based on a short pumping test in the water well drilled at the site by the Texas Low-Level Radioactive Waste Disposal Authority (app. 3A). No data are available on the thickness of the saturated zone of the Cretaceous aquifer in the area.

Bolson Fill

The thickness of the bolson fill in the site is approximately 400 to 500 ft (122 to 152 m) thick and may increase significantly across the Campagrande fault toward the Rio Grande. Near Fabens, transmissivity of the bolson is 25,000 gpd/ft (310 m²/d), and the storativity coefficient is 0.0003 (Leggat, 1962). Near El Paso, where the artesian bolson-fill aquifer provides the city with large amounts of water, transmissivities range from 50,000 to 120,000 gpd/ft (620 to 1,500 m²/d), and the storativity coefficient is 0.0004. In situ permeability measurements in shallow boreholes within the unsaturated zone of the bolson fill indicate values of 0.25 inch/d (0.63 cm/d) for the upper 40 to 50 ft (12 to 15 m) of sand and gravels and 0.12 inch/d (0.32 cm/d) for the 100-ft (30-m) interval of clays and thin sand lenses below these gravels (app. 7). These values represent horizontal permeabilities and therefore reflect the higher values of the sand lenses in the section. Vertical permeability values, more critical for flow in an unsaturated section, would be expected to be lower. Dames and Moore (1985) reported clay permeability in a core sampled in their test hole at the site, and their value was 0.002 inch/d (5.8×10^{-8} cm/s, or 0.005 cm/d). URM analyzed 6 silty clay (less than 20% sand) bolson cores taken from borehole LLWA 7 (fig. 23a) for vertical permeability, and their results varied from 3.4×10^{-5} inch/d to less than 4.7×10^{-6} (1×10^{-9} cm/s to less than 5×10^{-11} , or 9×10^{-5} cm/d to less than 4.3×10^{-6}) (app. 8).

Total porosity values in the bolson fill were determined in four boreholes (7, 11, 12, and 13, fig. 23), using LDT-CNL cross plots (app. 10). They ranged between 16 and 54 percent. Lower values (16 to 30 percent) characterize the gravel cover, and higher values (45 to 54 percent) are typical of the older fine grained bolson beneath the gravels. Effective porosity in the older bolson is expected to be much lower.

Rio Grande Alluvium

Rio Grande alluvium is about 200 ft (60 m) thick (Alvarez and Buckner, 1980). The alluvium is permeable, but no aquifer tests are known to have been conducted within this aquifer. An assumed specific yield of 0.2 and a transmissivity value of 30,000 gpd/ft ($370 \text{ m}^2/\text{d}$) were used for this aquifer in the verification stage of the Hueco Bolson model study (Alvarez and Buckner, 1980).

Recharge

Cretaceous Formations

Recharge into the Cretaceous aquifer is predominantly from direct precipitation on the plateau. Tritium data from wells in the Diablo Plateau (such as Head of Canyon well or Wilkey No. 2 well, fig. 28) indicate the presence of a recent recharge component (as indicated by 11.8 and 20.67 TU) mixed with older recharge sources identified by ^{14}C analyses (resulting in a mixture that has 42 to 60 Percent Modern Carbon [PMC]) or corrected ^{14}C "age" of 833 to 865 yr) (fig. 29). However, water from Gunsight No. 1 well, which is located farther east in the Finlay Mountains, does not show any indications of recent recharge (0 TU, ^{14}C age of 13,071 yr, and the most depleted values of $\delta^{18}\text{O}$ and $\delta^2\text{H}$). This water sample may be regarded either as the end member of the older flow component in the Cretaceous aquifer in the plateau area or as a sample from a separate aquifer whose current recharge is very slow or nonexistent. Recharge may also occur where the Cretaceous crops out in arroyos that cut the Campagrande fault.

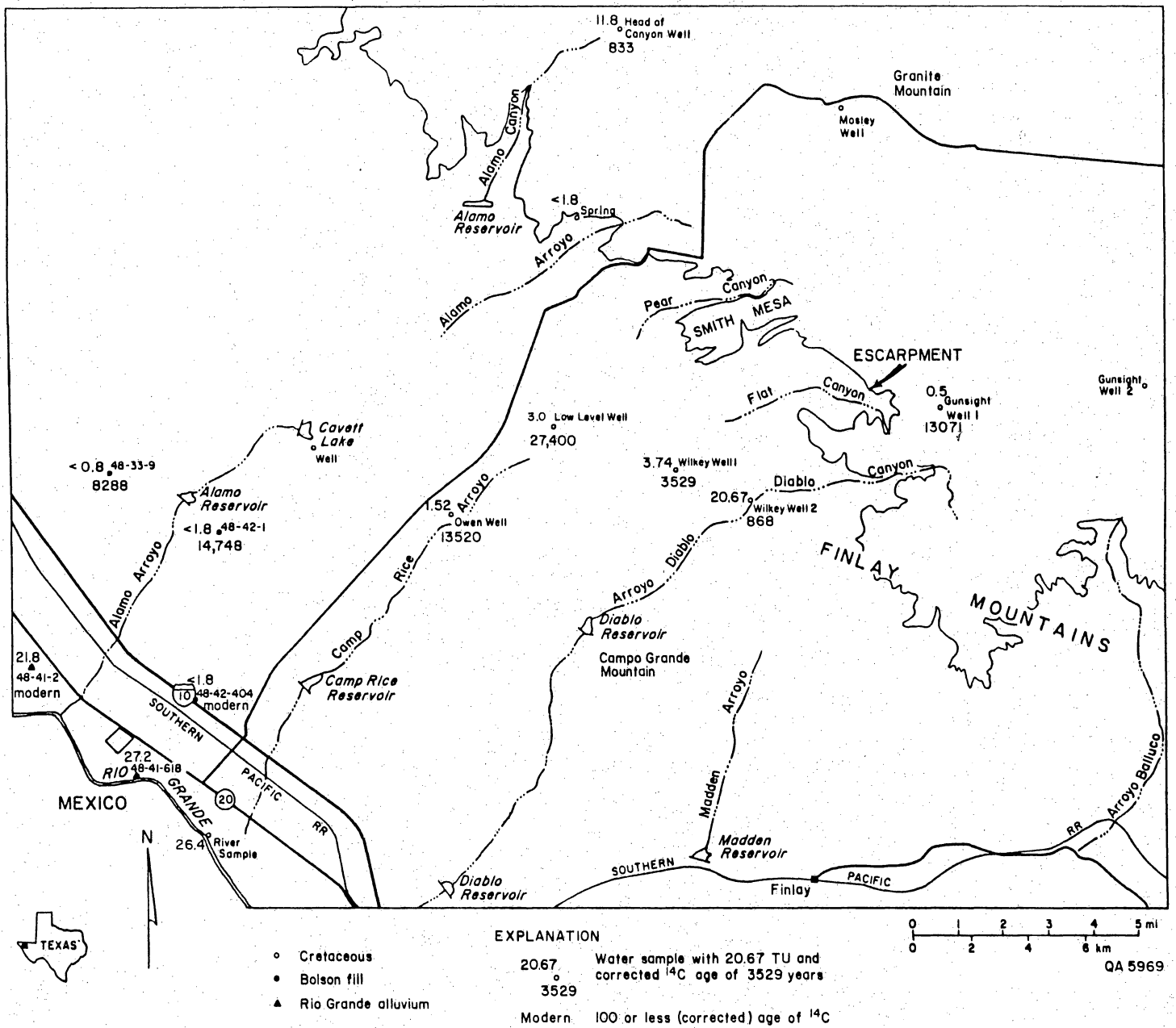


Figure 29. Tritium activity and ¹⁴C corrected ages in ground water of the Hudspeth County study area.

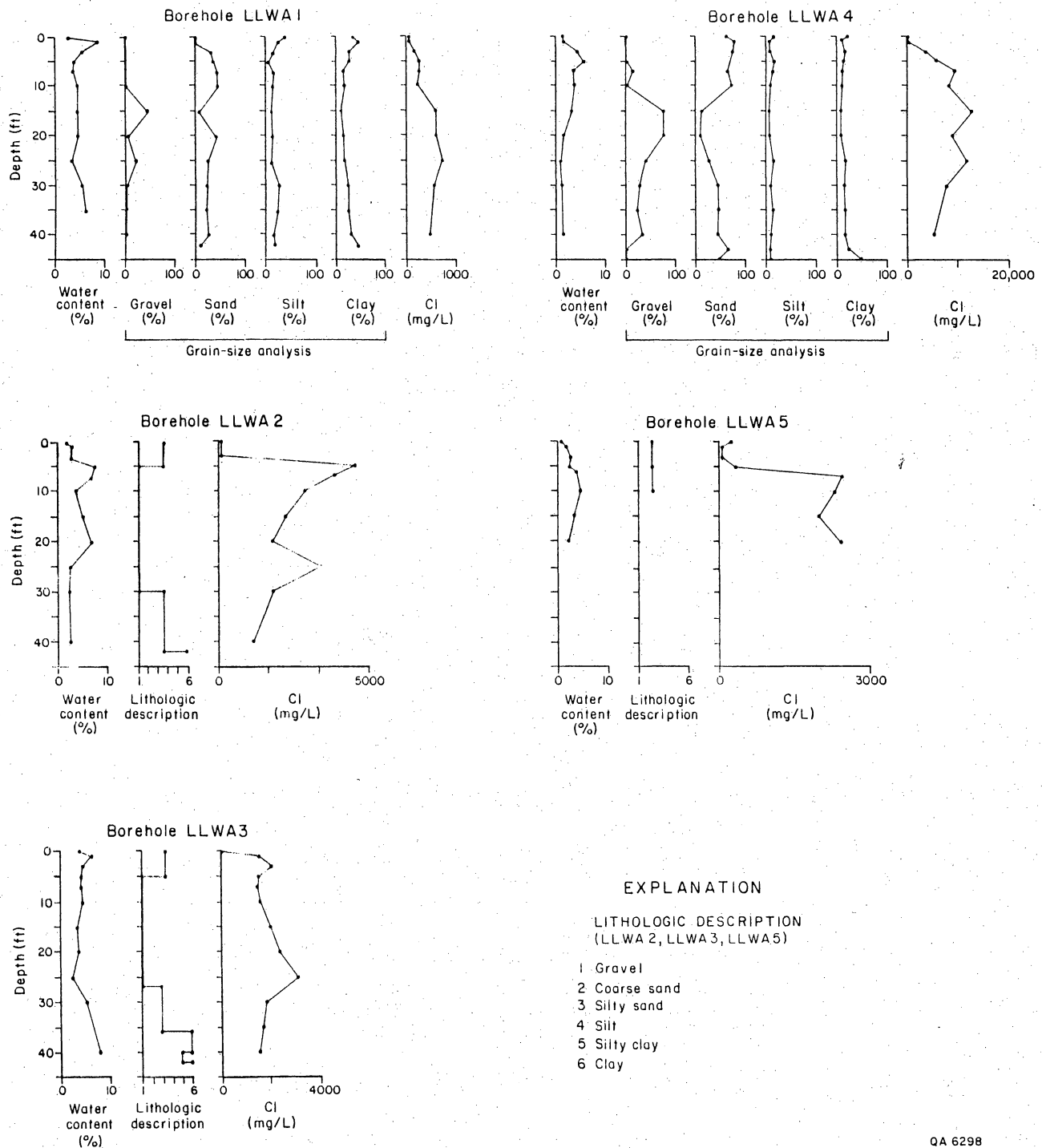
Bolson Fill

The bolson aquifer can be recharged by (1) precipitation that falls on the gravel veneer that covers the finer grained bolson fill, (2) surface water that flows during flash floods in the arroyos, (3) ground water moving upward from the underlying Cretaceous aquifer (Davis and Leggat, 1973), or by (4) ground water in the overlying Rio Grande alluvium, which may recharge bolson fill by vertical or lateral flow.

Recharge by upwelling water from the underlying Cretaceous aquifer is a possibility in the site area and its vicinity. Both Cretaceous and bolson aquifers contain old water, based on ^{14}C analyses ranging from 3,529 to 27,400 yr old in the Cretaceous wells (Wilkey No. 1 well, Low-level well, and Owen well) and from 8,000 to 15,000 yr old in the bolson wells (48-33-9 and 48-42-1). However, in the Rio Grande valley this is not a dominant recharge process. At bolson well 48-42-40, ^{14}C results indicate modern (less than 100 yr old) water, whereas the water from Cretaceous wells in the area is probably much older.

The annual rate of recharge through desert soils can be estimated by the distribution of chloride in the unsaturated soil zone. Qualitatively, if recharge rates are high, Cl is flushed from the soils. Conversely, if recharge is low due to low precipitation and high evaporation or low permeabilities, Cl will accumulate in the soil section, similarly to calcrete. In this study, recharge through the sand and gravel that overlie the bolson fill was estimated by the method of Allison and Hughes (1978). (See app. 11 for detailed description of techniques.) Samples of the sand and gravel (taken from five boreholes, LLWA 1 through 5, figs. 23a and 24a) augered by the BEG staff in the site area to total depth of 50 ft (15 m) were analyzed for chloride concentrations (app. 11). Chloride concentration in soil

profiles varied considerably from one borehole to another, ranging between 560 and 9,000 mg/L. Different distributions of chloride concentration with depth were observed in various boreholes (fig. 30). To determine the correlation between chloride distribution (and thereby the estimated recharge) and grain size of soil particles, soil samples from two boreholes (LLWA1 and 4, figs. 23 and 24) were analyzed for grain-size distribution (fig. 30). The soil profile of borehole LLWA1 has the lowest chloride concentration (560 mg/L), and no salinity peaks can be observed with depth. Chloride concentration of borehole LLWA4 is the highest (~9,000 mg/L), and several salinity peaks can be observed in the soil profile. According to grain-size analysis, clay and silt content is similar in both holes and therefore apparently chloride distribution and concentration do not depend on grain-size distribution of the soil profile. Topographic and flood-prone-area maps (figs. 23 and 24, pl. 4) show that borehole LLWA1 is located in one of the Alamo Arroyo tributaries and that flooding of this arroyo may result in higher recharge and lower chloride concentration. Conversely, borehole LLWA4 is located outside the flooded area of Arroyo Diablo, and therefore the chloride concentration and its distribution along the soil profile are not affected by the runoff in the arroyo. The calculated annual flux of rainwater into the gravels varies from a minimum of 0.0005 to 0.003 to a maximum of 0.009 to 0.05 inches with a mean ranging from 0.003 to 0.02 inches (0.07 to 0.5 mm). The higher values for estimated recharge represent arroyos that may be flooded more often, whereas the lower values are more typical of areas that are recharged only by direct precipitation. In the Southern High Plains, annual recharge calculated by similar methods (Stone, 1985) varied from 0.007 to 0.009 inches (0.18 to 0.24 mm). In the semiarid area of the River Murray, Australia, annual recharge calculated by this method ranged from 0.002 to 3.93 inches (0.06 to 100 mm) (Allison and others, 1985). Recharge of the fine-grained bolson fill beneath the gravel cover from water percolating from



QA 6298

Figure 30. Variations of grain size, water content, and chlorides in soil cores of five boreholes in the bolson gravel cover. Borehole location shown in figure 23.

the overlying sand and gravels along the area south and west of the Diablo Plateau has not yet been assessed. Annual flux is expected to be lower through the clays than through the sands and gravels. Bolson recharge may also occur by flood flow in the major arroyos and from the bottom of reservoirs such as the Alamo Reservoir.

In the Rio Grande valley, recharge occurs by the water stored in the Rio Grande alluvium that overlies the bolson fill near the Rio Grande. Both the Rio Grande and Rio Grande alluvium are characterized by modern ^{14}C activities and therefore agree with the ^{14}C data that indicate modern water in the bolson fill in the Rio Grande valley. However, bolson fill tritium data (0 TU in well 48-42-404) indicate that the bolson was recharged before 1952 and that the recharge process is slow.

Rio Grande Alluvium

Water in the Rio Grande alluvium is recharged by the water of the Rio Grande (Guyton and Associates, 1971; Davis and Leggat, 1973; Alvarez and Buckner, 1980). When the flow of the Rio Grande is sufficient, Rio Grande water is used for irrigation on the cultivated land adjacent to the river. Some of this water recharges the alluvium and then discharges to local drain canals and returns to the river. This assumption is supported by the rise of water levels in the aquifer since irrigation with river water began (Guyton and Associates, 1971) and by the results of ^{14}C and tritium analyses of water sampled from the Rio Grande and from wells that penetrate the Rio Grande alluvium. The water in the Rio Grande alluvium shows high ^{14}C and high tritium activities (21.8 and 27.2 TU), similar to the Rio Grande water (24.4 TU) (fig. 29).

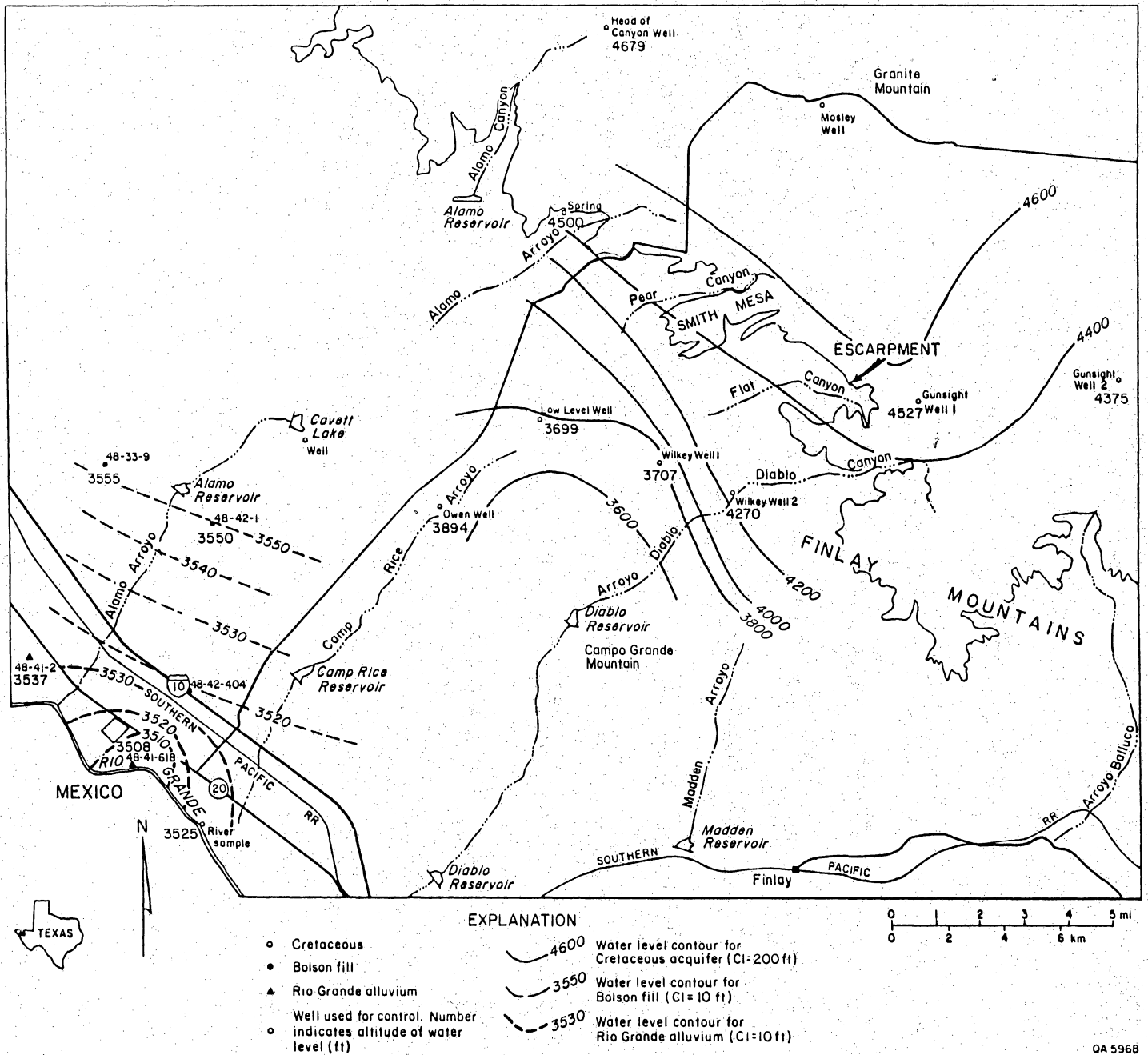
Discharge

Cretaceous Formations

Discharge from the Cretaceous aquifer occurs through pumpage from a few water wells that penetrate the aquifer and possibly through natural outlets such as leakage into the overlying bolson fill and Rio Grande alluvium in the Rio Grande valley. Amount of discharge into the Rio Grande alluvium or bolson fill in this area cannot be evaluated because no Cretaceous wells are located within the Rio Grande valley and therefore the difference between the potentiometric surface of the water in the Cretaceous aquifer and the water levels in the overlying aquifers in this area is unknown. If such vertical leakage occurs, it must be very small because in the Rio Grande valley water in both bolson and alluvium aquifers is modern, whereas water in the Cretaceous aquifer beneath the bolson fill is relatively old (fig. 29, app. 2). Discharge from the Cretaceous aquifer into the bolson fill at the site area and its vicinity is possible, considering the low tritium activities and old ^{14}C ages observed in two wells that pump from the bolson (48-33-9 and 48-41-1).

Bolson Fill

Discharge from the bolson fill occurs through pumpage from a few wells in the site area (toward the northwest the bolson fill is a major water supply source for the El Paso area). Water levels in the bolson fill (fig. 31) near the Rio Grande are similar to those in the Rio Grande alluvium and may suggest interconnectedness between both aquifers.



QA 5968

Figure 31. Potentiometric surfaces of ground water in the aquifers in S-34 study area (ft).

Rio Grande Alluvium

Water from the Rio Grande alluvium discharges (1) by evapotranspiration through the shallow water table or the crops, (2) through pumping wells, (3) through return flows into the Rio Grande by drainage channels, and (4) by leakage into the bolson fill.

Potentiometric Surface

Cretaceous Formations

The potentiometric surface of the water in the Cretaceous rocks (fig. 31) ranges between 4,679 ft (1,427 m) at the Diablo Plateau, where water flow is assumed to be under water-table conditions, to 3,745 ft (1,142 m) at the site area, where water is confined by the bolson fill. Ground water flows from the plateau toward the southwest. Potentiometric surface gradient ranges from 42 ft/mi (8 m/km) in the water-table area to 327 ft/mi (63 m/km) in the confined water area. The large gradient in the confined water zone may not reflect a decline in a potentiometric surface of a continuous aquifer but may indicate two hydrologic systems separated by possible faulting along the escarpment of the Diablo Plateau. Another possibility is that the aquifers that are exposed at the Diablo Plateau (Cox and Finlay Formations) are truncated and that the Cretaceous aquifer beneath the bolson fill south and west of the plateau is in the deeper Bluff Mesa Formation. Calculated horizontal flow velocity based on ^{14}C data (Vogel, 1970) is 2.8 ft/yr (0.85 m/yr), assuming a continuous aquifer.

Bolson Fill

Ground-water flow in the bolson aquifer is probably under water-table conditions south and west of the Diablo Plateau. Water may be confined in the Rio Grande valley, where the Rio Grande alluvium aquifer overlies the bolson

aquifer (Alvarez and Buckner, 1980). Sixty mi (90 km) to the north and west in the El Paso area, the water in the bolson is artesian (Alvarez and Buckner, 1980). Near Fabens, where the bolson fill is very thick (20 mi [30 km] to the northwest), a second artesian water zone was reported at a depth of 1,300 ft (400 m) (Alvarez and Buckner, 1980). The potentiometric surface of the water in bolson fill within the study area (fig. 31) ranges from 3,555 to 3,520 ft (1,084 to 1,073 m). Ground water follows the regional dip from northeast to southwest with a rather small gradient of 8.6 ft/mi (2.6 m/km). In the vicinity of the study area, water levels in the bolson aquifer are lower than in the underlying Cretaceous aquifer by 200 to 300 ft (60 to 90 m) and have water levels similar to those in the Rio Grande alluvium aquifer. It is assumed, therefore, that in the area of Fort Hancock, the bolson fill and the Rio Grande alluvium aquifer are hydrologically connected (Alvarez and Buckner, 1980).

Rio Grande Alluvium

Ground water in the Rio Grande alluvium aquifer flows under water table conditions along the Rio Grande valley from northwest to southeast (fig. 31; Alvarez and Buckner, 1980). Near Fort Hancock, the gradient of the water table is about 8 ft/mi (1.6 m/km). Water levels have risen since irrigation with Rio Grande water began in 1916 and it became necessary to construct drains. Water levels in the aquifer now fluctuate with the availability of Rio Grande water for irrigation. Ground-water levels decline as a result of intensive pumpage from the aquifer but recover when the flow in the river is at a higher stage. As a result, no long-term declines of water levels are encountered in the aquifer.

Ground-water Geochemistry

Cretaceous Formations

Ground water in the Cretaceous aquifer is slightly brackish, having total dissolved solids (TDS) of 801 to 1,850 ppm (fig. 32). Along the flow path from the escarpment to the confined ground-water zone south and west of it, water facies change from Na-mixed-cations or Ca-mixed-cations in the outcrop area (in Head of Canyon well, Thaxton Spring, and Wilkey No. 2 well) to Na-SO₄ facies in the confined water zone (Wilkey No. 1 and Owen wells) (fig. 33). These changes are also accompanied by increasing temperatures and age of ground water, reflected by a decrease of tritium activity from 20.67 and 11.8 TU (Head of Canyon and Wilkey No. 2 wells, respectively) to 3.75 and 1.52 TU (Wilkey No. 1 and Owen wells) and an increase in ¹⁴C ages from about 800 yr in the outcrop area to 27,000 yr in the confined water zone (figs. 29, 34, and 35). $\delta^{18}\text{O}$ and $\delta^2\text{H}$ values (figs. 36, 37, and 38) are heavier at the Diablo Plateau (Head of Canyon or Wilkey No. 2 wells) and become lighter along flow paths. Gunsight No. 1 well, with very light $\delta^{18}\text{O}$ and $\delta^2\text{H}$ values, is an exception in the plateau area. The above-mentioned changes in water chemical facies could result from evolution of the water chemistry from the recharge zone into the confined water zone but may also indicate a hydraulic discontinuity along the flow path of water in the aquifer resulting from faulting or separate aquifers.

It is important to note that even the water samples in the confined water zone (Wilkey No. 1 and Owen wells) that represent relatively old water (3,530 and 13,520 yr based on low ¹⁴C activities) have a small amount of tritium that may indicate recharge sources other than ground water flowing all the way into the Cretaceous rocks from the outcrop area. Vertical movement

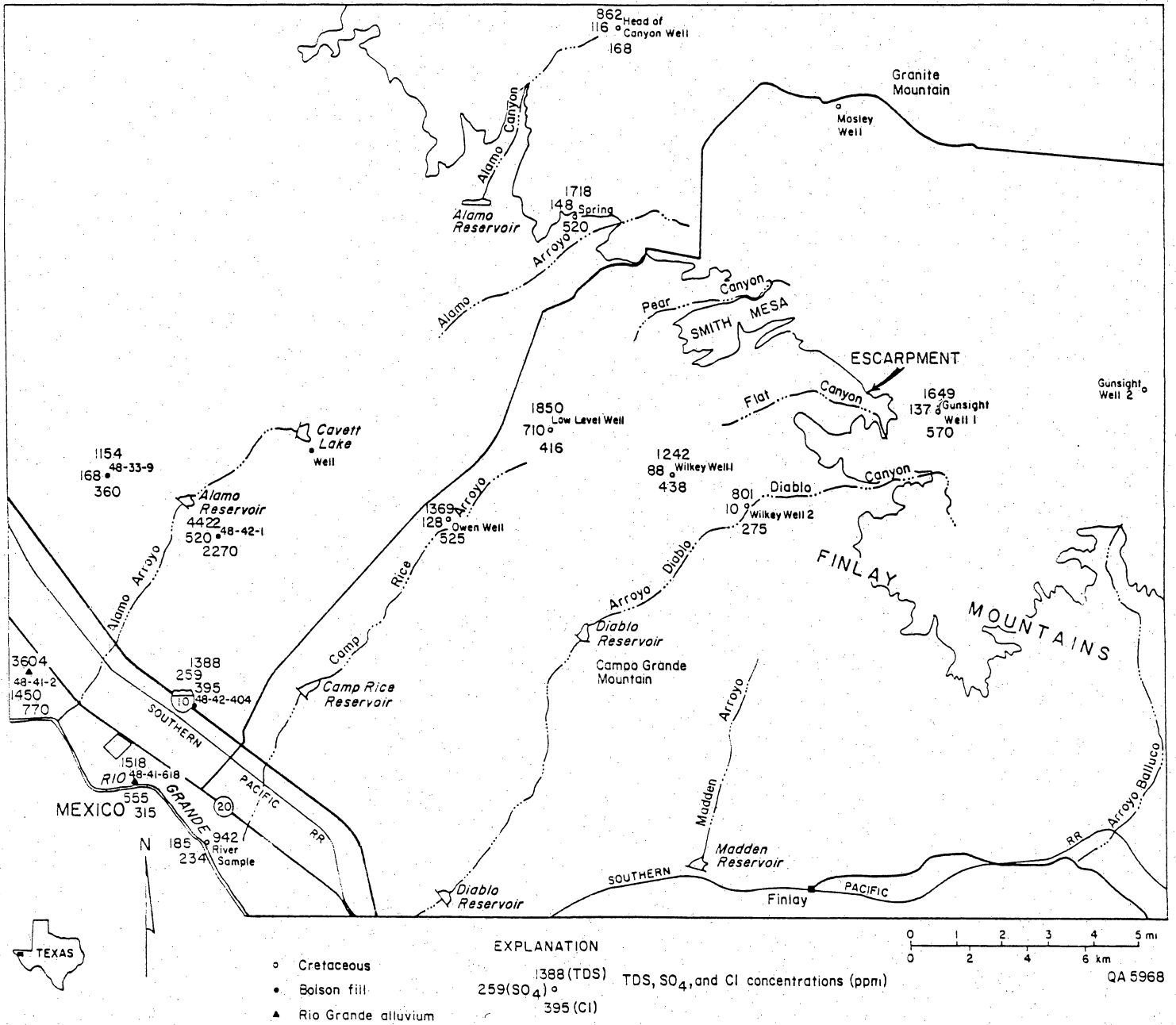


Figure 32. Total dissolved solids (TDS), SO₄²⁻, and Cl⁻ (mg/L) distribution in ground water of Hudspeth County study area.

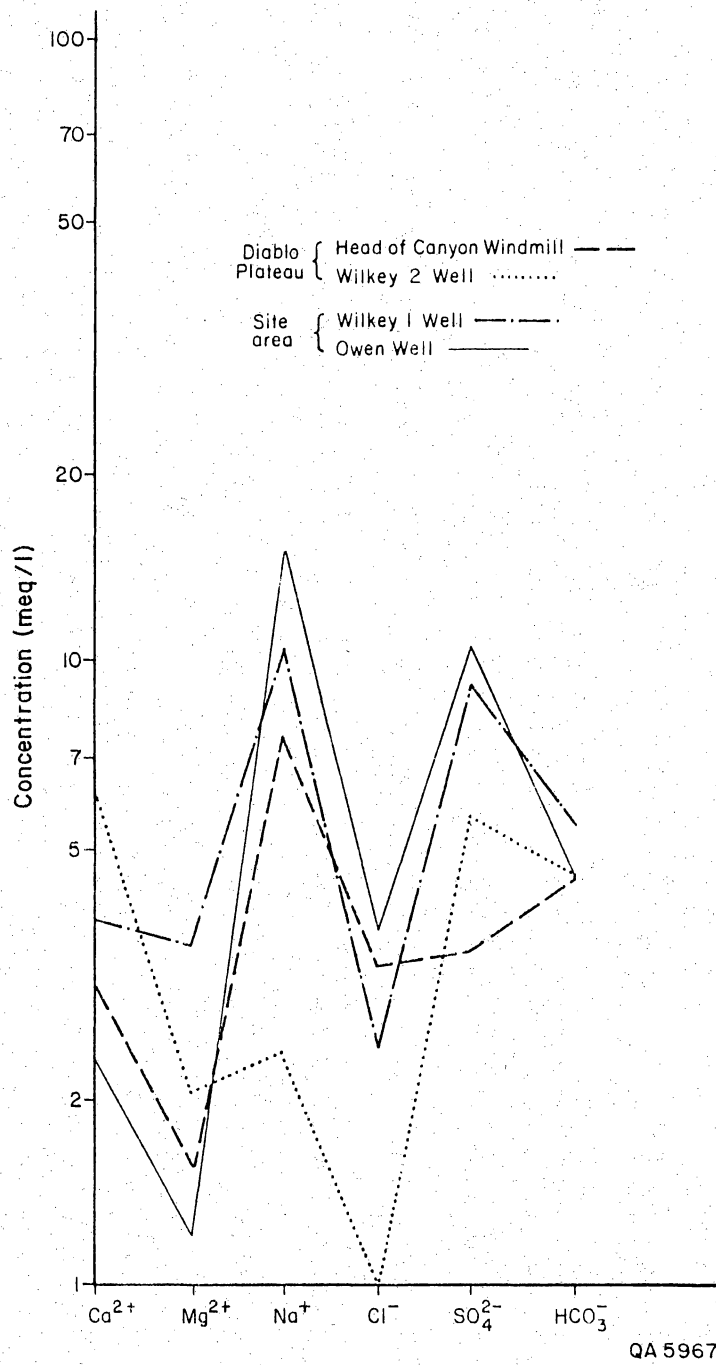


Figure 33. Salinity diagram of ground water from the Cretaceous aquifer in the S-34 study area. Well location is shown in figure 32.

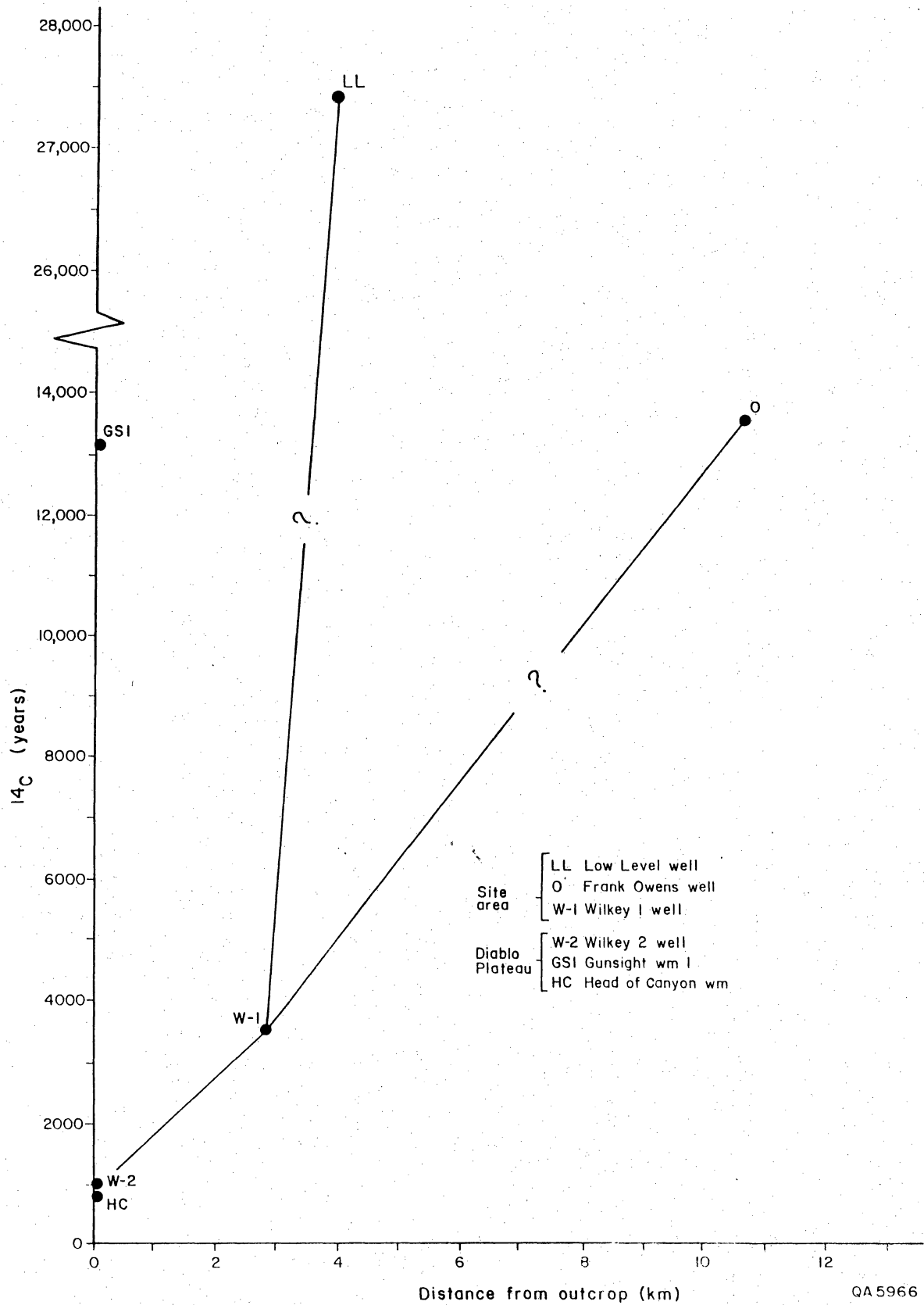


Figure 34. ^{14}C activity (yr) in ground-water samples of the Cretaceous aquifer versus the distance (km) from the recharge area at the Diablo Plateau. Well location is shown in figure 29.

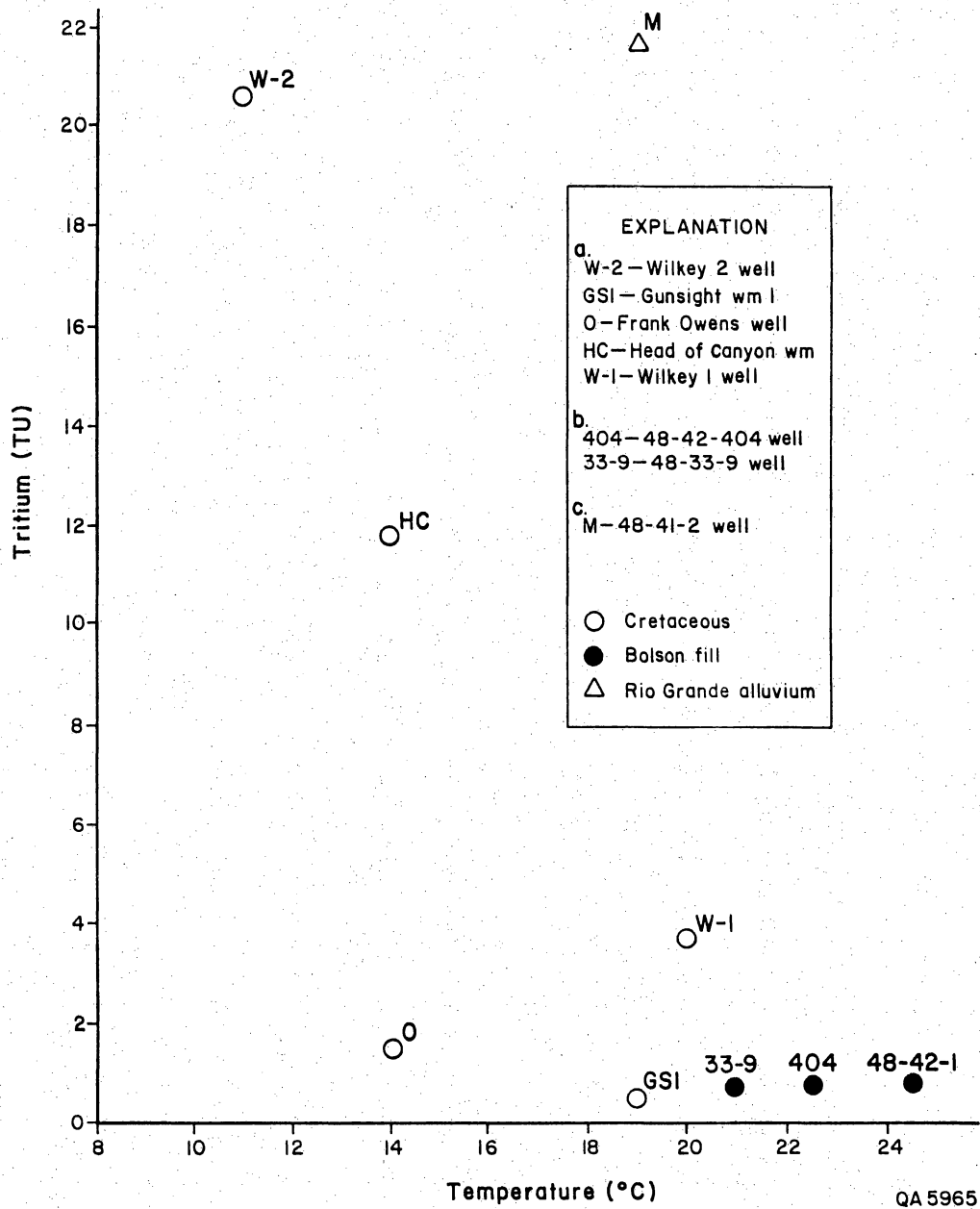
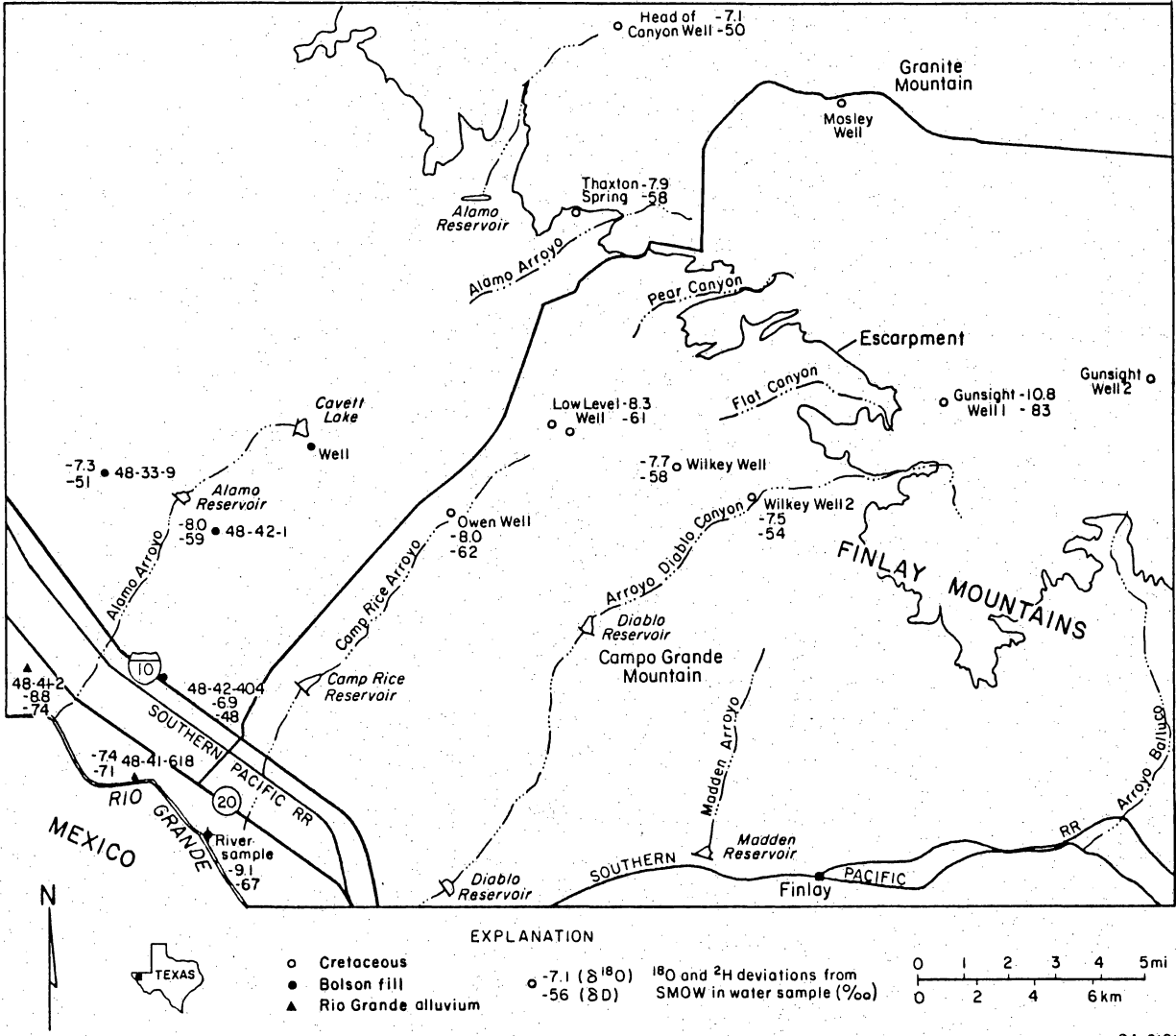
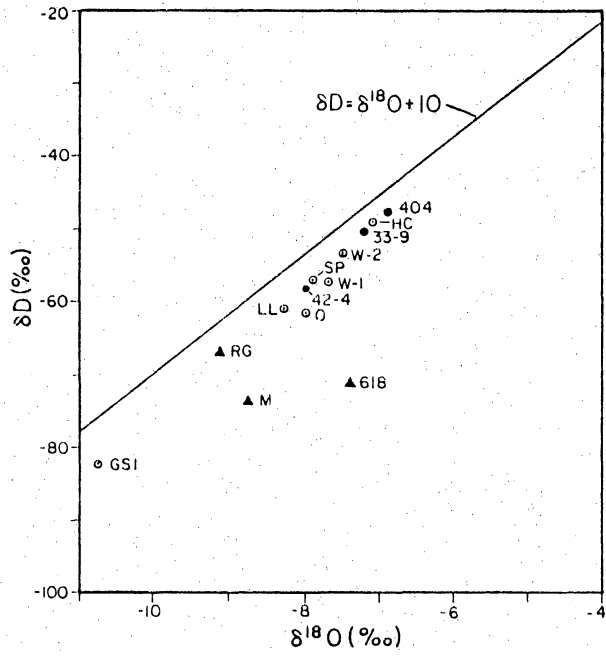


Figure 35. Tritium activity (TU) versus temperature (°C) in ground-water samples in S-34 study area. Well location is shown in figure 29.



QA 6121

Figure 36. $\delta^{18}\text{O}$ and $\delta^2\text{H}$ distribution in ground water in S-34 study area (in ‰/‰ deviation from SMOW).



EXPLANATION

<i>a</i>		<i>b</i>	
WS-1	Wilkey 1 Well	404	48-42-404 Well
WS-2	Wilkey 2 well	33-9	48-33-9 Windmill
GS-1	Gunsight 1 Windmill	42-4	48-42-4 Windmill
O	Frank Owens Well	<i>c</i>	
HC	Head of Canyon Windmill	M	48-41-2 Well
LL	Low Level Well	618	48-41-618 Well
SP	Thaxton Spring	RG	Rio Grande water

○ Cretaceous(a) ● Bolson fill(b) ▲ Rio Grande alluvium(c)

QA-6119

Figure 37. $\delta^{18}\text{O}$ versus $\delta^2\text{H}$ (‰) in ground water of S-34 study area (in ‰ deviation from SMOW). Well location is shown in figure 36.

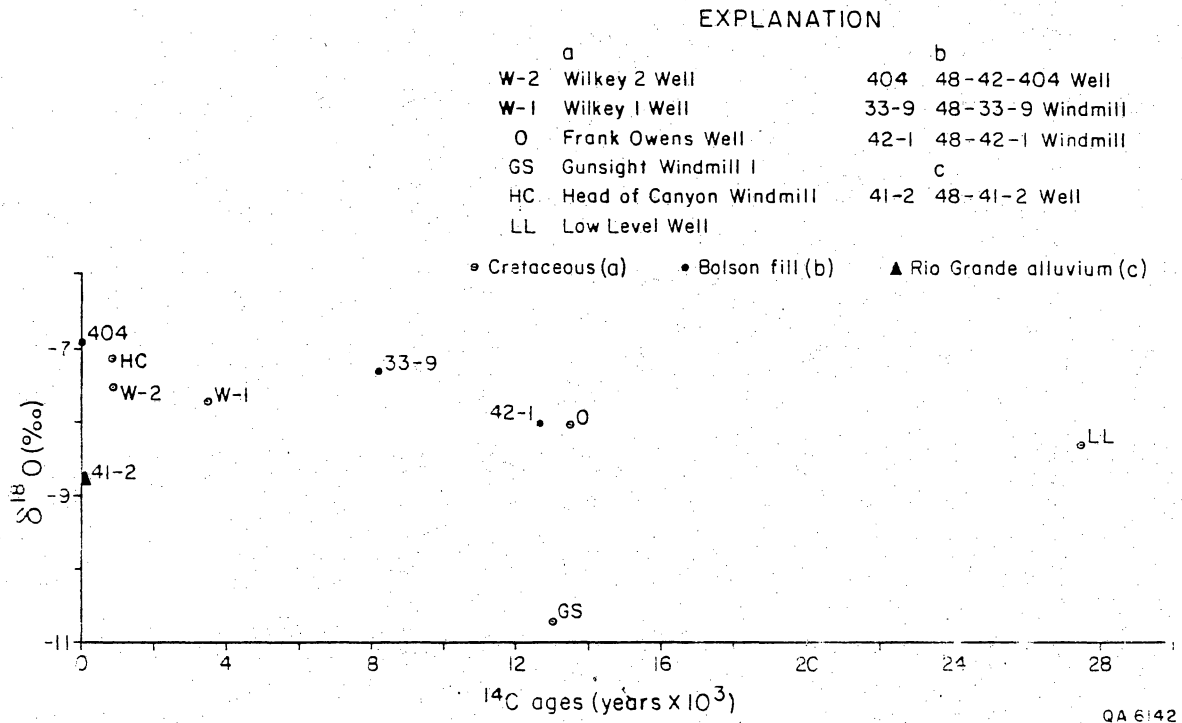


Figure 38. $\delta^{18}\text{O}$ (‰) versus ^{14}C corrected ages (yr) in ground water of S-34 study area. Well location is shown in figure 36.

of water through the bolson fill probably cannot account for the fast recharge rate needed to preserve tritium in ground water at the site.

A water flux range of 0.003 to 0.02 inches/yr (0.07 to 0.5 mm/yr) was calculated for the upper permeable veneer of gravels, whereas most of the bolson has lower permeabilities. Even with these relatively high values, it would take more than 6,000 yr to get water from land surface across the unsaturated section of 485 ft (148 m) into the Cretaceous. By that time, no tritium can be preserved in ground water. If the Campagrande fault zone is permeable, it could provide a shortcut for some recent recharge from surface water and precipitation into the aquifer.

Another interesting observation is the different chemical and isotopic features of the water sampled in Gunsight No. 1 well. The well is located in the outcrop area, but nevertheless its water exhibits characteristics of old water (0.5 TU and ^{14}C age of 13,071 yr), with Na-SO_4 chemical facies similar to the water in the confined water zone and the most depleted $\delta^{18}\text{O}$ and $\delta^2\text{H}$ values (-10.8 ‰ and -83 ‰, respectively).

Bolson Aquifer

Water in the bolson aquifer is brackish, with TDS varying from 1,154 to 4,421 ppm (fig. 32). Its chemical facies vary from Na-mixed-cations type to Na-SO_4 type (fig. 39). Brackish Na-SO_4 water was also found in the deep bolson aquifer near Fabens, northwest of Fort Hancock (Guyton and Associates, 1971). Ground water in the Cretaceous aquifer that underlies the bolson fill has similar Na-SO_4 water facies. Soluble material in the fine-grained, predominantly playa-lake deposits and the low level of interconnectedness between the sandy lens that



Figure 39. Salinity diagram of ground-water samples of the bolson-fill aquifer in the S-34 study area. Well location is shown in figure 32.

prevents efficient flushing of the salts from the bolson fill probably account for the mineralization of the water in this aquifer (Gates and others, 1980). Where horizontal movement is restricted, increase in dissolved salts may occur because there is no lateral influx of fresh water. Where vertical movement is constrained, zones of saline water may occur above or below zones of fresher water (Alvarez and Buckner, 1980). The tritium and ^{14}C activities of the water in the bolson aquifer near the site area indicate a very long residence time of ground water in the aquifer (8,000 to 15,000 yr and 0 TU), whereas in the Rio Grande valley they indicate recharge that occurred between 35 and 100 yr ago (0 TU and modern water, app. 2).

Rio Grande Alluvium

Water in the Rio Grande alluvium is more saline than water in the bolson aquifer, and in the study area TDS varies between 1,500 and 7,500 ppm (fig. 32; Alvarez and Buckner, 1980, their fig. 12). Water in the Rio Grande alluvium is fresher to the northwest (Alvarez and Buckner, 1980). Irrigation with Rio Grande water is probably the cause of the high salinities. The river is the source of and sink for irrigation water in the valley. Water is pumped from the river, but tail water and any ground water above a certain level in the alluvium drain back to the river by the open channels. The tail water is typically more saline than other water because of evapotranspiration and, as a result, contributes more minerals into the Rio Grande alluvium in this area. All chemical analyses of water from wells completed in the Rio Grande alluvium sampled for this study or older analyses taken from the Texas Water Commission files indicate Na-Cl chemical facies (fig. 40) and support the assumption that the salinity source is evaporation of recycled water and evapotranspiration. The tritium and ^{14}C activities of water

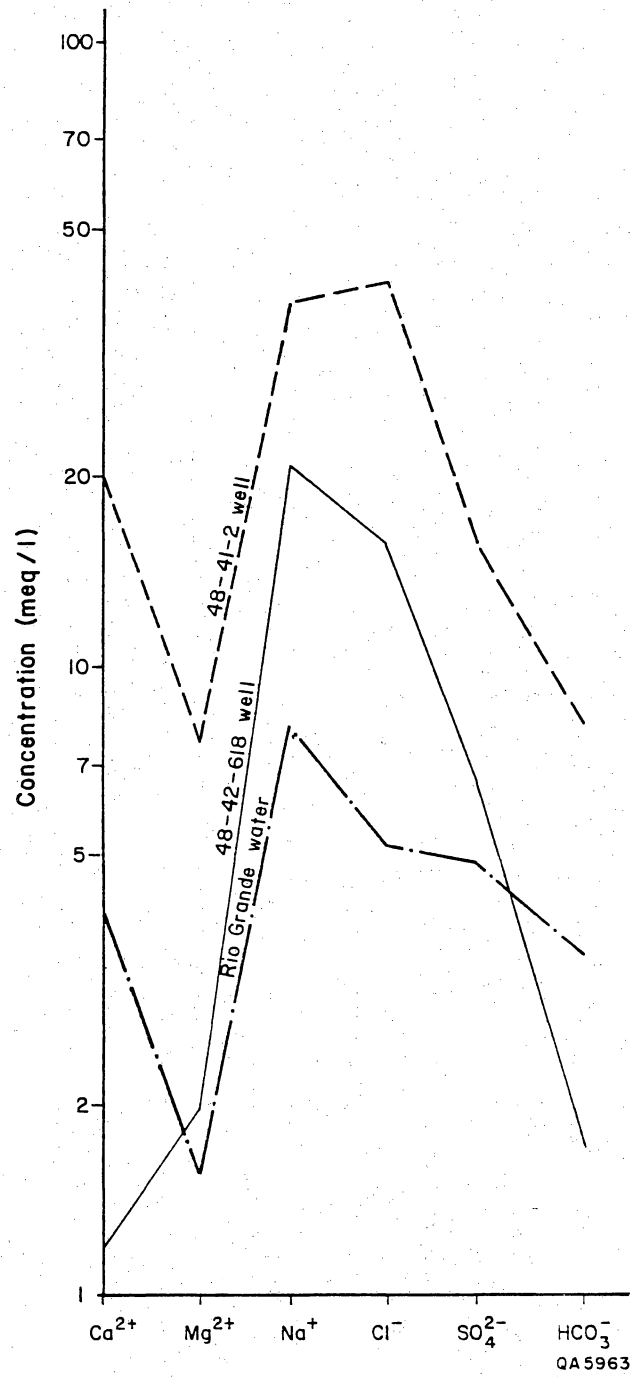


Figure 40. Salinity diagram of ground-water samples of the Rio Grande alluvium in the vicinity of the S-34 area. Well location is shown in figure 32.

from the aquifer (fig. 29) suggest a very fast recharge rate from the river (modern water having 21.8 and 27.2 TU, whereas the river has 24.4 TU). The Rio Grande alluvium water chemistry suggests that not much bolson-fill water is mixing with alluvium water; water-level data of Rio Grande alluvium suggest that mixing is possible.

Summary

Based on the geochemistry of the water in the Cretaceous, bolson, and Rio Grande alluvium aquifers, the Cretaceous and bolson formations appear to contain the oldest water but still receive some current recharge in areas that allow faster movement of water. Hydraulic discontinuity in the Cretaceous and bolson aquifers as a result of faulting is possible. According to geochemical and isotopic data, there is a possibility of upward movement of water from the Cretaceous aquifer into the bolson aquifer (this movement may also be hypothesized based on differences in potentiometric surfaces between these aquifers). On the other hand, water from the Rio Grande alluvium aquifer, mainly replenished by the Rio Grande, possibly recharges the bolson aquifer in the Rio Grande valley. Recharge to the bolson is slower than recharge to the Rio Grande alluvium aquifer and is governed by the lower permeabilities of the bolson fill.

Site-specific Hydrologic Features

No ground water was encountered in the bolson fill in the site area. The permeability and porosity of the bolson fill are expected to be heterogeneous because of the lenticular nature of the bolson clastics. Annual recharge from precipitation into the gravel cover of the bolson was estimated to range from 0.003 to 0.02 inches/yr (0.07 to 0.5 mm/yr). No information is available now about the recharge rate into the finer bolson sediments below the gravels. Another source of

recharge into the bolson fill in the site area is flash floods in the Alamo and Camp Rice Arroyo that drain the land surface toward the Rio Grande valley.

The only aquifer observed at the site is the Cretaceous. Two wells are located near the site area (Wilkey No. 1 and Owen wells). Aquifer thickness is unknown. The aquifer is confined in the site area and its potentiometric surface is 478 ft (145.7 m) below land surface. Estimated age of the ground water in the Cretaceous aquifer near and at the site area ranges from 3,500 and 27,400 yr old, which may suggest either a very low permeability of the aquifer or a hydraulic disconnection as a result of the regional fault. However, the presence of a small amount of tritium in the ground water may indicate shortcut paths of recent recharge. Water from the well that was drilled at the site is Na-SO_4 and brackish (TDS=1,850 ppm). Ground water flows from the site area to the southwest toward the Rio Grande valley. A small part of the site was indicated as a flood-prone area. Based on an earlier geologic reconnaissance, the site area was mapped as being within the extended outcrop of major and minor aquifers (Dames and Moore, 1985, their fig. 3.2). The hydrochemical, potentiometric, and geologic data from this investigation, however, suggest no significant hydrologic connection between the bolson deposits in the site area and the bolson deposits closer to the Rio Grande, where it is used as a water supply.

HUECO BOLSON - HUDSPETH COUNTY--CONCLUSIONS

The S-34 study area is underlain by bolson-fill sediments deposited on Cretaceous bedrock. Older bolson-fill deposits consist of a series of interbedded fine

sands, silts, and clays. Younger bolson deposits contain coarser sediments, including conglomerates, whose upper surface has been eroded to form a pediment surface. The only absolute date on the bolson deposits, about 2 million yr, is from an ash bed near the base of the younger bolson fill. Total thickness of the bolson fill is variable due to the highly irregular surface of the Cretaceous bedrock but is about 400 ft (120 m) or more thick in the vicinity of the primary study area.

The bolson-fill sediments are cut by the Campagrande fault. The Campagrande fault is a relatively discrete, easily mappable high-angle normal fault that strikes northwesterly across the bolson-fill deposits south of the S-34 area. Several meters of displacement are present in the older bolson fill, but the amount of displacement of the younger bolson deposits and the age of last movement along the fault are unknown. Other faults are present in Cretaceous rocks exposed along the margin of the Diablo Plateau and in the outcrops of the Finlay Mountains area.

Conclusions on the hydrogeology of the Hudspeth County site are as follows:

(1) Three regional aquifers, located in the Cretaceous rocks, the bolson fill, and the Rio Grande alluvium, occur in the study area.

(2) The uppermost aquifer near the site area is the bolson fill, but at the site no water was encountered in its sediments while drilling the water well. However, within a few miles of the site area, water levels in the bolson fill vary from 90 to 360 ft (27 to 110 m) below land surface. In the site area, the uppermost aquifer is in the Cretaceous formations, 478 ft (145.7 m) below land surface.

(3) Flow direction of the water in the Cretaceous and bolson aquifers is to the southwest toward the Rio Grande valley. The Campagrande fault may isolate aquifers beneath the site from aquifers in the Rio Grande valley. Flow direction in

the Rio Grande alluvium is along the valley and parallel to the river. Flow directions in the Rio Grande alluvium fluctuate depending on whether ground water or river water is being used for irrigation.

(4) Residence time of water in the Cretaceous aquifer varies from hundreds to thousands of years. The water in the bolson is old near the site area (8,000 to 15,000 yr) and modern (40 to 100 yr old) in the Rio Grande valley; the water in the Rio Grande alluvium is the current Rio Grande water.

(5) Recharge to the Cretaceous aquifer is from precipitation on the Cretaceous outcrop area. Presence of tritium in water of the Cretaceous aquifer beneath the bolson suggests mixing of young water with an older component of ground water. In the Rio Grande valley recharge to the Rio Grande alluvium and the bolson aquifers is through the Rio Grande. Recharge from the Cretaceous aquifer into the bolson fill in the vicinity of the site is a reasonable possibility based on the differences in potentiometric surfaces and on chemical and isotopic similarities. Based on the very low vertical permeability core values, vertical diffusion of rainwater into the bolson through the clays is extremely low. However, the presence of sand lenses and perhaps faults can result in shortcuts for vertical movement of water into the system.

(6) Ground water is pumped from the Rio Grande alluvium, the bolson fill, and the Cretaceous aquifers in the study area and its vicinity. Hydraulic continuity probably exists between the bolson and the Rio Grande alluvium in the Rio Grande valley, and the alluvium water discharges into the river. Water in the Cretaceous aquifer probably does not discharge into the upper aquifers in the Rio Grande valley because of the Campagrande fault. In the site area, chemical and isotopic similarities suggest that water in the Cretaceous discharges into the bolson fill.

DIABLO PLATEAU, HUDSPETH COUNTY INVESTIGATIONS

Location

The Texas Low-Level Radioactive Waste Disposal Authority selected two sites (HU1A and HU1B) within Hudspeth County, Texas, for consideration as the location of a low-level radioactive waste repository. The sites are on land owned and administered by The University of Texas System and are located approximately 15 mi (24 km) west of the Salt Basin in the vicinity of the Pump Station Hills on University Block K, sections 5, 6, 7, and 8, and University Block N, sections 16, 17, 31, 32, and 33, respectively (fig. 41). HU1A and HU1B are in the Hueco Station and Scratch Ranch 7.5-minute quadrangles, respectively. Site HU1A is 2 mi (3 km) south of the intersection of U.S. Highway 62-180 and Ranch-to-Market Road 1111. Site HU1B is about 1.5 mi (2.4 km) south of Scratch Ranch. Precambrian rhyolite porphyry bedrock is partly covered by alluvium at HU1A, whereas at HU1B alluvium covers Cretaceous limestone interbedded with some sandstone and mudstone. Both sites can be accessed from Ranch-to-Market Road 1111.

Methods

Aerial photographs at a scale of 1:12,000 (1 inch = 1,000 ft, 1 cm = 120 m) were acquired for a large area in the vicinity of the sites. Interpretations of aerial photographs were compared with published maps and refined through field studies. Fracture data were also collected.

Water-level data for the regional aquifers near the proposed sites were collected from several sources and are presented in appendix 1. Thirty-five static water-level

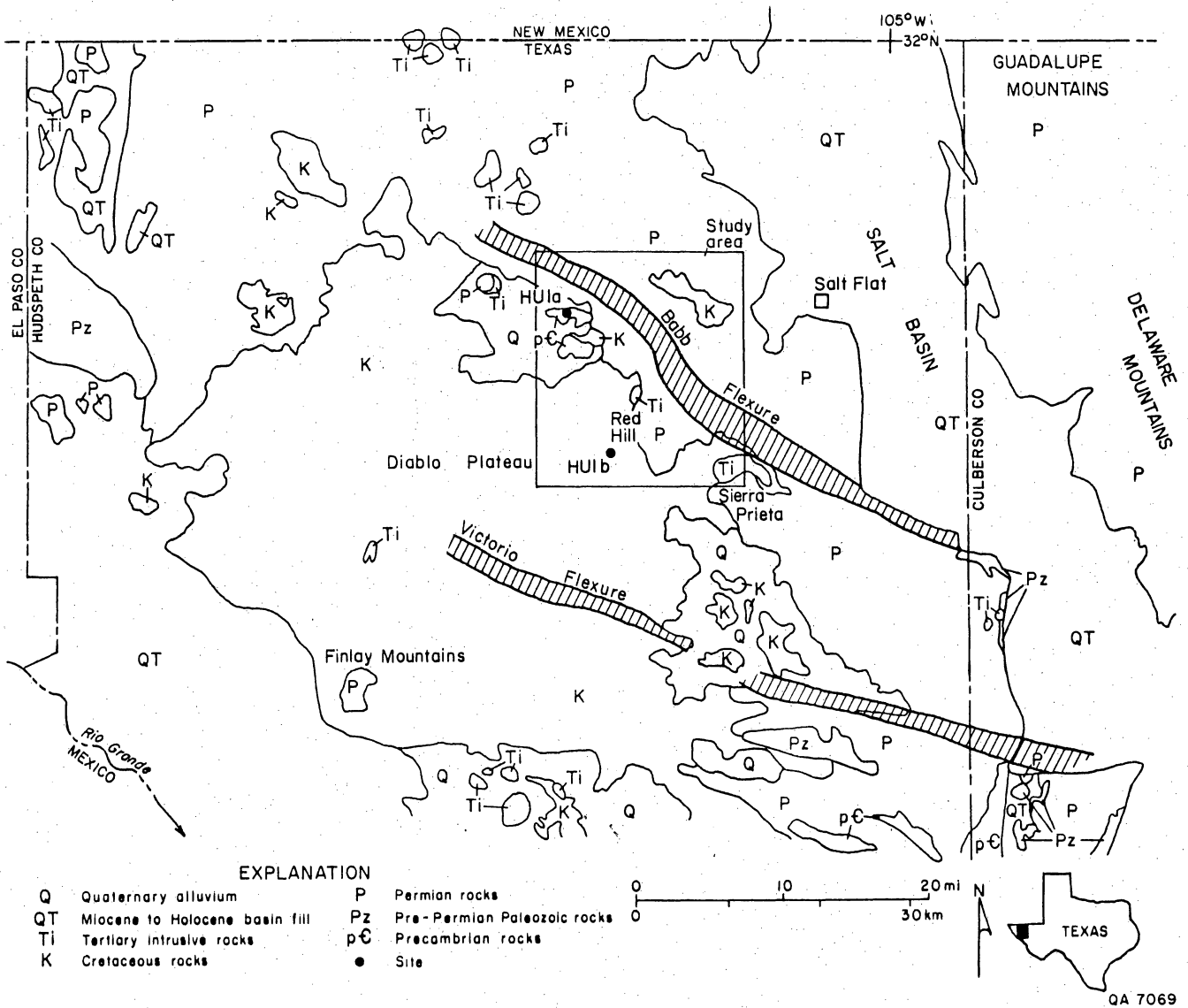


Figure 41. Location and regional setting of Pump Station Hills study area, Hudspeth County, Texas. Geology from Henry and Price (1985).

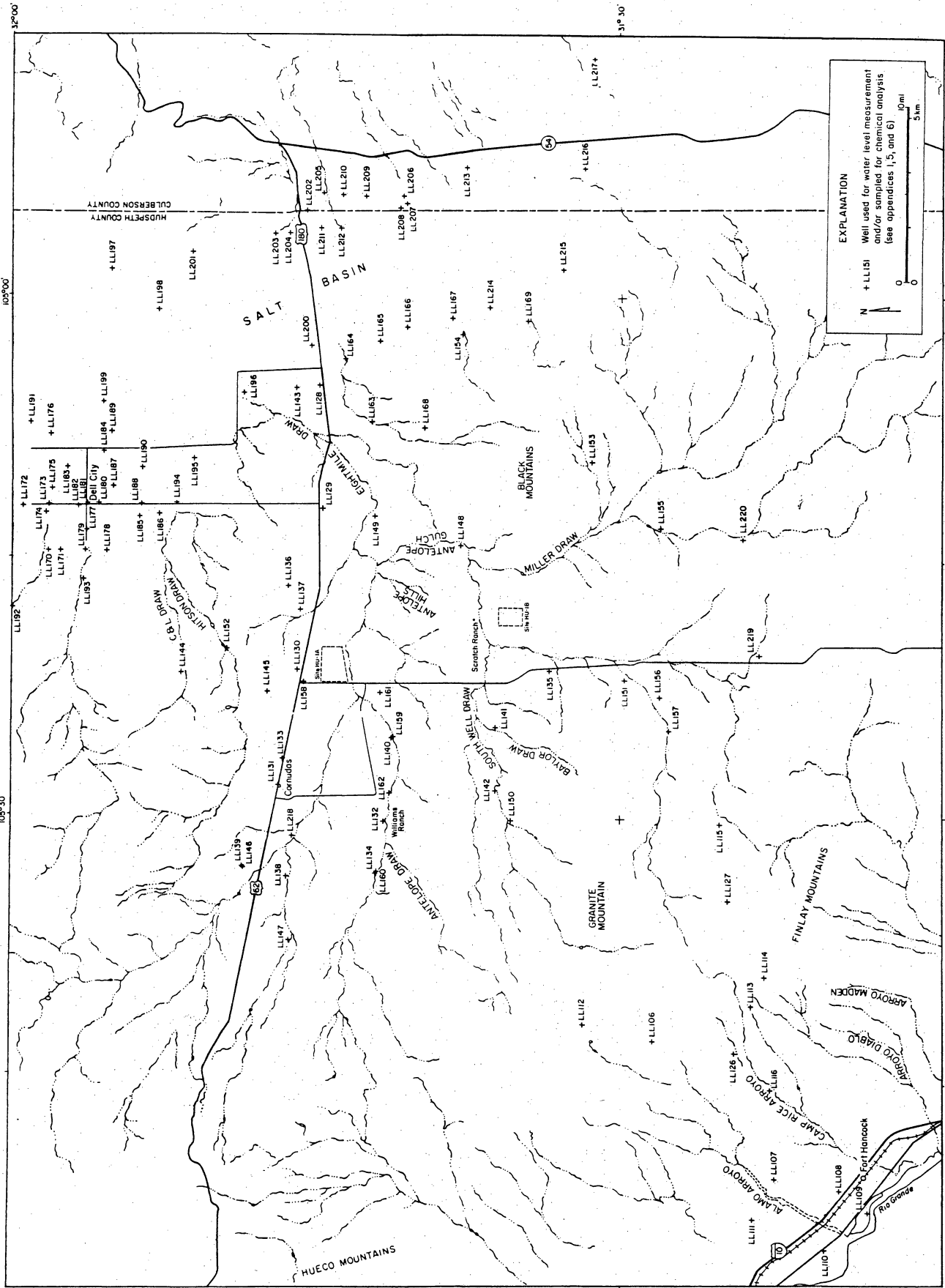
values were obtained either by direct measurement using an electric water probe and steel tape or from information provided by the well owner (fig. 42). Data for the Dell City and Salt Basin areas were taken from Texas Natural Resources Information System (TNRIS) computerized data base and from Nielson and Sharp (1985) and Boyd and Kreitler (1986). No data were available on porosities, hydraulic conductivities, or transmissivities of the unsaturated or saturated zones at the sites.

Drilling Programs

The first drilling program, conducted in July and August 1986 at sites HU1A and HU1B, was designed to provide data on the subsurface stratigraphy and rock characteristics at the sites and to drill boreholes for hydrologic testing. The second drilling program, accomplished in January 1987, was designed specifically for chloride profile investigations at HU1B. This second program was performed with the BEG drilling rig. Results of these investigations are included in the recharge section of this report and in appendix 11.

Byrl Binkley Drilling Contractor, drilled four test holes to complete initial drilling objectives. At each site a 150-ft (45.7-m) deep stratigraphic test hole was drilled (HU1A-BEG#1 and HU1B-BEG#1), and continuous core from top of bedrock to total depth was recovered to characterize the subsurface bedrock. The top of unweathered bedrock was determined at each site, and 15 ft (4.5 m) west of each stratigraphic test hole, a permeability test hole was cored (HU1A-BEG#2 and HU1B-BEG#2) to the top of unweathered bedrock. Casing was run to bottom and cemented to surface in each permeability test hole, and an additional 30 ft (9.1 m) was cored below casing. Constant head permeability tests were conducted for the intervals below casing to determine the hydraulic conductivity of the unweathered section of the unsaturated zone (appendix 7).

Figure 42. Surface drainage and location of wells within the study area. Thirty water-level measurements were taken, as were 30 ground-water samples that were analyzed for general chemistry, $\delta^{18}\text{O}$, δD , tritium, $\delta^{34}\text{S}$, $\delta^{13}\text{C}$, and ^{14}C . Water-level data and chemical analyses of ground water in the Dell City area taken from Texas Natural Resources Information System (TNRIS), Nielson and Sharp (1985), and Boyd and Kreitler (1986).



EXPLANATION

+ LL151 Well used for water level measurement and/or sampled for chemical analysis (see appendices 1, 5, and 6)

0 0 1 5 mi

The permeability test holes were drilled with fresh water circulated only once instead of using a gel-based mud system. This procedure was used to reduce potential contamination by mud-cake buildup on the walls of the borehole. The nature of the rhyolite and dense limestone prevented use of air for circulation because tremendous heat buildup occurred on the coring bit while drilling with compressed air. It was determined that drilling with compressed air was not feasible, and the system was converted to fresh water.

Previous drilling of the shallow subsurface (Dames and Moore, 1985) at both sites documented variability in thickness of bedrock cover and depths of weathered bedrock. Permeability tests on such heterogeneous units may be of only local significance and inapplicable to the site as a whole. Unweathered rhyolite penetrated at HU1A, however, may be homogeneous (assuming uniform fracture distribution), and permeability tests on this interval could be applicable to a larger area. The heterogeneity of alluvial cover and weathered bedrock strata at HU1B also indicates that permeability tests on these units are of only local significance.

Two permeability tests were performed during this study in the unsaturated zone. At HU1A the tested interval is the upper 30 ft (9 m) of unweathered rhyolite, and at HU1B the tested interval is the upper 30 ft (9 m) of unweathered Cretaceous Campgrande limestone. Seven pumping tests in the saturated zone of the Diablo Plateau (assumed to be in Permian Victorio Peak - Bone Spring strata) were conducted. Data from the permeability tests and pumping tests are presented in appendices 7 and 3, respectively.

Geologic and hydrologic data were obtained from eight water wells drilled and operated by the El Paso Natural Gas Company (EPNG) for their now-abandoned Pump Station #2 (appendix 12). Pump Station #2 is located 7.5 mi (12.2 km) west-southwest of site HU1A.

REGIONAL SETTING AND SEISMICITY

The study area lies within the Diablo Plateau region, Hudspeth County, Trans-Pecos Texas, at the eastern part of the Basin and Range structural province (fig. 41). This province consists of topographically high ranges separated by major normal faults from adjacent topographically low basins. Structural development of the province began about 24 million years ago (mya) during east-northeast-oriented extension. Faulting and associated relative subsidence of the basins began at that time and continue to the present. The basins were progressively filled by detritus eroded from the adjacent ranges. The study area lies about 15 mi (24 km) west of the Salt Basin, a large Basin and Range graben at the eastern edge of Hudspeth County. No Quaternary scarps have been found in the study area, although some parallel the eastern part of the Babb flexure in the Salt Basin (Goetz, 1977). The west-northwest-trending Babb flexure extends from the Salt Basin across the study area (fig. 41).

Geology

The sites lie on the Diablo Plateau, west of the Salt Basin. Rocks in the area range in age from Precambrian to Recent (fig. 41 and plate 5). Strata most important to this investigation are Precambrian rhyolite porphyry at site HU1A and Cretaceous limestone interbedded with sandstone and mudstone at site HU1B.

Precambrian rhyolite porphyry crops out in the northwestern part of the study area in low rounded hills (plate 5). The petrology and age of the rhyolite porphyry were discussed by King and Flawn (1953). Stead and Waldschmidt (1953). Flawn

(1956), Masson (1956), and Wasserburg and others (1962). The dark red rhyolite porphyry has pink feldspar and clear glassy quartz phenocrysts that range in size from 0.1 to 0.4 inches (0.2 to 1.0 cm). Chlorite is a common alteration product. It is unknown if the rhyolite is intrusive or extrusive. Masson (1956) suggested that a complex of both extrusive and intrusive Precambrian rocks is present. The general age determined by strontium isotopic analysis is 1,060 mya, whereas the age determined by the lead-uranium method on zircon is 1,150 to 1,200 mya (Wasserburg and others, 1962). Lithologic descriptions of core from HU1A are in appendix 13. Core and good exposures in an abandoned quarry indicate that fractures are locally abundant.

Permian strata that crop out in the study area include the Victorio Peak limestone and undivided Leonardian rocks (plate 5). These thin- to thick-bedded fossiliferous limestones and dolomites have interbeds of sandstone and siltstone (King, 1965). The Permian Cutoff shale also crops out in the eastern part of the study area, and the Hueco limestone is present on the south side of Sierra Prieta in the southeastern part of the area.

Cretaceous strata include the Campagrande Formation, Cox sandstone, and Finlay Formation (plate 5). Washita Group marl and fossiliferous shale also crop out at Sierra Prieta. The Campagrande Formation in the study area consists of thin-bedded, nodular, partly conglomeratic limestone with marl and clay interbeds (Barnes, 1983). It is commonly mottled yellow and red. The Cox conformably overlies the Campagrande Formation and consists of siltstone, sandstone, shale, and fossiliferous limestone (Barnes, 1983). Throughout most of the study area the Campagrande and Cox are poorly exposed and are undivided (plate 5). Test holes at site HU1B penetrate both Cox and Campagrande strata. Core descriptions are in appendix 13. Overlying the Cox are thick- to thin-bedded fossiliferous limestone interbedded with marl, shale, and sandstone of the Finlay Formation (Albritton and Smith, 1965; Barnes, 1983).

Two Tertiary intrusive bodies are present in the study area. The Red Hills (Antelope Hills) intrusion lies in the central part of the area and is about 6 mi (10 km) southeast of HU1A and 4 mi (6 km) north of HU1B (plate 5). The quartz trachyte intrusion is locally discordant but generally resembles a sill (Sullins, 1971). The intrusion has a Rb-Sr age of 28.2 ± 3.2 mya (Haley, 1971). The Sierra Prieta syenite intrusion (Black Mountains) lies 6 mi (10 km) east of HU1B. Hodges (1975) described Sierra Prieta as a "trap door" intrusion overlain by Permian strata and floored by Cretaceous rocks. Emplacement of the syenite intrusion was 35.0 ± 2.0 mya (Hodges, 1975).

Quaternary alluvial deposits cover much of the bedrock in the area. The alluvium consists of silt and sand with some pebbles and cobbles derived from local bedrock. Caliche layers up to 3 ft (1 m) thick occur near the surface.

Structure

Babb Flexure

The Babb flexure is a west-northwest-trending monocline with downward displacement of strata on the north side of the flexure (King, 1949, 1965). It can be traced about 40 mi (65 km) northwestward from the Salt Basin across the study area and is approximately 1 to 2 mi (1.5 to 3 km) wide (fig. 41 and plate 5). Permian rocks exposed on the flexure usually dip 10° to 15° north. The Victorio Peak Formation is displaced about 1,000 ft (305 m), and the Cutoff shale occurs only on the north side of the flexure (east of the study area). An angular unconformity exists between Permian and Cretaceous strata. Cretaceous rocks are not well enough exposed to determine if they have been warped by recurrent movement along the structure. Hodges (1975) mentioned that the flexure may be the Permian or post-Permian expression of a major pre-Permian strike-slip fault. Basement relief across the flexure

could be greater than 4,500 ft (1,370 m) based on the difference in elevation between exposed Precambrian rhyolite porphyry and the Jones No. 1 Mowry test hole, located 12 mi (19 km) northeastward, that bottomed in Ordovician strata at 500 ft (150 m) below sea level. The great amount of basement relief across the flexure indicates that the basement may be faulted.

Faults, Folds, and Joints

Faults present in outcrop are associated with the two Tertiary intrusions and do not extend far from the extrusive bodies. An east-west-trending anticline occurs west of Sierra Prieta. The anticline could have been caused by an unexposed intrusion that warped the overlying strata during emplacement. The buried intrusion may be related to the nearby Sierra Prieta intrusion.

Minor faults, flexures, and zones of closely spaced joints are mapped in well-exposed Permian strata in the northeastern part of the study area (plate 5). Displacement across the minor normal faults and flexures is commonly a few feet. Joint spacing in the fractured zones is as great as 10 joints per 3 ft (1 m) for limestone beds 1.5 ft (0.5 m) thick. Most of the fractured zones are about 6 ft (2 m) wide. These minor structures are probably related to the regional deformation along the Babb flexure but occur in strata well beyond the margins of the regional flexure.

Joints and minor normal faults also occur in the Precambrian rhyolite porphyry. Joint spacing of nearly vertical joints locally approaches 6 joints per 3 ft (1 m). Many of the joints extend vertically throughout the 15 to 20 ft (6 m) height of available exposures. Subhorizontal joints with dips of less than 30° also are abundant. Iron staining is a common feature on the joint surfaces, indicating that the joints have

acted as ground-water conduits. Limonite and hematite stains also occur on fracture surfaces in core, and some fractures are filled with dolomite and/or calcite (appendix 13). Fifty percent of the rhyolite porphyry core from site HU1A is fractured (appendix 13). Fractures in the core have dips ranging from horizontal to vertical, similar to fractures observed in outcrop.

Nearly vertical joints in the Precambrian rhyolite porphyry have multiple strike orientations (station 2 on plate 5, and fig. 41). Three minor normal faults present in the rhyolite strike west-northwestward, similar to the regional trend of the Babb flexure. Permian and Cretaceous strata usually have two major joint sets that vary in strike regionally across the area (plate 5). Across most of the study area, nearly vertical joints strike northwest at 300° to 340° and northeast at 050° to 070° (stations 2, 3, 4, and 5, plate 5). North of Sierra Prieta, joints striking 010° to 030° are also common (station 6, plate 5). West of Sierra Prieta, joints strike north-northwest at 330° to 000° and east-west at 250° to 290° (stations 7 and 8, plate 5). The east-west trend parallels the anticline axis and faults at Sierra Prieta. Joints at site HU1B may strike in the same direction as joints in bedrock at stations 7 and 8 (plate 5). Core from test holes at HU1B was not as fractured as core from HU1A.

HYDROLOGIC SETTING

Surface Flow

HU1A

All surface streams in this region are ephemeral and, except for small local depressions, discharge east of the sites into the Salt Basin (fig. 42). Antelope Draw,

one of the larger ephemeral streams in the area, is located 1.5 mi (2.4 km) south of HU1A. Dames and Moore (1985) report that this draw drains more than 650 mi² of the Diablo Plateau west of the site. Final discharge of Antelope Draw is into Eight Mile Draw, which discharges into the Salt Basin approximately 18 mi (28.9 km) east.

During field activities for this study, several thunderstorms occurred. Flooding of Ranch-to-Market Road 1111 created a body of water 2 ft (0.6 m) deep and as much 200 to 300 ft (60 to 91 m) across (fig. 43). Duration of the flooding was very brief, and the road became passable almost as soon as rainfall terminated.

A smaller unnamed draw in the northern part of this site drains a very small area and is not considered as potentially hazardous as the larger draws. The National Flood Insurance Rate Map (FIRM) for HU1A (Community-panel number 480361 0400 B) (fig. 44) classifies both Antelope Draw and this smaller unnamed draw as Zone A, defined as areas of 100-year flood; base flood elevations and flood hazard factors were not determined. The site itself is classified as Zone C, defined as areas of minimal flooding.

HU1B

The northern and western portions of HU1B are within the mapped floodplain of Antelope Gulch, a large ephemeral draw that discharges into Antelope Draw several miles to the north (FIRM, Community-panel number 480361 0550 B) (fig. 45). This draw is also classified as Zone A, and the remaining area is mapped as Zone C (U.S. Department of Housing and Urban Development, 1985).

Methodologies utilized by the National Flood Insurance Program (NFIP) to classify potential areas of flooding may be divided into three basic types: (1) existing sources, such as the U.S. Army Corps of Engineers; (2) USGS flood-prone area



Figure 43. Photograph of flooding at Antelope Draw where it crosses Ranch-to-Market Road 1111. The flood created a body of water 2 ft (0.6 m) deep and as much as 200 to 300 ft (60 to 91 m) across. Duration of flooding was very brief, and the highway became passable almost as soon as rainfall terminated.

Figure 44. Flood Insurance Rate Map (FIRM) for area around site HU1A (Community-Panel Number 480361 0400 B). Both Antelope Draw and a smaller unnamed draw are enclosed as Zone A, defined as a 100-year flood area. Base flood elevations and flood hazard factors were not determined. The site itself is classified as Zone C, defined as an area of minimal flooding (U.S. Department of Housing and Urban Development, 1985).

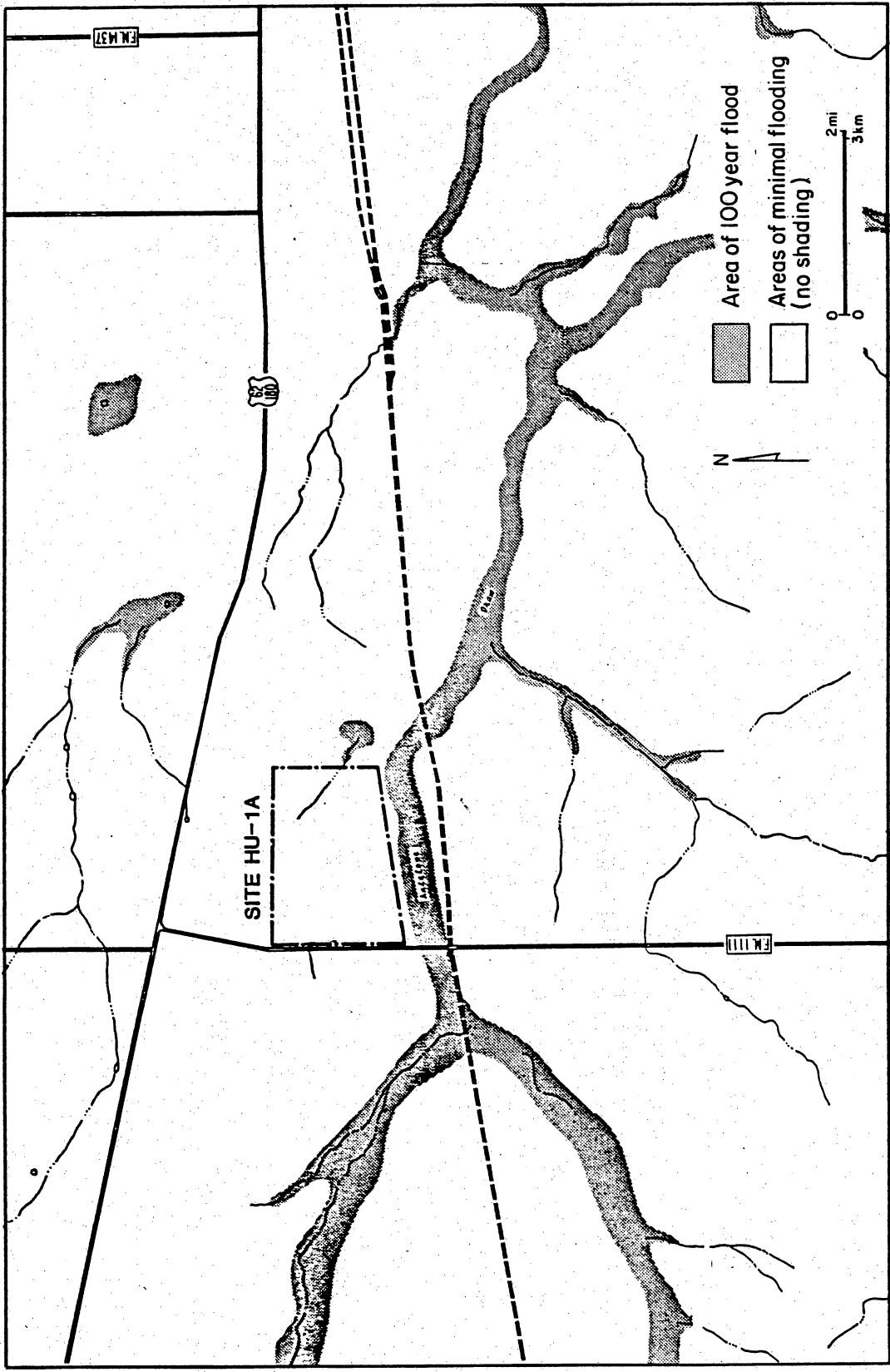


Figure 45. Flood Insurance Rate Map (FIRM) for area around site HU1B. The northern and western portions of HU1B are within the mapped floodplain of Antelope Gulch, a large ephemeral draw that discharges into Antelope Draw several miles to the north (FIRM, Community-Panel Number 480361 0550 B). This draw is also classified as Zone A, defined as a 100-year flood area. The remaining area is mapped as Zone C, defined as an area of minimal flooding (FIRM, 1985).

quadrangles; and (3) normal depth equations actually calculated for specific areas.

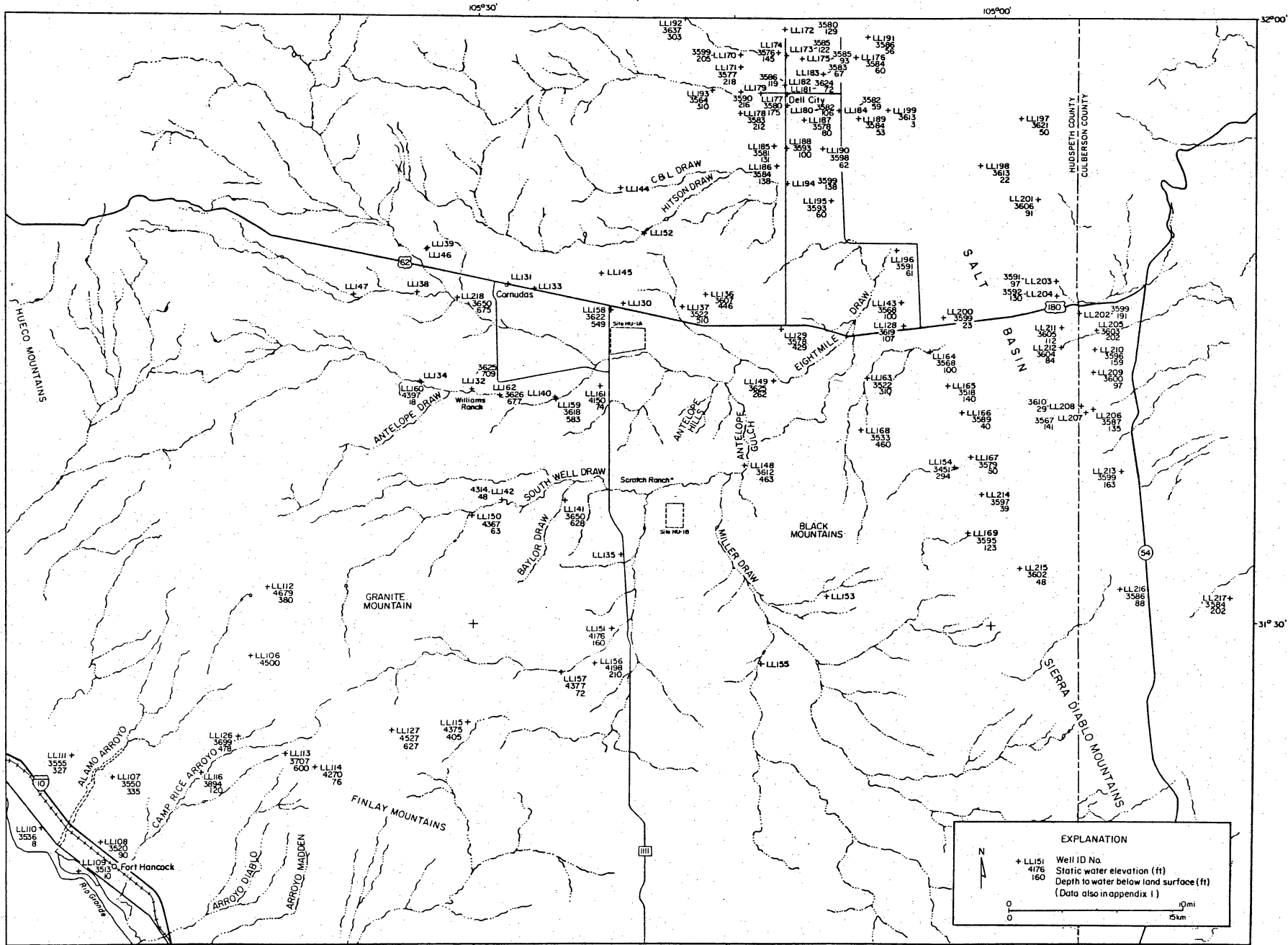
Extensive field investigations were conducted during January 1987 to determine the extent of flooding at HU1B, which resulted from heavy precipitation events observed in 1986. The main area of interest was Antelope Gulch, to the west and north of HU1B. Observations in this area did not locate any physical evidence of a previous flood event outside of the rather poorly defined arroyo. Other than the presence of the arroyo itself, no real evidence was recorded of flooding within the arroyo. Evidence indicates that actual flooding within the site boundary of HU1B would be of only minimal impact and engineering barriers constructed at the site would be sufficient to control future flood events.

Unsaturated Zone

The thickness of the unsaturated zone in the study area ranges from 3 ft (0.9 m) in the salt flats to 790 ft (240 m) in well LL138 (fig. 46). The unsaturated zone is made up of Cenozoic alluvium and colluvium, Cretaceous sandstones and limestones, Paleozoic carbonates and clastics, and Precambrian rhyolites.

Vertical permeabilities of cores through the alluvial cover at HU1A range from 2×10^{-4} cm/sec to 2×10^{-5} (63.072 m/yr to 6.3072 m/yr) (Dames and Moore, 1985). In situ horizontal permeability measurements from the upper 30 ft (9.1 m) of unweathered bedrock (Precambrian rhyolite) indicate a hydraulic conductivity value of 2.59×10^{-5} cm/sec (8.19 m/yr) (appendix 7). This value falls within the range of fractured igneous and metamorphic rocks as reported by Freeze and Cherry (1979, their table 2.2).

Figure 46. Map showing potentiometric surface elevations in the study area. Land-surface elevation changes from 3,450 ft (1,050 m) at the salt flats and Dell City area to greater than 4,500 ft (1,370 m) in higher regions in the west, but the elevation of the water table in Aquifer A rises only 200 ft (61 m) (from 3,445 ft to 3,650 ft, or 1,050 to 1,113 m) across the same region, resulting in increasing depth to water at higher elevation. Thickness of the unsaturated zone in the study area ranges from 3 ft (0.9 m) in the salt flats to 702 ft (214 m) in well LL132 in the west.



EXPLANATION

N

+ LL151 Well ID No.
4176 Static water elevation (ft)
160 Depth to water below land surface (ft)
(Data also in appendix I)

0 0 10mi
0 0 15km

Vertical permeabilities of cores through the alluvial cover at HU1B range from 7×10^{-4} cm/sec to 4×10^{-6} cm/sec (220.752 m/yr to 1.2614 m/yr) (Dames and Moore, 1985). In situ horizontal permeability measurements taken on the upper 30 ft (9.1 m) of Cretaceous Cox sandstone and Cretaceous Campagrande limestone below the alluvium indicate a hydraulic conductivity of 1.226×10^{-4} cm/sec (38.6 m/yr). This value is within the range of limestones, dolomites, and sandstones (Freeze and Cherry, 1979).

Natural fracturing occurs in cored bedrock at both sites and in an abandoned quarry southeast of the test holes at HU1A. Natural fractures are more abundant in the rhyolite. Most of the fractures in the rhyolite are still open with only thin layers of limonite and hematite lining the fractures and providing no appreciable restriction to ground-water flow. Fractures in the limestones of HU1B, however, are partially to totally occluded by brown calcite and dolomite cements. The degree of restriction to ground-water flow that results from these cements is unknown. At least two examples of fracture enlargement by solutioning were recorded from the limestone core. In addition to fracture solutioning, partially occluded biomolds, initially a result of solutioning, were also observed. The apparent increase in fracturing from HU1B to HU1A may be a result of closer proximity to the Babb flexure. Higher permeabilities at HU1B, however, could result from more efficient connection of fracture systems due to the effects of solutioning. Permeability tests on the unsaturated zone at HU1A (appendix 7) also confirmed the presence of fracture systems in the subsurface rhyolite.

Saturated Zone

The primary aquifer, Aquifer A, (see Potentiometric Surface section for a detailed discussion) in the study area is part of a regional aquifer that extends across much of

the Diablo Plateau. Previous studies of the Dell City area have reported that locally the water-bearing formation is the Bone Spring limestone of the Leonard series of Permian age (Scalapino, 1950; Peckham, 1963; Young, 1976; Gates and others, 1980; Logan, 1984). In the nearby Guadalupe Mountains, the Bone Spring limestone attains a thickness of several thousand feet (King, 1948). In the Dell City area, the Victorio Peak and Bone Spring limestones crop out, and locally the aquifer is referred to as the Victorio Peak - Bone Spring aquifer. Peckham (1963) reports that the Bone Spring limestone is a black, cherty, dense, fine-textured, thin-bedded limestone at least 500 ft (152 m) thick, and the Victorio Peak limestone is a thick-bedded succession of gray limestone with a total thickness of about 800 ft (243 m). Ground water has been reported to be encountered at depths from 200 ft (61 m) to 1,500 ft (457 m) (D'Appolonia, 1978).

Lithologic control for this aquifer outside the Dell City area is extremely limited. Two driller's logs were obtained from El Paso Natural Gas Company records (appendix 12) for water wells drilled at Pump Station #2. These logs record lithologies that could reasonably be correlated with Permian strata of the area.

The shallow aquifer, Aquifer B (fig. 47), is a local aquifer located in the southwestern portion of the study area. Although no previous studies report aquifer host rock, stratigraphic thicknesses, coring at HU1B, and discussions with local well drillers make possible some inferences. Aquifer B is probably a Cretaceous limestone aquifer with permeabilities controlled by the presence of fracturing and solutioning. Cretaceous rocks in the area are typically reported to have minimum thicknesses of 200 ft (61 m) and because all but one of the wells producing from Aquifer B are shallower than 200 ft (61 m), a Cretaceous host rock seems reasonable.

Figure 47. Potentiometric surface map, Aquifers A and B. Ground water flows predominantly to the northeast. A ground-water divide is located north of the Diablo Plateau scarp. The abrupt change of the potentiometric surface together with the difference in gradients and depth to water suggests the presence of two separate aquifers: the primary deep aquifer, Aquifer A, and a shallower aquifer, Aquifer B.

Water-bearing Characteristics

The occurrence and quantity of ground water both in the Dell City area and throughout this regional aquifer appear to be controlled by fractures. Subsurface joints and fractures, caused by structural movement along the Babb and Victorio flexures (fig. 41), have contributed to both porosity and permeability development of the aquifer. Logan (1984) reports that in the Dell City area, ground water occurs in open joints and fractures under both water table and confined conditions. Stratigraphic or facies controls on transmissivity values have not been reported.

Fractures in the carbonate rock may be enhanced by solution from the flow of fresh ground water through primary and secondary porosity. The presence of recent sinkholes 12 ft (3.6 m) deep and 12 ft (3.6 m) in diameter (Young, 1976) is evidence of active solution in the Dell City area. Well drillers in the area also report the regular occurrence of lost circulation zones indicative of large openings or caverns (Scalapino, 1950). Although the extent of fractures has not been clearly defined, inferences of highly permeable fracture zones may be drawn from the low hydraulic gradients recorded for Aquifer A.

Seven pumping tests have now been completed on wells spaced across the Diablo Plateau for this study. Six of the pumping tests were on water wells producing from Aquifer A while one was producing from Aquifer B. Water wells tested were (in the order of testing) LL162, LL156, LL155, LL148, LL141, LL132, and LL138 (fig. 42). Pumping test (PT) no. 1 at well LL162 was the only test where monitoring of observation wells was possible due to nearby wellbores LL219 and LL220 (figs. 42 and A3-1). No drawdown was observed, however, in these observation wells. Data collected from these tests are included in appendix 3. Values of transmissivity calculated by the methods of Walton, Jacob, and Theis and Logan's method of approximation for both semiconfined leaky aquifer and confined nonleaky aquifer

conditions range from 2.39 gpd/ft of drawdown to 1,713.9 gpd/ft of drawdown (0.32 ft²/d, or 0.03 m²/d to 229.1 ft²/d, or 21.3 m²/d) for Aquifer A whereas Aquifer B had significantly higher transmissivity values, ranging from 37,163.1 gpd/ft of drawdown (4,968.3 ft²/d, or 461.5 m²/d) to 49,986 gpd/ft of drawdown (6,683 ft²/d, or 621 m²/d). The mean transmissivity calculated from 26 separate interpretations for Aquifer A was 228.2 gpd/ft of drawdown (30.5 ft²/d, or 2.8 m²/d), with a large standard deviation of 343 gpd/ft of drawdown (45.8 ft²/d, or 4.2 m²/d). At present, these are the only known pumping tests for the study region outside of the Dell City area. In the Dell City area, specific capacity data range from 5 to 64 gpm/ft (93 to 1,141 m²/d) of drawdown (Peckham, 1963).

In each of the seven pumping tests, the data either directly or indirectly recorded the importance of fracture flow within the aquifers of the Diablo Plateau. Transmissivity within an individual water well is partially or totally dependent on the number and size of fractures encountered while penetrating the saturated section. Three of the seven tested water wells tested during this study were observed to be underproducing from both Aquifer A and Aquifer B. In these wells, drawdown stabilized after a few minutes of pumping with no more than a couple of feet of drawdown. This initial drawdown probably results from well bore storage (Driscoll, 1986) and does not reflect the hydrologic conditions of the aquifer. These pumping tests curves illustrate a short-term drawdown and then only minimal additional drawdown throughout the rest of the pumping tests. Only an approximation of a minimum transmissivity can be made by using Logan's method (Kruseman and De Ridder, 1976). Larger discharge pumping tests are needed on these wells to determine their true transmissivities.

Tectonic events on the Diablo Plateau that have been responsible for the creation of fracture systems have been numerous throughout the geologic history of the area. Successful siting of 11 water wells was achieved based on the location of lineaments and fractures mapped using aerial photographs of the Dell City area (H. Logan, Soil Conservation Service, personal communication, 1987). Only 1 out of 11 wells failed to encounter a sufficient amount of fractures to meet injection well transmissivity requirements of 2,000 gpm/ft of drawdown ($267.4 \text{ ft}^2/\text{m}$, or $24.8 \text{ m}^2/\text{m}$). Additional studies to better understand the unexpected water-bearing potentials of both Aquifer A and Aquifer B on the Diablo Plateau should include comparative studies between surface fractures and lineaments recorded on aerial photographs and the location of successful water wells (a successful water well being one capable of delivering acceptable quantities of water to the surface economically). Preliminary investigations indicate a potential for finding additional transmissive zones with good water quality for a large portion of the Diablo Plateau.

Potentiometric Surface

The potentiometric surface (fig. 47) on the Diablo Plateau shows that regional ground water flows predominantly to the northeast. A ground-water divide is located just to the north of the Diablo Plateau scarp. No divide is evident in the region of the Babb flexure as had been postulated during previous studies (Dames and Moore, 1985). Recharge from either site HU1A or HU1B would flow in the general direction of the Dell City irrigation region and toward the salt flats.

Two separate aquifers may exist. Aquifer A is located in the northeast section of the study area and includes the Dell City irrigation and salt flat areas (fig. 47).

Elevations of the water table range from 3,445 ft (1,050 m) in the Dell City and salt flat regions in LL154 to 3,650 ft (1,112 m) for wells LL141 and LL218. Depth to water varies from 3 ft (1 m) on the salt flats to more than 700 ft (213 m) in areas of higher land elevations (fig. 46). Land surface elevation changes approximately 1,000 ft (305 m) from \approx 3,450 ft (1,051 m) at the salt flats to more than 4,500 ft (1,372 m) in higher regions of the Diablo Plateau, but the elevation of the water table only rises 200 ft (61 m) across the same region. This explains why the depth to water increases significantly at higher elevations. The maximum hydraulic gradient measured between LL218 and LL154 is 6.9 ft/mi (1.3 m/km). A more typical gradient for the area, however, is 2.5 ft to 5 ft/mi (0.5 to 0.9 m/km), as measured between several wells.

Southwest of Aquifer A is a local aquifer (referred to as Aquifer B) with water-table elevations that are significantly higher than in Aquifer A (fig. 47). Aquifer B is bounded on the southwest by the escarpment of the Diablo Plateau. Water elevations for this area range from 4,397 ft (1,340 m) in LL160 to 4,176 ft (1,272 m) in LL151. The depth to ground water at Aquifer B is significantly less than that observed at Aquifer A; depth of water ranges from 18 to 210 ft (5 to 64 m), and the water depth for most wells is less than 100 ft (30 m). Ground water flows predominantly to the northeast. Limited flow is southwestward toward the Rio Grande valley. The hydraulic gradients measured for Aquifer B are higher than those of the regional Aquifer A, values being as high as 90 ft/mi (17 m/km) between wells LL156 and LL157.

The two different potentiometric surfaces in Aquifer A and Aquifer B suggest two permeable zones beneath the Diablo Plateau. Aquifer B represents a perched aquifer; Aquifer A is predicted to lie beneath Aquifer B in the southwestern part of the study area. In the north-northeastern part of the study area there are three examples of

Aquifer B overlying Aquifer A: (1) The water elevation of well LL161, a geothermal test well drilled on the flanks of one of the Pump Station Hills, is 4,150 ft (1,265 m), which is similar to water-table elevation of the shallow aquifer. This well was not used in potentiometric mapping of Aquifer A because of its apparently anomalous nature. (2) Wells LL160 and LL134 are located 100 ft (30 m) apart from each other on the Williams' Ranch at Hobo Tank, west of HU1A, and have significantly different water levels. LL160, a shallow windmill located in the bottom of an arroyo, has a depth to water of 18 ft (5.4 m), whereas the water depth in LL134, a deep pumpjack in the same area, was greater than 750 ft (229 m) (as reported by the owner). (3) The driller's logs for the abandoned El Paso Natural Gas Company Pump Station #2 well, which was used as an observation well for the pumping test (appendix 3), indicate that three water-bearing zones were encountered during drilling. During this study, water was always observed on the electric-line probe at depths of less than 200 ft (60.9 m), although static water level was recorded at 673 ft (205.1 m). In addition, water could be heard cascading down the borehole. (There was no casing below 100 ft (30.5 m) depth).

The difference in water levels, the difference in gradients, and the abrupt change in water levels that exist between the deep water table (Aquifer A) and the shallow water table (Aquifer B) found in the southwestern part of the study area suggest a change in hydrologic properties between the two regions. Aquifer A may be more fractured because of its location over or proximate to the Babb flexure. Fractures would permit greater leakage through possible aquitards between Aquifer A and Aquifer B and drain any ground water in overlying permeable zones. Greater fracture permeability would also permit a lower hydraulic gradient for Aquifer A than for Aquifer B. The Jacob plots for the aquifer tests of Aquifer A at wells LL132 and LL162 shows a segmented drawdown curve with time, which indicates drawdown in a

fractured medium (appendix 3). In the plot for well LL162 the first straight-line segment (a) represents drawdown in the fracture(s) penetrated by the well. These fractures have a transmissivity of 111 gpd/ft (1.38 m²/d). A barrier was hit at 40 minutes. The cone of depression hit another set of fractures at \approx 80 minutes. Transmissivity measured at the second set of fractures is 84 gpd/ft (1.05 m²/d); a higher transmissivity (158.6 gpd/ft; 1.97 m²/d) representing a third set was intersected at 900 minutes. The different transmissivities measured with increased time do not represent transmissivity values specific to each fracture set but do represent the cumulative value for the area affected by the cone of depression. The increased transmissivity evident at the end of the test may only indicate that more fractures are being intersected by the cone of depression, not that the fractures are more permeable. There was no drawdown in either of the adjacent observation wells, further indicating fracture control of ground-water flow and distribution. A similar pattern was also observed during the drawdown of well LL132. The abrupt change in water-table elevations between Aquifer A and Aquifer B may be due to a structural feature that functions as a hydrologic drain from Aquifer B into Aquifer A.

Recharge

Tritium levels measured on Diablo Plateau ground waters (appendix 2) indicate that a majority of the sampled wells (87 percent) contain recently recharged water. The major process responsible for this current recharge is infiltration of runoff in arroyos during occasional flash flooding (appendix 11). In the Dell City area, another probable source of current recharge is the recirculation of irrigation waters, through the thin vadose zone.

Several wells, particularly in the southwestern portion of the study area, also were found to contain high NO_3 levels. High nitrate levels may also be used as a qualitative tool for the documentation of local recent recharge. A detailed discussion of NO_3 in the study area and its implications for recharge appears in the Ground-Water Geochemistry section of this report.

Previous studies of the Diablo Plateau have dealt specifically with the identification of potential zones of recharge for the Dell City area. Peckham (1963) reported recharge zones to the west of Dell City and to the north in New Mexico. Principal recharge for the Dell City area has been attributed to the Sacramento River drainage basin located to the northwest of Dell City (Young, 1976). Peckham (1963) and Young (1976) also noted that to a lesser extent, recharge may occur in the Dell City area by the infiltration of precipitation on the land surface but apparently most of this evaporates (Dougherty, 1975; Boyd and Kreitler, 1986). Gates and others (1980) estimate annual recharge in the Dell City area as 31,000 acre-ft ($3.8 \times 10^7 \text{ m}^3$). The unsaturated section in the Dell City area consists of 5 to 150 ft (1.5 to 45 m) of alluvial cover. Recharge through the alluvium in the interarroyo areas is expected to be minor. Vegetation changes observed during field work may also influence or indicate active surface recharge. Preliminary studies dealing with climate and vegetation are presented in appendix 14.

Studies of recharge methods at HU1B

Reconnaissance field work in the study area indicates that recharge on the Diablo Plateau probably occurs by infiltration of runoff water in arroyos where erosion has transected Cretaceous bedrock. Detailed sampling of soil profiles for chloride analysis was conducted both in arroyos and in interarroyo areas to determine the relative recharge in each of these geomorphic areas. The recharge equation of Allison and

Hughes (1978) was then used to estimate the amount of precipitation and runoff that moves through the vadose zone annually.

Ten hollow-stem auger holes were drilled along two transects oriented east-west and north-south across HU1B (fig 48). One additional auger hole was drilled in a closed depression located southwest of the site. Two boreholes, C1 and C6, were located within the drainage channel of Antelope Gulch, west and north of the site respectively, and C4 was located within a minor unnamed north-south drainage channel along the eastern boundary of HU1B. Each borehole was drilled to auger refusal, which at all but one location could be confirmed to be the top of Cretaceous bedrock. Two cores drilled (plate 5) and limited outcrops in the area indicate the Cretaceous units encountered at the top of bedrock are limestones of the Finlay and Campagrande Formations and the Cox Sandstone.

Data specific to chloride concentration profiles at HU1B are present in appendix 11. The following discussion will be based on the Midland value of 0.79 mg/L chloride in rainfall. Borehole locations and chloride profiles are presented in figure 48.

Chloride profiles and calculated annual recharge document the very strong influence of the presence of arroyos on the amount of water moving in the vadose zone in the area of HU1B. Calculated annual recharge calculations for boreholes located in arroyos ranged from 0.180 to 0.011 inches/yr (0.457 to 0.028 cm/yr). Boreholes located in the interarroyo areas, however, recorded significantly lower annual recharge rates ranging from 0.008 to 0.002 inches (0.020 to 0.005 cm). Rates of recharge within a closed depression closest in the site region resembled those of arroyo areas, having an estimated annual recharge rate of 0.156 inches/yr (0.396 cm/yr). Recharge to bedrock within the boundary of HU1B, based on chloride concentration investigations, was found to be very small. These rates of recharge are

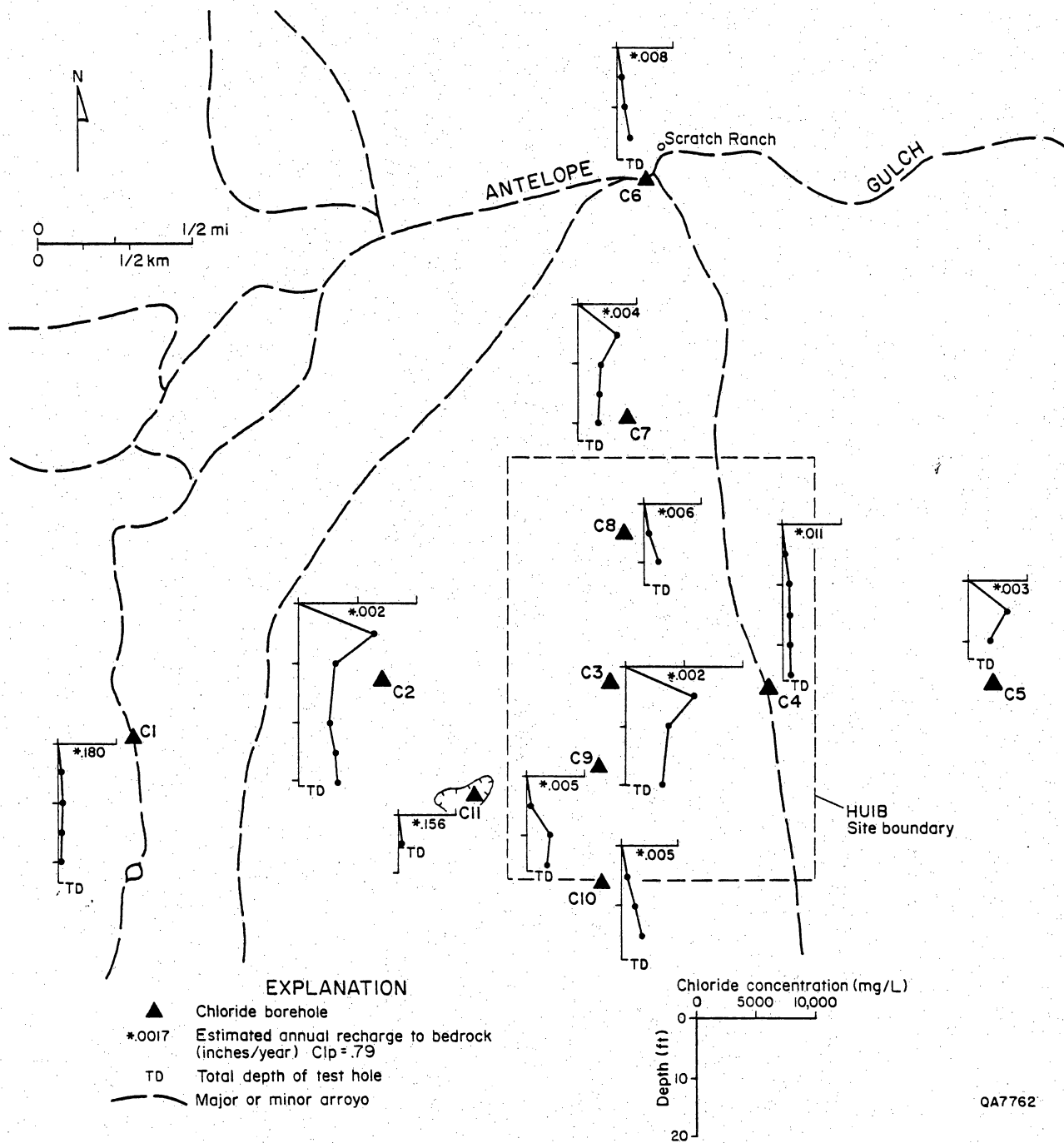


Figure 48. Map showing location of boreholes augered for chloride analysis at HU1B. Adjacent to borehole location is vertical profile of chloride concentrations measured in soil samples.

similar to rates measured in the area of S-34 to the southwest, which ranged from 0.009 to 0.0005 inches/yr (0.02 to 0.001 cm/yr).

Flood management and recharge in the Dell City area

Currently, a large flood-control program is under construction in the Dell City area. The flood control program is under the direction of the Soil Conservation Service (SCS), an agency of the U. S. Department of Agriculture (USDA). Major arroyos responsible for drainage through the Dell City area have only minor topographic definition and often fail to confine runoff during periods of heavy precipitation. Four retarding dams will eventually be completed to reduce costly damages resulting from flash flooding in the Dell City area. Currently, three dams have been completed and one is still under construction.

Man-induced ground-water recharge of floodwaters through a series of large-diameter (20-inch) recharge wells below each retarding dam is a secondary benefit of the flood control measures (Logan, 1984). The number of injection wells required per dam is dependent on the size of the drainage area above each structure. Current plans specify a total of 11 injection wells based on a ratio of 1 well per 30 mi² (77.7 km²) of drainage area. Injection is to be by gravitational flow. Three possible benefits from this effort, in addition to the obvious control of floodwaters, include (1) improved ground-water quality, which has steadily been declining since the inception and recycling of irrigation waters, (2) reduction or reversal of declining water levels due to the intensive ground-water production during peak irrigation periods, and (3) a better understanding of aquifer characteristics and potential for the area through geophysical logging, videologging, and pumping tests conducted in each injection well.

Discharge

The potentiometric map of Aquifer A (fig. 47) indicates that ground water flows toward the salt flats. Peckham (1963) and Young (1976) also reported that ground-water flow is in the direction of the salt flats. Discharge occurs naturally by evaporation in geographically extensive areas where depths to water may be as shallow as 3 ft (0.9 m) in the salt flats. Boyd and Kreitler (1986) and Chapman (1984) consider the salt flats to be the major discharge zone for the area. The potentiometric map of the study region confirms this hypothesis.

Abundant ground water was discovered in Dell City in 1947. By 1949, 32 water wells had been completed and 6,000 acres of farm land were under irrigation (Scalapino, 1950). The magnitude of irrigation continued to increase until as much as 40,000 acres of land had been converted to irrigated farming. According to D'Appolonia (1979), this represented the highest concentration of irrigated farm land within the state of Texas. Soil Conservation Service records indicate that as much as 150,000 acre ft ($1.8 \times 10^8 \text{ m}^3$) of irrigation water was produced in Dell City during 1979 (Logan, 1984).

Water levels measured in 1961 in the Dell City area had dropped an average of 18.5 ft total (5.6 m) since irrigation became prominent in the area around 1948. Young (1976) reports that water levels in the Dell City area have declined an average of 1.5 to 1.7 ft/yr (0.45 to 0.51 m/yr) from 1948 to 1968. During the same period of record, water salinity at Dell City tripled because of return flow from irrigation that leached salts from the soil. Production yields from these wells range from 160 to 2,240 gpm (875 to 12,250 m^3/d) (Peckham, 1963). In 1960, about 200 wells pumped 100,000 acre-ft ($123 \times 10^6 \text{ m}^3$) of water from the aquifer. This decline of the

potentiometric surface in the Dell City area has caused the wells in the Dell City area to be discharge points for the northern part of Aquifer A. It is uncertain whether flow from site HU1A would be toward Dell City. Based on the potentiometric map (fig. 47), however, flow from HU1B is expected to discharge at the salt flats.

Discharge of the aquifer has also occurred through naturally flowing springs. Crow Springs, located east-northeast of Dell City, was an important water oasis until the 1950's when an irrigation well was drilled adjacent to the spring. Flow of the spring terminated overnight (Brune, 1981). Other springs in the area that dried up due to pumpage are Washburn and Persimmon Springs north of Cornudas, Cove Spring on the south side of the Paint Waterhole Mountains, Shot Springs in the Antelope or Red Hills, Sulphur Springs on the east side of salt flat, Cottonwood Springs southeast of salt flat, and Aparejo or Harness Springs on the south side of Black Mountain (Brune, 1981).

No exterior drainage from Aquifer A was recorded during this study. Nielson and Sharp (1985) offer the possibility, however, that intrabasinal flow to the east may occur in the southern portion of the Salt Basin.

Ground-water Geochemistry

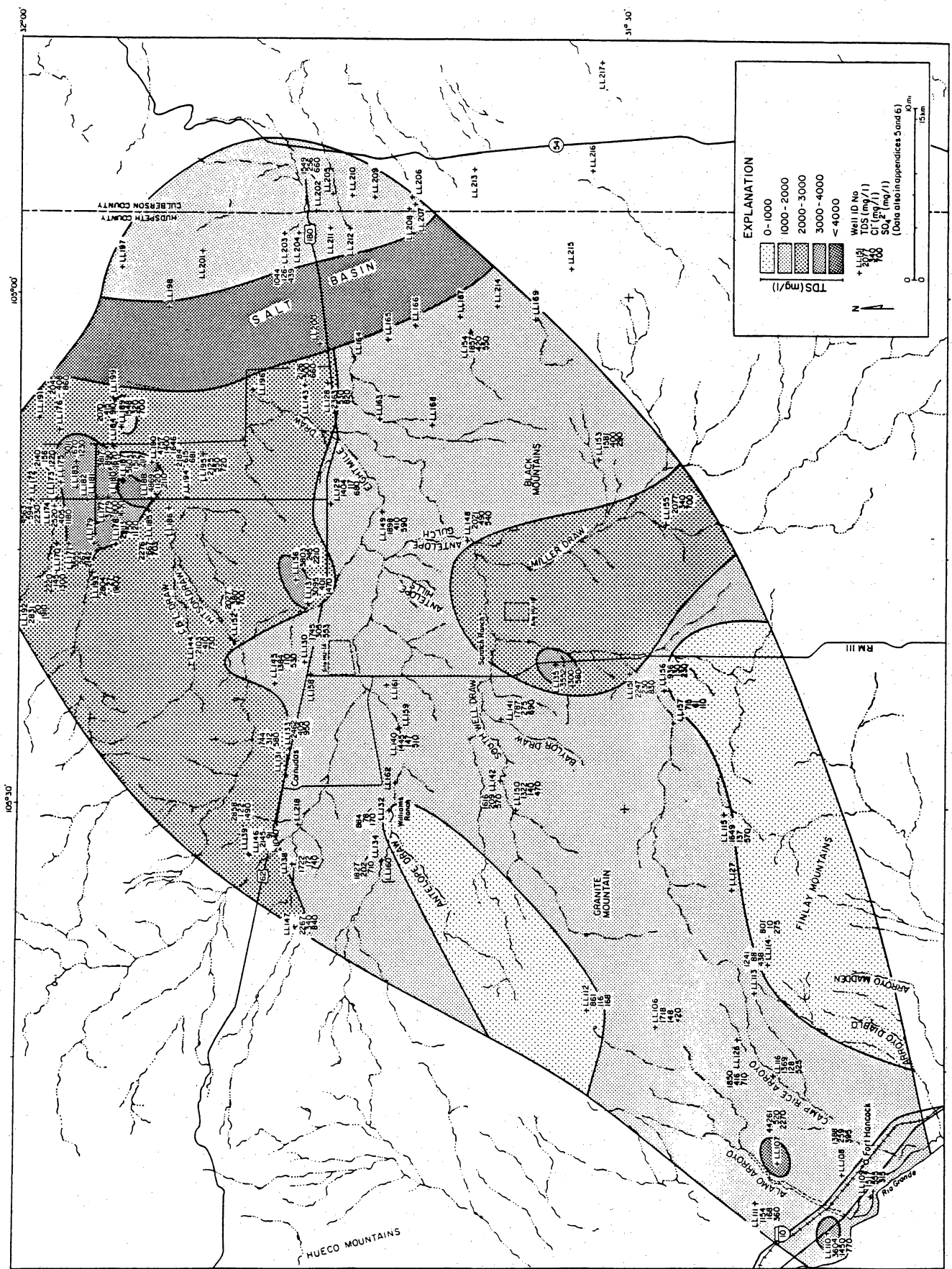
Chemical and isotopic analyses of ground-water samples from Hudspeth County collected during this study are presented in appendix 2. Additional chemical and isotopic analyses used during the evaluation of the southern site in Hudspeth County and chemical analyses from the Texas Water Development Board (1985) are also presented in appendix 2.

Ground water in the study area is fresh to brackish; total dissolved solids (TDS) range from 715 to 3,803 mg/L. Generally, there is no consistent pattern in TDS distribution (fig. 49); however, occurrence of relatively fresh water is restricted to Aquifer B and its vicinity, where elevation of the water table is higher and the unsaturated zone is thinner (figs. 46 through 48). Elevated values of TDS are a result of increasing concentrations of Na and SO_4 and, to a lesser extent, increasing concentrations of Ca and Cl (figs. 49 and 50).

Water facies vary from mainly Ca-Na- HCO_3 and Na- SO_4 types in the west (Aquifers A and B) to Na- SO_4 , Ca- SO_4 , and Na-Cl facies in the east (Aquifer A) (figs. 51 through 53). The shift in facies may be the result of the changing lithology from Cretaceous limestone interbedded with marl and clay to Permian limestone that may include Ca, SO_4 , and Cl-rich evaporites. Typically, high sulfate waters change chemically from Ca- SO_4 waters to Na- SO_4 waters as they flow because of cation exchange of Na for Ca. Waters in the study area, however, appear to change in the opposite direction, from Na to Ca facies, as they flow toward the salt flats, and this direction for chemical change is considered anomalous.

Aquifer B typically contains higher NO_3 concentrations (three wells had NO_3 concentrations of 100 mg/L or greater) than Aquifer A (fig. 54). The shallower depth to water table permits more rapid recharge. The source of the nitrate may be anthropogenic (stock water tanks, barnyards, corrals, septic tanks). High nitrate in wells typically relates to an animal waste or cultivation source. All high- NO_3 wells in Aquifer B were proximal to contaminant sources, and fracture permeability would facilitate rapid recharge of animal wastes. Some of the wells with high NO_3 , however, contain no tritium, which suggests that animal waste is not the source. At present the source of nitrates in these wells cannot be determined. High nitrates

Figure 49. Map of TDS, Cl, and SO₄ (mg/L) distribution. Ground water in the study area is fresh to brackish, TDS ranging from 715 to 3,803 mg/L. Generally, there is no consistent pattern in TDS distribution; however, occurrence of relatively fresh water is restricted to Aquifer B and its vicinity. Elevated values of TDS are a result of increasing Na and SO₄ concentrations and, to a lesser extent, increasing concentrations of Ca and Cl.



0A 7053

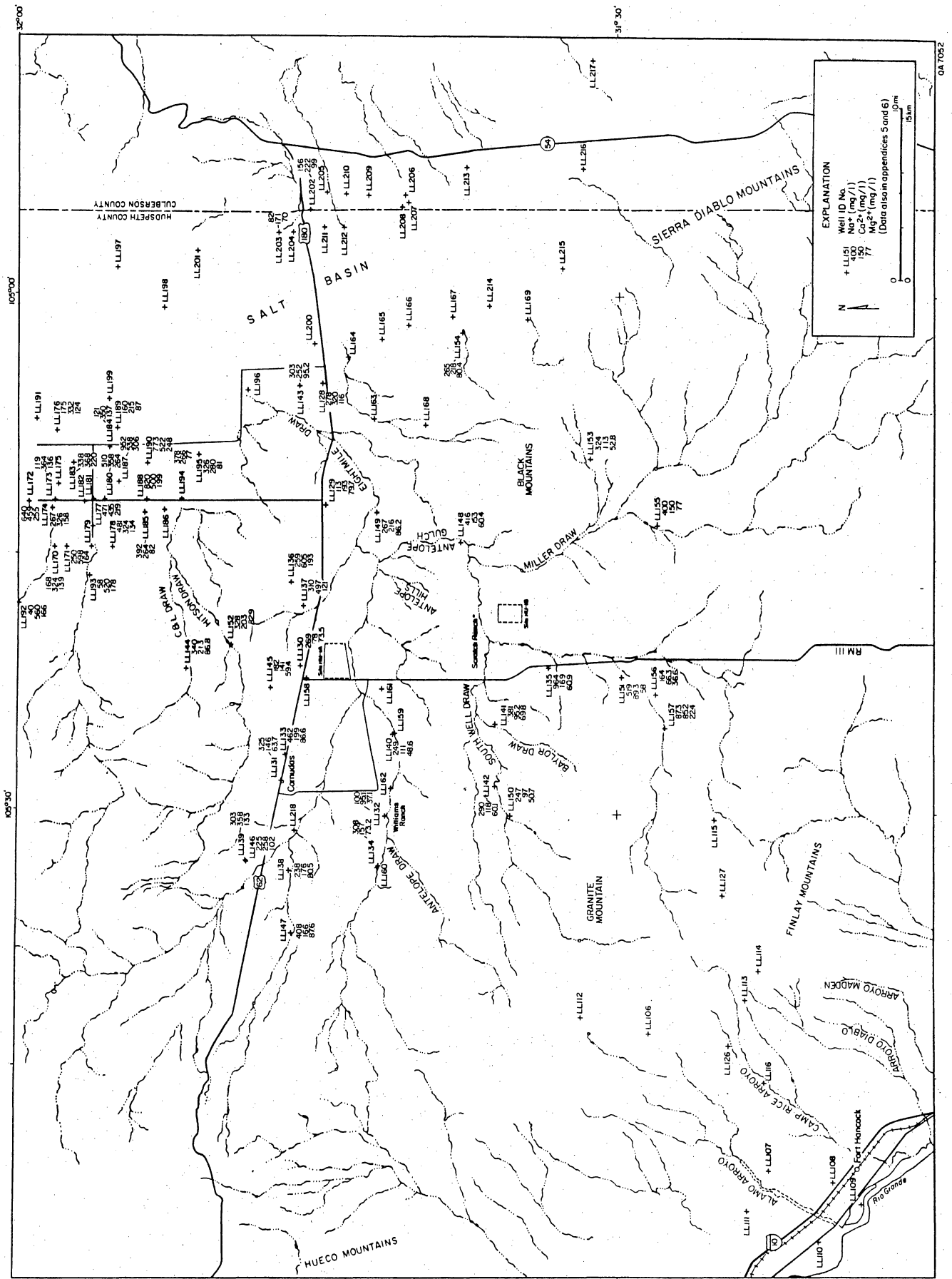


Figure 50. Map of Na, Ca, and Mg (mg/L) distribution.

Figure 51. Chemical facies map, Aquifers A and B. Water chemical facies vary from mainly Ca-Na-HCO₃ and Na-SO₄ in the southwest (Aquifers A and B) to Na-SO₄, Ca-SO₄, and Na-Cl facies in the northeast. This shift in facies may be the result of the changing lithology from Cretaceous limestone interbedded with marl and clay to Permian limestone that may include Ca, SO₄, and Cl-rich evaporites.

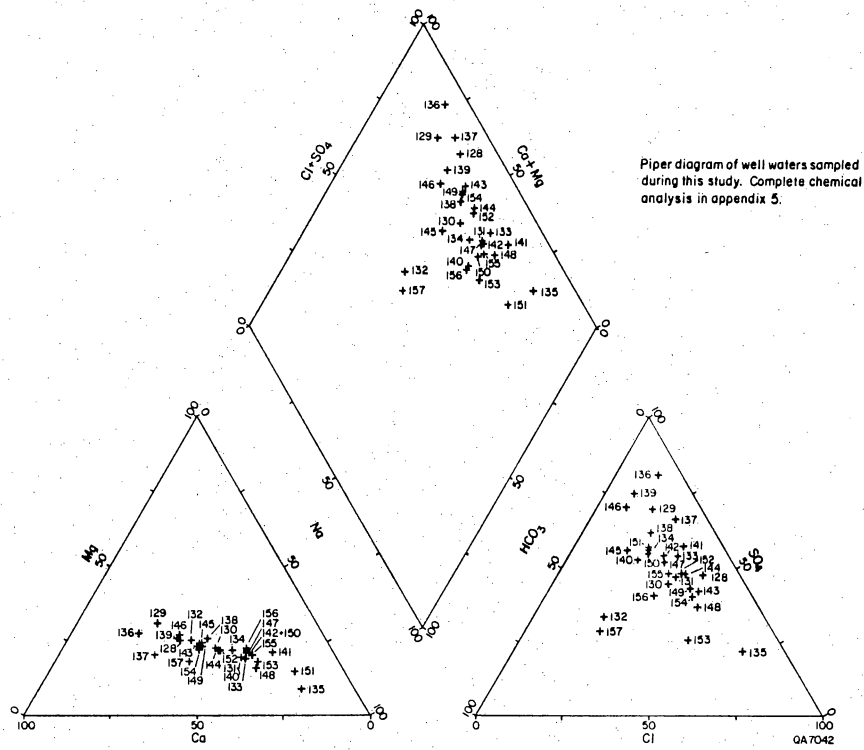


Figure 52. Piper diagram, Aquifers A and B.

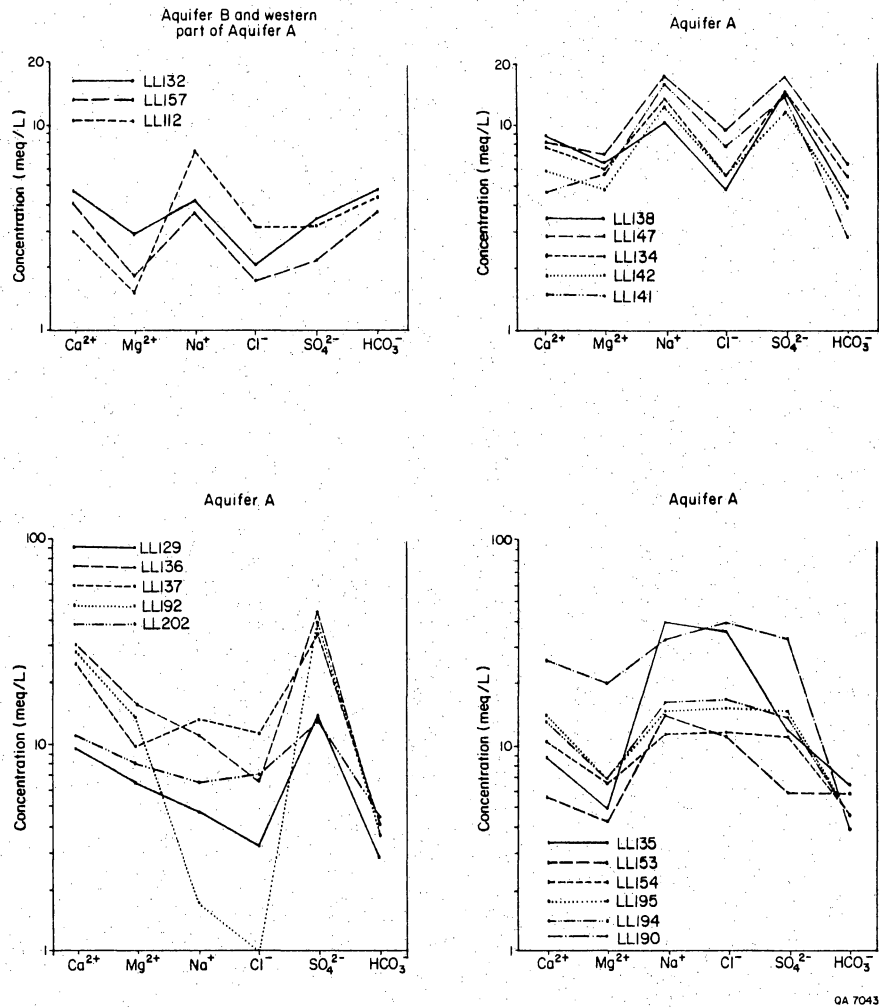
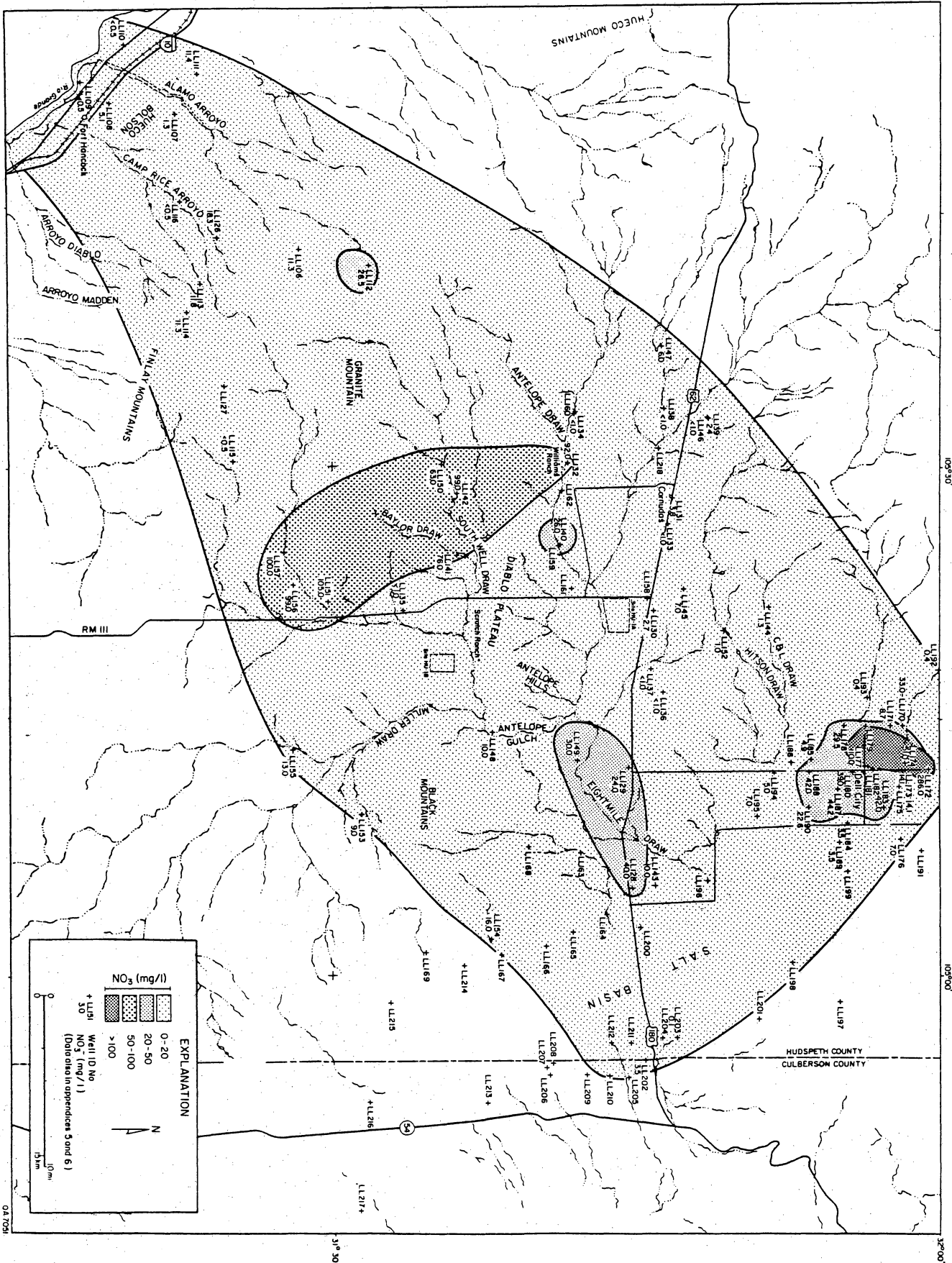


Figure 53. Salinity diagrams, Aquifers A and B, at different regions within the study area.

Figure 54. Map of NO_3 distribution. Higher NO_3 concentrations (mg/L) exist in Aquifer B than in Aquifer A. Shallower depth to ground water in Aquifer B permits more rapid recharge. The source of nitrates may be anthropogenic, and contaminant can rapidly reach water table through fracture permeability. Some of the wells with high NO_3 , however, contain no tritium, suggesting other sources of NO_3 .



EXPLANATION

NO₃ (mg/l)

0-20	20-50	50-100	>100
------	-------	--------	------

Well ID No
 NO₃ (mg/l)
 (Data also in appendices 3 and 6)

0 10m 15m

N

04704

31° 30'

106° 00'

106° 30'

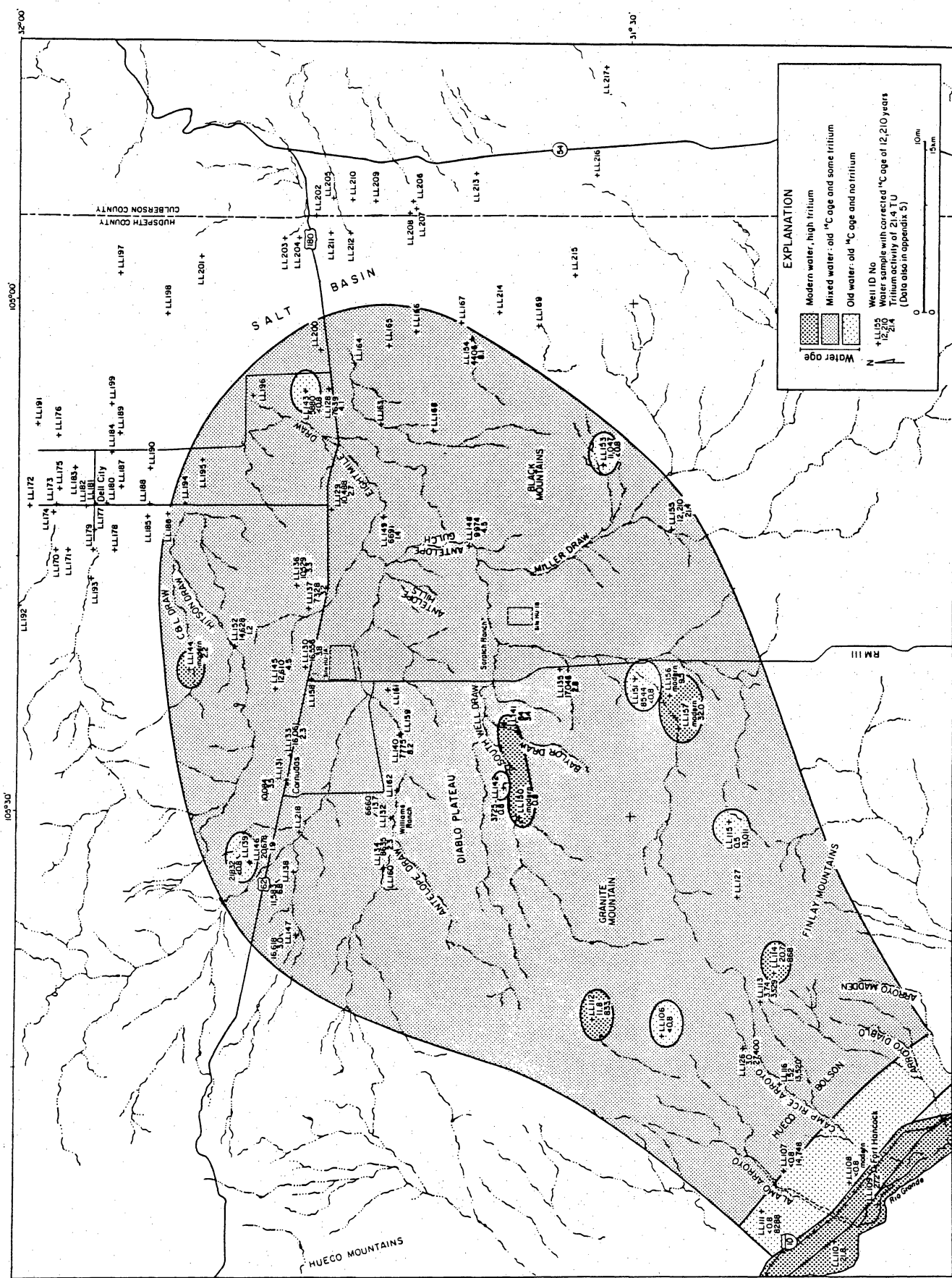
106° 00'

have been observed in other arid regions where they could not be related to anthropogenic sources.

Tritium activity data ranged from 0 to 32 TU and, except for four ground-water samples, all samples had varying amounts of tritium, indicating active recharge into both Aquifer A and Aquifer B (fig. 55). Ground-water ages determined by ^{14}C ranged from recently recharged modern water to 23,000-yr-old water (fig. 55). Tritium and ^{14}C activities vary significantly within short distances and do not show a clear distribution pattern. However, the youngest ^{14}C values and highest tritium values occur in the southwestern part of the study area in Aquifers A and B. The oldest water (> 20,000 yr old) can be found in the northern area of Aquifer A (fig. 55). The variable distribution of tritium (and variable chemical composition) across the study area strongly suggests the importance of fracture flow. The presence of tritium in ground water throughout the entire region and even where the water table is deeper than 700 ft (213 m) below land surface indicates that rapid recharge occurs along fractures in all regions of the study area and is not restricted to Aquifer B or to hydrologically updip areas in Aquifer A.

The ^{14}C ages are considered rough approximations. The presence of tritium in the waters indicates recharge that occurred post-1950. Some waters with high tritium concentrations have a low percent modern carbon (PMC) and old-corrected ages (e.g., LL155). This disparate situation may indicate mixing of very young waters with older waters or it may indicate that the calculated ^{14}C ages are erroneous. The $\delta^{13}\text{C}$ values of the bicarbonate are in a range of -10 to -3‰, heavier than those observed in most aquifers and significantly heavier than those of recently recharged ground waters. This suggests complex chemical reactions controlling the carbonate geochemistry and possibly altering the PMC values and the $\delta^{13}\text{C}$ values, both of which are necessary for calculating ^{14}C age.

Figure 55. Map of ^{14}C and tritium distribution. Tritium activity data range from 0 to 32 TU and, except for four ground-water samples, all samples have varying amounts of tritium, indicating active recharge into both Aquifer A and Aquifer B. Ground-water ages determined by ^{14}C ranged from recently recharged modern water to 22,831-yr-old water. Presence of tritium in water with old ^{14}C corrected age may indicate mixing of very young water with older waters, or it may indicate that the calculated ^{14}C ages are erroneous. Tritium and ^{14}C activities vary significantly within short distances and do not show a clear distribution pattern, suggesting the importance of fracture flow.



Ground-water samples vary in $\delta^{18}\text{O}$ values from -6.90 to -10.53 ‰, and δD values vary from -46.4 to 81.5 ‰ (with the exception of one sample [LL141] which had relatively enriched values of -2.72 and -35.3 ‰, respectively) (fig. 56). Heavier values (-6.90 to -8.27 ‰ for $\delta^{18}\text{O}$, and -46.4 to -64.2 ‰ for δD) are encountered at the western and southwestern parts of Aquifers A and B, where ground-water salinities are relatively low (fig. 49), and the age of water (determined by ^{14}C and tritium) is young (fig. 55). Annual weighted means of $\delta^{18}\text{O}$ and δD in rainfall sampled in Midland are -6.9 and -45 ‰, respectively (Nativ and Riggio, in preparation), similar to the values encountered in ground water in the western and southwestern parts of the study area. Based on these observations, it is suggested that the ground water of these areas represents the recharge end-member of the hydrologic system.

The most depleted values of $\delta^{18}\text{O}$ and δD occur in the northern part of Aquifer A where water has the oldest ^{14}C dates and lacks tritium (fig. 55). Similarly depleted values of $\delta^{18}\text{O}$ and δD were observed in Gunsight well (LL115) during investigations at S-34. Depleted values of stable isotopes in ground water can result from several mechanisms (Dansgaard, 1964). Cool, humid climatic conditions during recharge or an elevated recharge source are the more probable mechanisms relevant to this area. Occurrence of these exceptionally depleted values can be explained either by a cooler or more humid climate that may have prevailed in the area 20,000 years ago, when the water recharged the aquifer (based on the ^{14}C age of these ground-water samples), or by an elevated source of recharge to this area, other than the Diablo Plateau.

In the study area $\delta^{18}\text{O}$ and δD values of ground water generally plot parallel to and below the meteoric water line (Craig, 1961) (fig. 57). Ground-water samples collected from the southern Hudspeth County and Culberson County sites had similar

Figure 56. Map of $\delta^{18}\text{O}$ and δD distribution. Ground-water samples vary in $\delta^{18}\text{O}$ values from -6.90 to -10.53 ‰, and δD values vary from -46.4 to -81.5 ‰ (with the exception of well LL141). Enriched values, which resemble current annual mean rainfall values in Midland, are encountered at the west and southwest parts of the study area (in both Aquifer A and Aquifer B), where ground-water salinities are relatively low, tritium activities are high, and the age of the water is young. The most depleted values of $\delta^{18}\text{O}$ and δD occur in the north, where water has the oldest ^{14}C dates and lacks tritium.

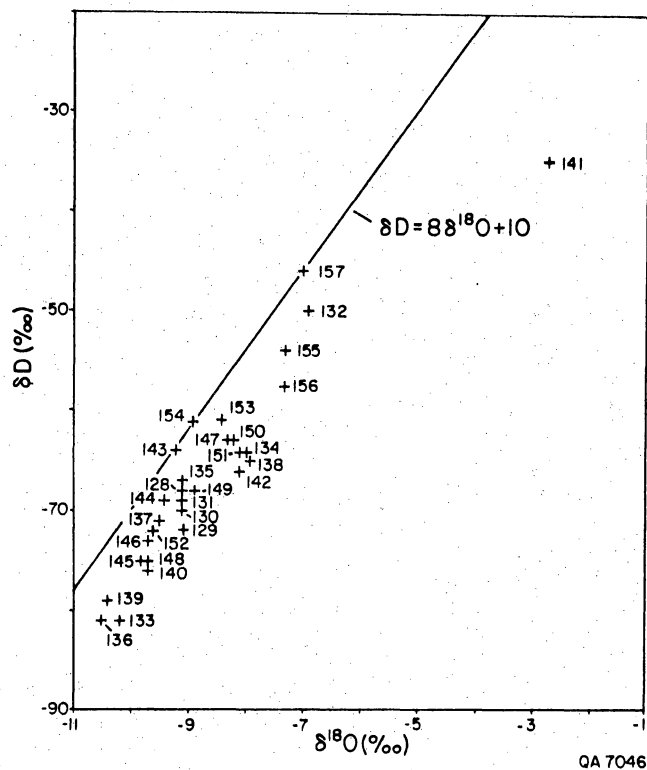


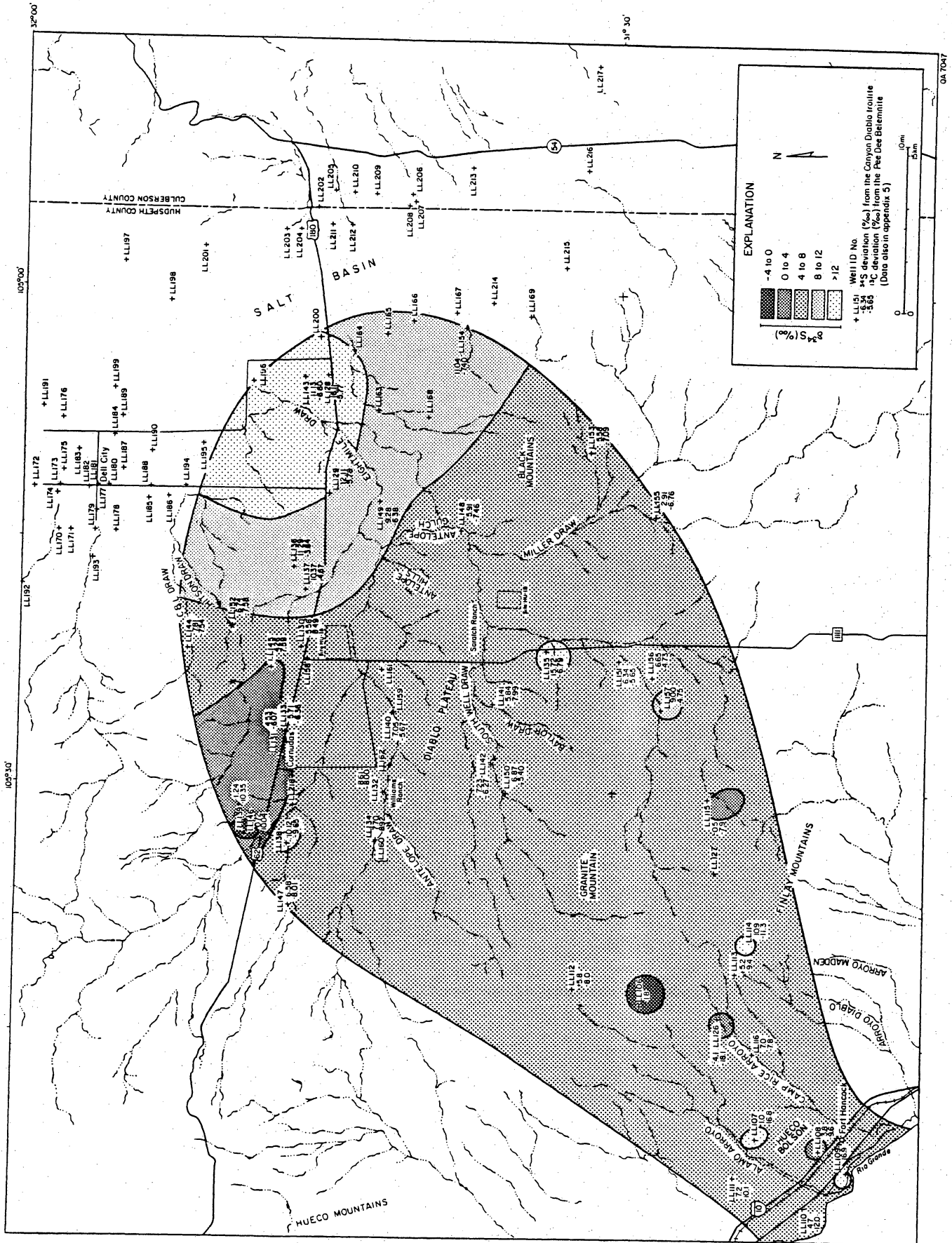
Figure 57. Plot of $\delta^{18}\text{O}$ versus δD . Values of $\delta^{18}\text{O}$ and δD in ground water in the study area generally plot parallel to and below the meteoric water line (Craig, 1961), similar to ground water in the southern Hudspeth County and Culberson County sites. These data may reflect a local version of the meteoric water line, controlled by high temperatures and evaporation rates prevailing in the study area.

plots. These data may reflect a local version of the world meteoric line. Stable isotope data of ground water from Roswell basin, eastern New Mexico (Hoy and Gross, 1982), indicate a shift of the local line to fit the line equation $\delta D = 7.27\delta^{18}O + 5.36$, rather than Craig's equation (1961) $\delta D = 8\delta^{18}O + 10$. Hoy and Gross (1982) related this shift to the higher temperatures and increased evaporation rates that prevail in eastern New Mexico. However, isotope data from the Ogallala, Dockum, and Cretaceous aquifers of the Texas Panhandle (Nativ and Smith, 1985), where climatic conditions are similar, plot along the world meteoric line, rather than below it.

Values of $\delta^{34}S$ range from -1.24 to $+16.11^{\circ}/\text{oo}$. (fig. 58); two-thirds of the samples have values above $+6^{\circ}/\text{oo}$. Heavier values (9.28 to $16.11^{\circ}/\text{oo}$) were encountered in the north and northeast of Aquifer A toward the discharge zone (fig. 47) and suggest that the dissolved SO_4 in ground water in this area is from dissolution of anhydrite in the host rock. These $\delta^{34}S$ values of dissolved sulfate are typical of Permian sulfate minerals (10 to $15^{\circ}/\text{oo}$) (Hoefs, 1973; Claypool and others, 1980). The $\delta^{34}S$ of the ground water SO_4 from Block 46 and S-15 (Culberson County) occupies a narrow range of $+9$ to $+11^{\circ}/\text{oo}$ and indicates simple Permian evaporite dissolution. In other parts of the study area, values are less enriched, possibly because of shorter reaction time with the host rock, or in the case of Aquifer B because of either different $\delta^{34}S$ values of sulfate minerals in the Cretaceous host rock or a mixing of sulfates from Cretaceous and Permian rocks. The most depleted $\delta^{34}S$ values are found in the northern part of Aquifer A, where ground water has other unique features regarding ^{14}C , tritium, $\delta^{18}O$, and δD values.

Values of $\delta^{13}C$ range from -10.35 to $-3.64^{\circ}/\text{oo}$ (fig. 57). These values are heavier than those encountered in the southern Hudspeth County site. Most marine carbonate rocks have $\delta^{13}C = 0^{\circ}/\text{oo}$, whereas common values for organic material and

Figure 58. Map of $\delta^{34}\text{S}$ and $\delta^{13}\text{C}$ distribution. Values of $\delta^{34}\text{S}$ range from -1.24 to $+16.11$ ‰; two-thirds of the samples have values above $+6$ ‰. Values of $\delta^{13}\text{C}$ range from -10.35 to -3.64 ‰ and are heavier than those in the southern Hudspeth County site. Old ground water in the north has the most depleted $\delta^{13}\text{C}$ values, whereas young water in the south and southwest has enriched values.



CO₂ in soil are -25 to -20‰. The concentration of δ¹³C in ground water is determined by the input with recharge water and by reaction with the rock. However, the assumption that the enriched values found in ground water in the study area can be related to longer interaction time with the host rocks is not supported by the distribution of δ¹³C values. Old ground water in the northern part of Aquifer A has the most depleted δ¹³C values, whereas young water with elevated tritium values in Aquifer B has enriched values. Therefore, a different mechanism controls the range and distribution of δ¹³C in this area.

CONCLUSIONS

Lithologies underlying HU1A and HU1B are Precambrian rhyolite porphyry and Cretaceous limestone interbedded with some silty and muddy interbeds, respectively. The rhyolite porphyry is fractured. The fractures strike in many directions, dip from vertical to horizontal, and have limonite and hematite stains on the fracture surfaces. Most fractures contain no mineral fillings, indicating that they are not sealed. Cretaceous limestone at HU1B is not as fractured as the rhyolite porphyry at HU1A.

The Babb flexure is north of both sites; however, fractures away from the inferred margins of this regional structure may be related to deformation of the flexure. The flexure may be the Permian or post-Permian expression of a major pre-Permian strike-slip fault (Hodges, 1975). It is unknown if Cretaceous rocks have been warped by recurrent movement along the structure.

Flooding down Antelope Draw at HU1A may be very intense for short durations and should be considered during site selection.

Regional ground-water flow is mainly from southwest to northeast. The ground-water divide is located close to the Diablo Plateau scarp, the escarpment that defines

the northern edge of the Rio Grande basin, not along the Babb flexure. In the study area two aquifers are present; a shallow aquifer in the southwestern area with depths to water generally less than 200 ft (60 m) and a deeper aquifer through most of the region with depths to water up to 700 ft (213 m).

Recharge occurs over the entire study area and is not restricted to the updip part of the potentiometric surface in the areas of higher elevation. Tritium is found in nearly all wells regardless of their location on the regional water table, indicating rapid recharge throughout the area. Most recharge probably occurs during flooding of the arroyos that drain the plateau. Minimal recharge is expected through the interarroyo areas. Fractures are probably important pathways for recharge. Recharge along fractures is the best mechanism to move recent recharge water rapidly through a thick unsaturated section.

Ground-water flow is predominantly fracture controlled. Three separate fracture sets were identified during a pumping test. Because of the fracture control on ground-water flow, aquifer permeabilities based on seven pumping tests were found to be extremely variable, ranging from 847 gal/day/ft² (34.63 m/day) to 8.2×10^{-3} gal/day/ft² (6.7×10^{-5} m/day). Transmissivities were found to range from 49,986 gpd/ft of drawdown (6,683 ft²/d or 621 m²/d) to 2.39 gpd/ft of drawdown (0.32 ft²/d or 0.03 m²/d). Water wells in the Dell City area have reported transmissivities greater than 388,000 gpd/ft of drawdown (51,872 ft²/d or 4819 m²/d) (Logan, 1984). Minimum transmissivity could be determined for only three wells because the pumps installed in the water wells never adequately stressed the aquifer. All of the calculated transmissivities should be used with caution because the calculations are based on assumptions of porous media flow and not fracture flow, and they represent only seven pumping tests. The fractures may cause a very

anisotropic system, and flow may not be directly down the regional potentiometric gradient. Discharge is either by evaporation on the salt flats or through pumping wells.

Total dissolved solids content ranges from 715 to 3,803 mg/L. The dominant water types are Na-SO₄ and CaSO₄. Many of the waters have high NO₃ concentrations, which suggests recent recharge and possible contamination by animal wastes. The chemical composition of the waters appears to be randomly distributed; there is no coherent chemical evolution of the water as it flows down the potentiometric gradient. This may be due to control of flow by fracture pathways and by local recharge across the entire Diablo Plateau.

The shallower aquifer may or may not be present at either site, although it is not used in the immediate vicinity of either site. Depth to ground water in the deeper aquifer beneath the sites is probably greater than 600 ft (180 m).

ACKNOWLEDGMENTS

We would like to thank Wheeler Wilson, Josef W. Mussey, Joe Crawford, and John Peters of the Pennzoil Sulphur Mine in Culberson County for the valuable information regarding ground water and land subsidence at the mine area and for their help in ground-water sampling during this study. Appreciation is extended to Steve Hartman of the University of Texas Land Office for his assistance in obtaining permission to conduct field work. Kenneth Moore and Syd Sullenger, also of the University of Texas Land Office, were a great help in water well locations and plant identification. Many people and well owners in Hudspeth County provided information and help. However, we owe special thanks to Mr. and Mrs. Scott Wilkey for their help and care, Mr. and Mrs. Dennis Walker for information and equipment, Mr. E. Franklin for information about well locations and owners, and Mr. J. Galvan for help in locating wells.

We would like to thank Skeet and Jay Williams of the Williams Ranch for their hospitality, time, information, and use of their water wells during this study. We would also like to thank James Baylor of the Baylor Ranch and Gary Hebbert of the Dyer Ranch for permission and assistance during pumping and sampling tests. Richard Bowen of El Paso Natural Gas Company provided assistance in locating water well records for Pump Station No. 2. All the ranchers in the study area of Hudspeth County were true "West Texans," as shown through their daily assistance and cooperation. We owe special thanks to George and Ethyl Temple of Salt Flat, Texas, for their always open door after a hot day in the field. Thanks are also given to Alan Dutton of the Bureau of Economic Geology for his technical assistance and supervision during pumping test no. 1 operations. James Doss and Alan Standen of the Bureau performed the second phase of drilling in

January 1987. Homer Logan of the Soil Conservation Service has been a valuable resource through his recharge studies in the Dell City area.

Saleem M. Akhter, Arten Avakian, and Gay Nell Gutierrez of the Bureau of Economic Geology helped with data processing, mapping, sample processing, proofreading, and drafting. Bernd C. Richter reviewed the report. Word processing was by Dottie Johnson, Kurt Johnson, Rosanne M. Wilson, and Ginger Zeikus, coordinated by Lucille C. Harrell. Base maps were drafted by Richard L. Dillon. Figures were drafted by Nan Minchow-Newman, Donald W. Thompson, Marty Thompson, T. B. Samsel III, and Annie Kubert-Kearns, under the supervision of Richard L. Dillon. The report was edited by Mary Ellen Johansen and Amanda R. Masterson. Funding for this study was provided by the Texas Low-Level Radioactive Waste Disposal Authority under contract no. IAC(86-87)-0828 and IAC(86-87)-1061.

REFERENCES

- Adams, J. E., 1944, Upper Permian Ochoa series of the Delaware Basin, west Texas and southeastern New Mexico: American Association of Petroleum Geologists Bulletin, v. 28, no. 11, p. 1596-1625.
- Albritton, C. C., Jr., and Smith, J. F., 1965, Geology of the Sierra Blanca area, Hudspeth County, Texas: U.S. Geological Survey Professional Paper 479, 131 p.
- Allison, G. B., and Hughes, M. W., 1978, The use of environmental chloride and tritium to estimate total recharge to an unconfined aquifer: Australian Journal of Soil Research, v. 16, p. 181-195.
- Allison, G. B., Stone, W. J., and Hughes, M. W., 1985, Recharge in karst and dune elements of semi-arid landscape as indicated by natural isotopes and chloride: Journal of Hydrology v. 76, p. 1-25.
- Alvarez, H. J., and Buckner, A. W., 1980, Ground-water development in the El Paso region, Texas, with emphasis on the Lower El Paso Valley: Texas Department of Water Resources Report 246, 346 p.
- Anderson, R. Y., Dean, W. E., Jr., Kirkland, D. W., and Snider, H. I., 1972, Permian Castile varved evaporite sequence, West Texas and New Mexico: Geological Society of America Bulletin, v. 83, p. 59-86.
- Askew, B., and Algermissen, S. T., 1983, An earthquake catalog for the Basin and Range province, 1803-1977: U.S. Geological Survey Open-File Report 83-86, 21 p.
- Askew, Bonny, and Algermissen, S. T., 1983, An earthquake catalog for the Basin and Range province, 1803-1977: U.S. Geological Survey Open-File Report 83-86, 21 p.

- Asquith, G. B., 1982, Basic well log analysis for geologists: Tulsa, Oklahoma, American Association of Petroleum Geologists, 210 p.
- Bachman, G. O., and Machette, M. N., 1977, Calcic soils and calcretes in the southwestern United States: U.S. Geological Survey Open-File Report 77-794, 162 p.
- Barnes, V. E., project director, 1983, Van Horn - El Paso Sheet: The University of Texas at Austin, Bureau of Economic Geology Geologic Atlas of Texas, scale 1:250,000.
- Bebout, D. G., and Loucks, R. G., 1984, Handbook for logging carbonate rocks: The University of Texas at Austin, Bureau of Economic Geology Handbook 5, 43 p.
- Boersma, L., 1965, Field measurement of hydraulic conductivity above water table, in Black, L. A., ed., Methods of soil analysis: American Society of Agronomy, p. 222-234.
- Bomar, G. W., 1983a, 1982--When a tornado hit Paris, a review of Texas' weather during the year: Texas Department of Water Resources Publication LP-195, 117 p.
- _____ 1983b, Texas weather: Austin, University of Texas Press, 265 p.
- Boyd, F. M., and Kreitler, C. W., 1986, Hydrology of a gypsum playa, northern Salt Basin, Texas: The University of Texas at Austin, Bureau of Economic Geology Report of Investigations No. 158, 37 p.
- Brown, J. B., Rogers, L. T., and Baker, B. B., 1973, Reconnaissance investigation of the ground water resources of the middle Rio Grande Basin, Texas: Texas Water Commission Bulletin 6502, p. M-1 - M-80.
- Brune, G., 1981, The springs of Texas: Fort Worth, Branch-Smith, 566 p.
- Carr, J. T., 1967, The climate and physiography of Texas: Texas Water Development Board Report 53, 27 p.

- Chapman, J. E. B., 1984, Hydrogeochemistry of the unsaturated zone of a salt flat in Hudspeth County, Texas: The University of Texas at Austin, Master's thesis, 132 p.
- Claypool, G. E., Holser, W. T., Kaplan, I. R., Sakai, H., and Zak, I., 1980, The age curves of sulfur and oxygen isotopes in marine sulfate and their mutual interpretation: *Chemical Geology*, v. 28, p. 199-260.
- Correll, D. S., and Johnston, M. C., 1970, *Manual of vascular plants in Texas*: Renner, Texas, Texas Research Foundation, 1881 p.
- Craig, H., 1961, Isotopic variations in meteoric waters: *Science*, v. 133, p. 1702-1703.
- Dames and Moore, 1985, Siting of a low-level radioactive waste disposal facility in Texas: Evaluation of State-owned lands: v. 2, Attachment C.
- Dames and Moore, 1985, Siting of a low-level radioactive waste disposal facility in Texas: Evaluation of State-owned lands, part III, appendix B.
- Dansgaard, W., 1964, Stable isotopes in precipitation: *Tellus*, v. 16, p. 436-469.
- Davis, M. E., and Leggat, E. R., 1973, Reconnaissance investigation of the ground water resources of the upper Rio Grande Basin, Texas: Texas Water Commission Bulletin 6502, p. U-1 - U-99.
- D'Appolonia Consulting Engineers, Inc., 1978, Phase I, ground-water recharge study, site 1: Cornudas, North and Culp Draws watershed, Site 2: Hitson, C & L and Washburn Draws watershed, Hudspeth County, Texas: United States Department of Agriculture, Soil Conservation Service, Temple, Texas, 65 p.
- Dougherty, J. P., 1975, Evaporation data in Texas: Texas Water Development Board Report 192, 237 p.
- Driscoll, F. G., 1986, *Groundwater and wells*, 2nd. ed.: St. Paul, Minnesota, Johnson Division, 1,089 p.

- Dumas, D. B., 1980, Seismicity in the Basin and Range province of Texas and northeastern Chihuahua, Mexico, in Dickerson, P. W., Hoffer, J. M., and Callender, J. F., eds., Trans-Pecos region, southeastern New Mexico and West Texas: New Mexico Geological Society 31st Annual Field Conference Guidebook, p. 77-81.
- Flawn, P. T., 1956, Basement rocks of Texas and southeast New Mexico: University of Texas, Austin, Bureau of Economic Geology Bulletin 5605, 261 p.
- Freeze, R. A., and Cherry, J. A., 1979, Groundwater: Englewood Cliffs, New Jersey, Prentice-Hall, Inc., 604 p.
- Gardner, J. S., and Dumanoir, J. L., 1980, Litho-density log interpretation: Society of Professional Well Log Analysts Transactions v. 21, p. I-1 - I-23.
- Gates, J. S., and Stanley, W. D., 1976, Hydrologic interpretations of geophysical data from the southeastern Hueco Bolson, El Paso and Hudspeth Counties, Texas: U.S. Geological Survey Open-File Report 76-650, 37 p.
- Gates, J. S., White, D. E., Stanley, W. D., and Ackermann, H. D., 1980, Availability of fresh and slightly saline ground water in the basins of westernmost Texas: Texas Department of Water Resources Report 256, 108 p.
- Gile, L. H., Hawley, J. W., and Grossman, R. B., 1981, Soils and geomorphology in the Basin and Range area of southern New Mexico--guidebook to the Desert Project: New Mexico Bureau of Mines and Mineral Resources Memoir 39, 222 p.
- Goetz, L. K., 1977, Quaternary faulting in Salt Basin graben: The University of Texas at Austin, Master's thesis, 136 p.
- Groat, C. G., 1972, Presidio Bolson, Trans-Pecos Texas and adjacent Mexico: geology of a desert basin aquifer system: The University of Texas at Austin,

- Bureau of Economic Geology Report of Investigations No. 76, 46 p.
- Guyton, W. F., and Associates, 1971, Availability of brackish water from Mesa area of Hueco Bolson, El Paso County, Texas: report prepared for El Paso Electrical Company, El Paso, Texas, 26 p.
- Haley, J. F., 1971, Rb-Sr geochemistry of alkalic igneous intrusions, northern Trans-Pecos Texas: The University of Texas at Austin, Master's thesis, 62 p.
- Henry, C. D., and Price, J. G., 1985, Summary of the tectonic development of Trans-Pecos Texas: The University of Texas at Austin, Bureau of Economic Geology Miscellaneous Map No. 36, 8 p.
- Hodges, F. N., 1975, Petrology, chemistry and phase relations of the Sierra Prieta nepheline-analcime syenite intrusion, Diablo Plateau, Trans-Pecos Texas: The University of Texas at Austin, Ph.D. dissertation, 184 p.
- Hoefs, J., 1973, Stable isotopes geochemistry: New York, Springer-Verlag, 112 p.
- Hoy, R. N., and Gross, G. W., 1982, A baseline study of oxygen 18 and deuterium in the Roswell, New Mexico, groundwater basin: New Mexico Water Resources Research Institute, partial technical completion report for U.S. Department of the Interior, Office of Water Research and Technology, Project No. B-059-nmex.
- Izett, G. A., and Wilcox, R. E., 1982, Map showing localities and inferred distributions of the Huckleberry Ridge, Mesa Falls, and Lava Creek ash beds (Pearlette family ash beds) of Pliocene and Pleistocene age in the western United States and southern Canada: U.S. Geological Survey Miscellaneous Investigations Series Map I-1325.

- King, P. B., 1948, Geology of the Southern Guadalupe Mountains, Texas: U.S. Geological Survey Professional Paper 215, 183 p.
- _____ 1949, Regional geologic map of parts of Hudspeth and Culberson Counties, Texas: U.S. Geological Survey Oil and Gas Investigations Preliminary Map 90.
- _____ 1965, Geology of the Sierra Diablo region, Texas: U.S. Geological Survey Professional Paper 480, 185 p.
- King, P. B., and Flawn, P. T., 1953, Geology and mineral deposits of pre-Cambrian rocks of the Van Horn area, Texas: University of Texas, Austin, Bulletin 5301, 218 p.
- Kruseman, G. P., and De Ridder, N. A., 1976, Analysis and evaluation of pumping test data (3d ed.): Wageningen, The Netherlands, International Institute for Land Reclamation and Improvement, Bulletin 11, 200 p.
- Larkin, T. J., and Bomar, G. W., 1983, Climatic atlas of Texas: Texas Department of Water Resources Publication LP-192, 151 p.
- Leggat, E. R., 1962, Development of ground water in the El Paso district, Texas, 1955-1960, Progress Report 8: Texas Water Commission Bulletin 6204, 56 p.
- Lodge, J. P., Jr., Pate, J. B., Basbergill, W., Swanson, G. S., Hill, K. C., Lorange, E., and Lazrus, A. L., 1968, Chemistry of United States precipitation, final report on the national precipitation sampling network: Boulder, National Center for Atmospheric Research, 66 p.
- Logan, H. H., 1984, A ground-water recharge project associated with a flood protection plan in Hudspeth County, Texas--supportive geologic applications: Texas Christian University, Master's thesis, 110 p.
- Masson, P. H., 1956, Age of igneous rocks at Pump Station Hills, Hudspeth County, Texas: American Association of Petroleum Geologists Bulletin, v. 40, no. 3, p. 501-518.

- Mazor, E., in press. Tracing ground water by its chemical, physical and isotopic parameters, a practical approach to field data.
- Miller, R. R., 1977. Composition and derivation of the native fish fauna of the Chihuahuan Desert region. in Wauer, R. H., and Riskind, D. H., eds., Transactions of the Symposium on the Biological Resources of the Chihuahuan Desert Region, United States and Mexico: Washington, D.C., U.S. Department of the Interior, National Park Service Transactions and Proceedings Series No. 3, p. 365-381.
- Motsch, S. A., 1951. Culberson County, Texas: The University of Texas at Austin, Master's thesis, 51 p.
- Muehlberger, W. R., Belcher, R. C., and Goetz, L. K., 1978, Quaternary faulting in Trans-Pecos Texas: *Geology*, v. 6, no. 6, p. 337-340.
- National Climatic Data Center, 1985, Texas, 1984: Asheville, North Carolina, National Oceanic and Atmospheric Administration, Climatological Data Annual Summary, v. 89, no. 13, 78 p.
- National Weather Service, 1986a, Texas water oriented data bank--NWS maximum temperature for ID 00002012: 328 p.
- _____ 1986b, Texas water oriented data bank--NWS minimum temperature for ID 00002012: 328 p.
- _____ 1986c, Texas water oriented data bank--NWS precipitation for ID 00002012: 411 p.
- Nativ, R., and Riggio, R., in preparation, Rain events in the Southern High Plains - their distribution and isotopic composition patterns.
- Nativ, R., and Smith, D. A., 1985, Characterization study of the Ogallala aquifer, northwest Texas: The University of Texas at Austin, Bureau of Economic Geology, prepared for the U.S. Department of Energy, Office of Nuclear Waste Isolation under Contract No. DE-AC97-83WM46651, 103 p.

- Nielson, P. D., and Sharp, J. M., Jr., 1985, Tectonic controls on the hydrogeology of the Salt Basin, Trans-Pecos Texas, in Structure and tectonics of Trans-Pecos Texas: West Texas Geological Society Guidebook, Publication 85-81, p. 231-234.
- Obert, L., and Duvall, W. L., 1967, Rock mechanics and the design of structures in rock: New York, John Wiley, 650 p.
- Olive, W. W., 1957, Solution-subsidence troughs, Castile Formation of Gypsum Plain, Texas and New Mexico: Geological Society of America Bulletin, v. 68, p. 351-358.
- Orton, R. B., 1969, Climates of the states -- Texas: Washington, D.C., United States Department of Commerce, Environmental Data Center, Climatography of the United States No. 60-41, 46 p.
- _____, 1964, The climate of Texas and adjacent Gulf waters: Washington, D.C., U.S. Department of Commerce, Weather Bureau, 195 p.
- Pearson, F. J., Jr., and White, D. E., 1967, Carbon-14 ages and flow rates of water in Carrizo Sands, Atascosa County, Texas: Austin, Water Resources Research, v. 3, p. 251-261.
- Peckham, R. C., 1963, Summary of the ground-water aquifers in the Rio Grande Basin: Texas Water Commission, Circular No. 63-05, 16 p.
- Porsch, E. L., Jr., 1917, The Rustler Springs sulphur deposits: University of Texas, Austin, Bulletin, 1722, 71 p.
- Reagor, B. G., Stover, C. W., Algermissen, S. T., 1982, Seismicity map of the state of Texas: U.S. Geological Survey Miscellaneous Field Studies, map MF-1388, U.S. Geological Survey, Denver, Colorado.
- Rightmire, C. T., 1967, A radioactive study of the age and origin of caliche deposits: The University of Texas at Austin, Master's thesis.

- Sanford, A. R., and Topozada, T. R., 1974, Seismicity of proposed radioactive waste disposal site in southeastern New Mexico: New Mexico Bureau of Mines and Mineral Resources Circular 143, 15 p.
- Scalapino, R. A., 1950, Development of ground water for irrigation in the Dell City area, Hudspeth County, Texas: Texas Board of Water Engineers, Bulletin 5004, 38 p.
- Schlumberger, 1974, Log interpretation manual/application, v. II: Houston, Schlumberger Well Services, Inc.
- _____ 1984, Log interpretation charts: Houston, Schlumberger Well Services, Inc., 106 p.
- Smith, A. R., 1980, Sulfur deposits in Ochoan rocks of the Gypsum Plain, southeast New Mexico and West Texas, in Dickerson, P. W., and Hoffer, J. M., eds., Trans-Pecos region, southeastern New Mexico and West Texas: New Mexico Geological Society 31st Field Conference Guidebook, p. 277-283.
- Snyder, R. P., and Gard, L. M., Jr., 1982, Evaluation of breccia pipes in southeastern New Mexico and their relation to the waste isolation pilot plant (WIPP) site: U.S. Geological Survey Open File Report 82-968.
- Stead, F. L., and Waldschmidt, W. A., 1953, Regional significance of the Pump Station Hills, in Haigh, B. R., and others, Sierra Diablo, Guadalupe, and Hueco areas of Trans-Pecos Texas: West Texas Geological Society Guidebook, p. 70-85.
- Stone, W. J., 1985, Recharge through calcrete, in Hydrogeology of rocks of low permeability: IAH conference, Tucson, Arizona, Memoires.
- Strain, W. S., 1966, Blancan mammalian fauna and Pleistocene formations, Hudspeth County, Texas: Texas Memorial Museum Bulletin No. 10, 55 p.
- Sullins, C. J., 1971, Red Hills intrusion, northern Hudspeth County, Texas: The University of Texas at Austin, Master's thesis, 63 p.

- Texas Water Development Board, 1985, Texas water oriented data bank--ground water quality system ID PD-115 for Hudspeth County, 24 p.
- Thornthwaite, C. W., 1931, The climates of North America according to a new classification: *Geographical Review*, v. 21, p. 633-655.
- U. S. Department of Commerce, Economic Development Administration, 1986, Dell City Water Feasibility Study: 37 p.
- U. S. Department of Housing and Urban Development, Federal Insurance Administration, 1985a, Flood hazard boundary maps, Hudspeth County, Texas: Community-- Panel Nos. 480361 0400 B and 480361 0550B.
- U.S. Department of Housing and Urban Development, Federal Insurance Administration, 1985b, Flood hazard boundary maps, Hudspeth County, Texas Community Panel Nos. 480361 0650B, 480361 0800B.
- Vogel, J. C., 1970, ^{14}C dating of ground water, in *Isotope hydrology*: Vienna, IAEA, p. 225-239.
- Walton, W. C., 1970, *Groundwater resource evaluation*: New York, McGraw-Hill, 664 p.
- Wasserburg, G. J., Wetherill, G. W., Silver, L. T., and Flawn, P. T., 1962, A study of the ages of the Precambrian of Texas: *Journal of Geophysical Research*, v. 67, no. 10, p. 4021-4047.
- Young, P. W., 1976, *Water resources survey of Hudspeth County: West Texas Council of Governments*, 156 p.

Appendix 1. Records of wells and springs in Culberson and Hudspeth sites (ft).

<u>BEG ID</u>	<u>Well name</u>	<u>TWC¹ ID</u>	<u>Coordinates</u>	<u>Ground- level elevation</u>	<u>Water- level depth</u>	<u>Water- level elevation</u>	<u>Total depth</u>
CULBERSON COUNTY							
Wells: S-15 Area							
LL100	Kohen Windmill		31°40'12" 104°10'50"	3331	75	3256	80
LL101	Smilin Jack Windmill		31°40'23" 104°12'22"	3480	70	3410	140
LL104	Monument Windmill		31°38'13" 104°10'52"	3455	150	3305	200
LL119	S-15 W. Windmill		31°39'10" 104°19'02"	3712			
LL120	Philips Windmill		31°40'06" 104°14'41"	3575			
LL121	S-15 N. Windmill		31°43'55" 104°14'59"	3560			
LL001	S-15 Scott Windmill		31°41'44" 104°09'48"	3348	115	3233	200
LL002	S-15 South Windmill		31°40'04" 104°08'09"	3310	58	3252	110
Wells: S-46 Area							
LL123	S-46 Seven L. Windmill		31°44'53" 104°28'18"	4055	20	4035	
LL124	S-46 High L. Windmill		31°42'46" 104°27'46"	4265			
LL125	S-46 Cave Well		31°40'03" 104°26'23"	4108	30	4078	
Springs: S-15 area							
LL102	Rustler Spring		31°38'42" 104°13'33"	3493		3493	
LL117	S-15 W. Sp		31°41'13" 104°17'33"	3730		3780	
LL118	S-15 S. Sp		31°38'43" 104°17'25"	3680		3680	
LL122	S-15 N. WM Sp		31°44'57" 104°15'19"	3572		3572	
LL400	Spring		31°50'43" 104°14'54"	3525		3525	
LL401	Toy Springs		31°49'16" 104°09'25"	3280		3280	
LL402	Springs		31°49'10" 104°10'37"	3355		3355	
LL403	Cotton Wood Sp		31°48'26" 104°11'50"	3445		3445	
LL404	Spring		31°45'48" 104°12'37"	3460		3460	
LL405	Springs		31°44'55" 104°12'38"	3485		3485	
LL406	Springs Well		31°44'42" 104°13'07"	3485		3485	
LL407	Horseshoe Spring		31°44'20" 104°09'52"	3275		3275	
LL408	Spring		31°46'30" 104°16'10"	3600		3600	
LL409	Spring		31°45'10" 104°18'23"	3700		3700	
LL413	Springs		31°39'33" 104°12'46"	3415		3415	
Springs: S-46 Area							
LL412	Burro Spring		31°46'41" 104°28'37"	4006		4006	
LL414	Spring		31°41'20" 104°26'06"	4130		4130	
LL415	Spring		31°39'26" 104°20'38"	3720		3720	

Appendix 1 (cont.)

BEG ID	Well name	TWC ¹ ID	Coordinates		Ground- level elevation	Water- level depth	Water- level elevation	Total depth
HUDSPETH COUNTY								
LL106	Thaxton Spring				4,500		4,500	
LL107		48-42-1	31°22'12"	105°50'52"	3,855	335	3,550	450
LL108		48-42-404	31°18'56"	105°51'27"	3,610	90	3,520	267
LL109		48-41-618	31°17'31"	105°52'45"	3,523	10	3,513	305
LL110	Miller Feedlot	48-41-2	31°19'37"	105°54'55"	3,545	8	3,536	160
LL111		48-33-9	31°23'18"	105°53'18"	3,882	327	3,555	367
LL112	Head of Canyon Wm		31°31'42"	105°42'05"	5,059	380	4,679	720
LL113	Wilkey Well No. 1		31°23'23"	105°40'48"	4,307	600	3,707	730
LL114	Wilkey Well No. 2		31°22'48"	105°39'07"	4,346	76	4,270	200
LL115	Gunsight Well 2		31°25'03"	105°30'20"	4,780	405	4,375	480
LL116	Owen Well		31°22'31"	105°45'50"	4,014	120	3,894	300
LL126	Low Level Well		31°24'14"	105°43'32"	4,179	478	3,699	530
LL127	Gunsight Well 1		31°24'43"	105°34'45"	5,154	627	4,527	690
LL128	Temple Well	48-24-1	31°44'40"	105°05'25"	3,726	107	3,619	
LL129	Guillen E on Well	48-23-201	31°44'48"	105°12'06"	4,007	429	3,578	
LL130	Desert Inn Well	48-14-7	31°45'56"	105°21'22"	4,135			
LL131	Cornudas Cafe Well	48-13-7	31°46'45"	105°28'09"	4,304			
LL132	Williams Ranch House Well	48-20-6	31°41'31"	105°30'09"	4,334	709	3,625	
LL133	Puett Well	48-13-8	31°46'38"	105°26'53"	4,341			
LL134	Hobo Well-Deep	48-20-5	31°41'44"	105°33'07"	4,416			
LL135	Jardin Well	48-30-4	31°33'27"	105°21'25"	4,282	528	3,754	
LL136	Sparks Windmill	48-14-9	31°46'18"	105°16'45"	4,053	446	3,607	
LL137	Sparks House Pump Well	48-14-8	31°45'39"	105°18'04"	4,032	510	3,522	
LL138	Williams #4 Well	48-12-8	31°46'21"	105°33'09"	4,409	790	3,619	
LL139	Stewart #2 Well	48-12-5	31°48'30"	105°32'52"	4,447			
LL140	Adobe House Tank Well	48-21-5	31°41'10"	105°25'18"	4,200			
LL141	Bravo Well	48-29-3	31°36'14"	105°24'27"	4,273	628	3,650	
LL142	Three Sisters Well	48-29-1	31°36'10"	105°28'18"	4,362	48	4,314	
LL143	Sumrall Well	48-16-7	31°45'57"	105°05'20"	3,668	100	3,568	
LL144	Foster House Well	48-14-1	31°51'44"	105°21'44"	4,186			
LL145	Foster South Well	48-13-9	31°47'15"	105°22'47"	4,182			
LL146	Stewart #1 Well	48-12-5	31°48'29"	105°32'56"	4,445			
LL147	Beard #1 Well	48-12-7	31°46'07"	105°37'02"	4,523			
LL148	Red Well	48-23-7	31°37'47"	105°14'20"	4,075	463	3,612	
LL149	Sampson Well	48-23-1	31°42'04"	105°12'45"	3,886	262	3,625	
LL150	South Well	48-28-3	31°35'29"	105°30'08"	4,430	63	4,367	
LL151	Moon Well	48-38-1	31°29'45"	105°21'59"	4,336	160	4,176	
LL152	Gibbs Well	48-14-4	31°49'17"	105°20'17"	4,081			
LL153	Hartnutt Well	48-31-9	31°31'20"	105°09'33"	4,509			
LL154	Flattop Well- Figure 2 Ranch	48-24-9	31°37'49"	105°02'10"	3,745	294	3,451	
LL155	Frederick Well	48-39-1	31°28'16"	105°13'16"	4,363	742	3,626	
LL156	Baylor-New Well	48-37-3	31°28'05"	105°22'59"	4,403	210	4,198	
LL157	Baylor-Old Well	48-37-3	31°27'38"	105°24'51"	4,449	72	4,377	

Appendix 1 (cont.)

BEG ID	Well name	TWC1 ID	Coordinates		Ground-level elevation	Water-level depth	Water-level elevation	Total depth
HUDSPETH COUNTY								
LL158	Desert Inn Abnd. Well	48-14-7	31°45'38"	105°22'05"	4,170	549	3,622	
LL159	Abnd. Adobe House Tank	48-21-5	31°41'06"	105°25'15"	4,201	583	3,618	
LL160	Hobo Well-Shallow	48-20-5	31°41'48"	105°33'08"	4,415	18	4,397	
LL161	Geothermal Well (UTEP)	48-21-6	31°41'47"	105°22'40"	4,224	74	4,150	
LL162	Williams Pump Jack #1	48-21-4	31°41'18"	105°28'50"	4,303	677	3,626	
LL163	Cavender Well	48-24-4	31°42'15"	105°07'19"	3,832	310	3,522	
LL164	Graham Well	48-24-2	31°43'34"	105°03'40"	3,668	100	3,568	
LL165	Bill Crane Well	48-24-5	31°41'54"	105°02'38"	3,658	140	3,518	
LL166	Morrison Well	48-24-6	31°40'34"	105°01'48"	3,629	40	3,589	
LL167	Wesley West Well	48-24-9	31°38'20"	105°01'11"	3,659	80	3,579	
LL168	Black Mountain Well	48-23-9	31°39'39"	105°07'34"	3,993	460	3,533	
LL169	Babbs Well	48-32-6	31°34'38"	105°01'22"	3,718	123	3,595	
LL170		48-07-101	31°58'08"	105°14'39"	3,804	205	3,599	700
LL171		48-07-102	31°57'33"	105°14'40"	3,795	213	3,577	962
LL172		48-07-206	31°59'25"	105°12'02"	3,709	129	3,580	215
LL173		48-07-207	31°58'10"	105°12'01"	3,707	122	3,585	712
LL174		48-07-210	31°58'15"	105°12'27"	3,721	145	3,576	240
LL175		48-07-214	31°57'56"	105°10'57"	3,678	93	3,585	500
LL176		48-07-304	31°58'00"	105°07'55"	3,644	60	3,584	
LL177		48-07-405	31°56'17"	105°13'27"	3,755	175	3,580	230
LL178		48-07-414	31°55'13"	105°14'39"	3,795	212	3,583	680
LL179		48-07-418	31°56'17"	105°14'39"	3,805	216	3,590	886
LL180		48-07-501	31°55'37"	105°11'51"	3,688	106	3,582	
LL181		48-07-504	31°56'11"	105°12'00"	3,696	72	3,624	175
LL182		48-07-516	31°56'37"	105°12'02"	3,705	119	3,586	300
LL183		48-07-606	31°57'10"	105°09'51"	3,651	67	3,583	
LL184		48-07-607	31°55'23"	105°08'51"	3,641	59	3,582	
LL185		48-07-706	31°53'34"	105°12'38"	3,712	131	3,581	835
LL186		48-07-708	31°52'37"	105°12'32"	3,722	138	3,584	1,583
LL187		48-07-801	31°54'53"	105°10'56"	3,658	80	3,578	200
LL188		48-07-803	31°53'31"	105°12'00"	3,693	100	3,593	278
LL189		48-07-901	31°54'56"	105°07'49"	3,637	53	3,584	300
LL190		48-07-904	31°53'27"	105°09'51"	3,660	62	3,598	780
LL191		48-08-102	31°59'03"	105°07'17"	3,642	56	3,586	392
LL192		48-06-201	31°59'59"	105°17'54"	3,940	303	3,637	1,100
LL193		48-06-601	31°56'20"	105°16'15"	3,874	310	3,564	1,505
LL194		48-15-203	31°51'43"	105°11'55"	3,715	138	3,599	325
LL195		48-15-301	31°50'53"	105°09'19"	3,652	60	3,593	320
LL196		48-16-402	31°48'26"	105°05'31"	3,652	61	3,591	140
LL197	(Eclipse Well)	47-01-7	31°54'57"	104°58'24"	3,671	50	3,621	
LL198		48-08-9	31°52'37"	105°00'45"	3,635	22	3,613	
LL199		48-08-4	31°55'23"	105°06'05"	3,616	3	3,613	
LL200		48-16-8	31°45'11"	105°02'50"	3,622	23	3,599	
LL201		47-09-1	31°50'58"	104°57'21"	3,697	91	3,606	
LL202		47-09-803	31°45'19"	104°55'01"	3,790	191	3,599	

Appendix 1 (cont.)

<u>BEG ID</u>	<u>Well name</u>	<u>TWC¹ ID</u>	<u>Coordinates</u>		<u>Ground- level elevation</u>	<u>Water- level depth</u>	<u>Water- level elevation</u>	<u>Total depth</u>
HUDSPETH COUNTY								
LL203		47-09-805	31°46'51"	104°56'17"	3,696	97	3,591	515
LL204		47-09-8	31°46'10"	104°56'16"	3,722	130	3,592	
LL205	(Black John Well)	47-17-3A	31°44'27"	104°53'57"	3,805	202	3,603	
LL206		47-17-6A	31°40'51"	104°53'50"	3,722	135	3,587	
LL207		47-17-6B	31°40'39"	104°54'06"	3,708	141	3,567	
LL208		47-17-6C	31°40'51"	104°54'59"	3,639	29	3,610	
LL209	(Hardluck Well)	47-17-3B	31°42'20"	104°54'06"	3,697	97	3,600	
LL210		47-17-3C	31°43'31"	104°54'02"	3,755	159	3,596	
LL211		47-17-2A	31°44'33"	104°56'00"	3,717	112	3,605	
LL212		47-17-2B	31°43'38"	104°56'03"	3,688	84	3,604	
LL213		47-18-4A	31°37'37"	104°52'25"	3,762	163	3,599	
LL214		48-32-3	31°36'30"	105°00'39"	3,636	39	3,597	
LL215	(Curton Well?)	47-25-4	31°32'45"	104°58'24"	3,650	48	3,602	
LL216		47-26-7	31°31'44"	104°52'30"	3,674	88	3,586	
LL217		47-26-9	31°31'18"	104°46'02"	3,786	202	3,584	
LL218	Abandoned Well	48-12-9	31°46'13"	105°30'51"	4,325	675	3,650	
LL219	Love Well	48-39-701	31°24'17"	105°13'50"	4,517	389	3,628	
LL220	Maupin Well	48-38-703	31°23'14"	105°20'37"	4,515	888	3,627	

¹TWC well identification system has 3 sets of numbers; preliminary wells have 1 number in the last set, permitted wells have 3.

Appendix 2. Chemical and isotopic composition of ground-water samples.
Major ions (mg/L) and temperatures (°C).

BEG ID	Well Name	Coordinates		Ca ²⁺	Mg ²⁺	Na ⁺	K ⁺	HCO ₃ ⁻	SO ₄ ²⁻	Cl ⁻	NO ₃ ⁻	TDS	Temp.
LL100	Kohen Windmill	31°40'12"	104°10'50"	517	229.0	367.0	16.2	223	2310	283	36.1	3993.9	17.6
LL101	Smilin Jack Windmill	31°40'23"	104°12'22"	587	83.3	38.0	7.3	121	1650	50	79.7	2627.7	19.0
LL102	Rustler Spring	31°38'42"	104°13'33"	595	49.8	68.7	6.7	133	1580	70	22.1	2534.2	14.9
LL103	Division Windmill	31°37'16"	104°13'03"	527	220.0	74.0	5.3	187	1960	91	0.4	3085	
LL104	Monument Windmill	31°38'13"	104°10'52"	277	115.0	45.0	3.2	258	900	40	10.3	1655.8	21.0
LL105	Rio Grande Water	31°16'23"	105°51'14"	86.9	18.5	186	7.8	214	234	185	6.6	941.9	11.0
LL106	Thaxton Sp	31°28'11"	105°42'57"	26.8	22.9	475	4.6	501	520	148	11.3	1718.3	9.0
LL107	48-42-1 Windmill	31°22'12"	105°50'52"	169.0	35.3	1250	7.7	161	2270	520	1.3	4421.6	24.5
LL108	48-42-404 Well	31°18'56"	105°51'27"	34.7	11.9	410	4.5	263	395	259	5.1	1388.1	22.5
LL109	48-41-618 Well	31°17'31"	105°52'45"	23.8	23.9	486	14.6	96	315	555	<0.5	1517.5	
LL110	48-41-2 Well	31°19'37"	105°54'55"	387.0	91.7	881	12.8	495	770	1450	<0.5	3604.1	19.0
LL111	48-33-9 Windmill	31°23'18"	105°53'18"	26.8	10.5	327	4.2	242	360	168	11.4	1154.4	21.0
LL112	Head of Canyon WM	31°31'42"	105°42'05"	61.6	19.3	177	5.4	282	168	116	26.5	861.7	14.0
LL113	Wilkey Well no. 1	31°23'23"	105°40'48"	77.1	43.1	237	3.4	336	438	88	11.8	1241.5	20.0
LL114	Wilkey Well no. 2	31°22'48"	105°39'07"	131.0	24.6	55	1.5	284	275	10	11.3	801.4	11.0
LL115	Gunsight Windmill no. 1	31°25'03"	105°30'20"	37.3	22.1	454	7.4	411	570	137	<0.5	1649.2	19.0
LL116	Owens Well	31°22'31"	105°45'50"	48.4	15.3	362	3.5	278	525	128	<0.5	1369.4	14.0
LL117	S-15 W. Sp	31°41'13"	104°17'33"	634	25.6	34.0	5.3	151	1500	34	26.5	2419.2	11.0
LL118	S-15 S. Sp	31°38'43"	104°17'25"	714	12.3	11.5	16.6	448	1490	13	<0.5	1203.0	14.0
LL119	S-15 W. Windmill	31°39'10"	104°19'02"	577	120.0	227.0	21.0	114	2040	190	22.6	3322.7	18.0
LL120	Phillips Windmill	31°40'06"	104°14'41"	614	34.0	47.9	4.6	84	1590	31	60.0	2476.0	19.0
LL121	S-15 N. Windmill	31°43'55"	104°14'59"	600	107.0	218.0	4.5	160	1900	221	35.5	3256.8	20.0
LL122	S-15 N. Windmill Sp	31°44'57"	104°15'19"	620	50.6	163.0	7.4	126	1730	127	44.6	2879.7	13.0
LL123	S-46 Seven L. Windmill	31°44'53"	104°28'18"	618	72.2	70.4	7.3	190	1680	73	<0.5	2724.4	17.0
LL124	S-46 High L. Windmill	31°42'46"	104°27'46"	634	25.8	68.4	10.2	201	1480	74	39.6	2539.9	18.0
LL125	S-46 Cave Well	31°40'03"	104°26'23"	676	55.9	73.2	13.0	320	1540	104	104.0	2898.9	
LL126	Low Level Well	31°24'14"	105°43'32"	70.7	6.9	549	4.4	60	710	416	18.3	1850.	17.0
LL128	Temple Well	31°44'40"	105°05'25"	320	116	278	11.3	236	820	530	40	2363	22
LL129	Guillen Exxon Well	31°44'48"	105°12'06"	193	79.7	113	5.2	178	680	117	24	1404	25
LL130	Desert Inn Well	31°45'56"	105°21'22"	178	73.5	269	7.0	345	553	305	2.7	1745	24
LL131	Cornudas Cafe Well	31°46'45"	105°28'09"	146	63.7	325	10.0	293	580	312	3.8	1744	24

Appendix 2. (cont.)
Major ions (mg/L) and temperatures (°C).

BEG ID	Well Name	Coordinates		Ca ²⁺	Mg ²⁺	Na ⁺	K ⁺	HCO ₃ ⁻	SO ₄ ²⁻	Cl ⁻	NO ₃ ⁻	TDS	Temp.
LL132	Williams Ranch House Well	31°41'31"	105°30'09"	95.1	37.1	100	2.7	299	170	78	92	884	25
LL133	Puett Well	31°46'38"	105°26'53"	199	86.6	462	12.7	332	950	405	<1.0	2462	23
LL134	Hobo Well-Deep	31°41'44"	105°33'07"	157	73.2	308	5.8	352	710	202	<1.0	1827	22
LL135	Jardin Well	31°33'27"	105°21'25"	169	60.9	964	40.5	412	580	1300	<1.0	3552	23
LL136	Sparks Windmill	31°46'18"	105°16'45"	605	193	259	11.7	243	2210	245	<1.0	3803	22
LL137	Sparks House Pump Well	31°45'39"	105°18'04"	497	121	310	9.2	263	1470	401	<1.0	3095	20
LL138	Williams #4 Well	31°46'21"	105°33'09"	176	80.5	238	5.9	283	740	172	<1.0	1722	22
LL139	Stewart #2 Well	31°48'30"	105°32'52"	358	133	303	5.8	430	1490	122	2.4	2859	21
LL140	Adobe House Tank Well	31°41'10"	105°25'18"	111	48.6	249	7.9	328	510	147	26	1445	22
LL141	Bravo Well	31°36'14"	105°24'27"	95.2	69.8	381	5.9	177	690	275	76	1787	25
LL142	Three Sisters Well	31°36'10"	105°28'18"	118	60.1	290	3.7	251	570	209	99	1616	22
LL143	Sumrall Well	31°45'57"	105°05'20"	252	95.2	303	9.1	290	660	500	10	2126	23
LL144	Foster House Well	31°51'44"	105°21'44"	213	86.8	340	8.4	300	730	410	1.3	2103	26
LL145	Foster South Well	31°47'15"	105°22'47"	141	59.4	182	4.3	340	530	110	7.0	1384	21
LL146	Stewart #1 Well	31°48'29"	105°32'56"	258	102	225	4.9	400	1040	91	<1.0	2145	19
LL147	Beard #1 Well	31°46'07"	105°37'02"	166	87.6	408	7.1	400	840	340	6.0	2267	22
LL148	Red Well	31°37'47"	105°14'20"	153	60.4	416	18.3	320	540	490	10	2021	20
LL149	Sampson Well	31°42'04"	105°12'45"	216	86.2	267	9.0	280	590	410	30	1898	22
LL150	South Well	31°35'29"	105°30'08"	97	50.7	247	4.3	240	470	140	63	1322	20
LL151	Dyer #1 Ranch House	31°29'45"	105°21'59"	89.3	58	519	6.7	400	830	230	105	2247	21
LL152	Gibbs Well	31°49'17"	105°20'17"	203	82.9	328	10.3	310	700	380	1.0	2027	21
LL153	Dyer #2 Black Mountain South Well	31°31'20"	105°09'33"	113	52.8	324	14.6	370	290	400	9	1581	22
LL154	Flattop Well-Figure 2 Ranch	31°37'49"	105°02'10"	218	80.4	265	9.7	290	550	420	16	1857	24
LL155	Dyer #3 Well	31°28'16"	105°13'16"	150	77	400	14.5	370	700	340	13	2077	19
LL156	Baylor - New Well	31°28'05"	105°22'59"	66.3	36.6	164	3.3	200	230	130	99	936	22
LL157	Baylor - Old Well	31°27'38"	105°24'51"	85.2	22.4	87.3	3.3	240	110	61	100	715	20

Appendix 2. (cont.)

Chemical composition (mg/L) of ground water from selected wells (Texas Water Development Board [TWDB], 1985).

BEG ID	TWDB ID	Ca ²⁺	Mg ²⁺	Na ⁺	K ⁺	HCO ₃ ⁻	SO ₄ ²⁻	Cl ⁻	F ⁻	NO ₃ ⁻	TDS
LL170	48-07-101	324	139	168	-	193	1,300	145	-	31.0	2,220
LL171	48-07-102	598	164	250	-	214	2,142	267	2.0	8.7	3,555
LL172	48-07-206	459	225	640	-	172	2,230	594	3.1	286.0	4,563
LL173	48-07-207	364	136	119	-	227	1,220	156	1.8	14.1	2,140
LL174	48-07-210	326	158	267	-	240	1,180	405	1.8	51.0	2,520
LL176	48-07-304	332	124	175	-	248	860	408	1.8	7.0	2,045
LL177	48-07-405	435	219	471	-	195	1,630	800	2.4	110.0	3,779
LL178	48-07-414	324	134	481	-	260	1,120	750	1.9	29.5	2,983
LL180	48-07-501	358	264	510	-	138	1,670	890	2.1	39.0	3,817
LL183	48-07-606	368	220	338	-	259	1,230	670	2.1	42.0	3,011
LL184	48-07-607	350	137	121	-	238	910	415	1.5	3.5	2,070
LL185	48-07-706	264	82	392	1.2	294	703	667	1.1	4.87	2,276
LL187	48-07-801	538	306	952	-	231	2,117	1,512	1.8	44.20	5,603
LL188	48-07-803	500	199	820	-	123	2,110	1,120	2.6	42.0	4,869
LL189	48-07-901	215	87	160	-	95	700	320	1.4	3.50	1,548
LL190	48-07-904	522	248	773	-	255	1,646	1,400	1.6	22.60	4,757
LL192	48-06-201	560	166	40	-	229	1,910	20	2.7	0.40	2,831
LL193	48-06-601	520	178	58	-	201	1,900	27	2.7	0.40	2,804
LL194	48-15-203	266	77	378	1.1	293	681	615	1.1	5.01	2,184
LL195	48-15-301	280	81	326	-	293	720	550	1.6	7.00	2,125
LL202	47-09-803	222	99	156	-	279	660	256	-	3.50	1,549
LL203	47-09-805	171	70	82	-	283	439	126	1.0	0.10	1,044

- 1) $\delta^{18}\text{O}$ and $\delta^2\text{H}$ are defined relative to SMOW. $\delta^{34}\text{S}$ is given as deviation from the Canyon Diablo Meteorite standard. $\delta^{13}\text{C}$ is defined relative to Pee Dee Belemnite carbonate.
- 2) PMC is percent of modern carbon.
- 3) ^{14}C age was corrected by using $\delta^{13}\text{C}$ values (Kreitler and others, 1986b), except for sample LL126.

Appendix 2. (cont.)

Trace ions (mg/L) and isotope composition¹ in ground-water samples.

BEG ID	Well Name	Coordinates	As ³⁺	Cd ²⁺	Li ⁺	Fe ²⁺	Sr ²⁺	Ba ²⁺	Br ⁻	F ⁻	δ ¹⁸ O	δ ² H	Tritium	δ ³⁴ S	δ ¹³ C	PMC ²	¹⁴ C Age ³
LL100	Kohen Windmill	31°40'12" 104°10'50"	<0.010	<0.03	0.10	0.02	9.79	0.01	1.17	1.50	-7.1	-47	13.7	+9.3			
LL101	Smilin Jack Windmill	31°40'23" 104°12'22"	<0.010	<0.03	0.05	0.24	9.78	0.01	0.18	1.05	-6.1	-42	12.0	+9.9			
LL102	Rustler Sp	31°38'42" 104°13'33"	<0.010	<0.03	0.04	0.03	11.20	0.01	0.22	1.45	-6.6	-48	6.7	+9.9			
LL103	Division Windmill	31°37'16" 104°13'03"	<0.010	<0.03	0.06	0.34	8.55	0.01	0.65	2.82	-7.3	-50	<0.8	+3.6			
LL104	Monument Windmill	31°38'13" 104°10'52"	<0.010	<0.03	0.04	0.07	4.65	0.02	0.22	2.37	-6.7	-43	6.3	+5.8			
LL105	Rio Gr. Water	31°16'23" 105°51'14"	<0.010	<0.03	0.11	0.69	1.36	0.06	0.22	0.66	-9.1	-69	24.4	+1.1			
LL106	Thaxton Sp	31°28'11" 105°42'57"	<0.010	<0.03	0.13	0.02	1.63	0.02	1.34	5.57	-7.5	-58	<0.8	-1.8			
LL107	48-42-1 Windmill	31°22'12" 105°50'52"	0.012	<0.03	0.26	0.04	3.20	0.02	2.66	1.05	-8.0	-59	<0.8	+1.0	-16.8	16.6	14,748
LL108	48-42-404 Well	31°18'56" 105°51'27"	0.017	<0.03	0.10	0.05	1.01	0.04	1.25	2.37	-6.9	-48	<0.8	+3.8	-9.6	61	Modern
LL109	48-41-618 Well	31°17'31" 105°52'45"	<0.010	<0.03	0.21	0.02	1.43	0.01	0.59	0.39	-7.4	-71	27.2	+16.9			
LL110	48-41-2 Well	31°19'37" 105°54'55"	<0.010	<0.03	0.26	1.35	6.69	0.06	2.27	0.61	-8.8	-74	21.8	+4.7	-12.0	116	Modern
LL111	48-33-9 Windmill	31°23'18" 105°53'18"	<0.010	<0.03	0.10	0.49	0.81	0.02	1.01	2.03	-7.3	-51	<0.8	+7.2	-10.1	21.8	8,288
LL112	Head of Canyon Windmill	31°31'42" 105°42'05"	<0.010	<0.03	0.06	0.10	1.72	0.02	1.14	2.79	-7.1	-50	11.8	+5.8	-8.0	43	833
LL113	Wilkey Well no. 1	31°23'23" 105°40'48"	<0.010	<0.03	0.05	0.71	3.90	0.03	0.77	1.60	-7.7	-58	3.74	+5.2	-9.4	36	3,529
LL114	Wilkey Well no. 2	31°22'48" 105°39'07"	<0.010	<0.03	0.03	<0.02	7.50	0.03	0.44	0.90	-7.5	-54	20.67	+10.9	-11.3	60	868
LL115	Gunsight Windmill no. 1	31°25'03" 105°30'20"	<0.010	<0.03	0.12	2.15	3.32	0.03	1.15	3.10	-10.7	-83	0.5	-0.5	-7.9	9.6	13,071
LL116	Owens Well	31°22'31" 105°45'50"	<0.010	<0.03	0.07	0.20	2.87	0.12	1.10	4.30	-8.0	-62	1.52	+7.0	-7.8	8.9	13,520
LL117	S-15 W. Sp	31°41'13" 104°17'33"	<0.010	<0.03	0.09	<0.02	7.62	0.02	0.23	0.70	-6.9	-51	15.76	+9.9			
LL118	S-15 S. Sp	31°38'43" 104°17'25"	<0.010	<0.03	0.03	0.07	4.16	0.07	0.19	0.30	-6.3	-48	13.16	+17.2			
LL119	S-15 W. Windmill	31°39'10" 104°19'02"	<0.010	<0.03	0.07	0.02	9.15	0.02	0.72	1.10	-6.7	-51	9.84	+9.4	-14.4	82	314
LL120	Phillips Windmill	31°40'06" 104°14'41"	<0.010	<0.03	0.03	0.04	9.35	0.01	0.24	0.80	-6.7	-51	8.67	+9.6	-17.0		
LL122	S-15 N. Windmill Sp	31°44'57" 104°15'19"	<0.010	<0.03	0.04	0.02	9.22	0.01	0.74	1.10	-6.7	-56	16.33	+9.9			
LL121	S-15 N. Windmill	31°43'55" 104°14'59"	<0.010	<0.03	0.06	0.07	8.27	0.01	1.10	1.30	-7.2	-54	13.46	+9.8	-18.0	90	1358
LL123	S-46 Seven L. WM	31°44'53" 104°28'18"	<0.010	<0.03	0.04	1.09	9.90	0.03	0.53	1.40	-7.4	-53	28.04	+11.5	-19.5	56	5906
LL124	S-46 High L. WM	31°42'46" 104°27'46"	<0.010	<0.03	0.03	0.04	5.86	0.03	0.33	0.60	-5.8	-40	11.35	+10.5	-12.0		Modern
LL125	S-46 Cave W.	31°40'03" 104°26'23"	<0.010	<0.03	0.05	0.07	11.00	0.03	0.66	0.90	-6.5	-50	21.78	+11.3	-18.8	110	Modern
LL126	Low Level well	31°24'14" 105°43'32"	<0.050	<0.03	0.10	0.13	8.30	0.19	2.10	4.30	-8.3	-61	no data ⁴	+4.1	-18.1	3.3	27,400

Appendix 2. (cont.)

Trace ions (mg/L) and isotope composition¹ in ground-water samples.

BEG ID	Well name	TWC ¹ ID	As	Cd ²⁺	Li ⁺	Fe ²⁺	Sr ²⁺	Ba ²⁺	Br ⁻	F ⁻	δ ¹⁸ O**	δD**	Tritium	δ ³⁴ S**	δ ¹³ C**	PMCT [†]	¹⁴ C Age ^{††}
LL128	Temple Well	48-24-1	<0.05	<0.03	0.07	*0.02	8.04	0.06	0.5	3.0	-9.18	-68.8	4.1	16.11	-5.77	13.47	7,639
LL129	Guillen Exxon Well	48-23-201	<0.05	<0.03	*0.05	0.08	8.25	0.06	0.5	5.2	-9.19	-72.7	2.7	12.11	-5.78	9.56	10,488
LL130	Desert Inn Well	48-14-7	<0.05	<0.03	0.08	0.04	6.14	0.03	0.7	5.1	-9.17	-70.3	3.8	5.56	-8.49	6.74	16,556
LL131	Cornudas Cafe Well	48-13-7	<0.05	<0.03	0.10	<0.02	4.49	0.05	0.7	5.0	-9.18	-69.8	3.5	4.53	-6.07	10.54	10,084
LL132	Williams Ranch House Well	48-20-6	<0.05	<0.03	*0.04	0.03	3.77	0.61	0.6	5.0	-6.90	-50.9	13.7	8.61	-8.00	21.02	6,660
LL133	Puett Well	48-13-8	<0.05	<0.03	0.16	1.62	5.58	0.03	1.0	5.0	-10.21	-81.1	2.3	5.71	-6.36	5.36	16,061
LL134	Hobo Well-Deep	48-20-5	<0.05	<0.03	0.09	1.42	0.09	0.02	0.8	7.2	-8.01	-64.2	2.3	7.70	-8.92	18.46	8,635
LL135	Jardin Well	48-30-4	<0.05	<0.03	0.45	6.97	0.45	0.08	1.4	9.0	-9.15	-67.4	2.8	15.72	-6.79	5.08	17,046
LL136	Sparks Windmill	48-14-9	<0.05	<0.03	0.14	16.3	0.14	0.03	0.7	6.6	-10.53	-81.5	3.3	11.29	-3.64	5.99	10,529
LL137	Sparks House Pump Well	48-14-8	<0.05	<0.03	0.14	2.24	0.14	*0.01	0.7	6.2	-9.53	-71.3	3.2	10.37	-4.67	11.32	7,328
LL138	Williams #4 Well	48-12-8	<0.05	<0.03	0.09	11.8	0.09	0.08	0.8	6.3	-7.91	-65.1	6.8	10.12	-9.65	13.98	11,583
LL139	Stewart #2 Well	48-12-5	<0.05	<0.03	0.10	0.25	0.10	0.03	0.8	5.7	-10.44	-79.6	<0.8	-1.24	-10.35	4.34	21,832
LL140	Adobe House Tank Well	48-21-5	<0.05	<0.03	0.11	5.24	0.11	0.04	0.9	8.5	-9.73	-76.0	8.2	7.05	-5.67	13.02	7,775
LL141	Bravo Well	48-29-3	<0.05	<0.03	0.15	<0.02	0.15	0.02	1.9	9.0	-2.72	-35.3	3.4	5.84	-7.99	46.52	84
LL142	Three Sisters Well	48-29-1	<0.05	<0.03	0.11	0.17	0.11	0.12	1.9	7.7	-8.16	-66.5	<0.8	7.23	-6.27	23.50	3,725
LL143	Sumrall Well	48-16-7	<0.05	<0.03	0.09	<0.02	0.09	0.04	0.39	1.3	-9.26	-64.8	<0.8	11.13	-6.80	19.64	5,880
LL144	Foster House Well	48-14-1	<0.05	<0.03	0.12	0.10	0.12	0.10	0.75	2.7	-9.47	-69.1	2.2	7.81	-7.54	49.5	modern
LL145	Foster South Well	48-13-9	<0.05	<0.03	0.08	0.07	0.08	0.02	0.81	3.0	-9.82	-75.4	4.5	4.26	-7.59	9.71	12,610
LL146	Stewart #1 Well	48-12-5	<0.05	<0.03	0.08	13.0	0.08	0.04	0.93	3.0	-9.79	-73.2	1.9	-0.72	-10.04	4.84	20,678
LL147	Beard #1 Well	48-12-7	<0.05	<0.03	0.13	0.11	0.13	0.09	0.92	3.0	-8.36	-63.8	3.0	6.58	-8.01	6.31	16,618
LL148	Red Well	48-23-7	<0.05	<0.03	0.22	3.10	0.22	0.06	0.96	3.3	-9.71	-75.0	4.5	5.91	-7.46	13.13	9,974
LL149	Sampson Well	48-23-1	<0.05	<0.03	0.11	0.05	0.11	0.03	0.63	2.3	-8.99	-68.6	1.4	9.28	-6.38	16.70	6,691
LL150	South Well	48-28-3	<0.05	<0.03	0.10	0.06	0.10	0.16	1.74	3.7	-8.27	-63.0	0.9	6.87	-5.40	35.77	modern
LL151	Dyer #1 Ranch House	48-38-1	<0.05	<0.03	0.14	0.03	0.14	0.02	2.06	3.7	-8.19	-64.7	<0.8	6.34	-5.65	11.82	8,544
LL152	Gibbs Well	48-14-4	<0.05	<0.03	0.13	0.03	0.13	0.11	0.69	2.7	-9.69	-72.9	1.2	6.74	-7.58	7.60	14,628
LL153	Dyer #2 Black Mountain South Well	48-31-9	<0.05	*0.03	0.16	0.07	0.16	0.04	0.82	2.7	-8.42	-61.8	<0.8	5.58	-7.09	10.96	11,047

Appendix 2. (cont.)

Trace ions (mg/L) and isotope composition¹ in ground-water samples.

BEG ID	Well name	TWC ¹ ID	As	Cd ²⁺	Li ⁺	Fe ²⁺	Sr ²⁺	Ba ²⁺	Br ⁻	F ⁻	$\delta^{18}\text{O}^{**}$	δD^{**}	Tritium	$\delta^{34}\text{S}^{**}$	$\delta^{13}\text{C}^{**}$	PMC [†]	¹⁴ C Age ^{††}
LL154	Flattop Well - Figure 2 Ranch	48-24-9	<0.05	<0.03	0.09	0.35	0.09	0.12	0.50	1.5	-8.90	-61.8	8.1	11.04	-7.40	25.54	4,406
LL155	Dyer #3 Well	48-39-1	<0.05	<0.03	0.19	0.65	0.19	0.07	1.46	3.0	-7.31	-54.8	21.4	2.91	-6.76	9.08	12,210
LL156	Baylor-New Well	48-37-3	<0.05	<0.03	0.07	<0.02	0.07	0.04	1.31	3.0	-7.38	-57.4	9.5	6.65	-4.73	39.43	modern
LL157	Baylor-Old Well	48-37-3	<0.05	<0.03	0.06	0.19	0.06	0.14	0.60	3.0	-7.04	-46.4	32.0	9.00	-4.75	90.77	modern

+ see fig. 7 for distribution

< less than indicated value

* reported value near detection limit

** $\delta^{18}\text{O}$ and $\delta^2\text{H}$ are defined relative to SMOW. $\delta^{34}\text{S}$ is given as deviation from the Canyon Diablo Meteorite standard. $\delta^{13}\text{C}$ is defined relative to Pee Dee Belemnite carbonate.

† PMC is percent of modern carbon.

†† ¹⁴C age was corrected by using $\delta^{13}\text{C}$ values (Kreitler and others, 1986b; their Appendix 5).

¹TWC's well identification system has 3 sets of numbers; preliminary wells have only one number in the last set, permitted wells have 3.

1) $\delta^{18}\text{O}$ and $\delta^2\text{H}$ defined relative to SMOW. $\delta^{34}\text{S}$ is given as deviation from the Canyon Diablo Meteorite standard. $\delta^{13}\text{C}$ defined relative to Pee Dee Belemnite carbonate.

2) PMC is percent of modern carbon.

3) ¹⁴C age was corrected by using $\delta^{13}\text{C}$ values (app. 5) except for sample LL126.

4) Tritium data for the Low Level well were not available by the time this report was submitted. Data will be provided in an addendum.

Appendix 3. Pumping test data and interpretation - Diablo Plateau

In order to determine the hydraulic properties of both aquifers A and B, seven pumping tests (PT) were conducted on water wells evenly spaced across the Diablo Plateau within the study area (fig. A3-1). The first pumping test was conducted in September 1986, and PT #2 through 7 were performed from January to March 1987. Three of the seven pumping tests resulted in only minimal, relatively instantaneous drawdown of the producing aquifer, because of inadequate production capacity of the water well required to stress the aquifer. Driscoll (1986) offers one method to determine whether or not this early drawdown is the result of wellbore storage or actual drawdown of the aquifer. In each of the three pumping tests where this was suspected, all or part of the drawdown was attributed to wellbore storage. When all or part of a very small drawdown curve is attributed to wellbore storage, no method can reliably be used to determine transmissivity. The following is a detailed discussion of each pumping test, methods used during analysis, and the resulting transmissivity. A summary of this data also appears within the hydrologic section, Water-bearing Characteristics (p. 132).

PT #1

To determine the hydraulic parameters of the regional aquifer, PT #1 was conducted in well LL162 at Williams Ranch, Hudspeth County (fig. A3-1). The well is located 6.7 mi (10.8 km) west-northwest of the intersection between Ranch-to-Market Roads 1111 and 2317 (fig. A3-2). This well was drilled by El Paso Natural Gas Company to serve as a water supply well for their pump station #2. It was drilled into probable Victorio Peak - Bone Spring limestones of Permian age to an original total depth of 1,214 ft (370 m). Wellbore diameter was 8 inches (20.3 cm).

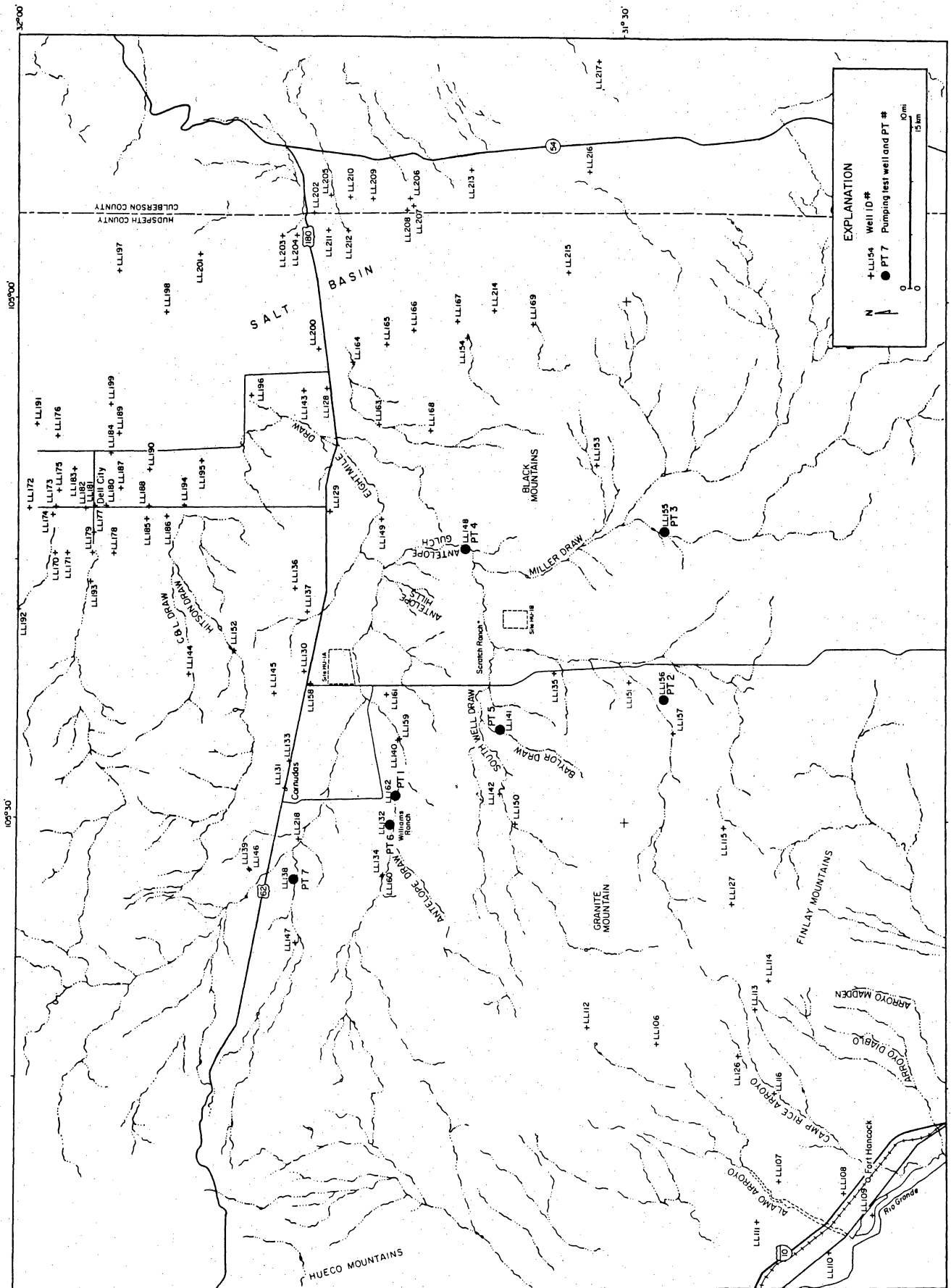


Figure A3-1. Location map of the seven wells in Hudspeth County tested during this study as part of hydrologic characterization studies.

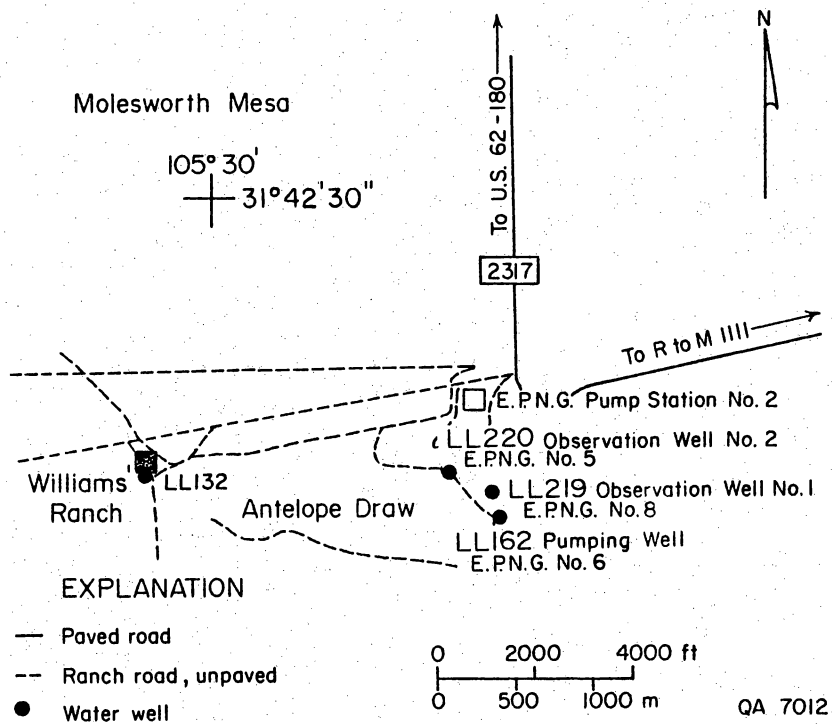


Figure A3-2. Location map of wells used in pumping test no. 1, Williams Ranch, Hudspeth County. Wells LL219 and LL220 served as observation wells during the pumping test.

Static water level in this well was measured at 677 ft (206.3 m) below land surface, and the saturated thickness is approximately 400 ft (121.9 m). Two adjacent wells, LL219 and LL220, located 468 ft (142.6 m) north-northwest and 1,326 ft (404 m) northwest of LL162, respectively, served as observation wells for the test. Water levels in these wells were measured at 671.5 ft (204.6 m) and 682.5 ft (208.0 m), respectively, below land surface. A shallow aquifer (see Hydrologic Setting, this report, p. 122) was found in observation well LL219 at a depth of about 200 ft (61 m) below land surface. Cascading ground water from this level to the bottom of the well was clearly audible in this borehole and was also observed on the electric line-probe from 200 ft (60.9 m) down to the producing aquifer.

The test started at 12:40 p.m. on September 26, 1986. Production rates were essentially constant throughout the drawdown phase at 9.7 to 10.1 gpm (table A3-1). During the pumping period, which lasted 32 hr and 50 min, the recorded water level dropped 60.5 ft (18.4 m) in the pumping well (figs. A3-3 and A3-4, table A3-1), but no drawdown was detected in the observation wells. When the pump was turned off at 9:31 p.m. on September 27, the recovery of water level was monitored for another 31 hr and 30 min, until 5:00 a.m., September 28. By that time 58.4 ft (17.8 m) of the 60.5 ft (18.4 m) of drawdown had recovered (fig. A3-5, table A3-2).

Two distinct segments appear on figures A3-3 and A3-5. The change in slope of drawdown curve with time could be the result of several possible scenarios that may affect interpretation of the data.

A. The tested deep aquifer is semiconfined, and the shallow aquifer may leak into it. Considering this interpretation, the early part of the test represents nonsteady flow and nonleaky conditions. Leakage from the shallow aquifer starts at

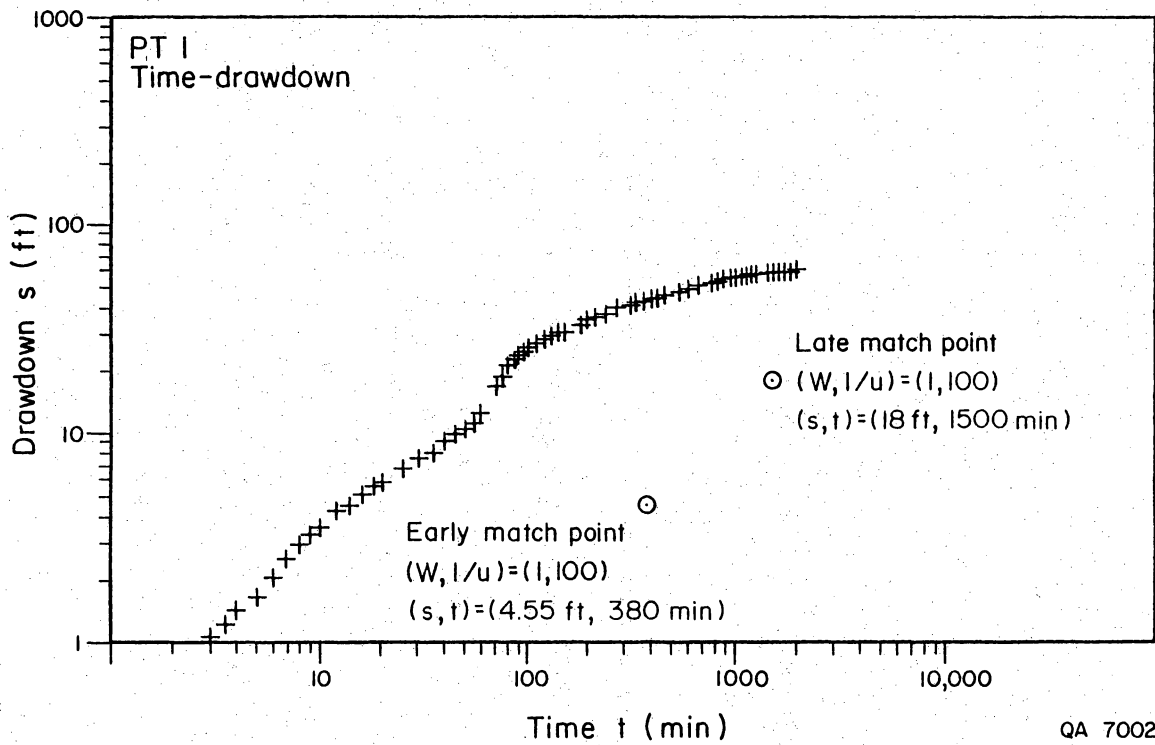


Figure A3-3. Time-drawdown curve that was matched to Walton type curves for pumping test no. 1 in well LL162. Two distinct segments appear on the curve, suggesting (1) leakage from Aquifer B to Aquifer A after a short drawdown that was caused by early pumpage or (2) dewatering of additional fracture systems as the test proceeded.

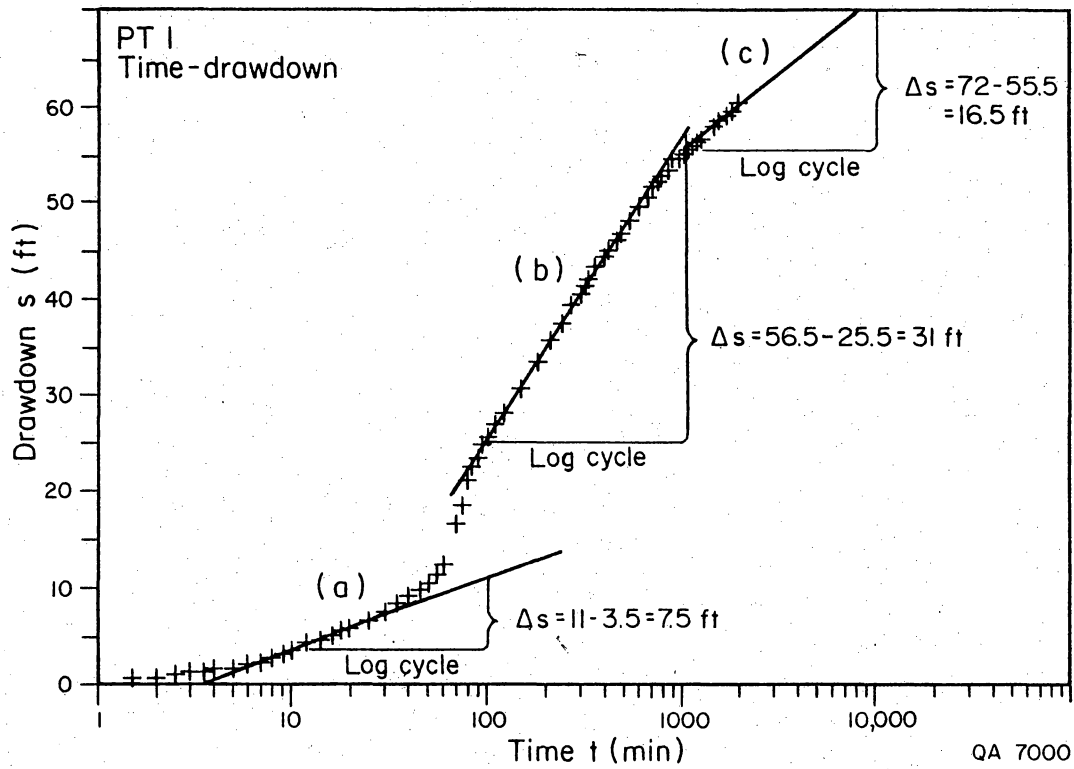


Figure A3-4. Time-drawdown plot interpreted using Jacob's method for pumping test no. 1 in well LL162. Three segments were found on the curve and may represent the dewatering of three separated fracture systems, as the cone of depression extended to greater distance from the pumping well.

Table A3-1. Drawdown data from pumping test no. 1 at well LL162.

Time (hr)	Time from beginning of pumpage (min)	Depth to water level (ft)	Water level drawdown (ft)	Flow meter reading (gal)	Well discharge (gpm)
12:40:00	0.0	680.00	0.00	3,353	0.0
12:40:30	0.5	680.00	0.00	-	-
12:41:00	1.0	680.27	0.27	3,361	8.0
12:41:30	1.5	680.625	0.625	3,365	8.0
12:42:00	2.0	680.792	0.792	3,371	12.0
12:42:30	2.5	680.917	0.917	3,378	14.0
12:43:00	3.0	681.083	1.083	-	-
	3.5	681.208	1.208	3,387	9.0
12:44:00	4.0	681.396	1.396	3,390.5	7.0
12:45:00	5.0	681.688	1.688	3,403	12.5
12:46:00	6.0	682.042	2.042	-	-
12:47:00	7.0	682.458	2.458	3,424	10.5
12:48:00	8.0	682.917	2.917	3,434	10.0
12:49:00	9.0	683.292	3.292	3,445	11.0
12:50:00	10.0	683.542	3.542	3,454	9.0
12:52:00	12.0	684.208	4.208	3,476	11.0
12:54:00	14.0	684.542	4.542	3,496	10.0
12:56:00	16.0	685.083	5.083	3,517	10.5
12:58:00	18.0	685.496	5.496	3,537	10.0
13:00:00	20.0	685.83	5.83	3,557	10.0
13:05:00	25.0	686.771	6.771	-	-
13:10:00	30.0	687.542	7.542	3,661	10.4
13:15:00	35.0	688.354	8.354	-	-
13:20:00	40.0	689.188	9.188	3,760	9.9
13:25:00	45.0	689.979	9.979	-	-
13:30:00	50.0	690.500	10.500	3,862	10.2
13:35:00	55.0	691.229	11.229	-	-
13:40:00	60.0	692.250	12.250	3,964	10.2
13:50:30	70.5	696.854	16.854	4,067	10.3
13:55:00	75.0	698.646	18.646	-	-
14:00:00	80.0	701.166	21.166	4,166	9.9
14:05:00	85.0	702.729	22.729	-	-
14:10:00	90.0	703.896	23.896	4,268	10.2
14:15:00	95.0	704.960	24.960	-	-
14:20:00	100.0	705.750	25.750	4,368	10.0
14:30:00	110	707.000	27.000	4,469	10.1
14:40:00	120	708.166	28.166	4,569	10.0
15:10:00	150	710.760	30.760	4,873	10.1
15:40:00	180	713.33	33.33	5,174	10.03
16:10:00	210	715.65	35.65	5,476.5	10.08
16:40:00	240	717.63	37.63	5,778	10.05
17:10:00	270	719.50	39.50	6,080	10.07
17:54:00	314	721.44	41.44	-	-
18:10:30	330.5	722.15	42.15	-	-
18:13:00	333			6,710	10.0
18:41:00	361	723.25	43.25	6,992	10.07
19:10:00	390	724.29	44.29	7,280.5	9.95
19:40:00	420	724.96	44.96	7,573	9.75
20:17:00	457	725.94	45.94	7,945	10.05
20:40:00	480	726.65	46.65	8,170.5	9.80

Table A3-1. (cont.)

Time (hr)	Time from beginning of pumpage (min)	Depth to water level (ft)	Water level drawdown (ft)	Flow meter reading (gal)	Well discharge (gpm)
21:40:00	540	728.00	48.00	8,761	9.84
22:10:00	570			9,045	9.80
22:40:00	600	729.33	49.33		
23:37:00	657			9,999	10.97
23:40:00	660	730.88	50.88	-	-
01:11:00	751	732.17	52.17	-	-
01:40:00	780	732.71	52.71	-	-
02:40:00	840	733.50	53.50		
02:42:00	842			11,710	9.25
03:40:00	900	734.08	54.08		
03:42:00	902			12,290	9.67
04:45:00	965	734.71	54.71	12,921.5	10.02
05:30:00	1,010			13,365.0	9.86
05:40:00	1,020	735.16	55.16		
06:47:00	1,087	735.58	55.58	14,112	9.70
07:40:00	1,140	736.0	56.00	14,637	9.91
08:40:00	1,200	736.44	56.44	15,223.5	9.78
09:40:00	1,260	736.63	56.63	15,820.0	9.78
13:23:00	1,483			18,000	9.82
13:25:00	1,485	738.17	58.17		
14:38:00	1,558			18,732	9.76
14:46:00	1,566	738.50	58.50		
16:54:00	1,694			20,065	9.80
16:56:00	1,696	739.00	59.00		
18:34:00	1,794			21,040	9.75
18:40:00	1,800	739.87	59.87		
21:08:00	1,948			22,570	9.94
21:10:00	1,950	740.35	60.35		
21:31:00	1,971	740.50	60.50	22,784.5	9.75

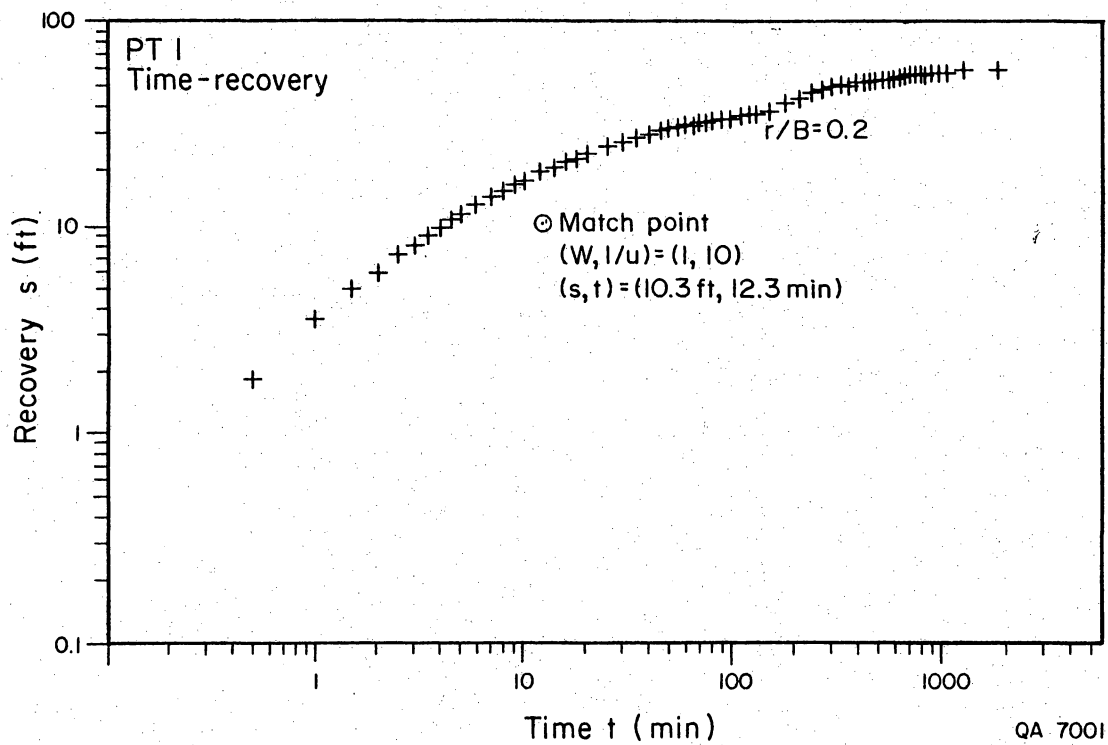


Figure A3-5. Time-recovery curve matched to Walton type curves for pumping test no. 1 in well LL162. Two distinct segments appear on the curve, similar to the time-drawdown curve.

Table A3-2. Recovery test data from pumping test no. 1 at well LL162.

Time (hr)	Time from beginning of recovery (min)	<u>Time since pump started</u> <u>Time since pump stopped</u> <u>(tp + Δt)</u> Δt	Depth to water level (ft)	Residual drawdown (s') (ft)	Water level recovery (ft)
21:31:00	0	∞	740.50	60.5	0
21:31:30	0.5	3,943	738.69	58.69	1.81
21:32:00	1.0	1,972	736.92	56.92	3.58
21:32:30	1.5	1,315	735.63	55.63	4.87
21:33:00	2.0	986.5	734.58	54.58	5.92
21:33:30	2.5	789.4	733.37	53.37	7.13
21:34:00	3.0	658.0	732.46	52.46	8.04
21:34:30	3.5	564.14	731.42	51.42	9.08
21:35:00	4.0	493.75	730.65	50.65	9.85
21:35:30	4.5	439.0	729.73	49.73	10.77
21:36:00	5.0	395.20	729.17	49.17	11.33
21:37:00	6.0	329.50	727.79	47.79	12.71
21:38:00	7.0	282.57	726.60	46.60	13.90
21:39:00	8.0	247.38	725.59	45.59	14.91
21:40:00	9.0	220.0	724.67	44.67	15.83
21:41:00	10.0	198.1	723.73	43.73	16.77
21:43:00	12.0	165.25	722.19	42.19	18.31
21:45:00	14.0	141.79	720.82	40.82	19.68
21:47:00	16.0	124.19	719.75	39.75	20.75
21:49:00	18.0	110.5	718.78	38.78	21.72
21:51:00	20.0	99.55	717.85	37.85	22.65
21:56:00	25.0	79.84	716.05	36.05	24.45
22:01:00	30.0	66.70	714.7	34.69	25.81
22:06:00	35.0	57.31	713.41	33.41	27.09
22:11:00	40.0	50.28	712.31	32.31	28.19
22:16:00	45.0	44.80	711.41	31.41	29.09
22:21:00	50.0	40.42	710.74	30.74	29.76
22:26:00	55.0	36.84	710.12	30.12	30.38
22:31:00	60.0	33.85	709.60	29.60	30.90
22:36:00	65.0	31.32	709.13	29.13	31.37
22:41:00	70.0	29.16	708.71	28.71	31.79
22:46:00	75.0	27.28	708.35	28.35	32.10
22:51:00	80.0	25.64	708.04	28.04	32.46
22:56:00	85.0	24.19	707.71	27.71	32.79

Table A3-2. (cont.)

Time (hr)	Time from beginning of recovery (min)	<u>Time since pump started</u> <u>Time since pump stopped</u> <u>(tp + Δt)</u> Δt	Depth to water level (ft)	Residual drawdown (s') (ft)	Water level recovery (ft)
23:01:00	90.0	22.90	707.40	27.40	33.10
23:06:00	95.0	21.75	707.11	27.11	33.39
23:11:00	100.0	20.71	706.83	26.83	33.67
23:21:00	110	18.92	706.35	26.35	34.15
23:31:00	120	17.43	705.89	25.89	34.61
24:01:00	150	14.14	704.23	24.23	36.27
24:31:00	180	11.95	701.28	21.28	39.22
01:01:00	210	10.39	698.17	18.17	42.33
01:31:00	240	9.21	695.85	15.85	44.65
02:01:00	270	8.30	694.34	14.34	46.16
02:31:00	300	7.57	693.10	13.10	47.40
03:01:00	330	6.97	692.25	12.25	48.25
03:31:00	360	6.48	691.46	11.46	49.04
04:01:00	390	6.05	690.98	10.98	49.52
04:34:00	423	5.66	690.35	10.35	50.15
05:01:00	450	5.38	689.90	9.90	50.60
05:31:00	480	5.11	689.37	9.37	51.13
06:31:00	540	4.65	688.59	8.59	51.91
07:01:00	570	4.46	688.20	8.20	52.30
07:34:00	603	4.27	687.83	7.83	52.67
08:10:00	639	4.08	687.42	7.42	53.08
08:31:30	660.5	3.98	687.13	7.13	53.37
09:01:00	690	3.86	686.88	6.88	53.62
10:00:00	749	3.63	686.30	6.30	54.20
11:00:00	809	3.44	685.72	5.72	54.78
12:00:00	869	3.27	685.31	5.31	55.19
13:38:00	967	3.04	684.63	4.63	55.88
15:19:00	1,068	2.85	684.03	4.03	56.47
19:00:00	1,290	2.53	683.29	3.29	57.21
05:00:00	1,890	2.04	682.08	2.08	58.42

early drawdown when water level approaches 10 to 20 ft (3.0 to 6.1 m). A similar effect can be seen on the recovery curve. When water level recovers to 10 to 20 ft (3.0 to 6.1 m) below its initial stage, a change in slope can be observed. The presence of a shallow aquifer at the adjacent observation well (LL219) may support this explanation. Interpretation of the test data based on these conditions can be done by matching Walton's (1970) set of type curves for unsteady flow in semiconfined leaky aquifers to the time-drawdown and time-recovery plots (figs. A3-3 and A3-5). Walton developed a method of solution that followed the Theis method (Kruseman and De Ridder, 1976), but, instead of one type curve, he used a family of type curves for several values of r/B (a ratio that includes the coefficient of transmissivity, permeability, and saturated thickness of the leaking aquitard). Transmissivity is calculated as follows:

$$T = \frac{114.6 Q W(u, r/B)}{s}$$

where

T = transmissivity (gpd/ft)

Q = discharge rate (gpm)

s = drawdown or the residual recovery (ft)

$W(u, r/B)$ = the well function (Kruseman and De Ridder, 1976) and the Y coordinate of the match point from the type curve.

The early part of the drawdown (30 min) may represent the flow in the pumped aquifer when no leakage from the upper aquifer was involved. The late part of the test may also include water contributed from the upper aquifer, as a result of the change in head in the deeper aquifer. Two transmissivity values were calculated for both parts of the drawdown. The early data set was matched to the nonleaky artesian type curve, and the match point had the coordinates $(W, 1/u)=(1.100)$ and $(s,t)=(4.55 \text{ ft}, 380 \text{ min})$. The late part of the data curve was matched with the

curve $r/B=0.2$, and the match point had the coordinates $(W,1/u)=(1.100)$ and $(s,t)=(18 \text{ ft}, 1500 \text{ min})$ (fig. A3-3). Pumpage rate used for the calculation was the mean value of 10.01 gpm. Transmissivity values calculated from both parts of the test were 252.1 gpd/ft for the early part, and 63.7 gpd/ft for the late part ($33.7 \text{ ft}^2/\text{d}$ or $3.1 \text{ m}^2/\text{d}$ and $8.5 \text{ ft}^2/\text{d}$ or $0.8 \text{ m}^2/\text{d}$), respectively.

The early recovery part of the test (120 min) was used to check on the values calculated for the pumping period that were significantly different. By matching the data to the curve $r/B=0.2$, we found that the match point had the coordinates $(W, 1/u)=(1.100)$ and $(s,t)=(10.3 \text{ ft and } 12.3 \text{ min})$ (fig. A3-5), and the calculated transmissivity was 111 gpd/ft ($14.9 \text{ ft}^2/\text{d}$ or $1.4 \text{ m}^2/\text{d}$). This value is higher than the value estimated for the symmetric late-pumping period during the drawdown part of the test.

B. Nonsteady flow, the aquifer is confined, and the two segments on both curves represent the permeability of the area around the borehole at the early time and the more regional pattern of permeability at a later stage. In this case, Jacob's method (Kruseman and De Ridder, 1976) can be used for interpretation of the late part of the drawdown, and the Theis recovery method (Kruseman and De Ridder, 1976) can be used for evaluation of both stages of recovery.

Jacob developed a method to calculate the transmissivity based on the Theis formula for cases in which the value of u is small ($u = r^2 S / 4 T t$; r is the well diameter, S is the storativity, T is the transmissivity, and t is the test duration). u is small as t (test duration) increases, and therefore the later part of the drawdown is suitable for the analysis. Transmissivity is calculated as follows:

$$T = \frac{2.3 Q}{4\pi\Delta s}$$

where

T = transmissivity (m²/d)

Q = discharge rate (m³/d)

s = drawdown (m).

Three segments were found on the drawdown curve and may represent the dewatering of three separated fracture systems, as the cone of depression extended further from the pumping well. For the calculation Δs were 7.5 ft/log cycle for the early phase, 31 ft/log cycle for the intermediate time, and 16 ft for the late part of the test (fig. A3-5). Calculated transmissivity values were 111, 84, and 158.6 gpd/ft (14.9 ft²/d, or 1.44 m²/d, 11.3 ft²/d, or 1.05 m²/d, and 21.5 ft²/d, or 1.97 m²/d), respectively.

The Theis method was used to calculate transmissivity from the time-recovery curve following the formula:

$$T = \frac{2.3 Q}{4\pi\Delta s'}$$

where

T = transmissivity (m²/d)

Q = discharge rate (m³/d)

s' = residual drawdown (m).

In their calculations $\Delta s'$ values were 20 and 21.5 ft/log cycle for the early and late periods of recovery, respectively. Calculated transmissivity values for the early and late part of the recovery curve (fig. A3-6) were 130.6 gpd/ft and 121.5 gpd/ft (17.4 ft²/d or 1.6 m²/d and 16.2 ft²/d or 1.5 m²/d), respectively.

Transmissivity values calculated by the methods of Walton, Jacob, and Theis for both a semiconfined leaky aquifer and a confined nonleaky aquifer range from

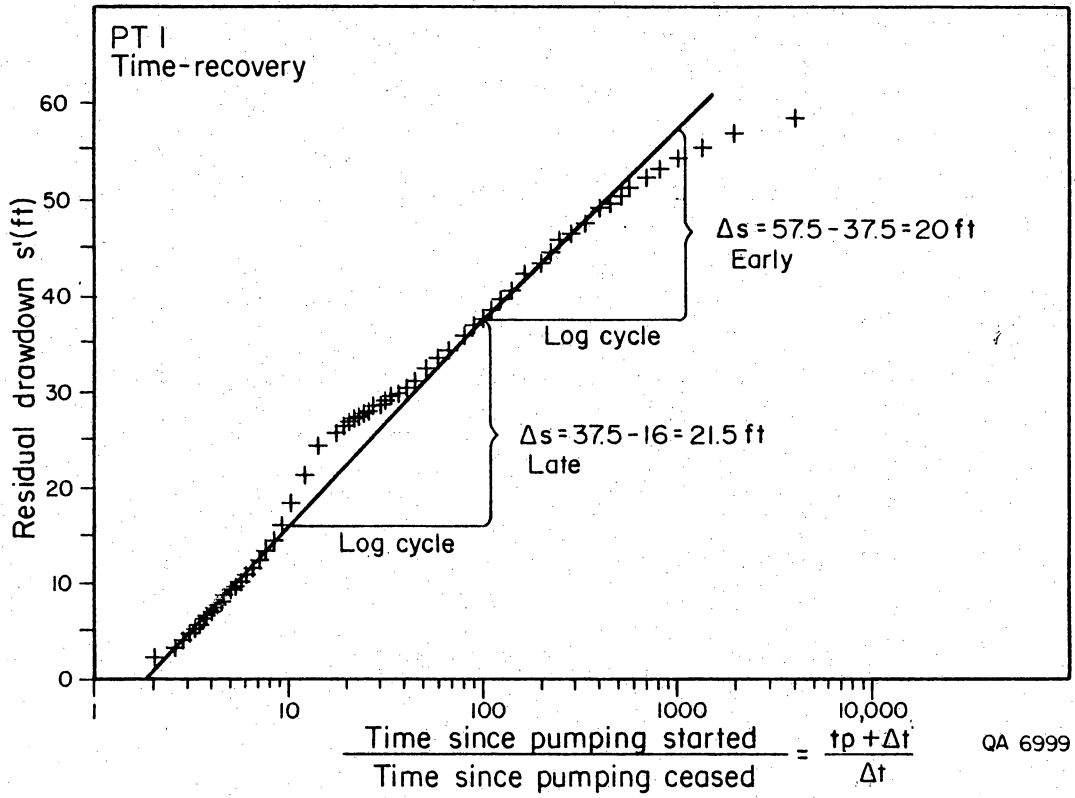


Figure A3-6. Time-recovery plot interpreted using Theis' method for pumping test no. 1 in well LL162.

63.7 gpd/ft to 252.1 gpd/ft, and the mean transmissivity calculated from all methods is 129.1 gpd/ft ($17.3 \text{ ft}^2/\text{d}$ or $1.6 \text{ m}^2/\text{d}$).

PT #2

PT #2 was conducted in well LL156 at the Baylor Ranch, Hudspeth County (fig. A3-1). The well is located approximately 1.9 mi (3.0 km) east-northeast of the Baylor Ranch Headquarters. The ranch road leading to this well is 20.7 mi (33.3 km) north of Sierra Blanca, Texas, and the well is 2.0 mi (3.2 km) west of Ranch to Market Road 1111. This well was drilled in the summer of 1986 by Leroy Perry of Dell City for the owner, James Baylor. It was drilled into probable Cretaceous Cox Sandstones and Campagrande Limestones, as indicated by local outcrops and by examination of cuttings by BEG personnel during the drilling of this well. Total depth of the well is approximately 265 ft (80.8 m), and wellbore diameter is 6 inches (15.2 cm). This well has 20 ft (6.1 m) of surface casing, and the producing interval was developed as an open-hole completion. Static water level in this well was measured at 206 ft (62.8 m) below land surface, and the saturated thickness in this wellbore is approximately 59 ft (17.9 m). No water wells or wellbores were available in the immediate area for use as observation wells. This well is producing NaSO_4 waters from aquifer B, and total dissolved solids were measured at 936 mg/L.

The drawdown phase of PT #2 was initiated at 10:30 a.m. on January 24, 1987. Although the well is equipped with a submersible pump, discharge rates varied considerably during the pumping period, from 14 gpm to 36 gpm, with a mean discharge rate of 27.5 gpm (table A3-3). During the pumping period, which lasted 50 hr, the recorded water level dropped only 1.3 ft (15.75 inches; 40.0 cm) (fig. A3-7), with 98% of the total drawdown occurring in the first 90 sec of the pumping test.

Table A3-3. Drawdown data from pumping test no. 2 at well LL156.

Time (hr)	Time from beginning of pumpage (min)	Depth to water level (ft)	Water level drawdown (ft)	Flow meter reading (gal)	Well discharge (gpm)
10:30:00	0.0	208.083	0.000	22,784	0.0
10:30:30	0.5	209.083	1.000	22,796	24.0
10:31:00	1.0	209.083	1.000	22,810	28.0
10:31:30	1.5	209.167	1.084	22,822	24.0
10:32:00	2.0	-	-	22,833	22.0
10:32:30	2.5	209.167	1.084	22,849	32.0
10:33:00	3.0	209.167	1.084	22,862	26.0
10:33:30	3.5	209.083	+1.000	22,876	28.0
10:34:00	4.0	209.083	1.000	22,892	32.0
10:34:30	4.5	209.083	1.000	22,904	24.0
10:35:00	5.0	209.083	1.000	22,911	14.0
10:36:00	6.0	209.083	1.000	22,943	32.0
10:37:00	7.0	209.083	1.000	22,975	32.0
10:38:00	8.0	209.083	1.000	23,005	30.0
10:39:00	9.0	209.083	1.000	23,033	28.0
10:40:00	10.0	209.083	1.000	23,061	28.0
10:42:00	12.0	209.083	1.000	23,115	27.0
10:44:00	14.0	209.083	1.000	23,169	27.0
10:46:00	16.0	209.083	1.000	23,229	30.0
10:48:00	18.0	209.083	1.000	23,285	28.0
10:50:00	20.0	209.083	1.000	23,339	27.0
10:55:00	25.0	209.083	1.000	23,485	29.2
11:00:00	30.0	209.083	1.000	23,615	26.0
11:10:00	40.0	209.083	1.000	23,880	26.5
11:20:00	50.0	209.083	1.000	24,130	25.0
11:30:00	60.0	209.083	1.000	24,408	27.8
11:40:00	70.0	209.083	1.000	24,705	29.7
11:50:00	80.0	209.083	1.000	25,017	31.2
12:00:00	90.0	209.083	1.000	25,315	29.8
12:10:00	100.0	209.083	1.000	25,639	32.4
12:30:00	120.0	209.083	1.000	26,292	32.65
13:00:00	150.0	209.167	1.084	27,075	26.1
13:30:00	180.0	209.167	1.084	27,860	26.167
14:00:00	210.0	209.167	1.084	28,779	30.633
14:30:00	240.0	209.167	1.084	29,778	33.3
15:00:00	270.0	209.167	1.084	30,786	36.6
15:30:00	300.0	209.167	1.084	31,816	34.333
16:00:00	330.0	209.167	1.084	32,890	35.8
16:30:00	360.0	209.167	1.084	34,032	38.067
17:30:00	420.0	209.167	1.084	36,192	36.0
18:30:00	480.0	209.167	1.084	38,324	35.533
21:00:00	630.0	209.167	1.084	43,468	34.293
23:10:00	760.0	209.250	1.167	47,480	30.862
7:30:00	1,260.0	209.250	1.167	63,419	31.878
13:30:00	1,620.0	209.250	1.167	72,680	25.725
18:30:00	1,920.0	209.250	1.167	80,130	24.833
7:30:00	2,700.0	209.250	1.167	98,120	23.064
12:00:00	2,970.0	209.250	1.167	104,553	23.826
12:30:00	3,000.0	209.167	1.083	105,292	24.633

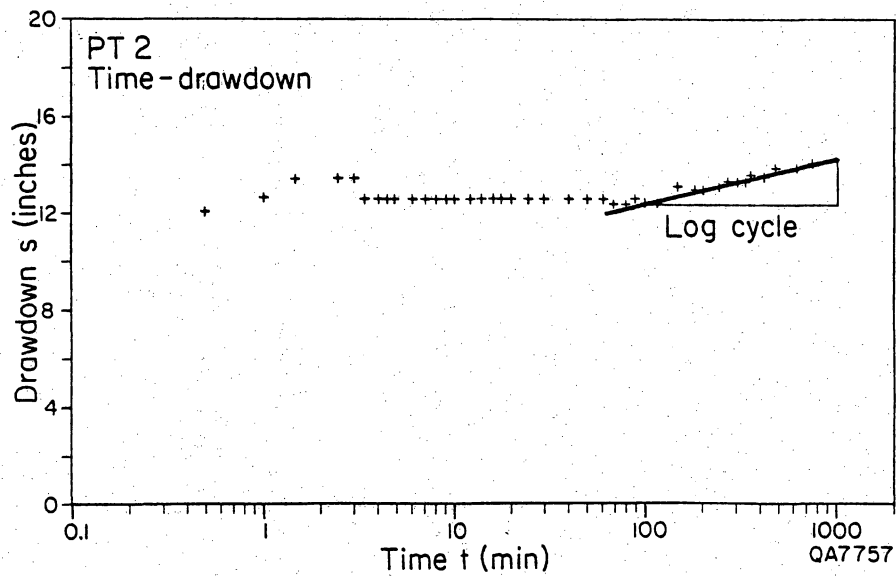


Figure A3-7. Time-drawdown plot interpreted using Theis' method for pumping test no. 2 in well LL156, Baylor Ranch. Fluctuations in water-level decline during early phase of testing due to changes in discharge rate. Segment illustrating minor decline during late phase of test used for transmissivity calculations.

During the drawdown phase, 82,508 gal of water were produced. When the drawdown phase was terminated at 12:30 p.m. on January 26, the recovery of water level was monitored for another 20 hr until 8:30 a.m., January 27 (table A3-4). At this point, 100% of the original water level had recovered.

Figure A3-7 illustrates the limited and brief drawdown observed in this well during testing. In pumping tests where drawdown is as limited as seen in this well and basically occurs instantaneously, only general approximations of transmissivity can be calculated. Using Jacob's method for drawdown data, a small trend does appear at the end of the test. Using this late phase, a calculated transmissivity of 49.986 gpd/ft of drawdown was obtained ($6.683 \text{ ft}^2/\text{d}$ or $621 \text{ m}^2/\text{d}$). The mean discharge rate (Q) used in this approximation was 27.5 gpm.

PT #3

PT #3 was conducted in well LL155, the Frederick Well, which is located on the Dyer Ranch (formerly the Frederick Ranch), Hudspeth County (fig. 2; fig. A3-1). The ranch road leading to this well intersects Ranch-to-Market Road 1111 21.6 mi (34.8 km) north of Sierra Blanca. The well is 8.0 mi (12.9 km) east of the highway. No data were available concerning the age of the well, lithologies encountered while drilling, or the actual producing formation. Total depth of the well is at least 1,200 ft (365.8 m), and during this test, water intake to the pump was set at 1,137 ft (346.5 m). The wellbore diameter is 8 inches (20.3 cm) with only limited surface casing, and the producing interval is an open-hole completion. Static water level in this well was measured at 745.25 ft (227.1 m) below land surface, and the apparent saturated thickness effective during this test was 391.75 ft (119.4 m). No

Table A3-4. Recovery test data from pumping test no. 2 at well LL156.

Time (hr)	Time from beginning of recovery (min)	<u>Time since pump started</u> <u>Time since pump stopped</u> <u>(tp + Δt)</u> Δt	Depth to water level (ft)	Residual drawdown (s') (ft)	Water level recovery (ft)
12:30:00	0.0	∞	209.167	1.083	0.0
12:30:30	0.5	6001.0	208.375	0.291	0.792
12:31:00	1.0	3001.0	208.334	0.249	0.834
12:31:30	1.5	2001.0	208.334	0.249	0.834
12:32:00	2.0	1501.0	208.334	0.249	0.834
12:32:30	2.5	1201.0	208.334	0.249	0.834
12:33:00	3.0	1001.0	208.334	0.249	0.834
12:33:30	3.5	858.14	208.334	0.249	0.834
12:34:00	4.0	751.0	208.334	0.249	0.834
12:34:30	4.5	667.67	208.334	0.249	0.834
12:35:00	5.0	601.0	208.334	0.249	0.834
12:36:00	6.0	501.0	208.334	0.249	0.834
12:37:00	7.0	429.57	208.334	0.249	0.834
12:38:00	8.0	376.0	208.334	0.249	0.834
12:39:00	9.0	334.33	208.334	0.249	0.834
12:40:00	10.0	301.0	208.334	0.249	0.834
12:42:00	12.0	251.0	208.334	0.249	0.834
12:44:00	14.0	215.29	208.313	0.229	0.854
12:46:00	16.0	188.5	208.313	0.229	0.854
12:48:00	18.0	167.67	208.313	0.229	0.854
12:50:00	20.0	151.0	208.313	0.229	0.854
12:55:00	25.0	121.0	208.292	0.208	0.875
13:00:00	30.0	101.0	208.292	0.208	0.875
13:10:00	40.0	76.0	208.292	0.208	0.875
13:20:00	50.0	61.0	208.292	0.208	0.875
13:30:00	60.0	51.0	208.292	0.208	0.875
13:40:00	70.0	43.86	208.292	0.208	0.875
13:50:00	80.0	38.5	208.292	0.208	0.875
14:00:00	90.0	34.33	208.292	0.208	0.875
14:10:00	100.0	31.0	208.292	0.208	0.875
18:30:00	360.0	9.33	208.250	0.166	0.917
0:30:00	720.0	5.17	208.167	0.083	1.000
8:30:00	1200.0	3.5	208.159	0.075	1.008

other water wells or wellbores were available during this test for use as observation wells. This well is producing NaSO_4 waters from Aquifer A, and total dissolved solids were measured at 2,077 mg/L.

Sampling of ^{13}C , ^{14}C , and ^3H for replicate analyses during the drawdown phase resulted in the need to perform two pumping tests. The first pumping test of LL155 started at 9:07 a.m. on February 6, 1987. This well is equipped with a cylinder pump and maintained a relatively constant discharge rate of 3.79 gpm (table A3-5). During the pumping period, the recorded water level dropped to the level of the pump intake at 1.137 ft (346.5 m) in 720 min (12 hr) for a total drawdown of 391.75 ft (119.4 m) (figs. A3-8, A3-9). As previously stated, sampling was also in progress, therefore the pumping test recovery phase was rescheduled for a later time in order to complete sampling. Monitoring of the drawdown phase was terminated at 9:07 p.m.

After sampling had been completed, the well was turned off and allowed to recover to the original static water level. A second drawdown phase, PT #3A, was started at 11:00 a.m., February 10, 1987 (table A3-6). During this phase, 200 ft of drawdown was measured during the first 180 min of the pumping test. It was determined that this would be the maximum drawdown for this test (PT #3A) because of difficulties encountered with probe movement below this depth during previous measurements. The drawdown phase was terminated at 2:00 p.m., and recovery measurements were immediately initiated (figs. A3-10, A3-11; table A3-7). Monitoring of water level recovery continued for 42 hr until 8:00 a.m., February 12, 1987. At this point in the recovery phase, 100% of the original water level had recovered.

In contrast to well LL156, LL155 is currently being overproduced as the inflow of ground water into the borehole only begins to reach equilibrium with the discharge of ground water as maximum drawdown is being approached (fig. A3-8), which occurs after a relatively short time. Although water-bearing fracture(s) may intersect the

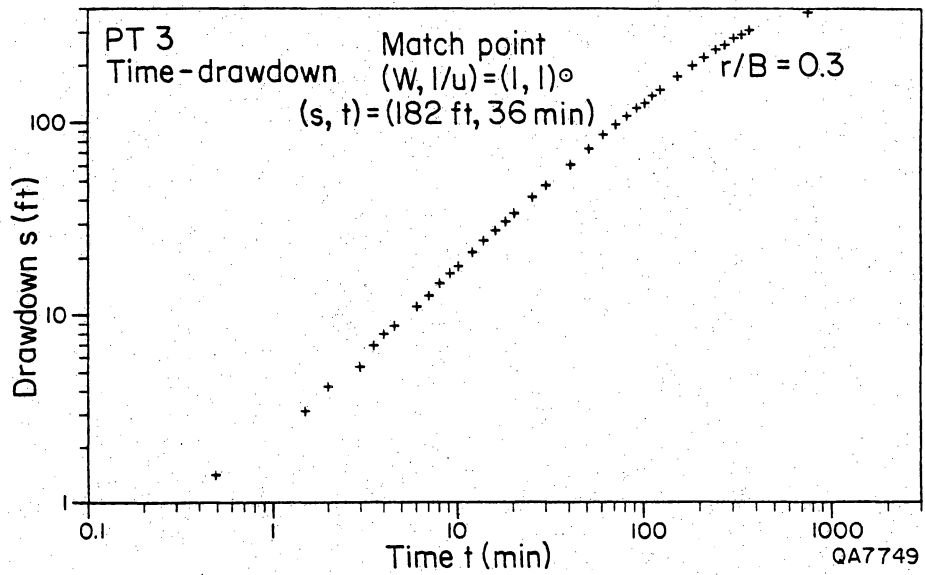


Figure A3-8. Time-drawdown curve matched to Walton type curve for pumping test no. 3 in well LL155, Dyer Ranch.

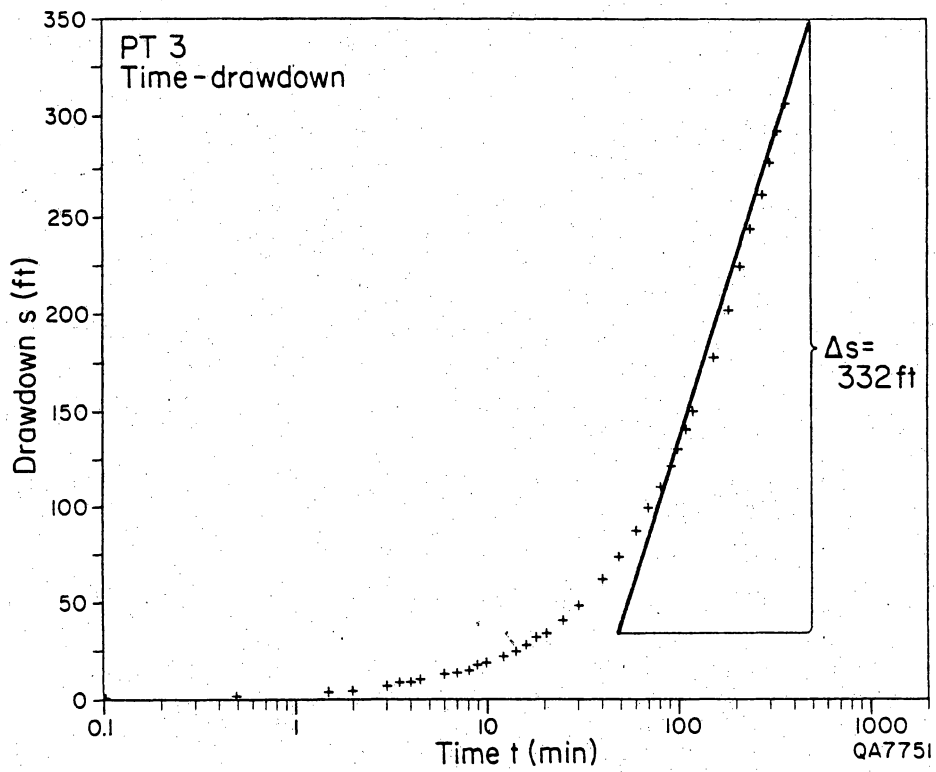


Figure A3-9. Time-drawdown plot interpreted using Jacob's method for pumping test no. 3 in well LL155, Dyer Ranch.

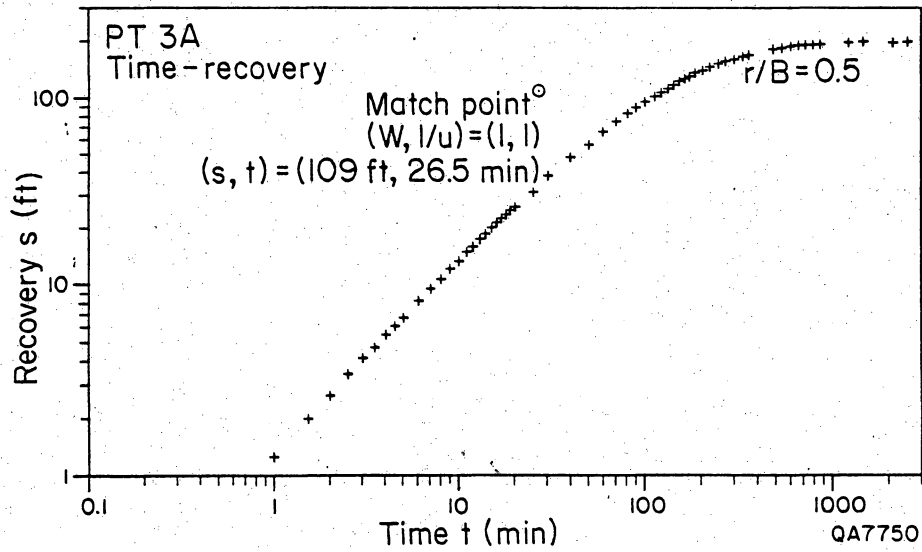


Figure A3-10. Time-recovery curve matched to Walton type curves for pumping test no. 3A in well LL155, Dyer Ranch.

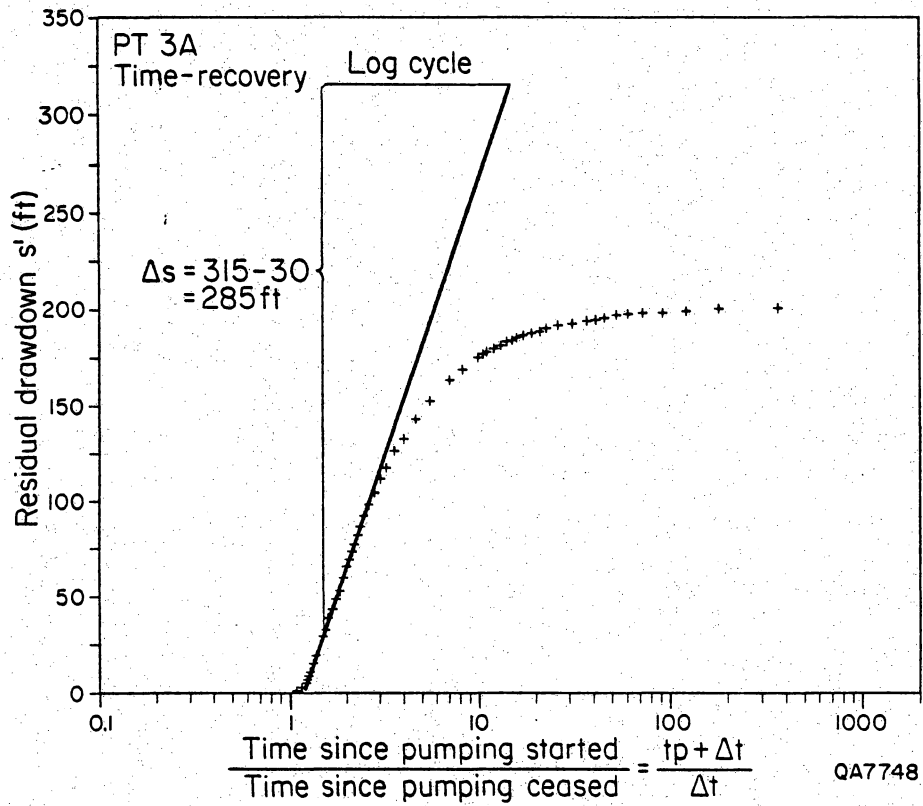


Figure A3-11. Time-recovery plot interpreted using Theis' method for pumping test no. 3A in well LL155, Dyer Ranch.

Table A3-5. Drawdown data from pumping test no. 3 at well LL155.

Time (hr)	Time from beginning of pumping (min)	Depth to water level (ft)	Water level drawdown (ft)	Flow meter reading (gal)	Well discharge (gpm)
09:07:00	0	747.917	0.000	105,393	-
09:07:30	0.5	749.333	1.416	105,393	-
09:08:00	1.0	-	-	105,395	4.0
09:08:30	1.5	751.000	3.083	105,397	4.0
09:09:00	2.0	752.000	4.083	105,398	2.0
09:09:30	2.5	-	-	105,301	6.0
09:10:00	3.0	753.083	5.166	105,303	4.0
09:10:30	3.5	754.917	7.000	105,305	4.0
09:11:00	4.0	755.833	7.916	105,306	2.0
09:11:30	4.5	756.667	8.750	-	-
09:12:00	5.0	-	-	-	-
09:13:00	6.0	759.083	11.166	105,310	2.0
09:14:00	7.0	760.833	12.916	105,315	5.0
09:15:00	8.0	762.583	14.666	105,320	5.0
09:16:00	9.0	764.750	16.833	105,327	7.0
09:17:00	10.0	765.917	18.000	105,333	5.0
09:19:00	12.0	769.333	21.416	105,345	6.5
09:21:00	14.0	772.500	24.583	105,356	5.5
09:23:00	16.0	775.333	27.416	105,367	5.5
09:25:00	18.0	778.583	30.666	105,379	6.0
09:27:00	20.0	781.417	33.500	105,390	5.5
09:32:00	25.0	788.667	40.750	105,429	7.4
09:37:00	30.0	795.667	47.750	105,448	3.8
09:47:00	40.0	809.667	61.750	105,530	5.5
09:57:00	50.0	821.667	73.750	105,569	3.9
10:07:00	60.0	835.583	87.666	-	-
10:17:00	70.0	846.167	98.250	105,735	3.9
10:27:00	80.0	857.167	109.250	-	-
10:38:00	91.0	868.667	120.750	105,725	4.1
10:47:00	100.0	877.833	129.916	-	-
10:57:00	110.0	887.833	139.916	105,804	4.2
11:07:00	120.0	897.00	149.083	105,906	4.25
11:37:00	150.0	923.917	176.000	105,956	2.90
12:07:00	180.0	948.500	200.583	106,103	3.90
12:37:00	210.0	969.833	221.916	106,200	3.90
13:07:00	240.0	989.500	241.583	106,315	3.8
13:37:00	270.0	1,007.167	259.250	-	-
14:07:00	300.0	1,024.500	276.583	106,545	3.8
14:37:00	330.0	1,040.000	292.083	106,656	4.0
15:07:00	360.0	1,055.000	307.083	-	-
21:07:00	720.0	1,137.000	389.083	-	-

Table A3-6. Drawdown data from pumping test no. 3A at well LL155.

Time (hr)	Time from beginning of pumpage (min)	Depth to water level (ft)	Water level drawdown (ft)	Flow meter reading (gal)	Well discharge (gpm)
11:00:00	0.0	744.667	0.000	108,095	--
11:00:30	0.5	745.750	1.083		
11:01:00	1.0	746.667	2.000		
11:01:30	1.5	747.667	3.000		
11:02:00	2.0	748.833	4.166		
11:02:30	2.5	749.583	4.916		
11:03:00	3.0	750.500	5.833		
11:03:30	3.5	751.500	6.833		
11:04:00	4.0	752.417	7.750		
11:04:30	4.5	753.750	9.083		
11:05:00	5.0	754.083	9.416		
11:06:00	6.0	755.667	11.000		
11:07:00	7.0	757.667	13.000		
11:08:00	8.0	759.167	14.500		
11:09:00	9.0	760.667	16.000		
11:10:00	10.0	762.500	17.833		
11:11:00	11.0	764.417	19.750		
11:12:00	12.0	765.833	21.166		
11:13:00	13.0	767.417	22.750		
11:14:00	14.0	769.000	24.333		
11:15:00	15.0	770.500	25.833		
11:16:00	16.0	771.750	27.083		
11:17:00	17.0	773.500	28.833		
11:18:00	18.0	774.833	30.166		
11:19:00	19.0	776.417	31.750		
11:20:00	20.0	777.917	33.250		
11:25:00	25.0	785.250	40.583		
11:30:00	30.0	792.333	47.666	108,125	1
11:40:00	40.0	805.583	60.916		
11:50:00	50.0	818.500	73.833		
12:00:00	60.0	830.833	86.166		
12:10:00	70.0	842.667	98.000		
12:20:00	80.0	853.750	109.083	108,330	4.02
12:30:00	90.0	864.083	119.416		
12:40:00	100.0	874.250	129.583		
12:50:00	110.0	884.167	139.500		
13:00:00	120.0	893.500	148.833	108,494	4.10
13:10:00	130.0	902.833	158.166		
13:20:00	140.0	912.000	167.333		
13:30:00	150.0	920.417	175.750		
13:40:00	160.0	929.000	184.333	108,655	3.93
13:50:00	170.0	937.000	192.333		
14:00:00	180.0	944.667	200.000	108,722	4.18

Table A3-7. Recovery data from pumping test no. 3 at well LL155.

Time (hr)	Time from beginning of recovery (min)	<u>Time since pump started</u> <u>Time since pump stopped</u> <u>(tp + Δt)</u> Δt	Depth to water level (ft)	Residual drawdown (s') (ft)	Water level recovery (ft)
14:00:00	0.0	∞	944.667	200.000	0.0
14:00:30	0.5	361.00	944.083	199.416	0.584
14:01:00	1.0	181.00	943.417	198.750	1.250
14:01:30	1.5	121.00	942.667	198.000	2.000
14:02:00	2.0	91.00	942.000	197.333	2.667
14:02:30	2.5	73.00	941.250	196.583	3.417
14:03:00	3.0	61.00	940.583	195.916	4.084
14:03:30	3.5	52.43	939.917	195.250	4.750
14:04:00	4.0	46.00	939.083	194.416	5.584
14:04:30	4.5	41.00	938.583	193.916	6.084
14:05:00	5.0	37.00	937.833	193.166	6.834
14:06:00	6.0	31.00	936.417	191.750	8.250
14:07:00	7.0	26.71	935.000	190.333	9.667
14:08:00	8.0	23.50	933.917	189.250	10.750
14:09:00	9.0	21.00	932.583	187.916	12.084
14:10:10	10.0	19.00	931.167	186.500	13.500
14:11:00	11.0	17.36	929.667	185.000	15.000
14:12:00	12.0	16.00	928.667	184.000	16.000
14:13:00	13.0	14.85	927.250	182.583	17.417
14:14:00	14.0	13.86	926.083	181.416	18.584
14:15:00	15.0	13.00	924.667	180.000	20.000
14:16:00	16.0	12.25	923.417	178.750	21.250
14:17:00	17.0	11.59	922.417	177.750	22.250
14:18:00	18.0	11.00	921.00	176.333	23.667
14:19:00	19.0	10.47	919.833	175.166	24.834
14:20:00	20.0	10.00	918.667	174.000	26.000
14:25:00	25.0	8.20	912.917	168.250	31.750
14:30:00	30.0	7.00	907.167	162.500	37.500
14:40:00	40.0	5.50	896.583	151.916	48.084
14:50:00	50.0	4.60	887.167	142.500	57.500
15:00:00	60.0	4.00	878.250	133.583	66.417
15:10:00	70.0	3.57	870.00	125.333	74.667
15:20:00	80.0	3.25	861.417	116.750	83.250

Table A3-7 (cont.)

Time (hr)	Time from beginning of recovery (min)	<u>Time since pump started</u> <u>Time since pump stopped</u> <u>(tp + Δt)</u> Δt	Depth to water level (ft)	Residual drawdown (s') (ft)	Water level recovery (ft)
15:30:00	90.0	3.00	855.250	110.583	89.417
15:40:00	100.0	2.80	848.833	104.166	95.834
15:50:00	110.0	2.64	842.667	98.000	102.000
16:00:00	120.0	2.50	836.833	92.166	107.834
16:10:00	130.0	2.38	831.417	86.750	113.250
16:20:00	140.0	2.29	826.250	81.583	118.417
16:30:00	150.0	2.20	821.750	77.083	122.917
16:40:00	160.0	2.13	817.667	73.000	127.000
16:50:00	170.0	2.06	813.833	69.166	130.834
17:00:00	180.0	2.00	810.167	65.500	134.500
17:20:00	200.0	1.90	803.917	59.250	140.750
17:40:00	220.0	1.82	798.500	53.833	146.167
18:00:00	240.0	1.75	793.750	49.083	150.917
18:30:00	270.0	1.67	787.667	43.000	157.000
19:00:00	300.0	1.60	782.667	38.000	162.000
19:30:00	330.0	1.55	778.500	33.833	166.167
20:00:00	360.0	1.50	774.833	30.166	169.834
22:00:00	480.0	1.38	764.417	19.750	180.250
23:00:00	540.0	1.33	760.917	16.250	183.750
00:00:00	600.0	1.30	757.917	13.250	186.750
01:00:00	660.0	1.27	755.333	10.666	189.334
02:00:00	720.0	1.25	753.333	8.666	191.334
03:00:00	780.0	1.23	751.583	6.916	193.084
04:00:00	840.0	1.21	750.250	5.583	194.417
10:15:00	1,215.0	1.15	746.167	1.500	198.500
13:45:00	1,425.0	1.13	745.333	0.500	199.500
00:00:00	2,040.0	1.09	745.00	0.333	199.667
08:00:00	2,520.0	1.07	744.667	0.000	200.000

borehole of this well, none of the methods used to calculate transmissivity documented or inferred their presence. Regionally, Aquifer A is unconfined although locally it may exhibit characteristics of a semiconfined aquifer. Interpretation of the test data was accomplished using four different methods (two using drawdown data and two using recovery data), as described in the discussion of PT #1.

By matching the time-drawdown and time-recovery plots from this well to Walton's set of type curves based on the Theis method for semiconfined aquifers (Kruseman and De Ridder, 1976), good agreement of calculated transmissivities resulted (figs. A3-8, A3-10). Matching the drawdown data for PT #3 with Walton's set of type curves, a calculated transmissivity of 2.39 gpd/ft of drawdown was obtained ($.32 \text{ ft}^2/\text{d}$, or $.03 \text{ m}^2/\text{d}$). Using the same method with recovery data from PT #3A, a transmissivity of 3.98 gpd/ft of drawdown was calculated ($.53 \text{ ft}^2/\text{d}$, or $.05 \text{ m}^2/\text{d}$).

Additional calculations of transmissivity were made using the Jacob method for drawdown (fig. A3-9) and the Theis method for recovery (fig. A3-11). The Jacob method is used with unsteady flow in confined aquifers. Using this method on drawdown data from PT #3, a calculated transmissivity of 3.01 gpd/ft of drawdown was obtained ($.40 \text{ ft}^2/\text{d}$, or $.04 \text{ m}^2/\text{d}$). The Theis recovery method may be used under the same conditions as those required for Jacob's method for drawdown. This method resulted in a transmissivity of 3.50 gpd/ft of drawdown ($.47 \text{ ft}^2/\text{d}$, or $.04 \text{ m}^2/\text{d}$).

Averaging the four values calculated for LL155 yields a mean transmissivity of 3.22 gpd/ft of drawdown ($.43 \text{ ft}^2/\text{d}$ or $.04 \text{ m}^2/\text{d}$) with a standard deviation of 0.68 gpd/ft. This is an extremely low value for transmissivity and, when compared to values from other wells tested in the area, may be used to infer either that only matrix permeability is contributing to the wellbore or that a considerably lower density of fractures was intersected.

PT #4

PT #4 was conducted in well LL148, the Red Well, which is located on the Baylor Lease of University of Texas Lands, Hudspeth County (fig. 2; fig. A3-1). The ranch road leading east from Ranch-to-Market Road 1111 toward Red Well is located 8.1 mi (13.1 km) south of the intersection between U. S. Highway 62-180 and Ranch-to-Market-Road 1111. East from Ranch-to-Market Road 1111, it is 4.2 mi (6.7 km) southeast to the Scratch Ranch and an additional 4.7 mi (7.5 km) east-northeast to the well. No data were available concerning the age of this well, lithologies encountered while drilling, or the actual producing formation. Total depth of this well is unknown, and during this test, water intake to the pump was set at 503 ft (153.3 m) below land surface. The wellbore diameter is 6 inches (15.2 cm) with limited surface casing because the producing interval is an open-hole completion. The static water level in this well was measured at 484.7 ft (147.7 m) below land surface, and the apparent saturated thickness effective during this test was 18.3 ft (5.6 m).

On July 31, 1986, the static water level in this well was measured during a previous phase of study at 462.7 ft (141.1 m) below land surface. Prior to this July 1986 measurement, above-average rainfall had been received in the area. Since the first measurement was taken, normal to below-normal rainfall has been recorded. The two static water level measurements record a decline in water levels between July 1986, and February 1987, of 22 ft (6.7 m). Production prior to the February measurement is not a cause of this decline in water level because the well had been inoperative for several months due to mechanical problems. No other water wells or wellbores were available during this test for use as observation wells. This well is producing NaCl waters from aquifer A and total dissolved solids were measured at 2020.67 mg/L.

The drawdown phase of PT #4 was initiated at 4:15 p.m. on February 11, 1987. This well is equipped with a cylinder pump and maintained a relatively constant rate of discharge of 4.33 gpm (table A3-8). The pumping or drawdown phase was terminated at 8:00 a.m. on February 12, when the pumpjack pulley mounted to the gas-powered motor sheared off the motor shaft. The last measurement taken before this mechanical failure had recorded 1.1 ft (.33 m) of drawdown after 945 min (15.75 hr). Measurements of recovery rates for this portion of the test were temporarily delayed while motor and pump shutdowns were completed. The first measurement of recovery was made at 8:05 a.m. on February 12, 1987, and was terminated at 10:00 a.m., 120 min after the start of recovery (table A3-9). At this point, all but 2 inches (5.1 cm) of the original drawdown had recovered.

After the motor assembly was repaired, another pumping test was performed (PT #4A) at an increased discharge rate of 6.74 gpm in an attempt to induce better drawdown data for the calculation of transmissivity (table A3-10). PT #4A was initiated 11:05 a.m. on February 12, 1987, and was terminated at 7:05 a.m. on February 13 (fig. A3-12). Total drawdown for PT #4 was measured at 1.1 ft (13 inches or 33 cm) while total drawdown for PT #4A was 1.6 ft (19 inches or 48.3 cm). In both tests, a majority of the drawdown, 68% and 80% respectively, occurred in the first minute of production. At the request of the rancher, no recovery test was conducted for PT #4A, so that depleted water supplies could be replaced.

The results of PT #4 and 4A were both similar to the results obtained from PT #2 in that insufficient drawdown was recorded to allow accurate, reproducible calculations of transmissivity. No transmissivity value can be calculated because the drawdown occurs during the early part of the test and is probably the result of wellbore storage.

Table A3-8. Drawdown data from pumping test no. 4 at well LL148.

Time (hr)	Time from beginning of pumpage (min)	Depth to water level (ft)	Water level drawdown (ft)	Flow meter reading (gal)	Well discharge (gpm)
16:15:00	0.0	486.167	0.000		
16:15:30	0.5	486.667	0.500		
16:16:00	1.0	486.833	0.666		
16:16:30	1.5	486.917	0.750		
16:17:00	2.0	486.917	0.750		
16:17:30	2.5	486.917	0.750		
16:18:00	3.0	486.917	0.750		
16:18:00	3.5	486.917	0.750		
16:19:00	4.0	486.917	0.750		
16:19:30	4.5	487.000	0.833		
16:20:00	5.0	487.000	0.833		
16:21:00	6.0	487.000	0.833		4
16:22:00	7.0	487.000	0.833		
16:23:00	8.0	487.083	0.916		
16:24:00	9.0	487.083	0.916		
16:25:00	10.0	487.083	0.916		
16:27:00	12.0	487.083	0.916		4.3
16:29:00	14.0	487.083	0.916		4.6
16:31:00	16.0	487.083	0.916		
16:33:00	18.0	487.083	0.916		
16:35:00	20.0	487.083	0.916		4.3
16:40:00	25.0	487.083	0.916		
16:45:00	30.0	487.083	0.916		4.0
16:55:00	40.0	487.083	0.916		4.3
17:05:00	50.0	487.083	0.916		4.0
17:15:00	60.0	487.083	0.916		4.3
17:25:00	70.0	487.083	0.916		
17:35:00	80.0	487.167	1.000		4.3
17:45:00	90.0	487.167	1.000		4.3
17:55:00	100.0	487.167	1.000		
18:05:00	110.0	487.167	1.000		4.3
18:15:00	120.0	487.167	1.000		
18:45:00	150.0	487.167	1.000		4.3
19:15:00	180.0	487.167	1.000		
19:45:00	210.0	487.250	1.083		4.3
20:15:00	240.0	487.250	1.083		
20:45:00	270.0	487.250	1.083		4.3
21:15:00	300.0	487.250	1.083		
21:45:00	330.0	487.250	1.083		
22:15:00	360.0	487.250	1.083		
23:15:00	420.0	487.250	1.083		4.3
00:15:00	480.0	487.250	1.083		
01:15:00	540.0	487.250	1.083		4.3
02:15:00	600.0	487.250	1.083		
03:15:00	660.0	487.250	1.083		4.0
04:15:00	720.0	487.250	1.083		
05:15:00	780.0	487.250	1.083		4.3
06:15:00	840.0	487.250	1.083		
07:15:00	900.0	487.250	1.083		

Table A3-9. Recovery data from pumping test no. 4 at well LL148.

Time (hr)	Time from beginning of recovery (min)	<u>Time since pump started</u> <u>Time since pump stopped</u> <u>(tp + Δt)</u> Δt	Depth to water level (ft)	Residual drawdown (s') (ft)	Water level recovery (ft)
08:00:00	0.0	∞	487.250	1.083	0
08:05:00	5.0	190.0	486.833	0.666	0.417
08:10:00	10.0	91.0	486.667	0.500	0.583
08:15:00	15.0	61.0	486.333	0.166	0.917
08:20:00	20.0	46.0	486.333	0.166	0.917
08:25:00	25.0	37.0	486.333	0.166	0.917
08:30:00	30.0	31.0	486.333	0.166	0.917
09:00:00	60.0	16.0	486.333	0.166	0.917
10:00:00	120.0	8.5	486.333	0.166	0.917

Table A3-10. Drawdown data from pumping test no. 4A at well LL148.

Time (hr)	Time from beginning of pumpage (min)	Depth to water level (ft)	Water level drawdown (ft)	Flow meter reading (gal)	Well discharge (gpm)
11:05:00	0.0	486.333	0.000		
11:06:00	1.0	487.167	0.834		
11:06:30	1.5	487.583	1.250		
11:07:00	2.0	487.625	1.292		
11:07:30	2.5	487.667	1.334		
11:08:00	3.0	487.750	1.417		
11:08:30	3.5	487.750	1.417		
11:09:00	4.0	487.750	1.417		
11:09:30	4.5	487.750	1.417		
11:10:00	5.0	487.833	1.500		
11:11:00	6.0	487.833	1.500		
11:12:00	7.0	487.833	1.500		
11:13:00	8.0	487.833	1.500		6.7
11:14:00	9.0	487.917	1.584		
11:15:00	10.0	487.917	1.584		
11:17:00	12.0	487.917	1.584		
11:19:00	14.0	487.917	1.584		
11:21:00	16.0	487.917	1.584		
11:23:00	18.0	487.917	1.584		
11:25:00	20.0	487.917	1.584		7.5
11:30:00	25.0	487.917	1.584		6.7
11:35:00	30.0	487.917	1.584		
11:45:00	40.0	487.917	1.584		
11:55:00	50.0	487.917	1.584		6.7
12:05:00	60.0	487.917	1.584		6.7
12:25:00	80.0	487.917	1.584		6.7
12:45:00	100.0	487.917	1.584		
13:05:00	120.0	487.917	1.584		6.7
14:05:00	180.0	487.917	1.584		6.7
15:05:00	240.0	487.917	1.584		6.7
16:05:00	300.0	487.917	1.584		7.5
17:05:00	360.0	487.917	1.584		6.7
18:05:00	420.0	487.917	1.584		6.7
19:05:00	480.0	487.917	1.584		
20:05:00	540.0	487.917	1.584		6.7
21:05:00	600.0	487.917	1.584		6.7
22:05:00	660.0	487.917	1.584		
23:05:00	720.0	487.917	1.584		6.7
00:05:00	780.0	487.917	1.584		6.7
01:05:00	840.0	487.917	1.584		
02:05:00	900.0	487.917	1.584		6.7
03:05:00	960.0	487.917	1.584		
04:05:00	1,020.0	487.917	1.584		6.7
05:05:00	1,080.0	487.917	1.584		
06:05:00	1,140.0	487.917	1.584		
07:05:00	1,200.0	487.917	1.584		6.7

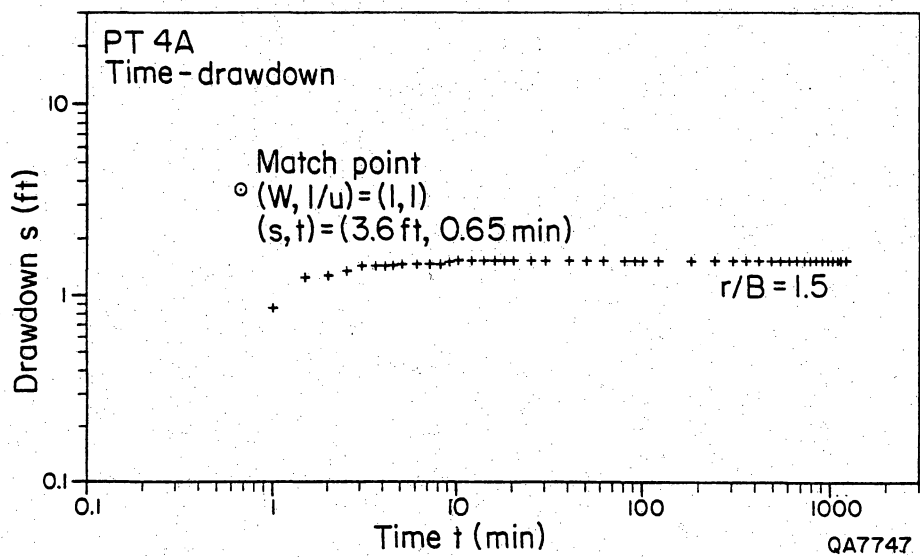


Figure A3-12. Time-drawdown curve matched to Walton type curves for pumping test no. 4A in well LL148. All of the drawdown occurs during the early testing period and can be explained by wellbore storage. In this case, no method of transmissivity determination is available. Additional testing will be required at an increased discharge rate so that the aquifer may be reasonably stressed.

Although other methods of analyses were attempted, including Jacob's method and Theis' method, the values obtained covered a wide range of transmissivities and were considered to be erroneous and of no real significance. As in PT #2, the discharge rate of this well will have to be increased to induce drawdown of a magnitude required for the determination of transmissivity.

PT #5

PT #5 was conducted in well LL141, the Bravo Well, which is located on the Baylor Lease of the University of Texas Lands, Hudspeth County (fig. 2; fig. A3-1). The ranch road leading west toward Bravo Well is located 10.2 mi (16.4 km) south of the intersection between U. S. Highway 62-180 and Ranch-to-Market Road 1111. West from Ranch-to-Market Road 1111, it is 2.3 mi (3.7 km) to the well. No data were available concerning the age of Bravo Well, lithologies encountered while drilling, or the producing formation. Total depth of this well is 663 ft (202.1 m) below land surface and during this test water intake was set at 661 ft (201.5 m) below land surface. The wellbore diameter is 8 inches (20.3 cm) with an unknown depth of surface casing and an open-hole completion. The static water level in this well was measured at 652.7 ft (198.9 m) below land surface, and the saturated thickness effective during this test was 9.3 ft (2.8 m).

The decline in static water level measured in LL148 (Red Well) was also recorded in LL141 (Bravo Well). On July 12, 1986, the static water level in this well was measured during a previous phase of study at 628 ft (191.4 m) below land surface. The two static water level measurements record a decline in water levels between July 1986 and February 1987 of 24.7 ft (7.5 m). Production prior to the February measurement is unlikely because arrangements had been made to allow the well

sufficient time to stabilize before testing. Both LL141 and LL148 are within the same drainage area, a series of connected arroyos. LL141 is within the drainage area of Baylor Draw, which feeds into South Well Draw, which feeds into Antelope Gulch, the arroyo within which LL148 is located. No other wells or wellbores were available during this test for use as observation wells. This well is producing NaSO_4 waters from aquifer A, and total dissolved solids were measured at 1786.92 mg/L.

Currently, this well only has 9.3 ft of drawdown potential. Attempts to lower the pump to allow for additional drawdown proved to be impossible as the current total depth is 1 ft (.3 m) deeper than the intake for the pump. The most likely scenario, based on discussions with ranch personnel, is that previously this well was deeper, but a large amount of pipe had been lost in the hole and attempts to recover the lost pipe were unsuccessful. In addition to lost pipe, caving of the open borehole during fishing operations may have contributed to the loss in total depth.

The drawdown phase of PT #5 was initiated at 10:00 a.m. on February 4, 1987. This well is equipped with a submersible pump and maintained a relatively constant rate of discharge at 11.1 gpm (table A3-11). The drawdown phase was terminated at 12:00 p.m., 120 min after starting the test. Recovery rates were monitored for 90 min, which was sufficient time to record 99% recovery of the original drawdown (table A3-12). Maximum drawdown occurred (water level dropped to level of pump intake) after 60 min 10 sec of the drawdown phase. The discharge rate at this point dropped to a constant rate of 8.6 gpm.

Using the same methods of analysis that were utilized for PT #1 and #3, excellent agreement was obtained for transmissivity values in this well. Time-drawdown and time-recovery plots were constructed and matched to Walton's set of type curves for semiconfined aquifers based on Theis' method (Kruseman and De

Table A3-11. Drawdown data from pumping test no. 5 at well LL141.

Time (hr)	Time from beginning of pumpage (min)	Depth to water level (ft)	Water level drawdown (ft)	Flow meter reading (gal)	Well discharge (gpm)
10:00:00	0.0	652.7	0.00		
10:00:30	0.5	652.96	0.26		
10:01:00	1.0	653.54	0.84		12
10:01:30	1.5	654.15	1.45		
10:02:00	2.0	654.7	2.00		12
10:02:30	2.5	655.15	2.45		
10:03:00	3.0	655.5	2.80		12
10:03:30	3.5	655.8	3.10		
10:04:00	4.0	656.2	3.50		12
10:04:30	4.5	656.5	3.80		
10:05:00	5.0	656.7	4.00		10
10:06:00	6.0	657.3	4.60		
10:07:00	7.0	657.6	4.90		10
10:08:00	8.0	657.9	5.20		
10:09:00	9.0	658.2	5.50		12
10:10:00	10.0	658.5	5.80		10
10:12:00	12.0	659.0	6.30		10
10:14:00	14.0	659.4	6.70		10
10:16:00	16.0	659.8	7.10		10
10:18:00	18.0	660.1	7.40		
10:20:00	20.0	660.5	7.80		10
10:25:00	25.0	660.7	8.00		10
10:30:00	30.0	661.1	8.40		12
10:40:00	40.0	661.7	9.00		12
10:50:00	50.0	661.9	9.20		12
11:00:00	60.0	662.0	9.30		10
11:10:00	70.0				8.6
11:20:00	80.0				8.6
11:30:00	90.0				6.7
11:40:00	100.0				8.6
11:50:00	110.0				8.6
12:00:00	120.0				8.6

Table A3-12. Recovery data from pumping test no. 5 at well LL141.

Time (hr)	Time from beginning of recovery (min)	$\frac{\text{Time since pump started}}{\text{Time since pump stopped}}$ $\frac{(tp + \Delta t)}{\Delta t}$	Depth to water level (ft)	Residual drawdown (s') (ft)	Water level recovery (ft)
12:00:00	0.0	∞	662.0	9.30	0.0
12:00:30	0.5	121.0	660.9	8.20	1.1
12:01:00	1.0	61.0	659.8	7.10	2.2
12:01:30	1.5	41.0	659.0	6.30	3.0
12:02:00	2.0	31.0	658.5	5.80	3.5
12:02:30	2.5	25.0	658.0	5.30	4.0
12:03:00	3.0	21.0	657.6	4.90	4.4
12:03:30	3.5	18.1	657.3	4.60	4.7
12:04:00	4.0	16.0	657.0	4.30	5.0
12:04:30	4.5	14.3	656.7	4.00	5.3
12:05:00	5.0	13.0	656.4	3.70	5.6
12:06:00	6.0	11.0	656.0	3.30	6.0
12:07:00	7.0	9.6	655.7	3.00	6.3
12:08:00	8.0	8.5	655.3	2.60	6.7
12:09:00	9.0	7.7	655.1	2.40	6.9
12:10:00	10.0	7.0	655.0	2.30	7.0
12:12:00	12.0	6.0	654.5	1.80	7.5
12:14:00	14.0	5.3	654.2	1.50	7.8
12:16:00	16.0	4.8	654.0	1.30	8.0
12:18:00	18.0	4.3	653.6	0.90	8.4
12:20:00	20.0	4.0	653.3	0.60	8.7
12:25:00	25.0	3.4	653.0	0.30	9.0
12:30:00	30.0	3.0	652.9	0.20	9.1
12:40:00	40.0	2.5	652.8	0.10	9.2
12:50:00	50.0	2.2	652.8	0.10	9.2
13:00:00	60.0	2.0	652.8	0.10	9.2
13:10:00	70.0	1.9	652.75	0.05	9.25
13:20:00	80.0	1.8	652.75	0.05	9.25
13:30:00	90.0	1.7	652.70	0.00	9.30

Ridder, 1976). The drawdown phase of this test yielded a calculated transmissivity of 410.3 gpd/ft of drawdown ($54.8 \text{ ft}^2/\text{d}$, or $5.1 \text{ m}^2/\text{d}$) (fig. A3-13). Using this method for the recovery data resulted in a transmissivity value of 480 gpd/ft of drawdown ($64.2 \text{ ft}^2/\text{d}$, or $6.0 \text{ m}^2/\text{d}$) (fig. A3-14).

Application of Jacob's method for drawdown data yields a calculated transmissivity of 417.9 gpd/ft of drawdown ($55.9 \text{ ft}^2/\text{d}$, or $5.2 \text{ m}^2/\text{d}$) (fig. A3-15) while the Theis method for recovery resulted in a transmissivity of 517.8 gpd/ft of drawdown ($69.2 \text{ ft}^2/\text{d}$, or $6.4 \text{ m}^2/\text{d}$) (fig. A3-16). Averaging the four calculated values for PT #5 on LL141 yields a mean transmissivity of 456.5 gpd/ft of drawdown ($61.0 \text{ ft}^2/\text{d}$, or $5.7 \text{ m}^2/\text{d}$) with a standard deviation of 51.5 gpd/ft of drawdown ($6.9 \text{ ft}^2/\text{d}$, or $.6^2/\text{d}$).

PT #6

PT #6 was conducted in well LL132 at the Williams' Ranch Headquarters (fig. 2; fig. A3-1). This well is located 7.8 mi (12.5 km) west-southwest of the intersection of Ranch-to-Market Roads 1111 and 2317. No precise data were available concerning the age of this well, lithologies encountered while drilling, or the producing formation. Discussions with the owner indicate that this well is probably more than 70 yr old. Total depth of this well is reported to be 1,200 ft (366 m), although this depth could not be confirmed. During this pumping test, water intake to the pump was set at 960.1 ft (292.6 m) below land surface. The wellbore diameter is 8 inches (20.3 cm) with surface casing down to an unknown depth. This well is producing from an open-hole completion. Static water level in this well was measured at 710.3 ft (216.5 m) below land surface, and apparent saturated thickness during this test was 249.8 ft (76.1 m). No other water wells or wellbores were available during this test for use as observation wells. This well is producing NaHCO_3 waters from

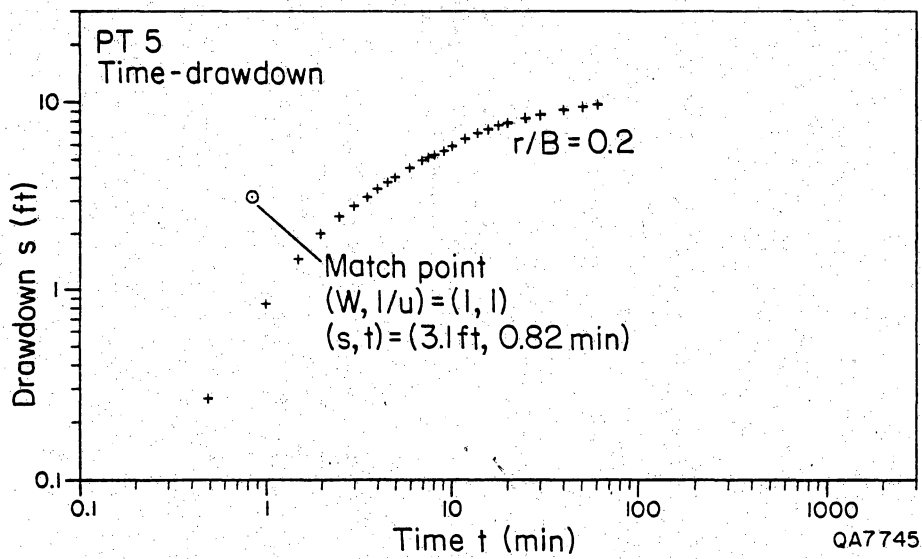


Figure A3-13. Time-drawdown curve matched to Walton type curves for pumping test no. 5 in well LL141, University Lands, Baylor lease.

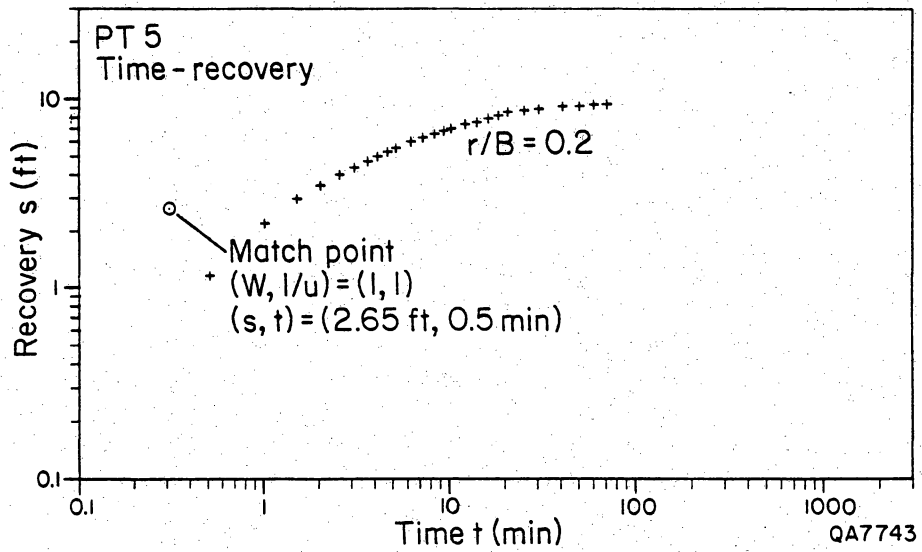


Figure A3-14. Time-recovery curve matched to Walton type curves for pumping test no. 5 in well LL141, University Lands, Baylor lease.

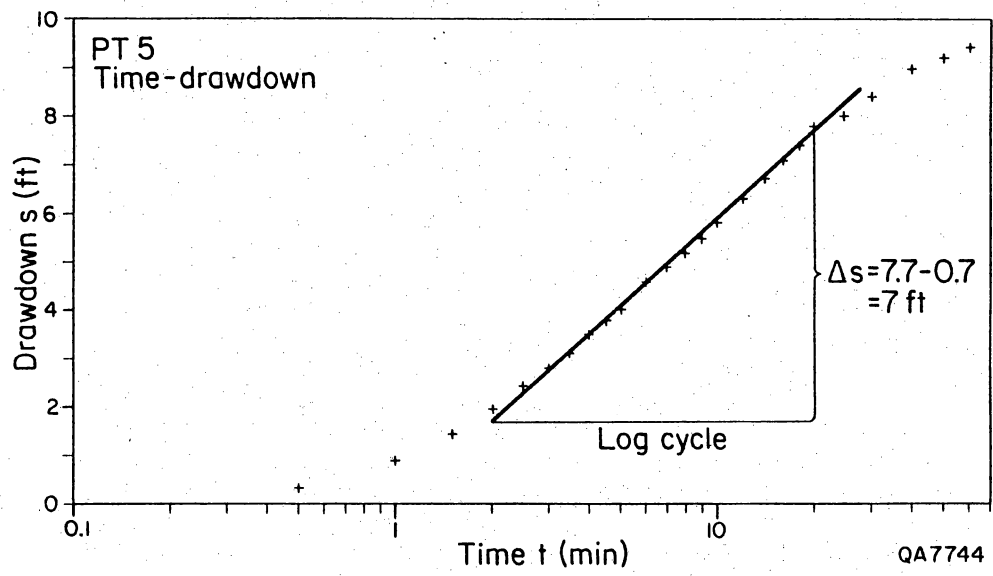


Figure A3-15. Time-drawdown plot interpreted using Jacob's method for pumping test no. 5 in well LL141, University Lands, Baylor lease.

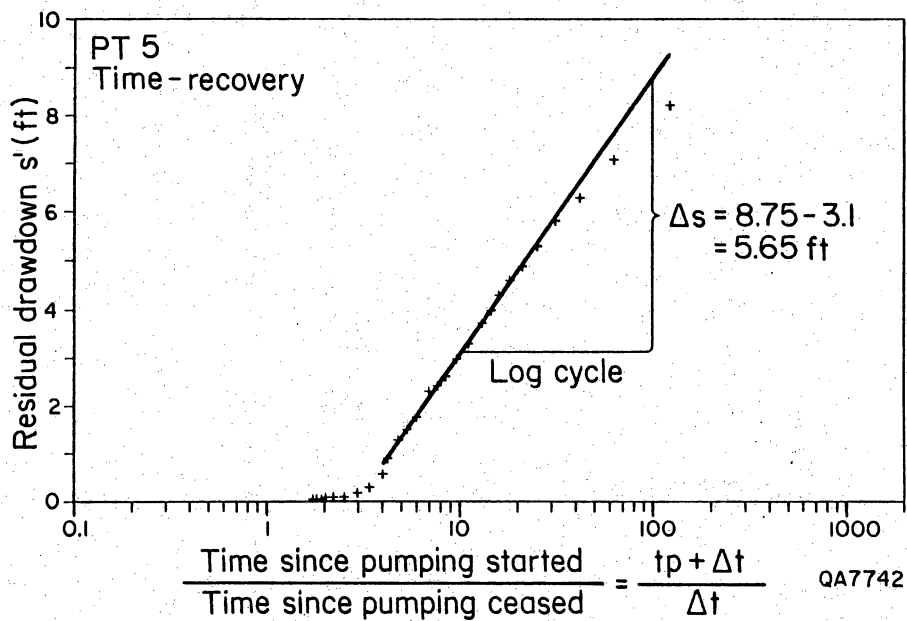


Figure A3-16. Time-recovery plot interpreted using Theis' method for pumping test no. 5 in well LL141, University Lands, Baylor lease.

aquifer A, and total dissolved solids were measured at 884.03 mg/L.

After this well had reached equilibrium during the drawdown phase, rainstorms in the area caused three power failures. The water level recovery was rapid and in each case had recovered more than 50% by the time recovery procedures could be initiated. After each power failure, the well was restarted and pumped until maximum drawdown was attained. These events explain the time lapse between the termination of drawdown and the beginning of recovery.

The drawdown phase of PT #6 was initiated at 6:00 p.m. on February 24, 1987. This well is equipped with a 2.75-inch (7.0 cm) cylinder pump, which maintained a relatively constant discharge rate of 10.6 gpm (table A3-13). During the drawdown phase, which lasted 2100 min (35 hr), the recorded water level dropped 121.3 ft (37.0 m) (fig. A3-17). During the drawdown phase, 22,260 gal of water were produced. When the final drawdown phase was terminated at 11:33 p.m., February 26, the water level recovery was monitored for 2,520 min (42 hr) until 5:33 p.m. on February 28 (table A3-14). At this point, 100% of the static water level had been recovered.

As with PT #3, PT #6 resulted in excellent agreement of transmissivity values calculated using the four methods discussed in detail for PT #1. Figures A3-17 and A3-18 represent the drawdown and recovery curves from this pumping test, which were used to match to Walton's set of type curves based on Theis' method for unsteady flow in semiconfined leaky aquifers (Kruseman and De Ridder, 1976). Based on a mean discharge rate of 10.6 gpm and a match point value for s (drawdown) of 42 ft (12.8 m) the calculated transmissivity is 28.9 gpd/ft of drawdown ($3.86 \text{ ft}^2/\text{d}$, or $.36 \text{ m}^2/\text{d}$). Using the same discharge rate and a match point for s of 50 results in a transmissivity of 24.3 gpd/ft of drawdown ($3.2 \text{ ft}^2/\text{d}$, or $.30 \text{ m}^2/\text{d}$).

Table A3-13. Drawdown data from pumping test no. 6 at well LL132.

Time (hr)	Time from beginning of pumpage (min)	Depth to water level (ft)	Water level drawdown (ft)	Flow meter reading (gal)	Well discharge (gpm)
18:00:00	0.0	711.958	0.0	108,703	0
18:00:18	0.3	713.333	1.375		
18:00:52	0.87	716.000	4.042		
18:01:08	1.13	716.667	4.709		
18:01:37	1.62	718.417	6.459		
18:02:00	2.00	719.750	7.792		
18:02:15	2.25	720.583	8.625		
18:02:30	2.50	721.333	9.375		
18:03:00	3.00	722.667	10.709		
18:03:26	3.43	724.083	12.125		
18:03:40	3.67	724.917	12.959		
18:04:00	4.00	725.667	13.709		
18:04:15	4.25	726.583	14.625		
18:04:45	4.75	728.750	16.792		
18:05:10	5.17	729.000	17.042		
18:05:30	5.50	729.750	17.792		
18:05:45	5.75	730.500	18.542		
18:06:05	6.08	731.417	19.459		
18:06:30	6.50	732.417	20.459		
18:07:00	7.00	733.583	21.625		
18:07:30	7.50	734.500	22.542		
18:08:00	8.00	735.583	23.625		
18:08:30	8.50	736.750	24.792		
18:09:00	9.00	737.750	25.792		
18:09:30	9.50	738.750	26.792		
18:10:00	10.00	739.917	27.959		
18:10:30	10.50	741.000	29.042		
18:11:00	11.00	742.167	30.209		
18:12:00	12.00	744.417	32.459		
18:13:00	13.00	746.417	34.459		
18:14:00	14.00	748.583	36.625		
18:15:00	15.00	750.667	38.709		
18:16:00	16.00	752.500	40.542		
18:17:00	17.00	754.417	42.459		
18:18:00	18.00	756.333	44.375		
18:19:00	19.00	757.833	45.875		
18:20:00	20.00	759.500	47.542		
18:21:00	21.00	761.500	49.542		
18:22:00	22.00	762.667	50.709		
18:23:00	23.00	764.250	52.292		
18:24:00	24.00	765.667	53.709		
18:25:00	25.00	767.083	55.125		
18:26:00	26.00	768.500	56.542		
18:27:00	27.00	769.833	57.875		
18:28:00	28.00	771.000	59.042		
18:29:00	29.00	772.250	60.292		
18:30:00	30.00	773.500	61.542		

Table A3-13. (cont.)

Time (hr)	Time from beginning of pumpage (min)	Depth to water level (ft)	Water level drawdown (ft)	Flow meter reading (gal)	Well discharge (gpm)
18:35:00	35.00	779.917	67.959		
18:40:00	40.00	783.833	71.875		
18:45:00	45.00	788.000	76.042	109,162	10.55
18:50:00	50.00	791.500	79.542		
18:55:00	55.00	794.583	82.625	109,297	10.0
19:00:00	60.00	797.417	85.459		
19:05:00	65.00	799.833	87.875	109,400	10.3
19:10:00	70.00	802.000	90.042		
19:15:00	75.00	804.083	92.125	109,505	10.5
19:20:00	80.00	805.917	93.959		
19:25:00	85.00	807.417	95.459	109,610	10.5
19:30:00	90.00	808.833	96.875		
19:35:00	95.00	810.083	98.125		
19:40:00	100.00	811.417	99.459	109,778	10.5
19:50:00	110.00	813.417	101.459		
20:00:00	120.00	815.167	103.209		
20:10:00	130.00	817.500	105.542	110,079	10.4
20:20:00	140.00	817.833	105.875		
20:30:00	150.00	818.833	106.875	110,282	10.15
20:40:00	160.00	819.667	107.709		
20:50:00	170.00	820.417	108.459		
21:00:00	180.00	821.083	109.125	110,592	10.3
21:10:00	190.00	821.750	109.792		
21:20:00	200.00	822.417	110.459	110,812	9.5
21:35:00	215.00	823.250	111.292		
21:40:00	220.00	823.667	111.709		
21:50:00	230.00	824.167	112.209		
22:00:00	240.00	824.667	112.709		
22:30:00	270.00	825.750	113.792	111,600	10.4
23:00:00	300.00	826.250	114.292		
23:30:00	330.00	826.375	114.417		
00:00:00	360.00	826.667	114.709	112,466	10.6
01:00:00	420.00	827.250	115.292		
02:00:00	480.00	827.917	115.959		
03:00:00	540.00	828.500	116.542		
04:40:00	640.00	829.833	117.875		
06:25:00	745.00	830.417	118.459	116,635	10.7
06:50:00	840.00	830.667	118.709	117,630	10.7
09:20:00	1050.00	831.583	119.625	119,875	10.7
10:33:00	1123.00	831.667	119.709	120,643	10.5
13:05:00	1275.00	831.917	119.959	122,282	10.6
15:50:00	1440.00	832.333	120.375	123,858	10.6
17:50:00	1560.00	832.833	120.875		
20:10:00	1700.00	833.250	121.292	126,815	10.7
01:05:00	1995.00	833.250	121.292	129,960	10.7
02:50:00	2100.00	833.250	121.292	130,963	10.6

Table A3-14. Recovery data from pumping test no. 6 at well LL132.

Time (hr)	Time from beginning of recovery (min)	<u>Time since pump started</u> <u>Time since pump stopped</u> ($t_p + \Delta t$) Δt	Depth to water level (ft)	Residual drawdown (s') (ft)	Water level recovery (ft)
23:33:00	0.0	∞	828.833	121.292	0.000
23:33:30	0.5	4201.0	826.000	118.459	2.833
23:34:00	1.0	2101.0	823.833	116.292	5.000
23:34:30	1.5	1401.0	821.667	114.126	7.166
23:35:00	2.0	1051.0	819.250	111.709	9.583
23:35:30	2.5	841.0	817.417	109.876	11.416
23:36:00	3.0	701.0	815.333	107.792	13.500
23:36:30	3.5	601.0	813.750	106.209	15.083
23:37:30	4.5	467.7	809.917	102.376	18.916
23:38:00	5.0	421.0	807.917	100.376	20.916
23:39:00	6.0	351.0	804.417	96.876	24.416
23:40:00	7.0	301.0	801.250	93.709	27.583
23:41:00	8.0	263.5	798.000	90.459	30.833
23:42:00	9.0	234.3	795.000	87.459	33.833
23:43:00	10.0	211.0	792.083	84.542	36.750
23:44:00	11.0	191.9	789.417	81.876	39.416
23:45:00	12.0	176.0	786.500	78.959	42.333
23:46:00	13.0	162.5	783.833	76.292	45.000
23:47:00	14.0	151.0	781.333	73.792	47.500
23:48:00	15.0	141.0	778.583	71.042	50.250
23:49:00	16.0	132.3	776.667	69.126	52.166
23:50:00	17.0	124.5	774.333	66.792	54.500
23:51:00	18.0	117.7	772.333	64.792	56.500
23:52:00	19.0	111.5	770.083	62.542	58.750
23:53:00	20.0	106	768.750	61.209	60.083
23:55:00	22.0	96.4	764.500	56.959	64.333
23:57:00	24.0	88.5	761.083	53.542	67.75
23:59:00	26.0	81.8	757.750	50.209	71.083
00:01:00	28.0	76.0	754.917	47.376	73.916
00:03:00	30.0	71.0	752.167	44.626	76.666
00:08:00	35.0	61.0	747.333	39.792	81.500
00:13:00	40.0	53.5	742.000	34.459	86.833
00:18:00	45.0	47.7	737.833	30.292	91.000

Table A3-14. (cont.)

Time (hr)	Time from beginning of recovery (min)	$\frac{\text{Time since pump started}}{\text{Time since pump stopped}}$ $\frac{(tp + \Delta t)}{\Delta t}$	Depth to water level (ft)	Residual drawdown (s') (ft)	Water level recovery (ft)
00:23:00	50.0	43.0	734.000	26.459	94.833
00:28:00	55.0	39.2	731.167	23.626	97.666
00:33:00	60.0	36.0	729.500	21.959	99.333
00:43:00	70.0	31.0	726.083	18.542	102.750
00:53:00	80.0	27.3	723.750	16.209	105.083
01:03:00	90.0	24.3	721.750	14.209	107.083
01:13:00	100.0	22.0	720.167	12.626	108.666
01:23:00	110.0	20.1	719.167	11.626	109.666
01:33:00	120.0	18.5	718.167	10.626	110.666
02:03:00	150.0	15.0	716.667	9.126	112.166
02:33:00	180.0	12.7	715.250	7.709	113.583
03:03:00	210.0	11.0	714.500	6.959	114.333
03:33:00	240.0	9.8	714.000	6.459	114.833
04:03:00	270.0	8.8	713.750	6.209	115.083
04:33:00	300.0	8.0	713.500	5.959	115.333
05:03:00	330.0	7.4	713.350	5.809	115.483
05:33:00	360.0	6.8	713.000	5.459	115.833
06:33:00	420.0	6.0	712.750	5.209	116.083
07:33:00	480.0	5.4	712.708	5.167	116.125
08:33:00	540.0	4.9	712.625	5.084	116.208
09:33:00	600.0	4.5	712.625	5.084	116.208
10:33:00	660.0	4.2	712.500	4.959	116.333
11:33:00	720.0	3.9	712.396	4.855	116.437
12:33:00	780.0	3.7	712.292	4.751	116.541
13:33:00	840.0	3.5	712.167	4.626	116.666
14:33:00	900.0	3.3	712.00	4.459	116.833
17:33:00	1080.0	2.9	711.833	4.292	117.000
20:33:00	1260.0	2.7	711.750	4.209	117.083
05:33:00	1800.0	2.2	711.667	4.126	117.166
17:33:00	2520.0	1.8	711.417	3.876	117.416

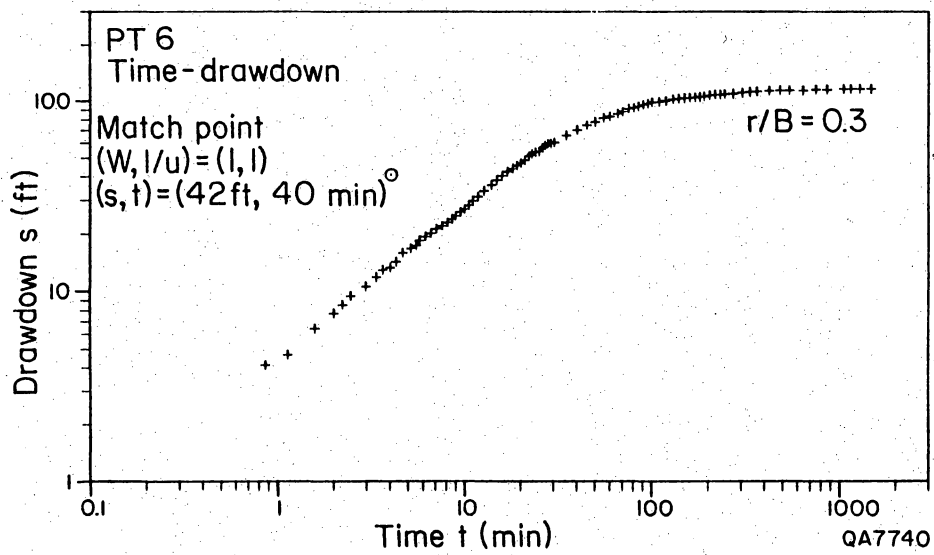


Figure A3-17. Time-drawdown curve matched to Walton type curve for pumping test no. 6 in well LL132, Williams Ranch. This well is approximately 1.4 mi (2.3 km) west of LL162, the site of pumping test no. 1.

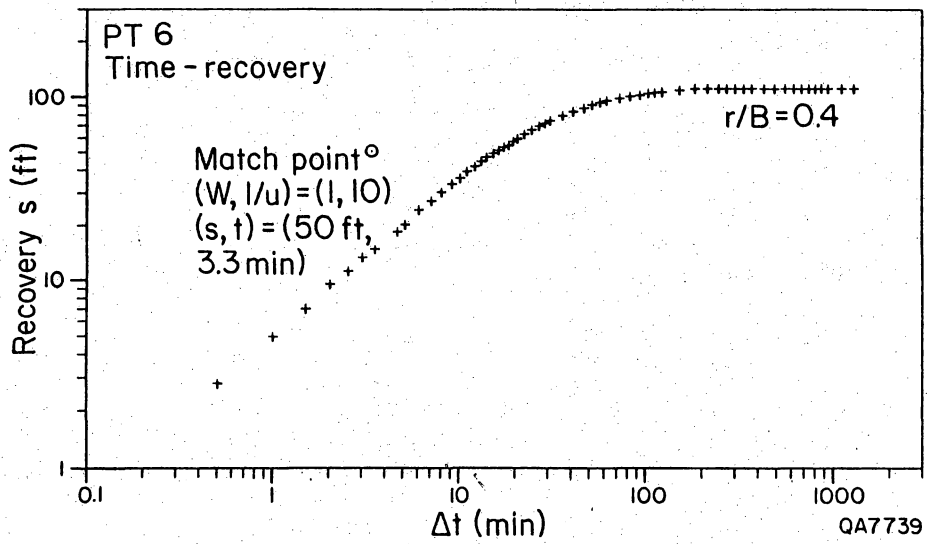


Figure A3-18. Time-recovery curve matched to Walton type curve for pumping test no. 6 in well LL132, Williams Ranch.

The Jacob method for drawdown data in confined aquifers with unsteady flow was also used with this well and resulted in three distinct segments representing the intersection of the cone of depression with separate fractures. The early phase had a Δs value of 76.5 ft (23.3 m) and a transmissivity of 27.4 gpd/ft of drawdown (3.7 ft²/d, or .34 m²/d) (fig. A3-19). The second segment recognized recorded a Δs value of 27 ft (8.2 m) and a transmissivity of 103 gpd/ft of drawdown (13.8 ft² or 1.3 m²) and the late segment before this well reached equilibrium had a Δs of 9 ft (2.7 m) with a transmissivity of 310 gpd/ft of drawdown (41.4 ft²/d or 3.8 m²/d). Using the Theis method for recovery data under the same aquifer conditions as required with the Jacob method, a single transmissivity of LL132 is 28.1 gpd/ft of drawdown (3.75 ft²/d, or .35 m²/d) (fig. A3-20). The segment observed using Jacob's method was not as apparent using Theis' method.

Averaging the six values calculated for LL132 yields a mean transmissivity of 86.95 gpd/ft of drawdown (11.6 ft²/d, or 1.1 m²/d) and a standard deviation of 113.4 gpd/ft of drawdown (15.2 ft²/d, or 1.4 m²/d). Both the drawdown data and recovery data illustrate the intersection with a fracture or fracture system during the later period of drawdown. In order to better define this occurrence, additional testing will be required and at a greater discharge rate, so that significant drawdown below this interval may be obtained.

PT #7

PT #7 was performed in well LL138, referred to as University #4 well, which is located on the Williams Ranch, Hudspeth County (fig. 2, fig. A3-1). The ranch road leading to this well is 4.7 mi (7.6 km) west of Cornudas, Texas, on U. S. Highway 62-180. The well is 1.6 mi (2.5 km) south of the highway. A USGS elevation benchmark is located at the intersection of the highway and the ranch road, where

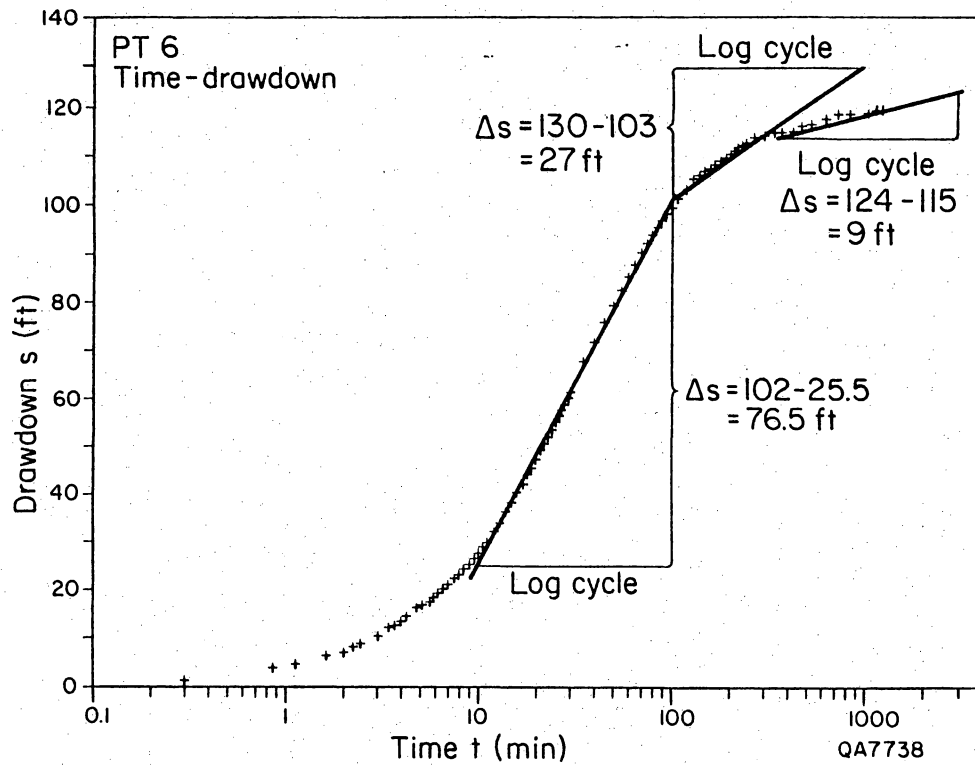


Figure A3-19. Time-drawdown plot interpreted using Jacob's method for pumping test no. 6 in well LL132, Williams Ranch. Three segments observed during drawdown similar to those recorded in pumping test no. 1, 1.4 mi (2.3 km) east of this well.

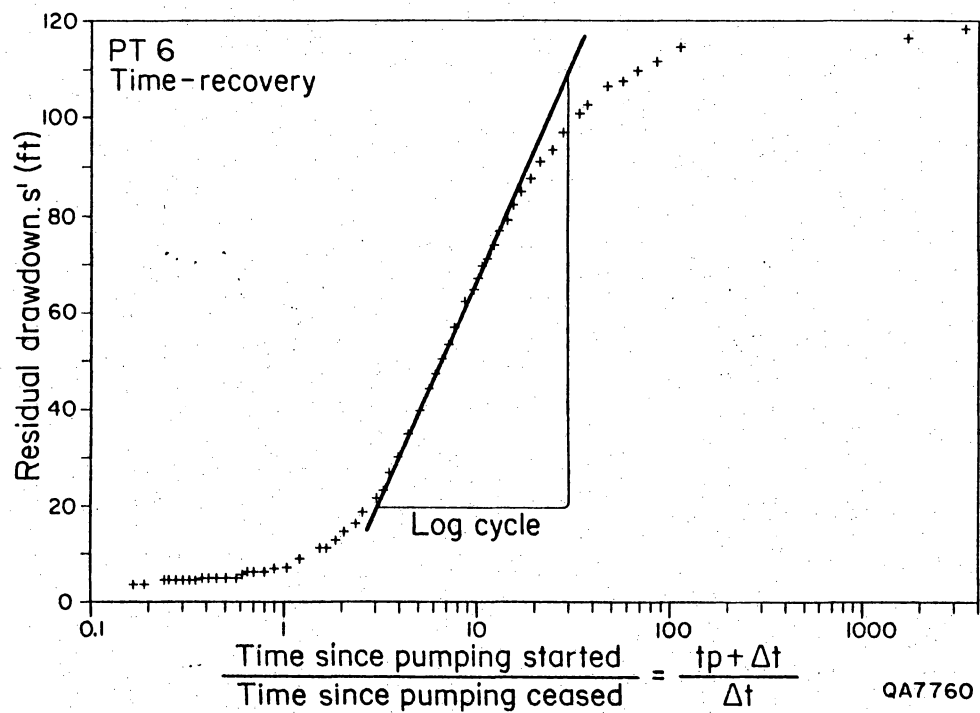


Figure A3-20. Time-recovery plot interpreted using Theis' method for pumping test no. 6 in well LL132, Williams Ranch.

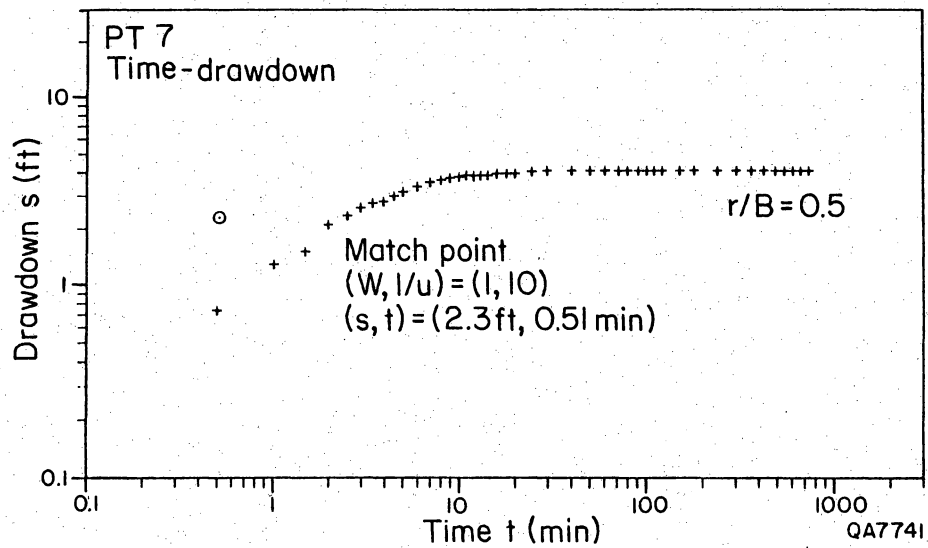


Figure A3-21. Time-drawdown curve matched to Walton-type curves for pumping test no. 7 in well LL138, Williams Ranch.

the elevation above sea level was measured at 4,408 ft (1,343.5 m). No data were available regarding the age of this well, lithologies encountered while drilling, or the producing interval. Total depth of this well is reported to be about 1,200 ft (366 m), but this depth could not be confirmed. For this pumping test, water intake into the pump was set at 850 ft (259.1 m) below land surface. The wellbore diameter is 8 inches (20.3 cm) with surface casing down to an unknown depth. This well, like all the wells tested, has been completed as an open-hole completion. Static water level in this well was measured at 789.9 ft (240.8 m) below land surface. Surface elevation of this well has been mapped at 4,409 ft (1,343.9 m) above sea level, yielding a water altitude in this well of 3,619.1 ft (1,103.1 m) above sea level. Saturated thickness effective during this test was 60.1 ft (18.3 m). No other wells or wellbores were available in the immediate area for use as observation wells. This well is producing NaSO_4 waters from aquifer A, and total dissolved solids were measured at 1,722.28 mg/L.

The drawdown phase of PT #7 was initiated at 6:00 p.m., March 1, 1987. Well LL138 is equipped with a 2 inch (5.1 cm) cylinder pump and maintained a relatively constant discharge rate of 4.0 gpm (table A3-15). During the pumping period, which lasted 1,440 min (24 hours), the recorded water level dropped only 4.1 ft (1.25 m) (fig. A3-21), and 93% of the total drawdown occurred in the first 10 min of pumping. During the drawdown phase, approximately 5,760 gal of water were produced. The drawdown phase of this test was terminated at 6:00 p.m., March 2, 1987. Owing to problems with upward movement of the probe resulting from friction with the installed polyhose, recovery measurements proved to be unsuccessful. This resulted in transmissivity calculations based strictly on drawdown data using Logan's method, and Walton's type curves based on the Theis method for drawdown data.

Table A3-15. Drawdown data from pumping test no. 7 at well LL138.

Time (hr)	Time from beginning of pumpage (min)	Depth to water level (ft)	Water level drawdown (ft)	Flow meter reading (gal)	Well discharge (gpm)
18:00:00	0.0	790.500	0.000		
18:00:30	0.5	791.250	0.750		
18:01:00	1.0	791.833	1.333		
18:01:30	1.5	792.000	1.500		
18:02:00	2.0	792.583	2.083		
18:02:30	2.5	792.833	2.333		
18:03:00	3.0	793.083	2.583		
18:03:30	3.5	793.250	2.750		
18:04:00	4.0	793.333	2.833		
18:04:30	4.5	793.500	3.000		
18:05:00	5.0	793.667	3.167		
18:06:00	6.0	793.833	3.333		
18:07:00	7.0	794.083	3.583		
18:08:00	8.0	794.167	3.667		
18:09:00	9.0	794.250	3.750		
18:10:00	10.0	794.333	3.833		
18:11:00	11.0	794.333	3.833		
18:12:00	12.0	794.333	3.833		
18:13:00	13.0	794.417	3.917		
18:14:00	14.0	794.417	3.917		
18:16:00	16.0	794.417	3.917		
18:18:00	18.0	794.417	3.917		
18:20:00	20.0	794.417	3.917		
18:25:00	25.0	794.500	4.000		
18:30:00	30.0	794.583	4.083		
18:40:00	40.0	794.583	4.083		
18:50:00	50.0	794.583	4.083		3.75
19:00:00	60.0	794.583	4.083		4.00
19:10:00	70.0	794.583	4.083		4.00
19:20:00	80.0	794.583	4.083		4.00
19:30:00	90.0	794.583	4.083		4.00
19:40:00	100.0	794.583	4.083		
19:50:00	110.0	794.583	4.083		4.0
20:00:00	120.0	794.583	4.083		4.0
20:30:00	150.0	794.583	4.083		
21:00:00	180.0	794.583	4.083		
22:00:00	240.0	794.583	4.083		
23:00:00	300.0	794.583	4.083		4.0
00:00:00	360.0	794.583	4.083		
01:00:00	420.0	794.583	4.083		
02:00:00	480.0	794.583	4.083		
03:00:00	540.0	794.583	4.083		
04:00:00	600.0	794.583	4.083		3.75
05:00:00	660.0	794.583	4.083		
06:00:00	720.0	794.583	4.083		
18:00:00	1440.0	794.583	4.083		

Transmissivity cannot be calculated because most of the decline in water level occurred in the first 5 minutes and is attributed to wellbore storage.

Additional testing with modifications in discharge rates and monitoring equipment would be of great value in determining a better approximation of transmissivity in this well. Once again, discharge rates should be increased by a factor of 2 or more to induce sufficient drawdown during a subsequent PT. Where a pump jack supplies lift for the water produced, discharge can often be increased simply by increasing the size of the motor pulley; this could be done at LL138 and LL148. When submersible pumps act as the lifting force, another pump of greater horsepower would have to be installed in the well; this would be required at LL156.

Appendix 3A. Hydrological parameters of the Cretaceous aquifer, Fort Hancock site, derived from a short-term pumping test.

Drilling the water well at the Fort Hancock site involved three major objectives in the following order of priority: measuring static water level in the Cretaceous aquifer, sampling its ground water for chemical and isotope analyses, and performing a pumping test in order to determine the aquifer transmissivity. The first and second objectives were completed successfully: water level at the well was measured at 478 ft (145.7 m) below land surface and water was sampled for chemical and isotopic analyses (app. 2). The pump test was not accomplished as previously planned. A detailed description of the drilling activities is included in appendix 15. Following is a summary of the pumping test.

Ground water was first observed while drilling at a depth of 485 ft (148 m). Drilling continued to a total depth of 530 ft (161 m) at an open borehole of 3.875 inches (9.84 cm) O.D. Hydrostatic water level was monitored for a few days at 478 ft (145.7 m) below land surface. The first pumping test failed owing to wall caving at the borehole that resulted in pump clogging. In the second attempt to pump the well, the pump was located at a depth of 489 ft (149 m) (it was not possible to lower it farther), only 11 ft (3.3 m) below water table. As a result, the pumpage rate had to be kept very low in order to prevent a large drawdown, which would have left the pump dry. Pumpage started at a rate of 0.26 gpm (0.98 lpm) (discharge was measured with 15-gallon containers) and lasted 68 minutes with no drawdown. At that point the pump plugged and had to be raised 5 ft (1.5 m) in an attempt to increase borehole clearance and to continue to clear up formation water for sampling. Pumpage was resumed at an increased and constant production rate of 0.789 gpm (2.98 lpm) with no drawdown for another

159 minutes. At that point, the pumping rate decreased to 0.75 gpm (2.83 lpm) and stopped at 167 minutes because the pump plugged again.

To calculate an approximate transmissivity, conventional solutions could not be used because no drawdown occurred in the borehole. A steady-state approximation method was used but provides only a minimum value for transmissivity. A minimum transmissivity of 27 gpd/ft d⁻¹ f¹ (0.33 m²/d) was calculated.

Logan's method for a steady-state flow in confined aquifers (Kruseman and De Ridder, 1976) represents an approximation of the Thiem formula for a confined aquifer and was used for the calculation of transmissivity. The ground water in the aquifer is assumed to be confined. The constant rate of pumpage and the absence of drawdown justify a steady-state condition.

$$kD = \frac{2.30Q \log r_{\max}/r_w}{2\pi s_{mw}}$$

where

kD = transmissivity of the aquifer, m²/d

Q = well discharge, m³/d

r_w = radius of the pumped well, m

r_{max} = radius of influence (=radius of depression cone, m)

s_{mw} = maximum drawdown in the pumped well, m.

The ratio of r_{max}/r_w cannot be accurately determined without the use of additional piezometers. However, although the variations in r_{max} and r_w may be substantial, the variation in the logarithm of their ratio is much smaller and can be approximated with an average value of 3.33. Substituting this value into the above equation yields

$$kD = \frac{1.22Q}{S_{mw}}$$

As was mentioned earlier, no drawdown was observed in the well, but a drawdown is needed to calculate transmissivity with this equation. The maximum drawdown possible at the well is 52 ft (15.85 m). Using the same discharge as in the pump test (0.789 gpm [4.3 m³/d, or 2.98 lpm]) with this maximum drawdown yields a minimum value of 27 gpd/ft (0.33 m²/d). Transmissivity must be higher because there was no drawdown.

Appendix 4. Application of isotope techniques to hydrology.

Stable Hydrogen and Oxygen Isotopes (modified from Mazor, in press)

Two oxygen isotopes are commonly measured in water samples, ^{16}O and ^{18}O . Concentration of heavy and rare ^{18}O is expressed as percent deviation from an international standard (Standard Mean Ocean Water [SMOW]). Similarly, two stable hydrogen isotopes are measured: a light one, ^1H , and a heavy and rare one, ^2H . These ^{18}O and ^2H concentrations are commonly written as $\delta^{18}\text{O}$ ‰ and $\delta^2\text{H}$ ‰, respectively, as an expression of their relative abundance in per mil deviation from the named SMOW standard. Craig (1961) published a $\delta\text{H}-\delta^{18}\text{O}$ diagram based on 400 water samples from rivers, lakes, and precipitation in various countries. These isotopic data follow a best-fit line of $\delta^2\text{H}=8\delta^{18}\text{O} + 10$ called the meteoric water line, which is applicable worldwide and is a convenient reference for tracing local ground-water origins and movement. Commonly, ground-water data are plotted on a $\delta^2\text{H} - \delta^{18}\text{O}$ diagram, using the meteoric line of local precipitation as a reference. Large isotopic deviations from present meteoric water isotopic composition indicate that ground water was recharged under different climatic conditions and therefore may indicate ancient water. Other deviations from the meteoric line occur when precipitation partly evaporates before reaching the water table. Water molecules with light hydrogen and oxygen, $^1\text{H}_2^{16}\text{O}$, are more volatile and upon evaporation pass more efficiently from the liquid to the vapor phase. As a result, the residual evaporating water gets relatively enriched with the heavier and less mobile molecules. Enriched ground water may indicate the evaporation that the rain and/or surface water go through before infiltration

occurs (and therefore may indicate low permeability of the soil cover) or the evaporation of ground water directly from a shallow water table. In deep aquifers, it may also indicate the equilibrium state between ground water and the host rock.

Tritium (modified from Mazor, in press)

Hydrogen has a radioactive isotope, ^3H , called tritium, in addition to its stable isotopes, ^1H and ^2H . The half-life of tritium is 12.3 years. The concentration of tritium in water is expressed by the ratio of tritium atoms to ^1H atoms. A ratio of $^3\text{H}/^1\text{H}=10^{-18}$ is defined as one tritium unit (TU). Cosmic rays that interact with the upper part of the atmosphere produce secondary neutrons that interact with nitrogen, producing tritium. Tritium is formed constantly, oxidized to water, $^1\text{H}^3\text{HO}$, and washed down by rains. The natural tritium abundance was completely masked by the hydrogen bomb tests, which began in 1952 in the Northern Hemisphere, which added large concentrations of tritium to the atmosphere. Tritium concentration peaked in 1963, when a single monthly rain sample in the U.S. revealed as much as 10,000 TU. When the anthropogenic tritium was noticed, the specific tritium pulses contributed by the individual tests were thought to provide an accurate means of ground-water dating; however, input precipitation values varied greatly from one location to another and during the seasons and years in each place. Semiquantitative dating, however, is possible and informative:

(a) Ground water with less than the amount of natural tritium left after decay indicates that all or most is pre-1952 (several decades old). Old water having 0 TU may be mixed with a small amount of post-1952 water.

(b) Ground water with 0 TU is all pre-1952, i.e., several decades or more old).

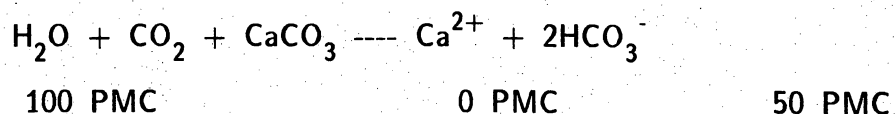
(c) Ground water with elevated tritium values indicates that all or most is post-1952. Tritium in ground water may be compared with the local tritium-precipitation curve to find its age range.

Radioactive Carbon, ^{14}C (modified from Mazor, in press)

Carbon has three isotopes in nature: ^{12}C (common, stable); ^{13}C (rare, stable); and ^{14}C (very rare, radioactive, 5,730-year half-life). ^{14}C forms in the upper parts of the atmosphere by secondary neutrons interacting with common nitrogen and decays radioactively into ^{14}N . The ^{14}C is oxidized upon production, to CO_2 and then mixed into the large atmospheric CO_2 reservoir. The concentration of ^{14}C is expressed relative to $^{14}\text{C}/^{12}\text{C}$ in an international standard (oxalic acid). The ^{14}C concentration in the bulk carbon of the standard is defined as 100 Percent Modern Carbon (PMC).

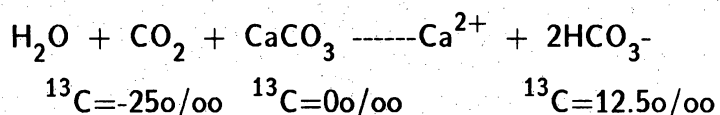
Large amounts of fossil fuels are continuously combusted, so far causing an increase of about 10% in the concentration of atmospheric CO_2 . This added fossil CO_2 is devoid of ^{14}C and correspondingly lowers the $^{14}\text{C}/^{12}\text{C}$ ratio in the air. Nuclear bomb tests introduced ^{14}C into the atmosphere, similar to the tritium increased, but the elevated values have decreased since, and present values are around 140 PMC. Rain and water dissolve small amounts of CO_2 . Significantly more CO_2 is added to water percolating through the soil layer because soil-air contains around 100 times more CO_2 compared with free air owing to biological action in the soil zone. This CO_2 is tagged by the atmospheric ^{14}C concentrations, for example, around 100 PMC in pre-nuclear-bomb test years and as much as 160 PMC in post-bomb test years. Once water reaches the saturated zone it is isolated from the atmosphere, and its ^{14}C decays with a half-life of 5,730 years. Thus, ^{14}C can serve as an age indicator of rain and surface water that reached the water table 30,000 to 40,000 years ago. Interactions of ground

water with carbonate rocks that form or are on the way to the aquifer (such as caliche layers) can add "dead" CO₂ (devoid of ¹⁴C) to ground water. Limestone and dolomite contain no ¹⁴C because they were formed much earlier than the ¹⁴C half-life (5,730 years). Recharged CO₂ containing water reacts with the carbonates to form dissolved bicarbonate:



Thus the dissolved CO₂ with 100 PMC reacts with the rock with 0 PMC to produce a 50 PMC bicarbonate.

The abundance of ¹³C in rocks, organic material, or ground water is expressed in per mil deviation of the ¹³C/¹²C ratio in the sample that is a standard (PDB, a Belemnite carbonate from the Pee Dee Formation of South Carolina). Most marine carbonate rocks have δ¹³C=0 o/oo, whereas frequent values for organic material and CO₂ in soil are -25 o/oo to -20 o/oo. The concentration of δ¹³C in ground water is determined by the input with recharged water and by reactions with rocks. For example, the reaction of water charged with CO₂ of δ¹³C=-25 o/oo with marine carbonate rock of δ¹³C=0 o/oo is:



whereas in reactions with silicates the original (organic) δ¹³C is retained because no carbon is contributed from silicate dissolution. It has been suggested that δ¹³C values may be applied to evaluate the extent to which ¹⁴C in ground water is altered by reaction with the aquifer matrix. Three values are needed: (a) the δ¹³C value of local soil material, representing the initial composition of ground water prior to the reaction with rocks, (b) the δ¹³C value of the local aquifer rocks, and (c) the δ¹³C value of the studied ground water. This correction

technique has been applied in this study as explained in appendix 6.

The main importance of ^{14}C isotopes in hydrologic studies is to determine relative ages and aquifer flow velocities; to check the continuity of proposed regional aquifers; and to study mixing of ground water from sources. Because of the complexities of the ^{14}C and its interactions with the aquifer minerals, ^{14}C ages represent approximations.

^{34}S (modified from Hoefs, 1973)

Sulfur has four stable isotopes with the following abundance: ^{32}S : 95.02 o/oo; ^{33}S : 0.75 o/oo; ^{34}S : 4.21 o/oo; ^{36}S : 0.02 o/oo.

The reference standard commonly used is sulfur from troilite of the Canyon Diablo iron meteorite with a $^{32}\text{S}/^{34}\text{S}$ ratio of 22.22. Variations in concentrations of sulfur isotopes have been observed. The "heaviest" sulfates show $\delta^{34}\text{S}$ values greater than +90 o/oo, and the "lightest" sulfides have values around -50 o/oo. Two types of reactions produce sulfur variations:

- (1) a kinetic effect during the bacterial reduction of sulfate to isotopically "light" H_2S , which gives by far the largest fractionations in the sulfur cycle, and
- (2) various chemical exchange reactions, e.g., between sulfate and sulfides, on the one hand, and between the sulfides themselves, on the other. In this mechanism, sulfides are being depleted in $\delta^{34}\text{S}$ by amounts up to 75% relative to sulfates.

Ground water flowing in marine rocks may reach chemical and isotopic equilibrium with the host rocks. $\delta^{34}\text{S}$ of sulfates in marine rocks has not remained constant during the geologic past. The general trends of evaporite $\delta^{34}\text{S}$

evolution are: high δ values (+20 to +30 o/oo) in the early Paleozoic, decreasing to +11 o/oo in Permian time, rapidly increasing in the early Mesozoic, and later on slightly oscillating around the present value of +20 o/oo. The trend of δ values of sulfate evolution in the world's oceans is so consistent, especially the very narrow range of Permian δ values, that it has been successfully used to determine the age of unknown salt deposits and the origin of sulfate-containing formation water.

The $\delta^{34}\text{S}$ of ground water sulfate may indicate whether SO_4 originated as sulfides or sulfates, and possibly the age of the formations through which ground water passed.

Appendix 5. Karst features of the Gypsum Plain.

Karst landforms and landforms possibly indicative of ancient karst processes are common throughout both of the potential low-level radioactive waste sites in Culberson County. These features include, from smallest to largest, karren, swallow holes, collapse sinks, dolines, blind valleys, and subsidence basins. A landform resulting from karst processes, but not a true karst feature, is the castile. Trough-like features in the western part of the study area have also been attributed to solution and subsidence (Olive, 1957).

Karren

Karren are small solution channels formed on fracture surfaces in gypsum and other soluble rocks and occur in many parts of the study area where gypsum of the Permian Castile Formation is exposed. The channels commonly exceed 1 cm in width and are separated by a knife-like ridge. Karren are oriented parallel to the slope of the exposed bedrock surface; they formed as surface waters infiltrated the gypsum and moved downward through fractures or across exposed surfaces. Presence of karren on fracture surfaces indicates that the process of dissolution of gypsum and solution widening of joints has occurred.

Sinkholes

The three types of sinkholes that occur in the study area are dolines, collapse sinks, and swallow holes (fig. 4). Sinkholes result from the collapse or subsidence of sediments overlying subsurface solution channels. Dolines are a special form of sinkhole that result either from surface solution beneath a soil mantle or from subsidence of an area over caverns. They are broad, closed, surface depressions

that show no evidence of abrupt collapse. Collapse sinkholes, on the other hand, are generally steep-sided and floored with rocky debris resulting from the collapse of the roof of a cavern. Another special form of sinkhole is the swallow hole. Swallow holes occur in stream valleys and mark the point where the discharge carried in the stream valley moves underground.

Several hundred sinkholes have been mapped from aerial photographs of the study area. Collapse sinkholes are far more common than dolines. Many additional sinkholes probably exist in the area, but they are not visible on aerial photographs because of their small size. The largest collapse sinkhole in the area is more than 820 ft (250 m) long. The abundance of sinkholes indicates that an extensive system of caverns exists in the subsurface. Large collapse sinkholes suggest the former presence of large cavern rooms.

Blind Valleys

Blind valleys occur where the surface drainage carried by a stream is diverted underground through a swallow hole. Surface runoff and erosion produce valley incision, but where valley incision ends at a swallow hole a blind valley results. Blind valleys are common in the terrane underlain by the Castile Formation; some of the larger blind valleys and associated sinkholes are shown in figure 4. The largest blind valley in the study area is nearly 1.2 mi (2 km) long.

Subsidence Basins

Subsidence basins, unlike sinkholes, are interpreted to have resulted from dissolution of soluble rocks over a large region. Two types of regional subsidence basins have been recognized: basins with extensive alluvial fill and basins with no appreciable alluvial fill.

The alluvium-filled subsidence basins illustrated in figure 4 are distinguished from other areas containing Quaternary alluvium by their low slope and unusually broad valley development. Drainage from these features is restricted and in some cases internal. The three larger subsidence basins are oriented east-west and are bounded on either the north or south by abrupt erosional escarpments. The floors of these features are heavily vegetated, and the alluvial fill is dark, suggesting a soil with a significant organic content. This is in contrast to the stark-white gypsite that mantles much of the Castile Formation that surrounds the basins. Alluvial fans have locally formed along the margins of the basins. Sinkholes are uncommon in the subsidence basins. Field observations and interpretations of aerial photographs indicate that these areas resulted from the gradual alluviation of broad basins. Basin shape, restricted or internal drainage, and the presence of numerous karst landforms in areas surrounding the basins suggest that these features resulted from solution of soluble rocks and subsidence of overlying strata.

A second type of subsidence basin with no evidence of alluvial filling consists of numerous small, irregularly shaped, closed depressions (fig. 4). The depressions are separated by irregular low ridges, and the entire group of ridges and depressions lies in a closed topographic basin. These features may become alluvium-filled subsidence basins if a source of alluvium is available.

Castiles

Numerous small, typically conical hills are present throughout the Gypsum Plain. Those developed strictly within the Castile Formation are typically capped by a resistant carbonate mass either formed by secondary processes or occurring as erosional remnants of limestone-rich portions of the Castile Formation. Other hills,

commonly developed in the upper Castile Formation near the eastern margin of the Gypsum Plain, are not true castiles because they contain exotic lithologies from units overlying the Castile Formation, particularly the Salado and Rustler Formations. These hills are capped by erosionally resistant sedimentary rocks, mostly Permian sandstones, limestones, and dolomites or siliceous gravels of unknown age. In some places the erosionally resistant material only partially caps the hills or castiles and provides only a partial measure of protection from the processes of erosion.

Well-exposed castiles were examined in the eastern half of Block 46 and along U.S. Highway 652 approximately 6 mi (10 km) west of Texas Highway FM 2185. All are capped by resistant bodies of carbonate, but the origins of the carbonate may be diverse and are open to interpretation. Textures within the carbonate vary from clearly secondary to apparently primary and from nearly massive to well bedded to brecciated. Castiles along U.S. 652 are capped by a very well bedded but highly brecciated rock that appears to be a limestone-rich unit within the Castile Formation. The brecciation is interpreted to be the result of downward collapse into the throat of a sinkhole, each castile in this cluster of hills apparently representing an individual sinkhole. Evidence of collapse is not as apparent in the castiles examined in Block 46. Some appear to have clearly secondary or replacement carbonate present, although the degree to which these processes have occurred may be variable and is open to further study. Many of the hills shown in figure 2 were recognized from aerial photographs and are interpreted to be castiles, although their origin has not been determined. Where collapse chimneys have been recognized, these features are identified in figure 4.

Troughs

Ridges oriented approximately N 85 E are located in the western Gypsum Plain within the outcrop area of the Castile Formation (King, 1949). Commonly, these ridges occur in pairs and bound a trough (fig. 4). The western ends of the pairs of ridges are open, and in several cases the eastern ends of the pairs of ridges converge to a blunt, rounded ridge. The trough between the ridges is usually topographically lower than the terrain beyond the ridges. These landforms range up to 9 mi (15 km) in length and up to 0.6 mi (1 km) from ridge crest to ridge crest. The ridges are underlain by gypsite or by disturbed and weathered bedded gypsum. Thin alluvium, gypsite, or relatively unweathered gypsum usually underlies the trough. The troughs and bounding ridges are at a high angle to the northeast-striking faults that occur near the western ends of these features. Olive (1957) suggested that these "solution-subsidence troughs" resulted from subsidence following solution of gypsum along joints in the Permian Castile Formation.

In one area, where a deeply incised stream channel cuts across a trough and its associated pair of ridges, only a few joints parallel to the trend of the trough were observed in exposures of bedrock along the stream. The incised stream channel is nearly normal to the orientation of the trough, and the stream follows joints nearly normal to the trend of the trough. There is no evidence of collapse or of significant dissolution of gypsum in the beds exposed beneath the ridges or in the intervening trough.

From interpretation of aerial photographs, sinkholes are known to occur in troughs, but the concentrations of sinkholes in troughs are no higher than in areas outside of troughs. Evidence in the literature (Olive, 1957) that pertains to the formation of these features is apparently contradictory to field observations made during this study. Although these features are an important aspect of the landscape of the study area, their origin cannot be determined from available data.

Distribution of Sinkholes

The widespread occurrence of sinkholes suggests that much of the area is underlain by a systems of caverns. Sinkholes are distributed throughout much of the study area without any recognizable relationship to fracture systems or other structural features. Locally, however, groups of sinkholes appear to occur preferentially along the northeasterly extensions of northeast-striking normal faults exposed in the western part of the study area. In certain cases, castiles and subsidence basins are associated with aligned groups of sinkholes. The aligned groups of sinkholes occur preferentially on the upthrown side of the faults. The flexures were most often recognized on the upthrown side of the faults. Development of the flexures parallel to and on the upthrown side of the faults apparently allowed fractures parallel to the faults to open. Solution of gypsum along these fractures and later collapse or subsidence of overlying strata resulted in the formation of subsidence basins, castiles, and sinkholes.

Surface Drainage of the Gypsum Plain

The surface drainage of the study region is intermittent and has formed a karst-deranged pattern (fig. 4). The presence of sinkholes, swallow holes, sinking streams, and blind valleys constitutes the karst drainage system. The remainder of the area is characterized by a deranged pattern of larger streams flowing into and out of alluvial and subsidence basins. These streams and the alluvial basins also have numerous short tributaries. Deranged drainage patterns indicate that insufficient time has passed for an integrated drainage to develop. Lack of an integrated drainage system also suggests that the surface of the study region is unstable and is changing as dissolution-induced subsidence continues.

Structural and topographic control of segments of streams has been recognized both in the field and from interpretation of aerial photographs. First- and second-order stream segments locally are parallel to or follow joints. In some places joint sets apparently weaken the rocks, and these rocks are preferentially eroded. In other areas joints widened by solution have been occupied by streams. Many drainage elements are aligned nearly east-west. These include numerous east-west stream segments and parts of the margins of most of the subsidence basins. In most of these areas it appears that valley or basin development has been influenced by jointing.

Appendix 6. Stratigraphic sections of bolson deposits cropping out
in Fort Hancock area, Hudspeth County.

Measured sections described in this appendix are shown in figure 4.
Section 1. Located on Arroyo Diablo ~ 1 km (0.63 mi) NE of Diablo
Reservoir No. 2 at 31°15'13" N, 105°45'26" W, ~ 7.6 km
(4.75 mi) SSW of the Campo Grande Fault.

Depth
Below
Surface

YOUNGER BOLSON DEPOSITS

0 m	Pedogenic calcrete. Surface eroded.
0.75	Matrix- to clast-supported limestone pebble to cobble gravel with clasts up to 20 cm in longest dimension. Gravels fine upward to flat-bedded medium to coarse gravelly sand. Hornblende diorite clasts common. This unit contains ~ 8 upward-fining sequences.
2.7	CaCO ₃ -cemented, pale-brown, laminated clayey silt.
3.0	Laminated, strongly bioturbated, clayey silt. Many plant fragments in lower 30 cm.
5.0	Medium sand with vague laminations. Pedogenic CaCO ₃ nodules up to 5 cm. Dispersed pebbles.
7.3	Pebbly, flat-bedded sand. Pebbles up to 5 cm. Pebbles mostly crystalline volcanics.
8.0	Flat-bedded, fine pebbly sand.
9.9	Section covered by Recent alluvium.

Section 2. Located on Arroyo Diablo ~ 1.75 km WSW of Diablo
Reservoir No. 2 at 31°19'46" N, 104°44'04" W, ~ 100 m
(300) ft WSW of the Campo Grande Fault.

Depth
Below
Surface

YOUNGER BOLSON DEPOSITS

0 m	Stage V calcrete with recemented fractures. Fracture fills are up 1 cm thick and laminated. Massive, dense; weathers to a tabular or platy appearance.
-----	--

2.5	Flat-bedded, clast-supported, gray limestone pebble-cobble gravel deposited on an erosion surface and overlain by medium to coarse flat-bedded sand with calcrete nodules.
3.0	Flat-bedded, clast-supported, gray limestone pebble-cobble gravel deposited on an erosion surface and overlain by medium to coarse flat-bedded sand with lenses of fine pebbles or granules.
4.2	Flat-bedded, clast supported, gray limestone pebble-cobble gravel deposited on an erosion surface and overlain by medium to coarse flat-bedded sand with lenses of fine pebbles or granules.
5.75	Three sequences of flat-bedded, gray pebble gravels fining upward to flat-bedded coarse to medium sand. Numerous lithoclasts of calcrete nodules in the basal gravel.
7.0	Matrix- to clast-supported, flat-bedded, gray limestone pebble to cobble basal gravel. Gravel is overlain by fine sand with gravel lenses and isolated pebbles. No primary sedimentary structures are preserved in the sand. Pedogenic CaCO_3 nodules occur throughout the fine sand and three massive pedogenic calcretes composed of CaCO_3 nodules are preserved in the fine sands. CaCO_3 films up to several millimeters thick occur on the lower surface of pebbles and cobbles. Calcretes are probably Stage III calcretes in the classification of Bachman and Machette (1977).
9.75	Base of section covered by Recent alluvium.

Section 3. Located on Arroyo Diablo ~ 0.8 km (0.5 mi) S of Campo Grande Mountain at 31°19'07" N, 105°42'30" W, ~ 10 to 0 m (30 to 60 ft) WSW of the Campo Grande Fault.

Depth
Below
Surface

YOUNGER BOLSON DEPOSITS

0 m	Stage IV to V calcrete. Massive CaCO_3 weathering to a platy or tabular structure. Fracture fillings are laminated. CaCO_3 content and density increases upward.
1.25	Poorly exposed, interbedded flat-bedded sand and gravel. Gravel content increases upward. Sand and gravel overlie an erosion surface developed on lower bolson deposits.

OLDER BOLSON DEPOSITS

26.5	Pale-brown, laminated, clayey silt.
28.5	Pale-red-brown silty clay. Massive, blocky fracturing with no preserved primary sedimentary structures. Fractures with slickensides.
28.8	Pale-brown, laminated, clayey silt.
31.8	Pale-red-brown silty clay. Massive, blocky fracturing with no preserved primary sedimentary structures. Fractures with slickensides.
34.8	Section covered by Recent alluvium.

Section 4. Located on Camp Rice Arroyo ~ 1.3 km (0.8 mi) N of the Lutich Ranch at 31°22'48" N, 105°46' W, ~ 1.6 km (1 mi) NE of the Campo Grande Fault.

Depth
Below
Surface

RECENT SEDIMENTS

0 m	Eolian sand.
-----	--------------

YOUNGER BOLSON DEPOSITS

1.8	Stage V calcrete, slightly laminated.
2.7	Flat-bedded sand and sandy pebble gravel.

OLDER BOLSON DEPOSITS

4.6	Pale-red-brown silty clay, no preserved primary sedimentary structures, blocky fractures with slickensides.
7.0	Laminated, pale-brown clayey silt.
7.3	Pale-red-brown silty clay, no preserved primary sedimentary structures, blocky fractures with slickensides.
9.4	Interbedded red-brown silty clay and pale-brown clayey silt. Characteristics of these beds are similar to those of silts and clays described above.
12.4	Base of section covered by Recent alluvium.

Section 5. Located on Arroyo Diablo ~ 1.75 km WSW of Diablo Reservoir No. 2 at 31°20'02" N, 104°44'06" W, ~ 100 m (300 ft) ENE of the Campo Grande Fault.

Depth
Below
Surface

YOUNGER BOLSON DEPOSITS

0 m

Stage IV to V calcrete. Dense, fractured, platy or tabular weathering. Fracture fillings laminated. Upper surface eroded.

0.5

Flat-bedded, partly clast-supported limestone pebble-cobble gravel with lenses of flat-bedded sand. Pedogenic CaCO_3 content increases upward. Gravel clasts up to 10 cm. Unit deposited on an erosion surface developed on lower bolson deposits.

OLDER BOLSON DEPOSITS

2.5

Pale-brown, laminated clayey silt with dispersed gravel clasts up to 10 cm.

3.5

Pale-red-brown silty clay. No preserved primary sedimentary structures. Fractures with slickensides.

3.75

Laminated clayey silt with clasts up to 8 cm at base.

4.3

Pale-red-brown silty clay. No preserved primary sedimentary structures. Blocky fracturing with slickensides on fracture faces.

5.1

Laminated, pale-brown, clayey silt.

6.0

Pale-red-brown silty clay. No preserved primary sedimentary structures. Blocky fracturing with slickensides on fracture faces.

6.4

Laminated pale-brown clayey silt.

6.9

Pale-red-brown silty clay. No preserved primary sedimentary structures. Blocky fracturing with slickensides on fracture faces.

7.8

Laminated pale-brown clayey silt. CaCO_3 -filled fractures.

8.4

Pale-red-brown silty clay. No preserved primary sedimentary structures. Blocky fracturing with slickensides on fracture faces.

9.25

Section covered by Recent alluvium.

Section 6. Located on Arroyo Diablo ~ 0.6 km (0.35 mi) NNW of Diablo Reservoir No. 1, at 31°20'34" N, 105°43' W.

Depth
Below
Surface

YOUNGER BOLSON DEPOSITS

0 m

Pedogenic calcrete, becomes more massive upward, tabular to platy, lamina in fractures, surface appears stripped. Probably a Stage IV to V calcrete.

1.1

Sandy matrix-supported pebble-cobble gravel with lenses of clast-supported pebble gravel.

4.0

Interbedded laminated silty sand and clayey silt. No primary sedimentary structures preserved in the clayey silt.

5.9

Red-brown, blocky-fracturing silty clay. Slickensides on fracture faces. No preserved primary sedimentary structures. CaCO₃ nodules up to 15 cm in diameter preserved near base.

6.4

Ripple-laminated fine silty sand.

6.4

Red-brown silty clay with CaCO₃ nodules.

6.6

Fine to medium horizontally laminated sand. Lower 2 m CaCO₃-cemented to form a ground-water calcrete. CaCO₃ nodules over a 0.5 to 1.0 cm-thick red-brown clay.

9.9

CaCO₃ nodules overlying a 1.0 cm-thick clay. CaCO₃ nodules up to 8 cm in diameter.

10.0

Fine- to medium-laminated silty sand.

OLDER BOLSON DEPOSITS

10.5

Red-brown, blocky-fracturing silty clay with CaCO₃ nodules. No preserved primary sedimentary structures. The upper contact of this unit is an erosional surface in which channels have been cut to a depth of as much as 2 m.

12.5

Laminated to ripple cross-laminated fine to medium sand. CaCO₃ nodules and thin CaCO₃-cemented lenses.

13.8

Horizontally bedded, fine to medium sand overlying couplets of silty clay and fine sand inclined up to 30° south. Couplets range from centimeters to nearly a meter thick. Inclined lamina overlie horizontal silty sand and sands. This unit is interpreted as a Gilbertian delta.

16.1

Red-brown, blocky-fracturing silty clay. No preserved primary sedimentary structures. Slickensides on fracture faces. CaCO_3 nodules preserved throughout.

Section covered by Recent alluvium.

Section 7. Located on Camp Rice Arroyo 0.9 ki (0.55 mi) NW of Lutich Ranch at $31^{\circ}22'26''$ N, $105^{\circ}46'24''$ W.

Depth
Below
Surface

YOUNGER BOLSON DEPOSITS

0 m

Massive calcrete, in part fractured with fracture fillings laminated. Nodular calcrete becoming massive upward. Surface of calcrete stripped. Probably a Stage IV or V calcrete.

1.6

Interbedded horizontally bedded sand and sandy clast-supported limestone gravel. Clasts up to 10 cm in long dimension.

3.6

Horizontally bedded, silty fine sand.

4.4

Massive, silty fine sand. No preserved primary sedimentary structures. Lightly CaCO_3 -cemented. CaCO_3 cement decreases upward.

OLDER BOLSON DEPOSITS

9.8

Red-brown, blocky-fracturing, silty clay. No preserved primary sedimentary structures. Slickensides on fracture faces.

11.5

Thinly laminated clayey silt.

11.8

Red-brown, blocky-fracturing silty clay. No preserved primary sedimentary structures. Slickensides on fracture faces.

13.5

Thinly laminated silt.

13.6

Red-brown, blocky-fracturing silty clay. No preserved primary sedimentary structures. Slickensides on fracture faces.

15.4

Massive silty fine sand. Rare preserved lamina marked by black stains. CaCO_3 nodules. Popcorn texture on exposed surface suggests a high expansive clay content.

17.8	Red-brown, blocky-fracturing silty clay. No preserved primary sedimentary structures. Slickensides on fracture faces.
22.3	Ripple cross-laminated fine sand and clayey silt. Fine sand lamina mark ripples.
24	Red-brown, blocky-fracturing silty clay. No preserved primary sedimentary structures. Slickensides on fracture faces.
25.3	Silty sand. No preserved primary structures.
25.4	Red-brown, blocky-fracturing silty clay. No preserved primary sedimentary structures. Slickensides on fracture faces.
25.5	Section covered by Recent alluvium.

Section 8. Located on Arroyo Diablo ~0.8 km (0.5 mi) S of Campo Grande Mountain at 31°19'17" N, 105°42'30" W, ~ 10 to 20 m (30 to 60 ft) ENE of the Campo Grande fault.

Depth
Below
Surface

OLDER BOLSON DEPOSITS

0 m	Calcrete. CaCO ₃ content increases upward. Stage of calcrete development unknown.
1	Interbedded red-brown, blocky-fracturing silty clay and pale-red-brown silty clay. Section partly obscured by colluvium.
12	Pale-red-brown clayey silt.
12.5	Red-brown silty clay.
16.5	Pale-red-brown clayey silt.
26.5	Section covered by Recent alluvium.

Section 9. Located in Alamo Arroyo ~ 1 km (0.6 mi) WNW of Cavett Lake dam at 31°24'20" N, 105°49'40" W.

Depth
Below
Surface

RECENT

0 m

Eolian sand

OLDER BOLSON DEPOSITS

3

Red-brown, blocky-fracturing silty clay. No preserved primary sedimentary structures. Slickensides on fracture faces.

4

Trough crossbedded silty sand. The base of this unit is an erosional surface.

5.5

Red-brown, blocky-fracturing silty clay. No preserved primary sedimentary structures. Slickensides on fracture faces.

6.0

Laminated to cross-laminated silty fine to medium sand. CaCO₃ nodules.

6.9

Red-brown, blocky-fracturing silty clay. No preserved primary sedimentary structures. Slickensides on fracture faces. CaCO₃ nodules.

19.4

Laminated to cross-laminated silty fine sand. Some zones massive with no preserved primary sedimentary structures.

20.9

Section covered by Recent alluvium.

Appendix 7. Hydraulic conductivity measurements in the unsaturated zone.

Hueco Bolson

The hydraulic conductivity of two sequences of gravels and clays-and-sand in the bolson fill was measured in the Fort Hancock site area. Hydraulic conductivity of unweathered bedrock at HU1A and HU1B was also measured. Procedure and interpretations follow the determination of hydraulic conductivity in soil above water table (Boersma, 1965; Freeze and Cherry, 1979). This method is known as the shallow well - pump-in method, the piezometer method, or the dry-auger-hole method. According to this method, an auger hole or cored hole is dug, and then water is supplied to the hole. The water in the hole is maintained at a constant level. The rate of water input is determined until a steady state is obtained. Hydraulic conductivity is calculated from the following equation:

$$K = \frac{[\ln(h/r + \sqrt{(h/r)^2 - 1}) - 1] Q}{2\pi h^2}$$

where

K = hydraulic conductivity (cm/hr)

h = depth of water maintained as measured from the bottom of the hole (cm)

r = the radius of the test hole (cm)

Q = rate at which water flows into the test interval (cm³).

Two different lithologies within the bolson fill were tested: The gravels that cover the finer materials from land surface to a depth of 9 to 15 m (30 to 50 ft) and the clays, silts, and fine sands that underlie the gravels to a depth of 148 m (485 ft) below land surface (B-1 and B-8 respectively, fig. 23a). Each of the boreholes was filled with coarse sand to prevent caving in the sides of the holes.

The gravel interval was cased when testing the finer materials' sequences of sand and clays.

Results of the test are presented in the following table:

Tested lithology	Depth of the borehole (cm)	Length of the tested interval (cm)	Radius of the borehole (cm)	Final rate of flow into the borehole (cc/hr)	Hydraulic conductivity (cm/hr)
gravel	1,311	1,311	11.43	64,000	0.026
clays and silty sand	4,628	3,165	4.37	4,440	0.013

Hydraulic conductivity of the gravels was calculated to be 2.3 m/yr (7.56 ft/yr) and that of the clays and sands is 1.15 m/yr (3.8 ft/yr).

Diablo Plateau

The hydraulic conductivity of two intervals of unweathered bedrock was measured at sites HU1A and HU1B to characterize potential migration rates in the area. At site HU1A, the interval to be tested consisted of unweathered rhyolite porphyry. Attempts to core this section with air to reduce borehole contamination proved unsuccessful (because of tremendous heat buildup), and fresh water had to be used to circulate cuttings and cool the core bit. To a lesser extent, a similar situation existed at HU1B in Cretaceous Campgrande limestones and was also cored with fresh water. To reduce borehole contamination, the fresh water was circulated only once to keep the borehole flushed of cuttings. Water was then supplied to the test interval and maintained at a constant level.

Tests performed during this study were conducted on two different units, unweathered rhyolite porphyry at HU1A and unweathered limestone at HU1B. In tests at the Fort Hancock site, uniform coarse sand was added to the test hole

before adding water to stabilize the walls of the hole. This was not necessary for these tests, however, due to the competent nature of the intervals tested. Results of the two tests are presented in the following table.

Tested lithology	Depth of borehole (cm)	Length of the tested interval (cm)	Radius of the borehole (cm)	Final rate of flow into the borehole (cm ³ /hr)	Hydraulic conductivity (cm/hr)
Rhyolite	1,524	914	3.7846	240,000	.0935
Limestone	1,524	914	4.8133	1,182,000	.4415

Hydraulic conductivity of the rhyolite at HU1A was calculated to be 26.8 ft/yr (8.19 m/yr) and that of the limestone at HU1B was 126.6 ft/yr (38.6 m/yr).

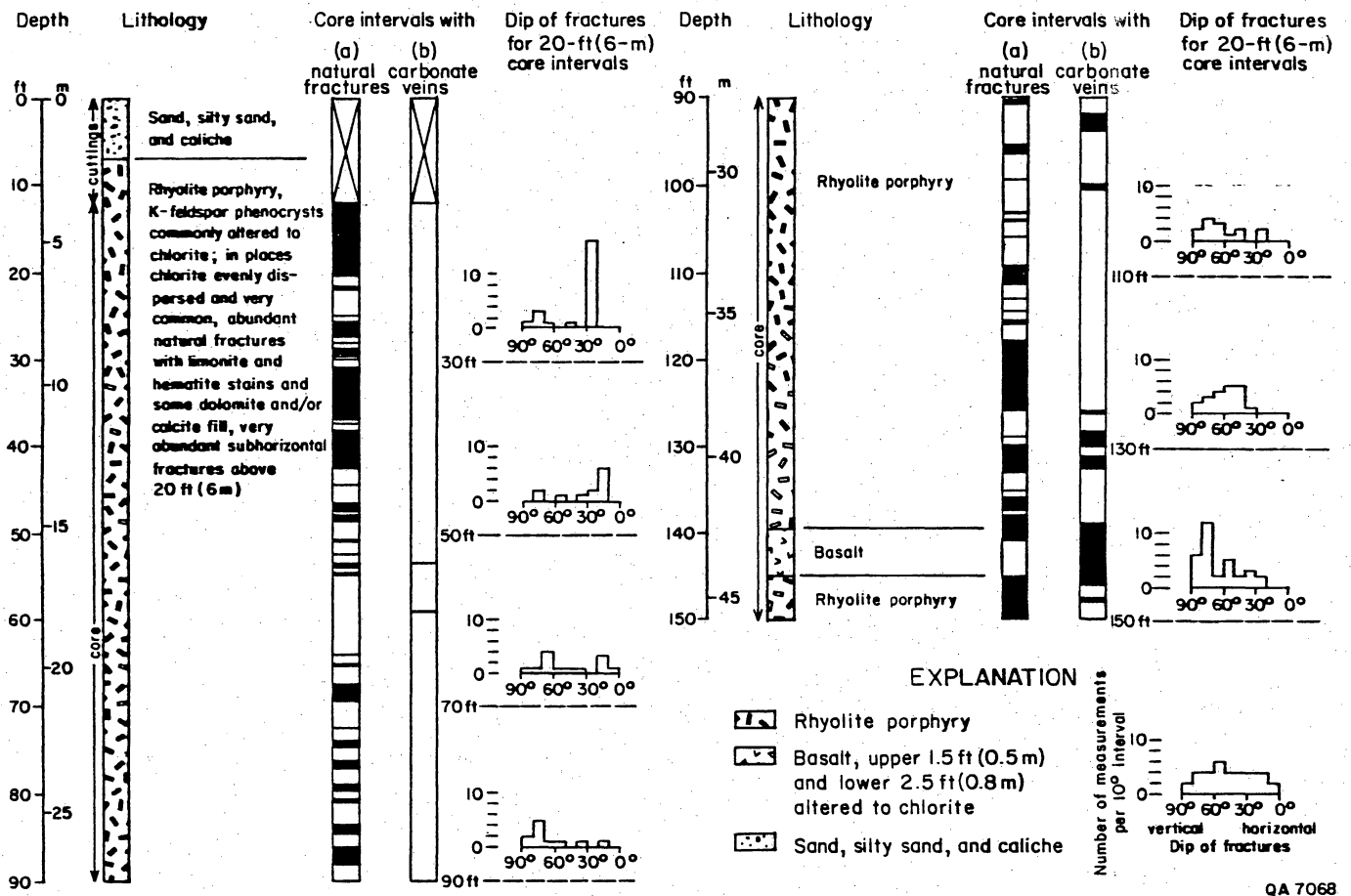


Figure A7-1. Lithologic log for the rhyolite core from HU1A site.

Appendix 8. Permeability of bolson fill based on core and grain size analyses.

Three boreholes (B-7, B-12, and B-13, fig. 23a in the geology section, this report) were cored by URM in the bolson fill from below the gravel cover to total depth of 150 ft for grain size and permeability analyses. B-7 was selected for the analysis because an in situ permeability test on nearly the same section was performed earlier in adjacent borehole (B-8). It is assumed that the permeability measured in the in situ test is mainly horizontal permeability of the more permeable sandy layers. Conversely, lab tests are biased toward the finer grain sized samples because the sandy samples are not cohesive enough for handling and measurement. As a result, a complementary set of data was achieved. Following are the results of the lab tests on B-7 performed by URM:

Sample #	Depth below land surface (ft)	Sand (%)	Silt (%)	Clay (%)	Perm. (cm/sec)
3	65-70	45	30	25	
4	73.5-74	23	47	30	
5	77-77.5	22	38	40	$<1 \times 10^{-9}$
6	82-82.5	0	18	82	$<1 \times 10^{-10}$
7	85-90	6	49	45	$<3 \times 10^{-10}$
8	100-101	41	26	33	
9	105-110	22	25	53	
10	110-111	27	40	33	
11	116-116.5	0	5	95	$<6 \times 10^{-11}$
12	120-125	3	21	76	$<4 \times 10^{-10}$
13	126-126.5	16	30	54	
14	142-142.5	5	23	72	$<3 \times 10^{-10}$

Sand percentage varies from 0 to 45 within this section, whereas clay percentage varies from 25 up to 95 (fig. A8-1). The upper limit of sand percentage for lab permeability tests in these samples was 22 and resulted in the highest permeability value of less than 1×10^{-9} cm/sec. The in situ test that measured the permeability of the entire section between 48 and 149.8 ft below land surface yielded a higher value of 3.7×10^{-6} cm/sec (app. 12). Horizontal permeability is usually higher than vertical permeability. The sandy layers, whose permeability could not be tested in the lab, dominated the field test. Dames and Moore (1985) reported clay permeability of 5.8×10^{-8} cm/sec in a core sampled in their test hole at this site. Porosity data derived from the geophysical logs of B-7 showed negative correlation with core vertical permeability data (fig. A8-2) as expected from the high percentage of clay and silt present in the cores.

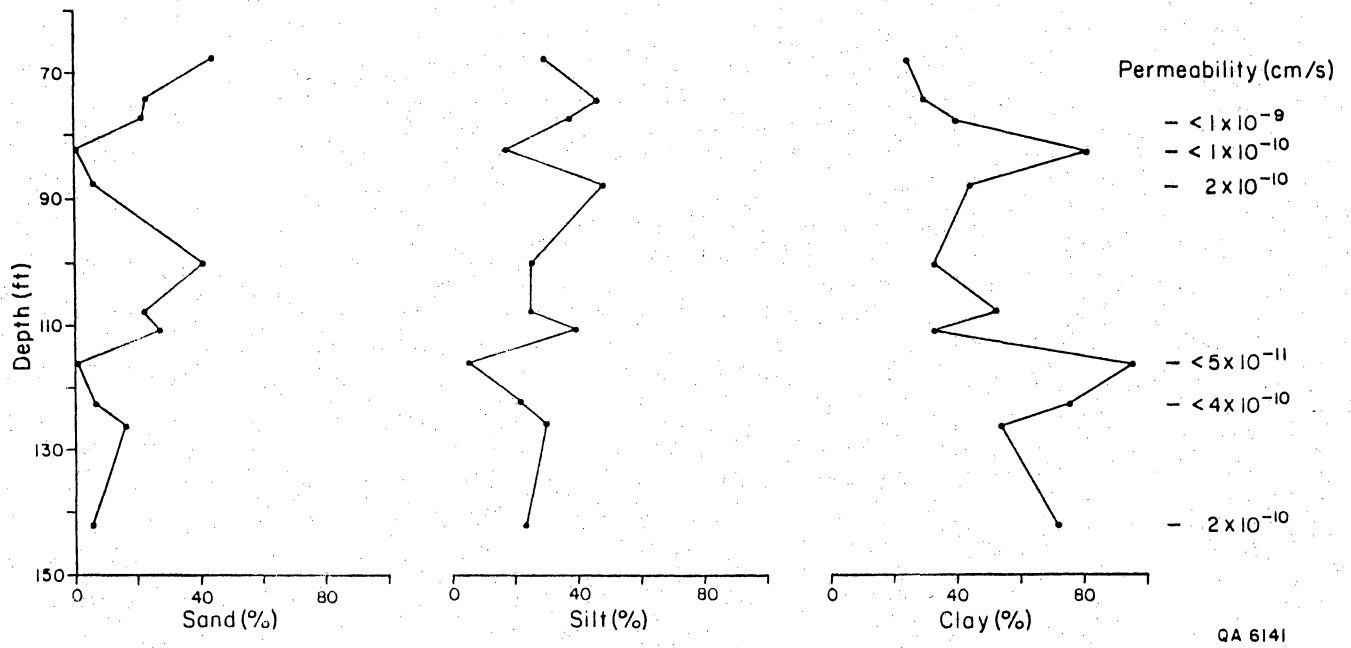


Figure A8-1. Variations in grain size (°/o) and vertical permeability (cm/s) with depth (ft) in borehole 7. Location of the borehole is shown in figure 23a.

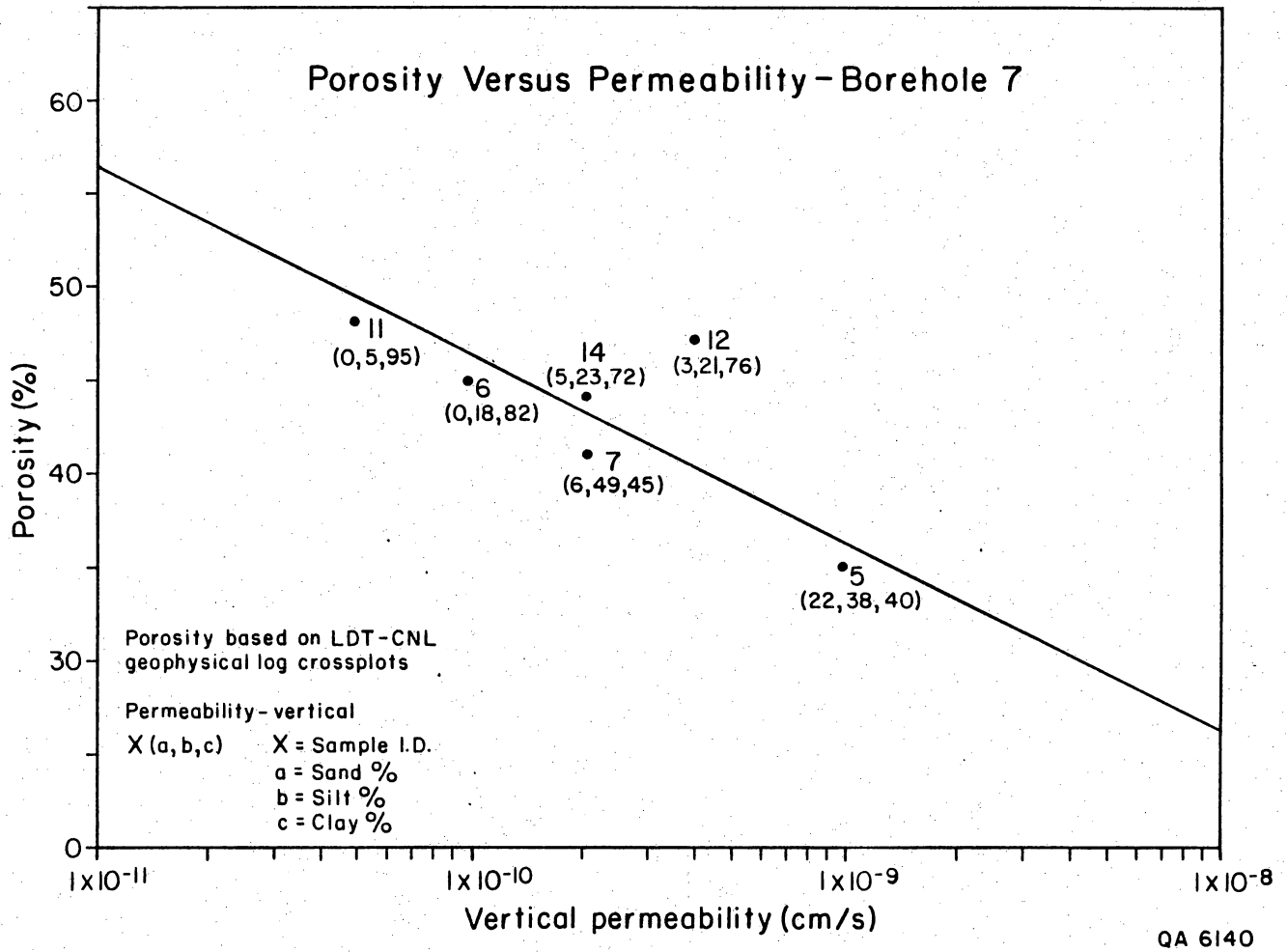


Figure A8-2. Correlation of porosity (°/o) and vertical permeability (cm/sec) in borehole 7. Location of the borehole is shown in figure 23a.

Appendix 9. Lithologic logs for Hudspeth County test holes.

LLWA 1

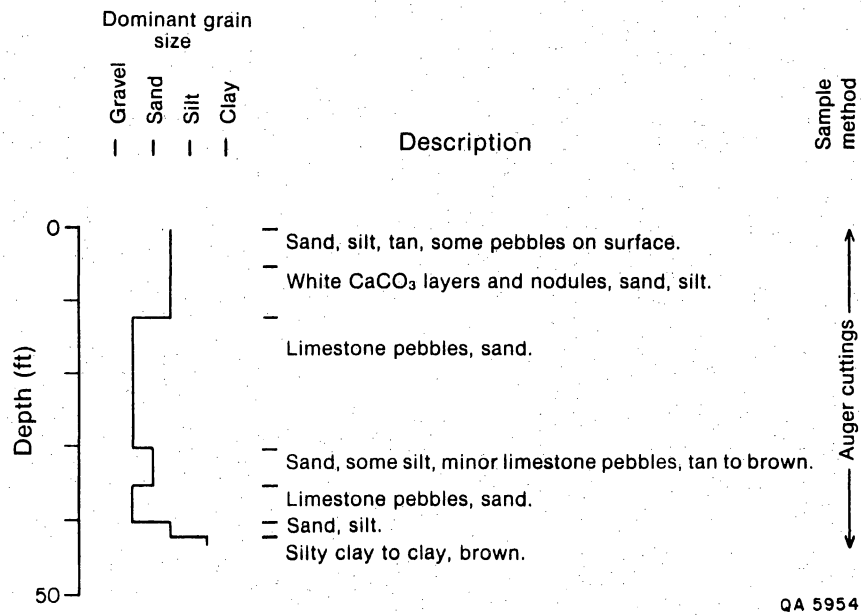


Figure A9-1. Lithologic log, LLWA1, Hudspeth County.

LLWA 2

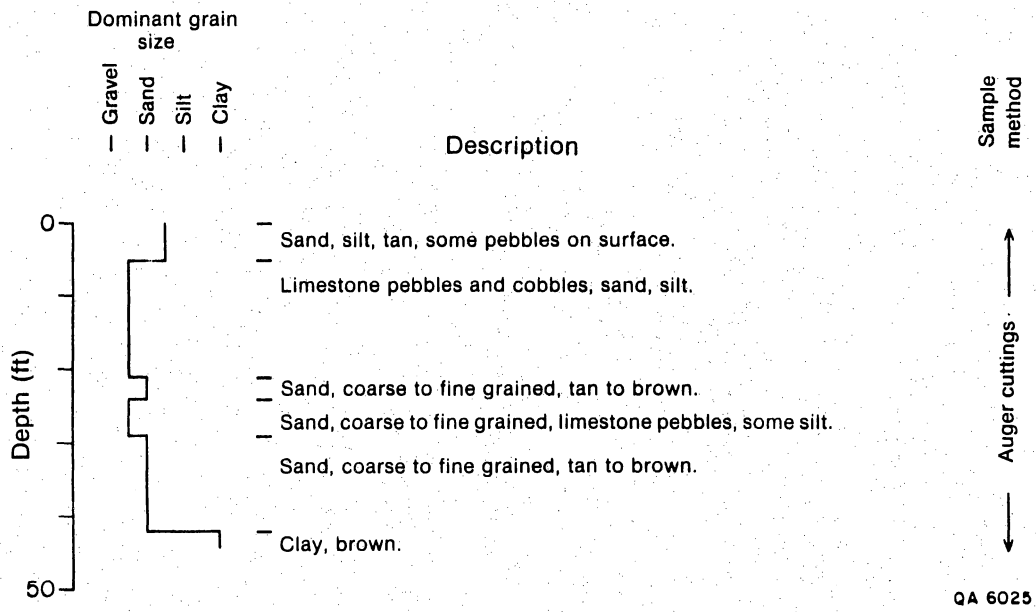


Figure A9-2. Lithologic log. LLWA2, Hudspeth County.

LLWA 3

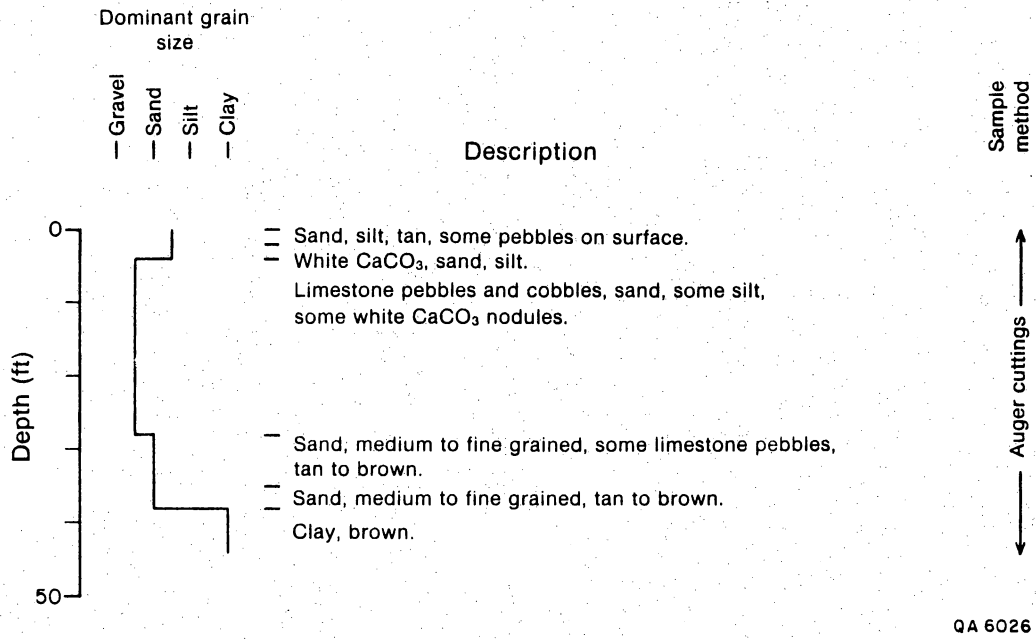


Figure A9-3. Lithologic log, LLWA3, Hudspeth County.

LLWA 4

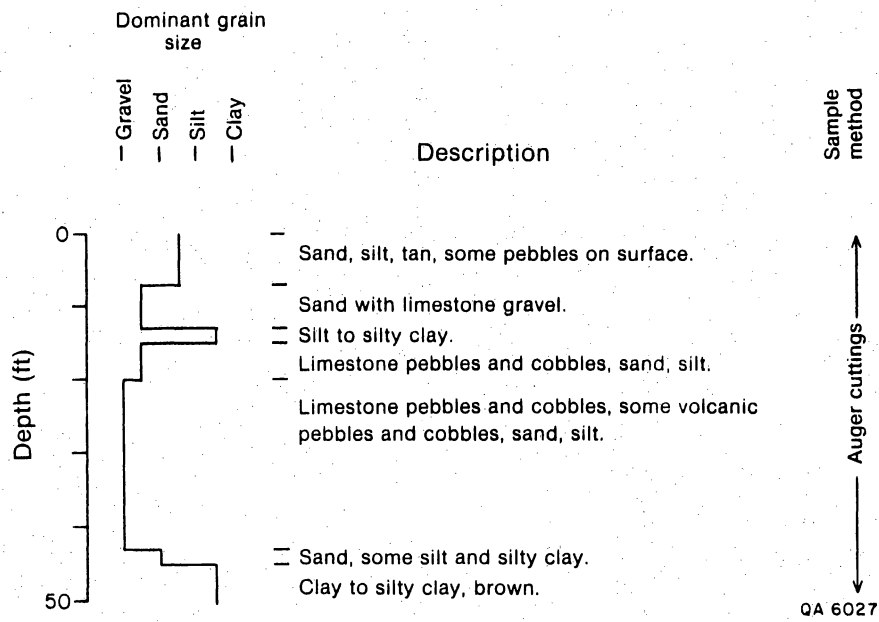


Figure A9-4. Lithologic log. LLWA4, Hudspeth County.

LLWA 5

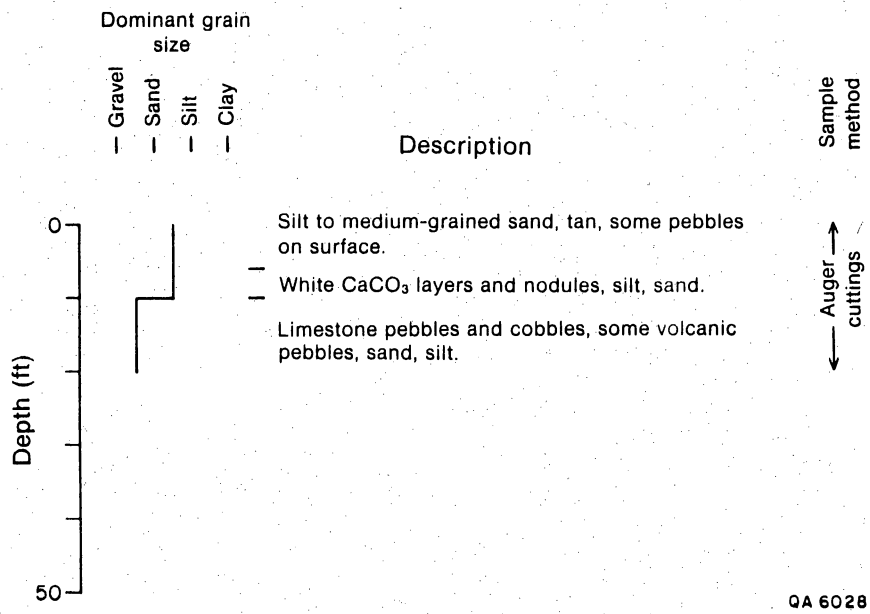


Figure A9-5. Lithologic log, LLWA5, Hudspeth County.

LLWA 6

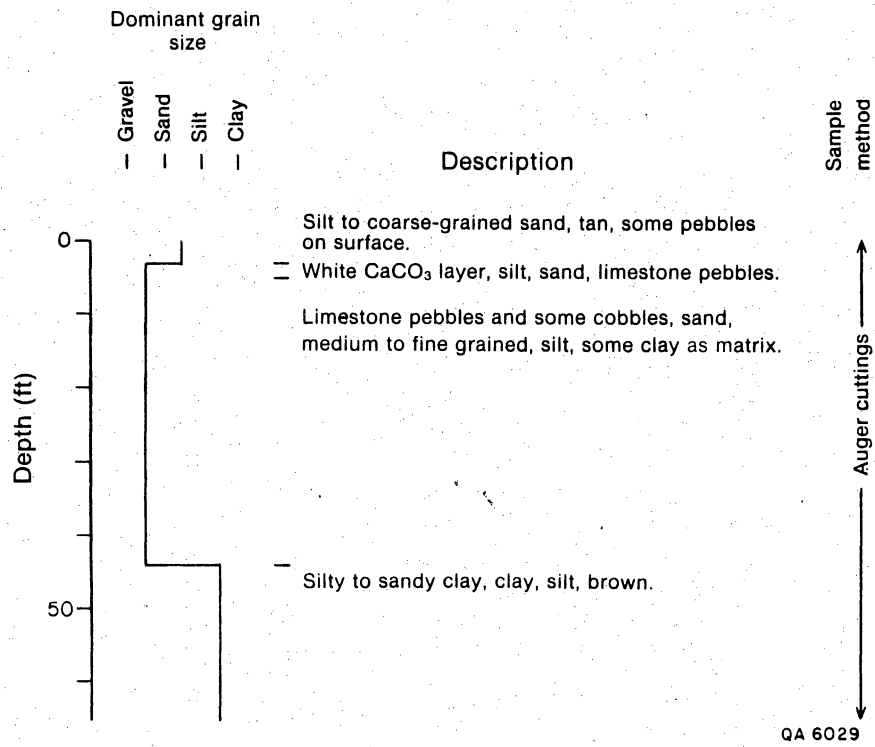


Figure A9-6. Lithologic log. LLWA6. Hudspeth County.

LLWA 7

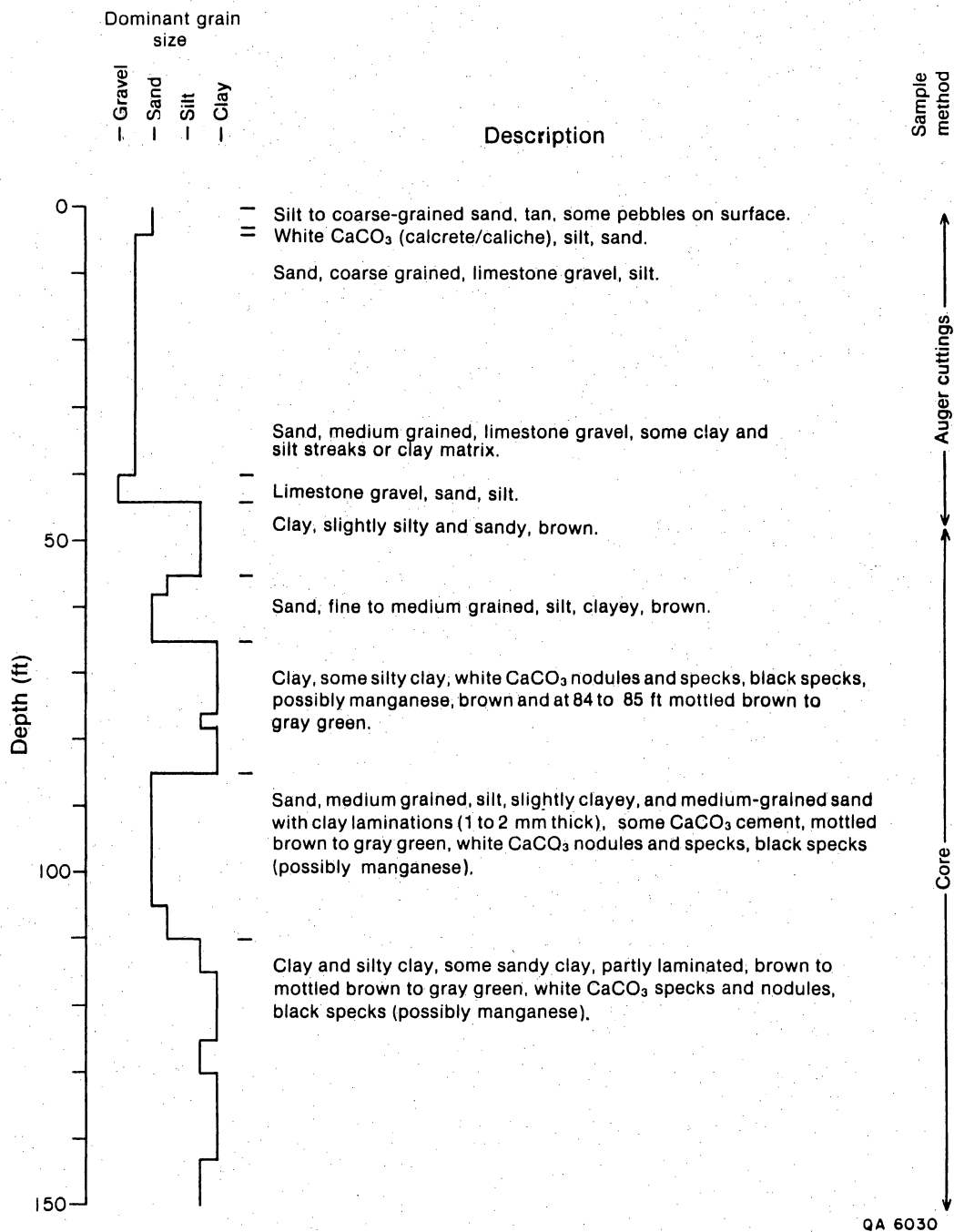


Figure A9-7. Lithologic log, LLWA7, Hudspeth County.

LLWA 11

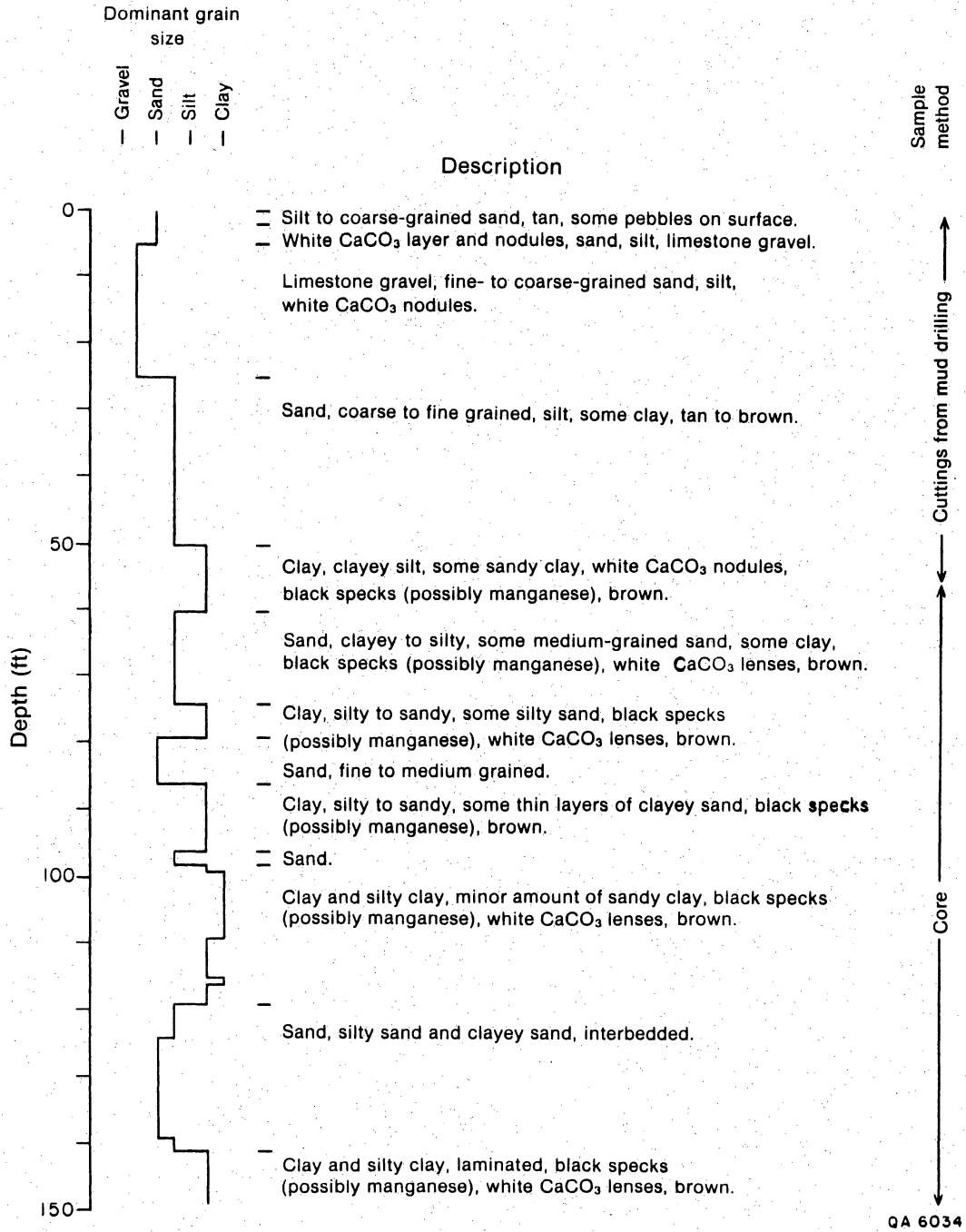


Figure A9-8. Lithologic log, LLWA11, Hudspeth County.

LLWA 12

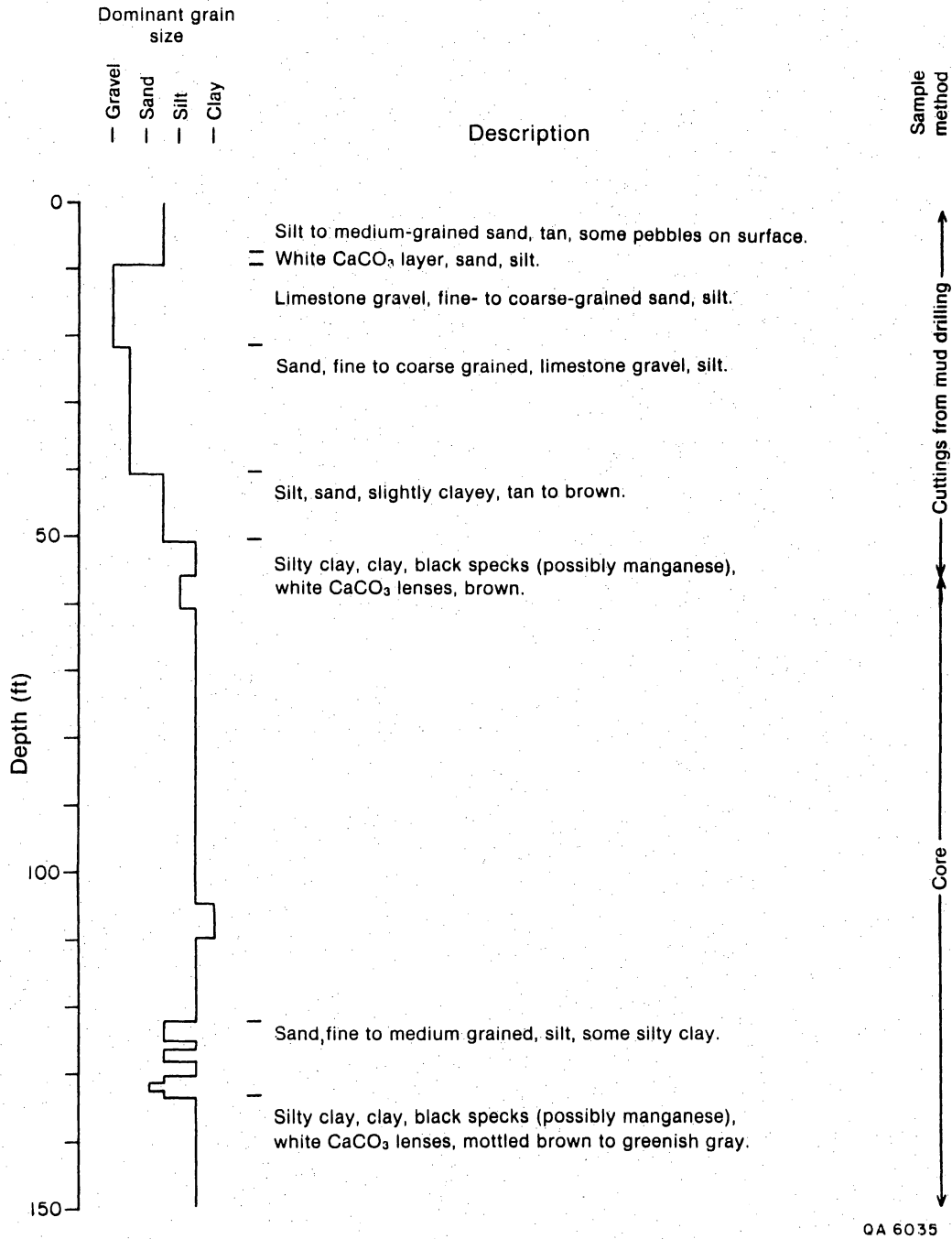


Figure A9-9. Lithologic log. LLWA12. Hudspeth County.

Appendix 10. Geophysical log data.

The following data are based on analysis of geophysical logs run in four open boreholes and are cased borehole (figs. A10-1, A10-2, A10-3, A10-4, A10-5). Schlumberger Well Services performed the logging on April 17-18, 1986. It should be noted that all five boreholes were unsaturated (above the water table) and certain tools were directly affected by this environment.

Lithologic Determination

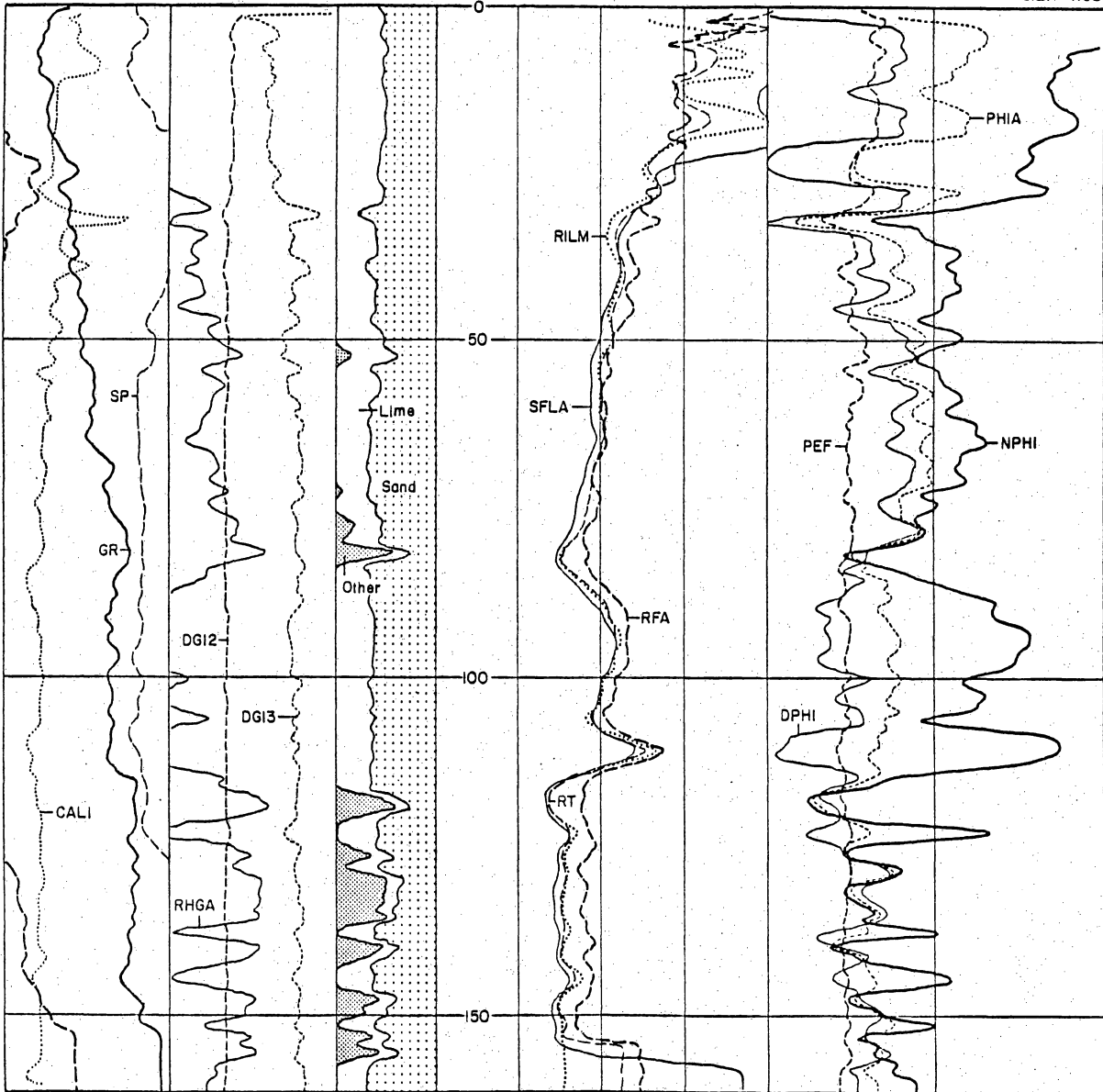
Three of the logging tools may be used to determine lithologies in open boreholes. These are the Spontaneous Potential curve (SP), Gamma Ray log (GR), and Litho-Density log (LDT).

The SP log is commonly used to determine the presence of permeable beds, bed boundaries, formation water resistivity, and shale content (Asquith, 1982). The SP log may also be an effective tool in stratigraphic and structural correlations. Typically, the SP log measures the contrast in salinities between the drilling mud filtrate and formation water. In this case (boreholes at S-34), formation water is limited to the irreducible water content trapped between and coating grains of sand, silt, and clay. This factor essentially eliminates the potential for electrochemical conduction and contrast through the formation. The SP log may have limited use in stratigraphic and structural correlations but should be used in combination with other logs such as GR or DIL.

The GR log measures natural radioactivity of a formation. In typical sequences, radioactive materials tend to be concentrated in shales and clays. The higher GR readings indicate shalier units, whereas lower GR readings indicate cleaner sandstones and limestone. Since formation water is not required, GR logs are useful to

L.L.R.W.D.A.
Well B-7 Test Borehole
Hudspeth County, Texas

G.L. = 4168'



EXPLANATION

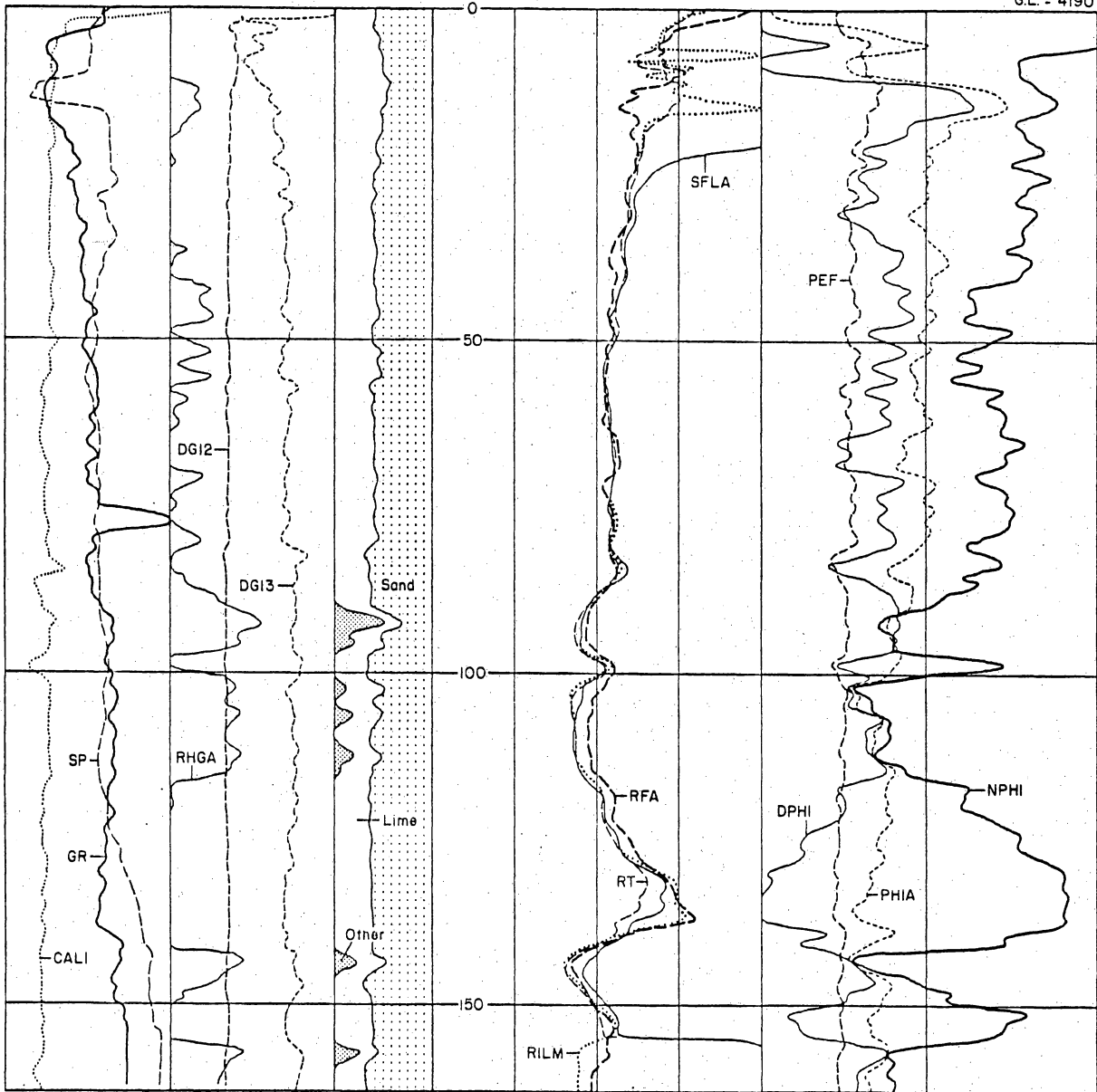
6.0000	CALI (IN)	26.000					
2.0000	DGI3 (G/C3)	3.0000	.10000	SFLA (OHMM)	1000.0	0.0	PEF
2.0000	DGI2 (G/C3)	3.0000	.10000	RT (OHMM)	1000.0	.60000	PHIA
2.0000	RHGA (G/C3)	3.0000	.10000	RILM (OHMM)	1000.0	.60000	DPHI
2.0000	SP (MV)	3.0000	.01000	RFA (OHMM)	100.00	.60000	NPHI
-160.0	GR (GAPI)	240.00					
0.0		300.00					

QA 6042

Figure A10-1. Composite geophysical log for borehole 7. Location of the borehole is shown in figure 23.

L. L. R. W. D. A.
 Well B-11 Test Borehole
 Hudspeth County, Texas

G.L. = 4190'



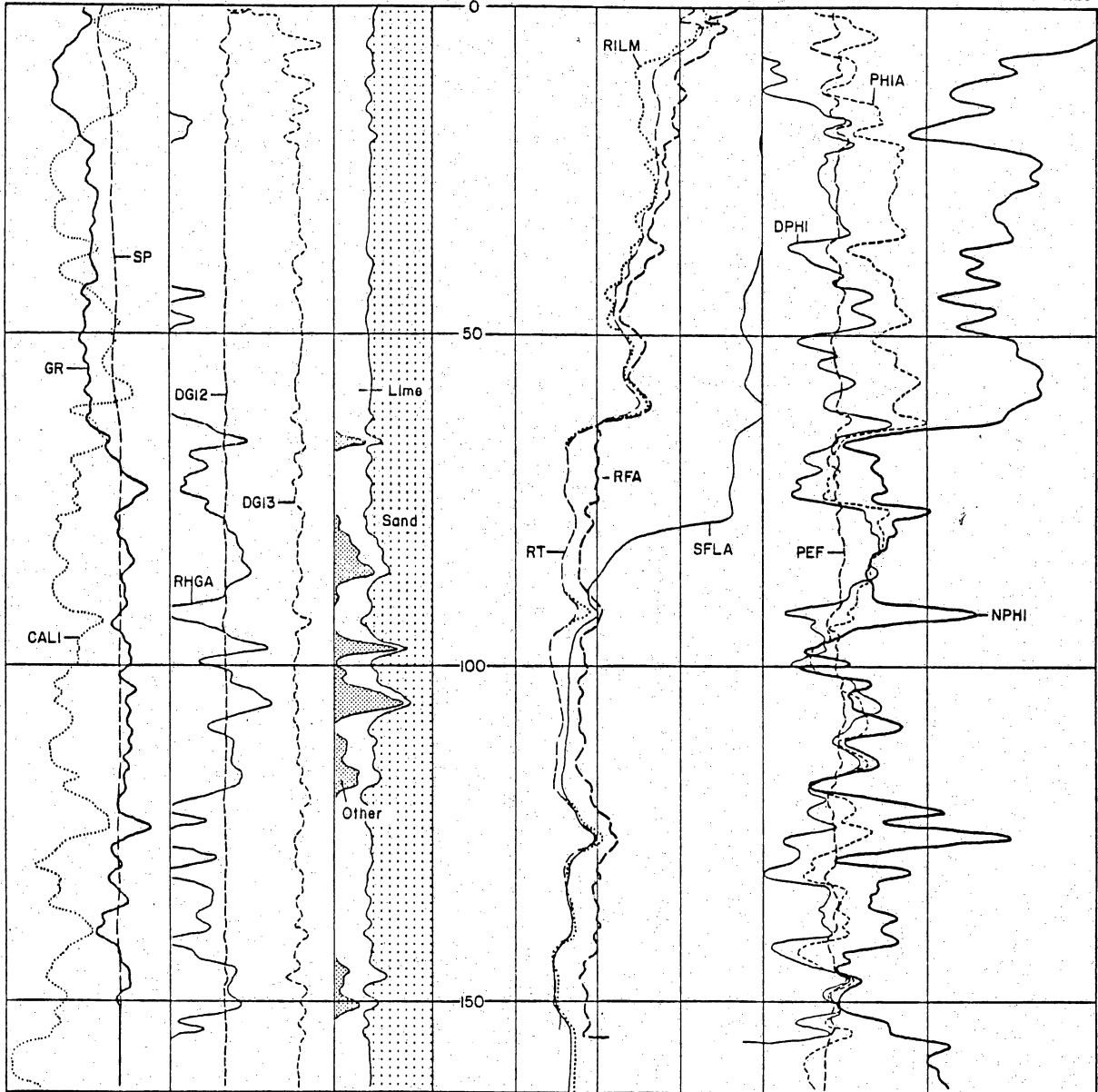
EXPLANATION			
6.0000	CALI (IN)	26.000	
2.0000	DG13 (G/C3)	3.0000	.10000 SFLA (OHMM)
2.0000	DG12 (G/C3)	3.0000	.10000 RT (OHMM)
2.0000	RHGA (G/C3)	3.0000	.10000 RILM (OHMM)
2.0000	SP (MV)	3.0000	.10000 RFA (OHMM)
-160.0	GR (GAPI)	240.00	.01000
0.0		300.00	
			10000.0 PEF
			.60000 PHIA
			.60000 DPHI
			.60000 NPHI
			10.000
			0.0
			0.0
			0.0
			0.0

QA 6044

Figure A10-2. Composite log for borehole 11. Location of the borehole is shown in figure 23.

L.L.R.W.D.A.
Well B-12 Test Borehole
Hudspeth County, Texas

G.L. = 4129'



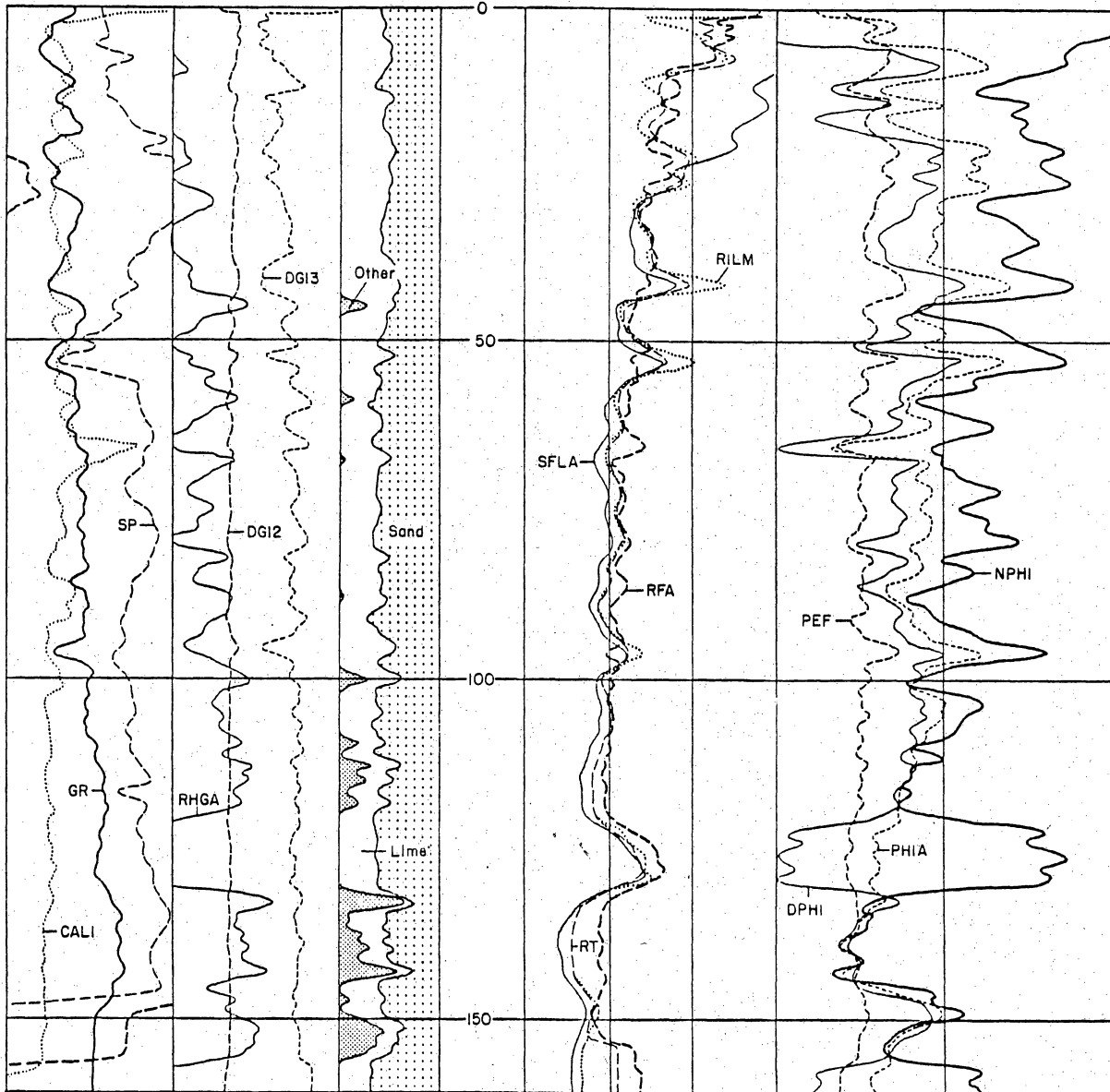
EXPLANATION			
6.0000	CALI (IN.)	26.000	
2.0000	DGI3 (G/C3)	3.0000	.10000 SFLA (OHMM)
2.0000	DGI2 (G/C3)	3.0000	.10000 RT (OHMM)
2.0000	RHGA (G/C3)	3.0000	.10000 RILM (OHMM)
2.0000	SP (MV)	3.0000	.10000 RFA (OHMM)
-160.0	GR (GAPI)	240.00	.01000
0.0		300.00	
			10000.0 PEF
			10000.0 PHIA
			.60000 DPHI
			.60000 NPHI
			10.000
			0.0
			0.0
			0.0
			0.0

QA 6045

Figure A10-3. Composite geophysical log for borehole 12. Location of the borehole is shown in figure 23.

L. L. R. W. D. A.
 Well B-13 Test Borehole
 Hudspeth County, Texas

G.L. = 4212'



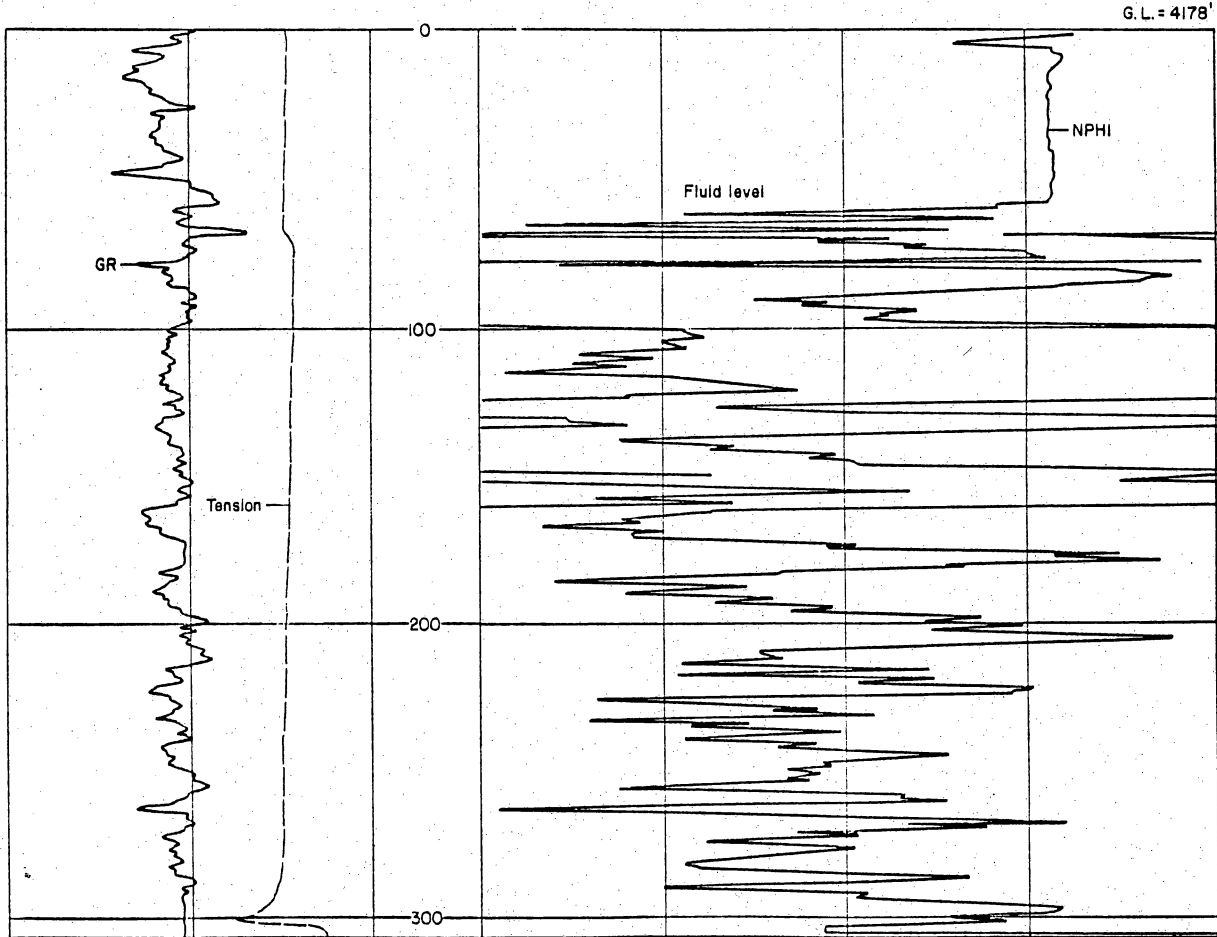
EXPLANATION

6.0000	CALI (IN.)	26000.					
2.0000	DGI3 (G/C3)	3.0000	.10000	SFLA (OHMM)	1000.0	0.0	PEF
2.0000	DGI2 (G/C3)	3.0000	.10000	RT (OHMM)	1000.0	.60000	PHIA
2.0000	RHGA (G/C3)	3.0000	.10000	RILM (OHMM)	1000.0	.60000	DPHI
2.0000	SP (MV)	3.0000	.01000	RFA (OHMM)	100.00	.60000	NPHI
-160.0	GR (GAPI)	240.00					0.0
0.0		300.00					

QA 6042

Figure A10-4. Composite geophysical log for borehole 13. Location of the borehole is shown in figure 23.

L.L.R.W.D.A.
 Well B-10 Test Borehole
 Hudspeth County, Texas



EXPLANATION

2000.0	TENS (LB)	0.0	.30000	NPHI	-1.000
0.0	GR (GAPI)	150.00			

QA 6046

Figure A10-5. Composite geophysical log for borehole 10. Location of the borehole is shown in figure 23.

determine lithology and to quantify shale or clay content of the formation.

One method used to determine percent clay or shale content for an individual unit or to establish base lines over a specified interval involves the following equation (Schlumberger, 1974).

$$I_{GR} = \frac{GR_{log} - GR_{min}}{GR_{max} - GR_{min}}$$

where I_{GR} = gamma ray index
 GR_{log} = gamma ray reading of formation
 GR_{min} = gamma ray minimum
 GR_{max} = gamma ray maximum

Using this method to determine percent clay lines for individual logs, the following data were compiled.

Clay (%)	B-7	B-11	B-12	B-13
0-25	59'-39%	28'-19%	65'-43%	91'-61%
26-50	44'-29%	69'-46%	59'-39%	34'-23%
51-75	30'-20%	34'-23%	22'-15%	15'-10%
76-100	17'-11%	19'-13%	4'- 3%	10'- 7%

The LDT has recently become important in identifying single and multiple lithologies within a borehole. One component of the LDT is a photoelectric curve (P_e), which is used to determine the mineralogy of the matrix based on the apparent photoelectric absorption cross section of a mineral. P_e values are recorded in barns per atom (one barn = 10^{-27}cm^2). In this case, the P_e proved valuable in recording the presence of bolson gravels because of the gravel's calcite content. Basic divisions case were (1) clean sands: 1.4-1.8, (2) sandy clays to clays: 1.8-2.8, and (3) calcite gravels-composed of Cretaceous limestones from the Finlay, Cox, and Bluff Mesa Formations: 2.8-5.1 (based on Gardner and Dumanoir, 1980).

Thickness to (ft)	B-7	B-11	B-12	B-13
Clean sands	2	0	4	0
Sandy clays to clays	119	121	146	119
Calcareous gravels	29	31	0*	31
Base of upper gravels	53	56	64*	54
Total footage-sandy silt to silty clay	82	47	144	35

*Although log response does not record the presence of limestone gravels in B-12 as in other boreholes, its presence was confirmed during coring operations. Reasons for this absence of calcite response may result from an increase in clay content that masks the calcite or possibly be a result of significant borehole invasion by drilling fluids as recorded by resistivity logs.

Porosity Determination

The LDT may also serve as a porosity tool when combined with the CNL, another porosity device. Accurate porosity analysis for both consolidated and unconsolidated sediments is possible when both tools are used. Using Schlumberger porosity chart CP-5 (Schlumberger, 1984) appropriate corrections can be made to determine real porosity. In this case, true porosity is 1-2 porosity units greater than the computer derived average porosity (labeled PHIA). The following data are compiled from LDT-CNL crossplots for the four open boreholes.

	B-7	B-11	B-12	B-13
Maximum porosity (percent)	54	45	54	50
Minimum porosity (percent)	21	16	30	19
Depth of maximum porosity (ft)	32	142	142	115
Depth of minimum porosity (ft)	5	14	63	41
Total footage < 36% porosity (ft)	51	84	18	98
Total footage > 48% porosity (ft)	6	0	15	2
Total footage 36-48% porosity (ft)	93	66	117	50

Formation Resistivity

Resistivity logs are typically used to delineate water-bearing versus hydrocarbon-bearing intervals. They may also be used to locate permeable zones and to make stratigraphic or structural correlations. Like SP logs from the area, resistivity logs are hampered by the absence of formation water, which restricts possible quantification of true formation water resistivity values. Qualitative observations can be made, however, concerning the location of more permeable intervals and the detection of potential perched aquifers.

The Dual Induction Focused log (DIL) is a standard resistivity tool composed of a deep-reading induction device (ILd), a medium-reading induction device (ILm), and a shallow-reading spherically focused device (SFL). Differences in resistivity values between ILd and SFL curves may be used to differentiate between true resistivity and drilling fluid resistivity. At the Fort Hancock S-34 area, the only water present in the unsaturated zone is the irreducible water content trapped and coating the sand- to clay-size grains. Since permeabilities were also found to be low for these intervals based on in situ and laboratory testing, minimal borehole invasion by the drilling fluids occurred. As a result, all three logging tools are reading similar if not identical conditions in the unsaturated sediments.

Variations in resistivity values may be used qualitatively to indicate higher versus lower water contents and permeability values. Two sequences in B-7 illustrate this. The gravel section from 0 to 50 ft records higher resistivity values than do the predominantly clay sections from 50 to 80 ft and 120 to 150 ft. This is also true of the sand from 80 to 116 ft, which indicates a higher content of irreducible water

within the larger grained deposits. Higher permeability sections are best illustrated where some separation between ILd and SFL is recorded, as in B-7 from 0 to 22 ft. The ILd in this example is measuring resistivity at a borehole depth of 64 inches while the SFL records conditions 16 inches deep. The separation that occurs in B-7 from 0 to 22 ft indicates that drilling fluids have invaded the borehole at least 16 inches but less than 64 inches because of the fluid resistivity contrast.

Appendix 11. Estimation of annual recharge based on soil coring and chloride analysis.

Annual recharge into the gravels overlying bolson fill at the Fort Hancock site and Cretaceous bedrock at HU1B was estimated based on soil cores analyzed for chloride concentrations. Procedures and interpretation followed a method suggested by Allison and Hughes (1978). When rainwater containing chloride percolates into a soil subject to water loss by transpiration, chloride concentrations at a steady state in soil water will increase monotonically through the root zone. Below the root zone, chloride concentrations remain constant with depth. Assuming that the only source of chloride in the soil is rainfall, annual recharge can be calculated using the equation:

$$R = \frac{Cl_p}{Cl_s} \times P$$

where R is annual recharge, Cl_p is chloride concentration in local rainfall, Cl_s is chloride concentration in the soil profile below the root zone, where it is constant with depth, and P is annual precipitation.

Five holes were augered in the gravels overlying the bolson fill at the Fort Hancock site, to depths of 9 to 15 m (30 to 50 ft) below land surface (LLWA 1 to LLWA 5, figs. 23 and 24). Core samples were taken in each borehole at depths of 0.3, 1, 1.5, 2.1, 3, 4.6, 6.1, 7.6, 9.1, 12.2, and 15.2 m (1, 3, 5, 7, 10, 15, 20, 25, 30, 40, and 50 ft). No drilling fluids were used while augering. All samples were weighed at the site and immediately sealed in airtight containers. Water content was determined gravimetrically using 20 g of sample. Soil samples were reweighed in the lab, oven-dried at 105°C for 24 hr, and then weighed again. Water content was used for calculating chloride concentration in the soil solution.

Chloride concentration was measured on the oven-dried samples used in determining water content. These were stirred with 50 ml distilled water for more than 2 days. Aliquots of filtrate were titrated potentiometrically to obtain chloride concentration and are reported as the concentration in the soil water solution. Variations in lithology, water contents, and chloride concentrations along each borehole are presented in figure 29. Annual rainfall amount was assumed to be 20.3 cm (8 inches). The chloride concentration in rainfall used for recharge calculations (3.71 ppm) was taken from rainfall measured in San Angelo (Lodge and others, 1968). Rainfall and vegetation cover are less in Hudspeth County than in the San Angelo area. Therefore, the amount of suspended particles in the Hudspeth County atmosphere may be larger, and its rainwater may contain more chlorides. Based on the above equation, higher annual recharge rates will result from a higher chloride concentration in the local rainfall. These annual recharge values were calculated:

Borehole no.	Cl concentration used (mg/L)	Calculated recharge (inches/yr)
1	14.6	2.03
2	54.0	0.55
3	43.8	0.68
4	57.0	0.52
5	35.0	0.9

Mean annual recharge into the gravel cover of the bolson fill, based on results from all boreholes, is 2.36 cm/yr (0.93 inch/yr), which is 11.6 percent of the annual rainfall.

Recharge was also calculated in 11 boreholes at HU1B on the Diablo Plateau using this procedure. Results are presented in the following table.

Table A11-1. Chloride and annual recharge data at HU1B.

Borehole I.D.	Total depth (ft) [A+ top of bedrock]	Total number of chloride samples collected	Test hole geological setting	Bulk density of soil at surface (gm/cm ³)	Cl _s	Calculated Recharge to Cretaceous Bedrock (inch/year)		
						Clp = 3.71 mg/l San Angelo	Clp = 0.6 mg/l Amarillo	Clp = 0.79 mg/l Midland
C1	23.5	4	Arroyo	1.37	51.9	.843	.136	.180
C2	30.5	6	Interarroyo	1.41	3,652.5	.012	.002	.002
C3	21.0	4	Interarroyo	1.33	4,237.5	.010	.002	.002
C4	26.0	6	Minor arroyo	1.29	814.9	.054	.009	.011
C5	13.0	3	Interarroyo	1.36	2,637.4	.016	.003	.003
C6	18.0	4	Arroyo	1.39	1,126.7	.039	.006	.008
C7	23.0	5	Interarroyo	1.42	2,107.7	.021	.003	.004
C8	14.0	3	Interarroyo	1.41	1,452.2	.030	.005	.006
C9	16.0	4	Interarroyo	1.42	1,911.9	.023	.004	.005
C10	19.0	4	Interarroyo	1.23	1,803.0	.024	.004	.005
C11	5.5	2	Closed depression	1.27	59.6	.734	.119	.156

P (average annual precipitation) = 11.8 inches, the average of Cornudas (10.2 inches) and Sierra Blanca (13.45 inches).

Appendix 12. Geologic and hydrologic data from El Paso Natural Gas Company Pump Station #2 water wells, Hudspeth County, Texas.

The following is a synthesis of operational and maintenance records for eight wells drilled by El Paso Natural Gas Company (EPNG) to supply water to Pump Station #2. This pump station, now abandoned, is located 5.8 mi (9.4 km) south of Cornudas, Texas, and 7.5 mi (12.2 km) southwest of site HU1A. Number (#) at the beginning of each section denotes the BEG ID number for EPNG documents.

Well #1

(1) History of drilling - On November 18, 1954, it was reported that well was drilled in approximately 1929. Location is NE 1/4, NE 1/4, Sec. 24, Blk. 123 PSL.

(2) Operational data - On November 29, 1954, depth of well at 1,125 ft with a static water level of 950 ft. Capacity of well reported as 7 gpm from June 1950 to present. Water level will decrease below the pump at a higher rate and also at 7 gpm if kept at that rate longer than 30 days. Pump is a rod type cylinder pump.

(3) Well water chemical analysis - On November 29, 1954, two chemical analyses were reported (mg/L).

	5/2/50	6/2/50
pH	7.3	7.6
Total hardness as CaCO ₃	376	428
Calcium as CaCO ₃	190	223
Magnesium as CaCO ₃	186	205
P alkalinity as CaCO ₃	0	0
Total alkalinity as CaCO ₃	230	235
Chloride as Cl	188	200
Sulfate as SO ₄	295	293
Silica as SiO ₂	15	14
Iron as Fe	trace	0.1

(4) Water well data. Based on the November 15, 1954 report, the following well data were summarized:

Drilling completion date	1929
Total depth (TD) of well	1,200 ft
Static water level	950 ft
Pumping capacity	7 gpm
Make of pump	Jenson Brothers
Rod size	3/4 inches
Column size	2 1/4 inches
Rated HP of pump	5
Pumping column	44 rods-25 ft @ 1,100 ft with 7-ft barrel and 8-ft perforated anchor.

This well is described as having an optimum capacity of 7 gpm and that water level will decrease below the pump at a higher pumping rate. It is also noted that water level will decrease below the pump when used at 7 gpm for more than 30 days. A production screen of unknown length was installed at 791 ft, 8 inches. This well was later plugged back to 1,125 ft.

(5) This driller's log describing the encountered section of water well #1 was prepared by M. E. Hawkins on June 20, 1950. Closing statement of the document is that well was plugged back to 1,100 ft.

Interval (ft)

<u>From</u>	<u>To</u>	<u>Lithology and comments</u>
110	132	Tan cream and pink dense limestone
132	140	Dense cream limestone
140	160	Cream yellow-tan and deep pink limestone, partly dolomitic
160	170	Tan and cream dense limestone (partly dolomitic) partly silty, trace chert
170	180	Yellow-tan, some cream and pink partly earthy dense dolomitic limestone
180	185	Light and limestone pebbles, some fragments of reddish-brown breccia, 20% fine to coarse clear worn sand, 20% gray clay, 80% chert
185	195	Sand and limestone conglomerate including siliceous pebbles
195	200	Light tan limestone, some quartzite pebbles
200	220	Cream partly dolomitic limestone, 30% pale gray chert

220	260	Cream limestone and pale gray chert
260	290	Cream limestone, gray and trace green tuff, 20% pyrite
290	310	Dark yellow-tan, some reddish slightly granular dolomite, 20% light chert
310	320	Dark tan granular dolomite, trace red stain and chert
320	330	Dark tan granular dolomite, 20% pink chert
330	340	Dark tan and pink dolomite, 25% gray-white and pink chert
340	360	Dark tan dolomite, trace light chert
360	370	Dark tan granular dolomite, 20% dense white chert
370	390	Dark tan dolomite
390	400	Light and dark tan and dark gray dolomitic limestone
400	410	Tan brown, some gray-black limestone
410	415	Brown and brownish gray limestone, trace dark chert
415	425	Dull tan to gray-brown limestone, trace chert and black shale
425	435	Tan and light brown limestone
435	455	Tan limestone, 10% white chert
455	475	Tan limestone, 20% cream chert
475	500	Tan limestone, 10% chert
500	520	Light and dark tan limestone, trace chert
520	530	Dark gray-brown limestone, 20% black limey shale, trace dark chert
530	545	Dark brown-gray limestone, trace chert and shale
545	560	Dark brown-gray and light tan limestone, trace black shale and chert
560	575	Tan fine crystalline limestone, 20% white chert
575	625	Brown irregular textured limestone, partly mixed with some lighter limestone
625	650	Tan and light brown limestone, 20% dark chert, trace black shale
650	660	Light tan with some gray limestone, trace black shale
660	680	Tan limestone, trace light fine-grained chert
680	690	Gray-tan partly dolomitic irregular textured limestone
690	705	Irregular textured gray-tan, some cream limestone
705	715	Brown-tan mixed with some cream limestone, 20% finer, granular dull tan chert
715	720	Limestone as above

720	730	Dark tan, some brown-black shaly granular limestone
730	745	Brown, irregular textured limestone, 20% black shale
745	760	Gray-brown irregular textured limestone
760	780	Limestone similar to above
780	800	Gray-brown, some tan limestone, 10% light chert, trace black shale
800	830	Tan limestone, <u>Show Water</u>
830	845	Gray-brown limestone, 25% calcite
845	875	Gray-tan limestone, trace calcite, black shale and white chert
875	900	Tan, some dark gray irregular textured limestone
900	930	Gray-tan irregular textured limestone, trace black chert
930	950	Gray-tan limestone, trace black shale
950	990	Brown limestone, some darker and shaly
990	1000	Tan to brown limestone
1000	1040	Irregular textured brown-gray limestone
1040	1060	Light and gray-tan limestone, trace black shale
1060	1070	Gray-tan rather dense limestone
1070	1090	Irregular textured light and gray-tan limestone
1090	1110	Irregular textured gray-tan limestone, 25% dark gray chert
1110	1120	Gray-tan partly shaly limestone
1120	1130	Gray-tan slightly granular dolomitic limestone
1130	1150	Tan limestone, 30% dark gray shale
1150	1170	Slightly granular and dolomitic limestone, 20% dark gray shale
1170	1190	Very coarse partly worn clear sand, 20% dark gray shale, 25% gray and tan limestone, trace glauconite <u>Water 1190</u>
1190	1235	Slightly dolomitic gray-tan limestone, trace black shale

Wells 2, 3, 4, and 7

(6) Memorandum dated November 24, 1954, reports the following status of water wells 2, 3, 4, and 7. Wells 2 and 3 were drilled in approximately 1929 and were abandoned in approximately 1938. The casing was pulled from both wells, and remaining boreholes were then filled with dirt. Well #4 location is listed as NE 1/4, NE 1/4, Sec. 24, PSL Blk. 123, Hudspeth County, Texas. This is 1/4 mi south of the pump station. Well #4 was also abandoned, but the dates for drilling or abandonment are not given. A plate was attached to a surface nipple on top of the

casing at time of abandonment. This well was 700 ft deep. Well #7 was drilled in 1947 and was never completed. A plate was secured to the surface casing when this well was abandoned.

Well #5

(7) Location reported as NE 1/4, NE 1/4, Sec. 24, PSL Blk. 123, 900 ft south of the pump station. Well was drilled on August 18, 1936, to a total depth of 713 ft. Casing string is given as 60 ft of 10-inch pipe and 703 ft of 4-inch pipe. Pumping equipment at this time consisted of an Allis Chalmers electric motor pump jack. This borehole is reported to be crooked at 400 ft.

(8) Driller's log (source of driller's log listed as Compressor Department, El Paso Natural Gas Company):

Interval (ft)

<u>From</u>	<u>To</u>	<u>Lithology and comments</u>
0	4 ft	Surface
4	21	Caliche-hard
21	45	White lime
45	80	Sandy blue limestone
80	110	White lime
110	125	Sandy blue limestone
125	185	White limestone
185	198	Black limestone
198	250	Red rock-hard
250	270	White limestone
270	295	Yellow sandy limestone
295	389	Hard gray limestone
389	400	White limestone
400	402	Gray limestone
402	452	Yellow sandstone, some limestone
452	515	Yellow limestone crevis, 479-485
515	530	White limestone
530	550	Gray limestone
550	624	White limestone
624	647	Gray limestone, crevis at 637, lost drilling water
647	700	Yellow limestone, crevis 647-653, no lost returns
700	713	Corrected to 703 water sand

(9) The chemical analysis of ground-water in well #5 given below was dated November 18, 1954:

	3/49	No date
pH	8.2	7.8
Total hardness as CaCO ₃	376	300
Calcite as CaCO ₃	240	223
Magnesium as CaCO ₃	136	77
P alkalinity as CaCO ₃	0	0
Total alkalinity as CaCO ₃	230	260
Chloride as Cl	136	170
Sulfate as SO ₄	165	---
Silica as SiO ₂	36	17
Iron as Fe	0.1	0
Total solids	1092	958

(10) Appropriate portions of the maintenance record for Well #5 are listed below.

Drilling operations for Well #5 began July 7, 1936, and were completed on August 18, 1936. September 18, 1957 entry includes (1) total depth of hole is 697.5 ft (212.6 m); (2) static water level is at 675 ft (205.7 m); (3) initial capacity after service of well was 8.5 gpm on 13 cycles per minute of pump jack; (4) On January 21, 1958, production rate was measured at 10.0 gpm after replacing pump parts and rods; (5) On February 17, 1958, production rate still recorded at 10 gpm.

(11) Water well maintenance report dated August 12, 1965. Reports that static water level rose from 693 ft (211 m) to 684 ft (208 m) after replacing a portion of pipe string and pump. Before servicing, the production capacity fell from 11 gpm to 5 gpm, and production barrel was faulty and sanded up.

(12) Undated operational memorandum repeats that this hole is crooked at 400 ft (121.9 m) and recommends that in the future a cable tool rig be used to reclaim all of hole (from caving). This memo also reports the static water level at well #5 for August 1965 to be ranging from 693 to 684 ft (211.2 to 208.4 m) and in October 1965 to be static at 690 ft (210.3 m). Original total depth of borehole (TD) reported to be 713 ft (217.3 m).

Well #6

(13) Location of well is NE 1/4, NE 1/4, Sec. 24, PSL Blk. 123. This is located 1/4 mile south of pump station. This well was completed at a total depth of 1,209 ft (368.5 m) in 1938. Production was reported as 12 gpm through 8-inch casing.

(14) Operational record dated November 29, 1954, states that well has a total depth of 1,214 ft (370 m) and a static water level of 1,044 ft (318.2 m). Production capacity for this well is given as 20 to 30 gpm, and it is reported that water level will decrease below the pump if rates are greater.

(15) Chemical analyses reported for two consecutive days for well #6 on November 18, 1954.

	<u>7/24/52</u>	<u>7/25/52</u>
pH	7.5	7.6
Total hardness as CaCO ₃	430	450
Calcium as CaCO ₃	250	250
Magnesium as CaCO ₃	180	200
P alkalinity as CaCO ₃	0	0
Total alkalinity as CaCO ₃	290	270
Chloride as Cl	72	64
Sulfate as SO ₄	288	310
Silica as SiO ₂	9	12
Iron as Fe	trace	---
Total solids	980	1000

(16) Driller's log for Well #6.

<u>Interval (ft)</u>		<u>Lithology and comments</u>
From	To	
25	35	Buff and gray lime
35	45	Buff and gray lime, scattered sand grains
45	55	Buff and gray lime, scattered sand grains
55	65	Buff gray lime, fewer sand grains
65	80	Buff gray lime, few quartz grains
80	95	Gray buff lime, rust-colored limy shale
95	105	Gray lime, few quartz grains
105	115	40% gray buff lime, 60% calcite crystals, and few pyrite inclusions
115	127	Gray and buff lime

127	136	Brown dolomite and calcitic lime, crystalline
136	140	90% gray lime, 5% black lime, 5% black limey shale
140	150	Blue lime
150	160	Blue and gray lime
160	196	Blue and gray lime
196	208	Blue and gray lime, scattered sand grains
208	218	80% blue and gray lime, 20% sand with some pyrite
218	229	Blue and gray lime, scattered sand grains
229	233	Blue and gray lime
233	237	70% buff and blue lime, 30% partly rounded quartz grains
237	240	80% buff lime, 20% sand
240	249	90% buff lime, 10% calcitic sand
249	259	Buff lime some calcitic and quartz sand
259	269	Gray buff lime
269	271	Gray buff lime
271	295	Brown dolomitic lime, few calcitic and quartz grains
295	305	Gray buff lime, few calcite grains
305	315	Light brown lime
315	320	Dark brown lime, few calcite grains, some pyrite
320	330	Blue gray lime
330	340	Dark brown lime, few calcite grains
340	360	Dark brown and gray lime
360	370	Dark brown and gray lime, few calcite grains
370	380	Dark gray and light gray lime
380	400	Dark gray and some light brown lime
400	424	Very dark gray lime
424	430	Dark brown lime, few calcite grains
430	440	Brown lime, few calcite grains
440	450	Brown and lighter brown lime
450	490	Dark brown and gray lime
490	500	Light brown and brown lime
500	530	Brown lime
530	540	Dark brown lime
540	550	Dark brown and light lime
550	560	Light brown lime and few calcite grains
560	570	Light brown and little white lime, few calcite grains
570	580	Light and dark brown lime

580	590	Brown lime, 5%-10% calcite grains
590	600	-skipped interval on log-
600	610	Light gray lime, few calcite grains
610	620	Light brown lime
620	640	Dark brown lime
640	650	Dark brown and light brown lime
650	670	Dark gray lime, few calcite grains
670	680	Dark gray and brown lime
680	690	Light brown lime
690	715	Dark brown and brown lime
715	729	Dark brown lime
729	750	Dark gray lime, few calcite grains
750	770	Brown lime, few calcite grains
770	800	Dark brown lime, few calcite grains
800	830	Dark brown lime and brown lime
830	840	Brown lime
840	850	Brown and light brown lime
850	870	Brown lime
870	900	Dark brown lime
900	930	Brown lime
930	940	Dark brown lime
940	950	Brown lime
950	960	Dark brown and brown lime
960	980	Brown lime
980	1000	Brown and light brown lime
1000	1010	Light brown lime
1010	1018	Dark brown lime
1018	1030	Brown lime
1030	1038	Dark brown lime
1038	1062	Brown lime
1062	1068	Brown and light brown lime
1068	1086	Brown lime, semi-frosted quartz grains
1086	1087	Dark brown lime
1087	1094	Light brown lime, few green limey shale flakes, few quartz grains, light brown lime contains fossil remnants
1094	1099	Dark brown lime, numerous frosted quartz grains
1099	1104	Brown lime, numerous frosted quartz grains

1104	1115	Light brown lime, few frosted quartz grains
1115	1120	Light brown lime, some pyrite inclusions
1120	1128	Dark brown lime
1128	1150	Brown lime
1150	1160	Brown lime, few frosted quartz grains
1160	1170	Brown lime, few calcite grains
1170	1175	Dark brown fossiliferous grains
1175	1180	Dark brown lime
1180	1189	Brown lime
1189	1204	Dark brown lime
1204	1209	Dark brown lime and gray lime--TD

Well #8

(17) Well data sheet gives location for this well as NE 1/4, NE 1/4, Sec. 24, PSL Blk. 123 (outside southwest corner of plant location). This well, completed on June 26, 1951, was drilled by Holland Page, Jr., to a TD of 1,288 ft (392.5 m). Well was temporarily plugged and abandoned March 28, 1956, and restored to production on January 20, 1958.

(18) This document is a memorandum to W. H. Miller from M. E. Hawkins reporting the results of pump tests on well #8.

<u>Date</u>	<u>Time</u>	<u>Gallons per minute (gpm)</u>
11/26/51	12:30 p.m.	start test
11/26/51	12:30-4:30 p.m.	45
11/26/51	4:30-11:30 p.m.	30
11/26-27/51	11:30 p.m.-8:30 a.m.	25
11/27/51	8:30 a.m.-10:00 p.m.	20
11/27-28/51	10:00 p.m.-6:30 a.m.	15
11/28-12/5/51	6:30 a.m. to present	12

(19) The following is a synthesis of a combined driller's log and operational report for water well #8.

<u>Date</u>	<u>Interval (ft)</u>	<u>Lithology and comments</u>
6/2/51	0-43	Caliche
6/3/51	43-45	Lime
	45-65	Yellow lime
	65-75	Brown lime
	75-80	Yellow lime
	80-86	Yellow lime
	86-94	Gray lime
6/4/51	94-95	Light brown hard lime
	95-100	Light brown hard lime
	100-106	Lime ballard gray lime
6/5/51	106-114	Lime gray
	114-120	Lime brown hard
	120-124	Lime brown hard
	124-134	Gray lime
	134-140	Gray lime
	140-143	Gray shale
	143-155	Gray lime shells
6/6/51	155-165	Lime, broken medium, little water at 158-160
	165-171	Lime gray hard
	171-175	Lime, broken, little more water at 171-175
	175-190	Broken lime
	190-195	Gray shale
	195-205	Gray lime
6/7/51	205-225	Lime hard sharp
	225-233	Lime hard sharp
	233-239	Sand, report increase in water
	239-240	Hard gray lime
6/8/51	240-245	Lime gray hard
	245-253	Lime broken
	253-270	Lime-sand medium
	270-276	Lime-sand
	276-295	Yellow lime hard

6/9/51	295-310	Lime gray brown hard
	310-325	Brown lime hard
6/10/51	325-340	Lime brown hard
	340-348	Lime
6/17/51	348-355	Lime hard
	355-358	Lime hard
6/18/51	358-360	Lime hard
	360-370	Lime hard
	370-377	Black lime
6/19/51	377-383	Hard lime
	383-397	Hard lime, testing water, 1.5 bailers per hour
6/20/51	397-401	Hard lime
	401-410	Brown lime
	410-421	Brown lime
6/21/51	421-443	Brown lime
	443-450	Brown lime
6/24/51	450-455	Brown lime hard
	455-464	Brown lime hard
	464-480	Brown lime
6/25/51	480-493	Brown lime
	493-513	Brown lime
6/26/51	513-525	Brown lime hard
	525-557	Brown lime
6/27/51	557-571	Lime shells
	571-607	Brown lime
6/28/51	607-618	Broken lime hard
	618-649	Black lime, tested production at 0.5 bailer per hour
6/29/51	649-685	Lime
6/30/51	685-698	Lime
7/1/51	698-710	Lime hard
	710-743	Black lime
7/3/51	743-760	Black lime

7/4/51	760-771	Lime black
	771-777	Gray lime
	777-790	Brown lime
	790-804	Black lime
7/5/51	804-825	Gray lime
	825-843	Blue lime
7/6/51	843-875	Gray lime
7/7/51	875-885	Gray lime hard
	885-908	Gray lime
7/8/51	908-920	Gray lime
	920-933	Gray lime hard
	933-940	Gray lime, tested water production, rate at 1.5 bailers per hour
7/9/51	940-952	Gray lime
	952-963	Hard gray lime
	963-973	Hard gray lime
7/10/51	973-983	Gray lime
7/13/51	983-985	Black lime
7/14/51	985-997	Black lime
	997-1021	Blue gray lime
7/15/51	1021-1051	Blue gray lime hard
7/16/51	1051-1070	Black lime
	1070-1093	Blue gray lime
7/17/51	1093-1131	Blue gray lime
7/18/51	1131-1150	Shale-gray lime
7/19/51	1150-1180	Blue gray lime, possible water from 1170 to 1180, begin testing water-no results
	1180-1200	Black lime
7/20/51	1200-1217	Blue gray lime, testing production-initial rate of 2.5 bailers per hour, increased to 10 bailers per hour
7/21/51	1217-1235	Blue gray lime, tested 5 bailers per hour, hit small crevice at 1225
7/22/51	1235-1266	Shale and lime

7/23/51	1266-1288	Shale and lime, recorded 400 ft (121.9 m) of fluid in the hole, bailed from 11:30 a.m. to 5:30 p.m. (75 bailers full), during one hour delay for equipment repair-water level rose 100 ft, at 530 ft, 65 bailers water 500 ft
7/24/51	1288	Continued bailing, water rose approximately 25 ft (7.6 m) averaged bailing 15 bailers per hour-lowered the water level 40 ft (12.2 m) -shut down 45 minutes and water level rebounded to original level of 250 ft (76.2 m) (Note-the water level of 250 ft mentioned in this entry is unclear because the last entry noted water level of approximately 530 ft (161.5 m))
7/25/51	1288	Started production test. Before starting-water level measured at 590 ft (179.8 m), recovered 23 bailers in 1 hour, water level at 948 ft (288.9 m), after bailing 1,640 gallons bailed (6207.4 L)-bailed 23 to 24 gallons per hour-maximum drawdown measured was 200 ft (60.9 m)
7/26/51	1288	420 ft (128.0 m) of fluid in the hole at beginning of production test-recovered 21 bailers containing 1,425 gal (5393.6 L) lowering water table 100 ft (30.4 m) unable to lower water table below 200 ft (60.8 m)-end of test.

(20) The following chemical analysis as prepared for water well #8 by D. C. Kelly is dated November 18, 1954.

	<u>7/24/51</u>	<u>12/--/51</u>
pH	7.6	7.4
Total hardness as CaCO ₃	400	405
Calcium as CaCO ₃	230	240
Magnesium as CaCO ₃	170	265
P alkalinity as CaCO ₃	0	0
Total alkalinity as CaCO ₃	215	230
Chloride as Cl	80	104
Sulfate as SO ₄	108	336
Silica as SiO ₂	18	17
Iron as Fe	trace	---
Total solids	---	1578

(21) An operational report dated March 1952 provides information about water found in the following intervals in water well #8:

158 ft- 165 ft

171 ft- 175 ft

1170 ft-1190 ft

Static water level is recorded at 626.5 ft (190.9 m). Other remarks in this memo include (1) well does not have a sand trap, (2) is not gravel packed, (3) does have a foot valve, and 4) well does not pump sand.

Appendix 13. Lithologic and structural descriptions of test holes.

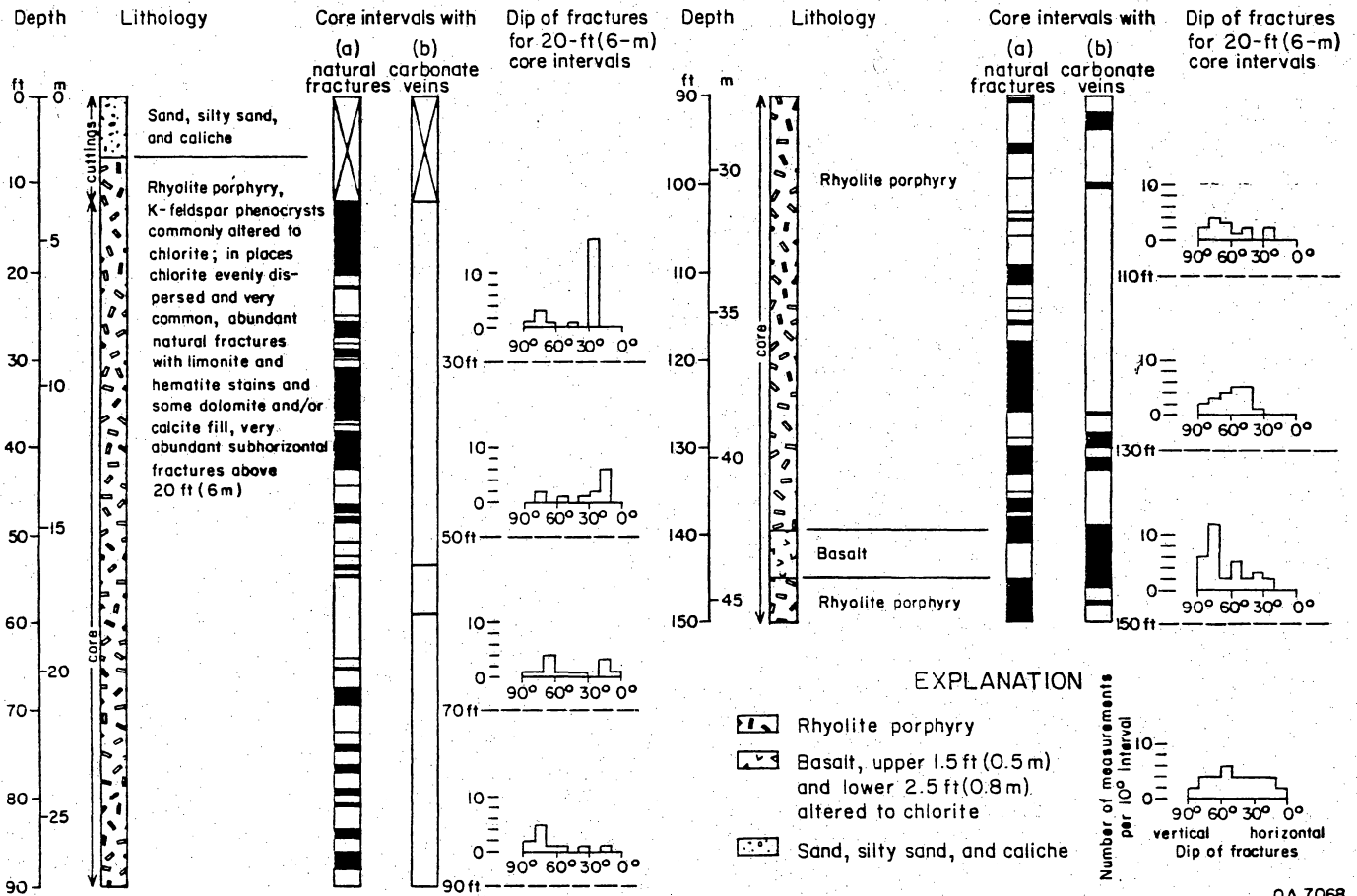
Two boreholes drilled as part of this study were continuously cored from the top of bedrock to a total depth of 150 ft (46 m). Lithologic logs for both boreholes are presented below.

HU1A (fig. A13-1)

Bedrock was encountered in HU1A-BEG #1 at a depth of 8 ft (2.4 m). Alluvial cover from 0 to 5 ft (0 to 1.5 m) consisted of tan to brown, sand to silty sand, with minor occurrences of caliche. From 5 ft (1.5 m) to 8 ft (2.4 m) the alluvium became increasingly coarser with gravels of predominantly rhyolite composition. The dark-red rhyolite porphyry has pink feldspar and clear glassy quartz phenocrysts that range in size from 0.1 to 0.4 inches (0.2 to 1.0 cm). Chlorite is a common alteration product. Limonite and hematite stains also occur on fracture surfaces in the core. Fifty percent of the rhyolite porphyry core from site HU1A is fractured.

HU1B (fig. A13-2)

Bedrock was encountered in HU1B-BEG#1 at a depth of 18 ft (5.4 m). Alluvial cover at this site consisted of tan to brown sand with abundant caliche nodules from 0 to 8 ft (0 to 2.4 m); tan to yellow clay with variable amounts of brown sandstone gravels and minor inclusions of interbedded silts and sands from 8 to 18 ft (2.4 to 5.4 m). Cretaceous bedrock encountered at 18 ft (5.4 m) consisted of a limestone breccia to 20.3 ft (6.2 m). Cretaceous Cox sandstone consists at



QA 7068

Figure A13-1. Lithologic log for rhyolite core from HU1A site.

this location of a predominantly gray crossbedded sandstone interbedded with thin purple layers of quartz grains, and was recorded from 20.3 ft (6.2 m) to 30.8 ft (9.3 m). This interval recorded variable amounts of fracturing. Oxidation of iron minerals in this interval was prevalent.

From 30.8 ft (9.2 m) to total depth at 150 ft (45.7 m) the stratigraphic interval was Cretaceous Campagrande limestones. This interval is dominated by nodular limestones in the upper section, becoming more conglomeratic in the lower section. Logging descriptions used are based on the system of Bebout and Loucks (1984).

Appendix 14. Climate and vegetation controls on surface recharge.

Differences in annual rates of precipitation, evaporation, temperature, and dominant plant ecosystems between sites HU1A and HU1B on the Diablo Plateau and the Fort Hancock site in the Hueco Bolson may influence the potential for surface recharge. Distinct differences between the two areas in climate, surface and near-surface lithologies, and vegetation have been reviewed to determine how they may affect surface recharge. Further study is required to quantify actual levels of evapotranspiration at both areas before final conclusions are drawn.

Trans-Pecos Climate

The Trans-Pecos region has a subtropical arid climate (Larkin and Bomar, 1983) characterized by (1) high mean temperatures and marked fluctuations over broad diurnal and annual ranges and (2) low mean precipitation with widely separated annual extremes (Orton, 1964). Rainfall in this climate is inadequate to support vegetation other than desert and semi-desert types.

Precipitation and temperature (minimum and maximum) data were selected for five monitoring stations in the area (fig. A14-1; table A14-1) (National Weather Service, 1986a, b, c). Three stations are within the Hueco Bolson at the El Paso Airport, in Fabens, and in Fort Hancock. Two stations on the Diablo Plateau are at Sierra Blanca, south of the study area, and at Cornudas, to the northwest. Only the El Paso Airport station had complete records for extended lengths of time; data from the other four stations are incomplete.

National Weather Service (NWS) records were used to describe the climate of the study area. Monthly totals for precipitation and monthly averages for minimum and maximum temperatures were recorded at the five stations. No year with

incomplete data was used; data from some stations represent different years. Ten complete years of data were assembled for each station except Fort Hancock, which had only 7 years of precipitation data. Mean annual, monthly, and summer (June to September) values for precipitation and temperatures were calculated, along with standard deviation. Results are presented in table A14-1.

Most annual precipitation occurs as afternoon thundershowers from June to September. These thundershowers are the result of moist air from the Gulf of Mexico moving northwest into the Trans-Pecos area during the hurricane season. At the Cornudas service station, annual precipitation has averaged 10.2 inches (25.9 cm) and average summer precipitation is 6.24 inches (15.8 cm) or 61% of the annual total over 33% of the time. Similar values were observed at the other stations.

Changes in elevation have a direct effect on both temperature and precipitation patterns. The difference in elevation between Cornudas and Fort Hancock is approximately 708 ft (215 m), and the difference in average temperatures is 2.1°F for maxima and 1.6°F for minima. Average precipitation totals for both Cornudas and Fort Hancock are 10.2 inches (25.9 cm) and do not reflect the difference in elevations. Sierra Blanca, however, records a greater average annual precipitation of 13.45 inches (34.1 cm).

How temperature increases within the Hueco Bolson affect potential evaporation, and thus evapotranspiration changes, between the bolson and plateau is unknown. Quantitative data on potential evaporation in the area are from two stations in Ysleta, both of which are in the bolson east of El Paso. The adjusted annual mean evaporation for these stations ranges from 93.1 inches (2.4 m) in 1944 to 116.4 inches (3 m) in 1956 (Dougherty, 1975). Scalapino (1950) reported that the annual potential evaporation in the Dell City area is nine times greater than the annual precipitation. If the only variables in the two systems were precipitation and

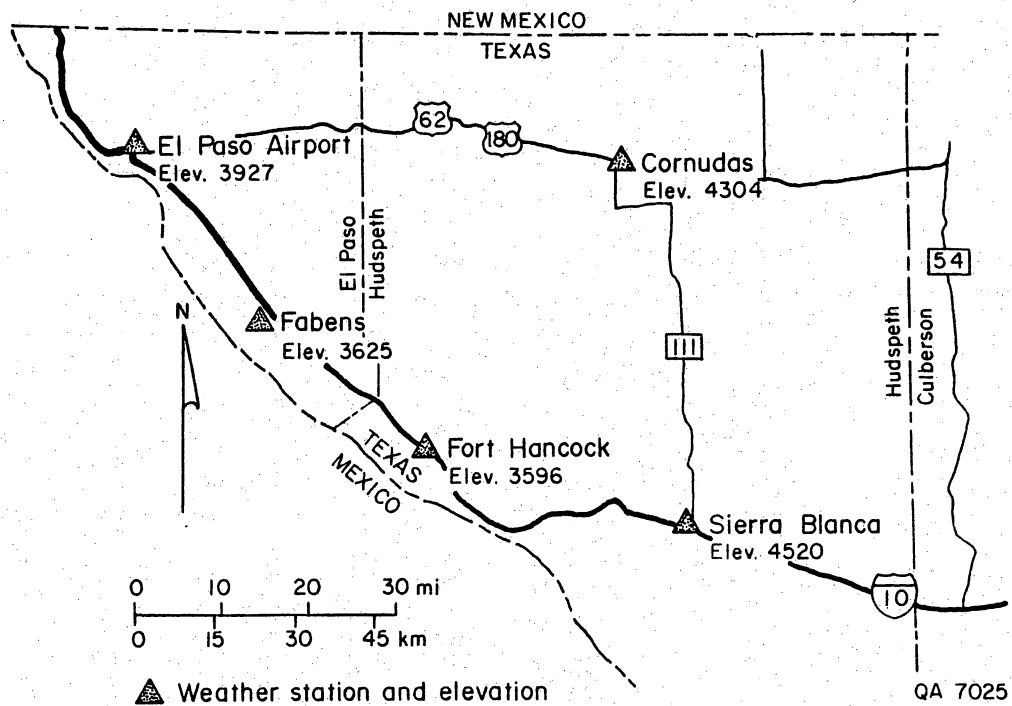


Figure A14-1. Weather station location map. Three stations (El Paso, Fabens, and Fort Hancock) are in the Hueco Bolson area, whereas two stations (Sierra Blanca and Cornudas) are on the Diablo Plateau.

Table A14-1. Climatic data for Hueco Bolson and Diablo Plateau in the study area.

Monitor Station (Elevation in ft)	Latitude/ Longitude	Annual Average			Summer Average (June - Sept.)		
		Rainfall (inches)	Minimum Temperature (°F)	Maximum Temperature (°F)	Rainfall (inches)	Minimum Temperature (°F)	Maximum Temperature (°F)
Cornudas Service Station (4304)	31°47'00" 105°28'00"	10.2	42.5	77.7	6.24	59.1	91.9
El Paso WSO AP (3927)	31°48'00" 106°24'00"	9.53	49.0	77.9	5.56	65.5	94.0
Fabens (3625)	31°30'00" 106°09'00"	9.65	45.2	77.8	6.96	62.5	91.6
Fort Hancock (3596)	31°17'00" 105°51'00"	10.27	44.1	79.8	6.48	61.9	95.0
Sierra Blanca (4520)	31°11'00" 105°21'00"	13.45	43.9	77.3	9.28	59.7	90.2

temperature, evapotranspiration in the bolson would be greater, and thus surface recharge to the water table would be more probable on the Diablo Plateau.

Fort Hancock Area - Hueco Bolson Plant Ecosystems

Common plant ecosystems in the Hueco Bolson north of Fort Hancock are representative of desert shrublands (taxonomic identification assisted by Kenneth Moore, personal communication, 1986; Correll and Johnston, 1970). Most of the annual vegetative production is from woody plants with running mesquite (*Prosopis sp.*) dominant in areas of rolling sandy loams and the creosote bush (*Larrea tridentata*) more dominant in gravelly areas. Annual plant production from herbaceous plants is low, averaging 500 pounds per acre (ppa). Commonly, bare land surface exists between woody plants, a controlling factor in the low plant production. Annual grasses may also constitute a large part of the plant production.

Other woody plants common in the area are javelina bush (*Condalia ericoides*), yucca (*Yucca sp.*), and cactus (Cactaceae family). Minor populations of four-wing salt bush (*Atriplex canescens*) and broomweed or snakeweed (*Xanthocephalum sp.*) are also present. Perennial grasses in the area include bush muhly (*Muhlenbergia porteri*), dropseed (*Sporobolus sp.*), fluffgrass (*Erioneuron pulchellum*), and burro grass (*Scleropogon brevifolius*).

HU1A - HU1B Diablo Plateau-Plant Ecosystems

The Diablo Plateau in the vicinity of HU1A and HU1B is a desert grassland. Numerous annual and perennial grasses may be found in the area but only sparse occurrences of woody vegetation. Annual plant production from desert grasslands may be considerably higher than has been reported for desert shrublands, ranging from 1,000 to 5,000 ppa. Dominant annual grasses of the area include blue grama (*Bouteloua gracilis*), black grama (*Bouteloua eriopoda*), tobosa grass (*Hilaria mutica*), plains bristlegrass (*Setaria macrostachya*, *S. texana*, and *S. leucopila* collectively), and side-oats grama (*Bouteloua curtipendula*).

Perennial grasses may also represent a large segment of the desert grassland ecosystem. Several of these species are *Muhlenbergia*, *Sporobolus*, along with vine-mesquite (*Panicum obtusum*), burro grass (*Scleropogon brevifolius*), and fluffgrass (*Erioneuron pulchellum*). In local areas that receive additional water from runoff, such as draws, Cane bluestem (*Andropogon sp.*) and Sacaton grass (*Sporobolus sp.*) may also be a dominant part of the ecosystem.

Woody vegetation is rare in the desert grassland, except where the soil is sandy or gravelly. Woody vegetation that occasionally dominates the draws includes vine-ephedra (*Ephedra pedunculata*), several species of the cactus family, the creosote bush (*Larrea tridentata*), desert sumac (*Rhus microphylla*), yucca (*Yucca sp.*), and the javelina bush (*Condalia cricoides*).

Discussion

The correlation between temperature, precipitation, and dominant plant ecosystem discussed above influences evapotranspiration rates and potential for surface recharge. High tritium levels in several sampled wells on the Diablo Plateau indicate surface recharge activity significantly higher than that measured in the Hueco Bolson, north of Fort Hancock (fig. 14). Greater rainfall and lower temperatures may be directly related to active surface recharge on the Diablo Plateau. However, increased precipitation may not affect surface recharge in the Diablo Plateau because the denser plant populations may absorb more water, whereas shrublands lose water during runoff infiltration due to less extensive or less efficient root systems. There is a large difference between plant production in the bolson (500 ppa) and on the plateau (up to 5,000 ppa). Quantification of evapotranspiration rates in both areas would facilitate a better understanding of recharge mechanism and recharge potential both in the bolson and on the plateau.

Appendix 15. B-14 water well summary.

On April 4, 1986, drilling of water well B-14 at Fort Hancock Site S-34 began. This additional well was necessary because the cement packer in B-10 (the first water well) failed during cementing operations. Two purposes for drilling the new well were to determine the static water level at the site and to sample for standard chemistry and isotopes. Total depth of B-14 is 530 ft* with a static water level of 478 ft. Final drilling operations on this well were completed on April 16, and all sampling and testing completed on April 23. This section documents (1) drilling and completion activities, (2) recommendations for possible completion of this well, and (3) lithologies encountered. Results of chemical and isotopic analysis are in appendix 4.

April 4--Located and rigged up for drilling B-14 213 ft east-northeast of B-10. Began drilling at 10:45 a.m. with fresh-water gel-based mud system. Drilled to 135 ft with 7-7/8 inch tri-cone rock bit. Drilled to 180 ft with 7-7/8 inch drag bit.

April 5--Drilled to 393 ft, where cuttings indicated presence of limestone, rate of penetration slowed due to increased hardness of formation, and suction pit water level dropped 2 inches due to presence of lost-circulation zone. Based on local information, the first sign of lost circulation usually indicates both porosity and water-bearing strata. Conditioned the hole and pulled pipe in preparation to run casing. Ran 4-inch steel casing to T.D. at 393 ft. Successfully cemented casing from T.D. to surface.

*All depths reported in this appendix were measured below land surface.

April 6--Ran 3-1/2 inch tri-cone in hole and staged out drilling mud with air in 100-ft increments. Had circulation problems while drilling with compressed air due to small size differential between drill bit and drill pipe (1/4 inch clearance). Drilled out from bottom of casing to 399 ft.

April 7--Ran new 4-inch drag bit into hole in attempt to increase clearance differential. Drilling with circulation problem continued, however. Ran split spoon to T.D. in attempt to determine lithology responsible for circulation problem. Sample recovered was moderately compacted and cemented, tan to brown, medium grain sand with occasional small limestone gravels. Sample was only slightly damp, a result of uphole drilling fluids and not formational water. Due to circulation problems, only 18 inches of new hole drilled.

April 8--Waited on air compressor repairs. Switched to drilling with a foam system. Lithology determination while drilling with foam difficult. To accurately determine depth of water strata from 400 to 500 ft, drilling was stopped after each 10-ft interval, cuttings were circulated bottoms-up, then foam was cut off and dry air circulated for 20 minutes. After air was circulated, returns were checked for presence of moisture content. No moisture was detected while drilling from 400 to 480 ft. After drilling 480 to 490 ft and following above procedure, definite presence of moisture was detected at a constant rate. Drilled to 500 ft as temporary T.D. so that water levels could be monitored.

April 9--Tripped pipe into hole to T.D. to determine amount of fill and to condition borehole for water-level measurements. Two feet of borehole caving into bottom of open hole was recorded. Water level was measured at 478 ft below land surface. Attempts to bail well unsuccessful due to insufficient bailing line on rig to reach water level.

April 14--Measured water level to confirm that previous measurement was static. Water level static at 478 ft below land surface. Attempts to bail well unsuccessful due to insufficient bailing line on rig to reach water level.

April 16--To increase depth of water in borehole for pump test, well was deepened to 530 ft T.D. This depth was approaching maximum depth capacity of drilling rig. Final conditioning before pump test involved slugging hole with foam and then circulating dry air for 30 minutes. This process was repeated three times. After final circulation, returns were still observed to have high moisture content.

April 18--Difficulty anticipated for successful pump test because of extremely small clearance between submersible pump (3-3/4 inch O.D.) and open borehole (4-inch O.D.). Tight hole conditions were confirmed as maximum depth of free clearance for the pump was 489 ft below land surface, allowing only 11 ft of water coverage over the pump at the start of the test.

Pump test started with empty return pipe and no check valve to restrict backflow of water into formation during a pump shutdown. During first 4 minutes of pump test, water-level drawdown was measured then water level rose, indicative of pump failure. Attempts to correct pump failure were unsuccessful, and pump test was temporarily abandoned so that pump could be pulled from well and inspected. Results of inspection indicated that turbine intakes on pump had been completely packed off with loose sand, a result of borehole wall caving. Two possible remedies were to install check valve in pump at the return pipe connection and to fill return pipe with formation water obtained during bailing. Reasoning for this solution was that initial surge of pump at start of test with no restriction in return pipe resulted in large amounts of sand caving into openhole and subsequently into pump intakes.

April 23--In addition to previous measures taken to enhance the pump test, the submersible pump was also wrapped with Dupont filter fiber to reduce sand intake. Depth for which pump was set to start test was again 489 ft below land surface. Measures taken to correct pump test #1 results proved partially successful as returns at the surface were monitored and collected from the start of the test. Restriction to flow, however, was still apparent, as returns were measured at only 0.26 gpm. The low yield was insufficient to reduce water level; rates of recharge exceeded rates of production.

Obtaining a clean water sample from the pump test for chemistry and isotope analysis was also a high priority, and so the pump test was continued. After approximately 68 minutes, discharge at the surface dropped to a trace. The pump was raised 5 ft to 484 ft below land surface to increase borehole clearance and continue to clear up formation water for sampling. This increased production to approximately 0.8 gpm. Although it was clear that rate of return could be increased by opening control valve at the surface, only 4 ft of water covered the pump intakes, and caution had to be used to maintain water levels above the intake level. To determine quality of formation water, temperature, salinity, and conductivity were constantly monitored using a battery-powered conductivity meter. After 139 minutes of pumping, temperature, salinity and conductivity had stabilized at 17°C, 1.7%, and 2,550 micromhos, respectively. Formation water was then collected and sampled for cations, anions, ^{13}C , ^{14}C , ^{18}O , ^2H , ^{34}S , and tritium. Production began to decrease at 159 minutes and stopped at 167 minutes.

It was determined that with current bottomhole conditions, a successful drawdown pump test was unlikely because of low clearance differential, and further modifications would have to be employed before new attempts would be made.

One possible solution would be to re-enter the well with an underreaming drill bit and increase the diameter of the openhole from 393 ft to T.D. at 530 ft. This would greatly reduce pump intake restriction and allow pump positioning at a deeper depth for greater drawdown potential. The greatest risk in this operation occurs after underreaming has been completed and reamer blades are closed for removal. If the blades do not close due to mechanical problems there would be no alternative to economically salvage the well.

Another possibility with greater risks would be to attempt a cement squeeze job over the entire open hole from 393 ft to the top of water-bearing strata at 480 ft. This might be attempted by (1) filling the borehole with sand from 530 ft to 480 ft, (2) placing a 2-4 ft bentonite plug on top of sand, (3) filling rest to open hole from 476 to 393 ft with a wet cement slurry to allow for formation penetration, and (4) after allowing adequate time for cement to cure, drill back to T.D. with 4 inch bit. If all steps were successful, then a cement liner would restrict any possible sand caving into submersible pump intakes during testing and production. This method would, however, involve significantly greater risks than the first method.

The current design of B-14 is as follows:

- 4 inch steel casing from -393 ft to +2 ft.
- open borehole from -393 ft to -530 ft
- 3 ft square cement pad at surface with locking well cap.

Although drilling conditions were not conducive to accurate lithologic determination, some conclusions could be made as to the general sequences encountered.

*0-6 ft-tan silty sand

*7-33 ft-limestone gravels and silts

*34-44 ft-silt to silty clay

*51-100 ft-silt to silty clay

*100-125 ft-unconsolidated fine sand, some silt

*125-345 ft-predominantly clay with minor amounts of silt, occasional thin lenses with higher silt and sand content

*345-392 ft-silty clay with well cemented lenses of sand and occasional limestone gravels

*393-393 ft-hard, apparently well cemented limestone gravel. Encountered partial loss of circulation in this interval.

*480-530 ft-lithology determination complicated while drilling with foam. Of two scenarios, the most reasonable is that, based on rates of penetration and returns, Cretaceous rocks were encountered at 487 ft of either the Finlay or Bluff Mesa formations. The returns during this interval were predominantly black limestones. Another possible conclusion is that this interval was simply a well-cemented basal bolson gravel.

Future testing in this area should definitely include continuous coring in at least one borehole from 150 ft to 700 ft so that stratigraphic and hydrologic questions raised by inadequate sample returns can be answered.